

**FEDERAL UNIVERSITY OF ITAJUBÁ - UNIFEI  
POST GRADUATE PROGRAM IN  
ELECTRICAL ENGINEERING**

Dynamic Emulation and Analysis of  
Synchronous and Induction Generators in  
Parallel Operation Mode in an Isolated  
Electric System

**Vinicius Zimmermann Silva**

Itajubá, November 16, 2020

**FEDERAL UNIVERSITY OF ITAJUBÁ - UNIFEI  
POST GRADUATE PROGRAM IN  
ELECTRICAL ENGINEERING**

**Vinicius Zimmermann Silva**

**Dynamic Emulation and Analysis of  
Synchronous and Induction Generators in  
Parallel Operation Mode in an Isolated  
Electric System**

Thesis submitted to the Post Graduate Program in Electrical Engineering as part of requirements to obtaining of Doctor Degree in Electrical Engineering Science

**Concentration field: Analysis Methods, Planning and Operation of Electric System**

**Supervisor: Prof. Dr. Angelo José Junqueira Rezek**

**November 16, 2020  
Itajubá**

FEDERAL UNIVERSITY OF ITAJUBÁ - UNIFEI  
POST GRADUATE PROGRAM IN  
ELECTRICAL ENGINEERING

Dynamic Emulation and Analysis of  
Synchronous and Induction Generators in  
Parallel Operation Mode in an Isolated  
Electric System

Vinicius Zimmermann Silva

Thesis approved by examination bench in April  
24, 2020, granting the author the degree of **Doctor  
in Science in Electrical Engineering**

*Examination bench:*

Prof. Dr. José Carlos de Oliveira  
Prof. Dr. Nery de Oliveira Junior  
Prof. Dr. Ricardo Elias Caetano  
Prof. Dr. José Carlos Grilo Rodrigues  
Prof. Dr. Angelo José Junqueira Rezek

Itajubá  
2020

---

Vinicius Zimmermann Silva

Dynamic Emulation and Analysis of Synchronous and Induction Generators  
in Parallel Operation Mode in an Isolated Electric System/ Vinicius Zimmermann  
Silva. – Itajubá, November 16, 2020-

172 p. : il.; 30 cm.

Supervisor: Prof. Dr. Angelo José Junqueira Rezek

Thesis (Doctorate)

FEDERAL UNIVERSITY OF ITAJUBÁ - UNIFEI

Post Graduate Program in Electrical Engineering , November 16, 2020.

1. Induction Generator 2. Synchronous Generator I. Angelo José Junqueira  
Rezek II. Federal University of Itajubá III. Electrical System IV. Doctorate in  
Electrical Engineering

CDU 07:181:009.3

---

Vinicius Zimmermann Silva

# **Dynamic Emulation and Analysis of Synchronous and Induction Generators in Parallel Operation Mode in an Isolated Electric System**

Thesis submitted to the Post Graduate Program in Electrical Engineering as part of requirements to obtaining of Doctor Degree in Electrical Engineering Science

Work approved. Itajubá, April 24, 2020:

---

**Prof. Dr. Angelo José Junqueira  
Rezek**  
Professor adviser

---

**Prof. Dr. José Carlos de Oliveira**

---

**Prof. Dr. Nery de Oliveira Junior**

---

**Prof. Dr. Ricardo Elias Caetano**

---

**Prof. Dr. José Carlos Grilo Rodrigues**

---

**Prof. Dr. Angelo José Junqueira  
Rezek**

Itajubá  
November 16, 2020

# Acknowledgements

I owe my most sincere and deepest thanks to God due to the grace of our lives, to my professor adviser and friend Angelo José Junqueira Rezek who always motivated and helped me, as well as to my parents Maria das Graças Zimmermann Silva and Jose Carlos Ferreira da Silva who have always been together with me to overcome my challenges.

I also thank my friend and university co-worker Christel Enock Ghislain Ogoulola for assistance in thesis conversion to LATEX.

Finally, I thank the UNIFEI technicians José Airton de Freitas, Adair Salvado Junior and Jorge Wilson Rosa for assistance in my workbench at laboratory of research development of electrical didactic laboratory of Federal University of Itajubá.

*"You don't start out writing good stuff. You start out writing crap and thinking it is good stuff, and then gradually you get better at it. That's why I say one of the most valuable traits is persistence."  
(Octavia E. Butler)*

# Resumo

Este trabalho tem a finalidade de apresentar novas contribuições para os estudos de aplicações de máquinas elétricas, principalmente sobre análise de geradores de indução e síncrono em modo de operação paralelo, incluindo estudos de transientes de geração e carga e contingências contra efeitos indesejáveis do aumento da frequência. Assim, em resumo, os principais tópicos apresentados neste trabalho são: (a) uma análise dos geradores de indução e síncrono em modo de operação em paralelo, (b) estudos de transientes de carga e geração e, finalmente, (c) estudos de frequência aumentada para esta citada topologia de geradores, as causas do aumento da frequência e alternativas para controlar esses efeitos. Todo este conteúdo principal é suportado por anexos e apêndices que contribuem com práticos e originais estudos relacionados a cada subsistema que fazem parte dos experimentos principais, tais como: (i) reguladores de corrente e tensão para máquinas de corrente contínua, (ii) circuito de disparo, (iii) reguladores de tensão para geradores síncronos, (iv) sistema de acionamento em quatro quadrantes para máquinas de corrente contínua e (v) placas de controle digital e analógica.

**Palavras-chaves:** Controle em malha fechada; Gerador de Indução; Gerador Síncrono; Gerador Assíncrono; Geradores em Paralelo, Sistema Elétrico Isolado.

# Abstract

This work aims to present new contributions for electrical machines application studies, mainly about analysis of induction and synchronous generators in parallel operation mode, including studies of generation and load transients and contingencies against undesirable effects of frequency increasing. Then, in summary, the main topics presented in this work are: an analysis of induction and synchronous generators in parallel operation mode, studies of load and generation transients and, finally, studies of increasing frequency for this cited generator topology, the causes of increasing frequency and alternatives to control these effects. All of this main subject are supported by appendixes that contributes with practical and original studies related to each subsystem that is part of main experiments such as: (i) voltage and current regulators for DC machines, (ii) firing circuit, (iii) voltage regulators to synchronous generators, (iv) four-quadrant Driven System for DC Machine and (v) analogical and digital control boards.

**Key-words:** Asynchronous Generator; Closed loop Control; Induction Generator; Isolated Electric System; Generators in Parallel; Synchronous Generator.

# List of Figures

Figure 1.1 – Electric Scheme . . . . .	30
Figure 1.2 – MP 410T in Speed Control loop . . . . .	31
Figure 1.3 – MP 410T in Voltage Control loop . . . . .	31
Figure 1.4 – Speed Control Loop . . . . .	34
Figure 1.5 – Field Voltage Control Loop . . . . .	34
Figure 1.6 – Converter Configuration used for control Operational Scenarios . . . . .	34
Figure 1.7 – Electronic Board MP410T and Connections . . . . .	35
Figure 1.8 – Circuit boards MP410T used to implement the Control Loops . . . . .	35
Figure 1.9 – Laboratory assembly in the laboratory of research development of electrical didactic laboratory of Federal University of Itajubá . . . . .	41
Figure 1.10–Synchronous and Induction Generators in parallel Operation Mode with Steady Armature Voltage for $DCM_{IG}$ (Variation of $DCM_{IG}$ field flux by field Rheostat) . . . . .	42
Figure 1.11–Synchronous and Induction Generators in Parallel Operation mode with Variable Armature Voltage for $DCM_{IG}$ ( $DCM_{IG}$ Steady field flux) . . . . .	42
Figure 1.12–Synchronous and Induction Generators in Parallel Operation mode with Variable Armature Voltage for $DCM_{IG}$ and an Induction Motor as Load ( $DCM_{IG}$ Steady field flux) . . . . .	43
Figure 1.13–Conjugate vs rpm - Induction Motor and Generator . . . . .	43
Figure 1.14– $PIG$ vs $PSG$ with $DCM_{IG}$ Field Variation and $V_{aDCMIG}$ kept Constant . . . . .	48
Figure 1.15– $PIG$ vs $PSG$ with $V_{aDCMIG}$ Variation and Field flux kept Constant (Only resistive load) . . . . .	49
Figure 1.16– $PIG$ vs $PSG$ with $V_{aDCMIG}$ Variation and Field Flux kept Constant (Resistive load & IM) . . . . .	49
Figure 1.17– $P_{DCMIG}$ vs $P_{DCMSG}$ with $DCM_{IG}$ Field Flux Variation and $V_{aDCMIG}$ Kept Constant . . . . .	50
Figure 1.18– $V_{SG}$ ( <i>Synchronous generator voltage</i> ) x $f_{SG}$ ( <i>Synchronous generator frequency</i> ) x $I_{load}$ ( <i>Load current</i> ) . . . . .	50
Figure 1.19– $P_{DCMIG}$ vs $P_{DCMSG}$ with $V_{aDCMIG}$ Variation and Field Flux Kept Constant (Only resistive load) . . . . .	51
Figure 1.20– $P_{DCMIG}$ vs $P_{DCMSG}$ with $V_{aDCMIG}$ Variation and Field Flux Kept Constant (Resistive load plus IM) . . . . .	51
Figure 1.21– $n_{IG}$ vs $n_{SG}$ with $DCM_{IG}$ Field Flux Variation and $V_{aDCMIG}$ Kept Constant . . . . .	52
Figure 1.22– $n_{IG}$ vs $n_{SG}$ with $V_{aDCMIG}$ Variation and Field Flux kept Constant (Only resistive load) . . . . .	52

Figure 1.23– $n_{IG}$ vs $n_{SG}$ with $V_{a_{DCMIG}}$ Variation and Field Flux kept Constant (Resistive load plus IM) . . . . .	53
Figure 2.1 – Laboratory Assembly . . . . .	58
Figure 2.2 – Connections Arrangement of MP410T and Devices . . . . .	58
Figure 2.3 – Synchronous and Induction Generators in Parallel Operation Mode . . . . .	59
Figure 2.4 – Speed Control Loop . . . . .	59
Figure 2.5 – Field Voltage Control Loop . . . . .	59
Figure 2.6 – $I_{IG}$ and $V_{pn}$ (Scenario 1) . . . . .	61
Figure 2.7 – $I_{SG}$ and $V_{pn}$ (Scenario 1) . . . . .	61
Figure 2.8 – $I_{IG}$ and $V_{pn}$ (Scenario 2) . . . . .	61
Figure 2.9 – $I_{SG}$ and $V_{pn}$ (Scenario 2) . . . . .	61
Figure 2.10–Channel 1- $I_{SG}$ , Channel 2- $V_{pn}$ . (2/3 kW is removed and then inserted) (Scenario 2) . . . . .	62
Figure 2.11–Channel 1- $I_{IG}$ , Channel 2- $V_{pn}$ . (2/3 kW is removed and then inserted) (Scenario 2) . . . . .	62
Figure 2.12–Channel 1- $n_{SG}$ , Channel 2- $I_{IG}$ . (2/3 kW is removed and then inserted.) (Scenario 2) . . . . .	62
Figure 2.13–Channel 1- $n_{SG}$ , Channel 2- $I_{SG}$ . (2/3 kW is removed and then inserted.) (Scenario 2) . . . . .	62
Figure 2.14– $V_{pn}$ , $SG$ is removed and then inserted. Scenarios 4 & 5 . . . . .	63
Figure 2.15– $V_{pn}$ in load. $IG$ is removed and then inserted. Scenarios 4 & 5 . . . . .	63
Figure 2.16– $SG$ speed. $IG$ is removed and then inserted. Scenarios 6 & 7 . . . . .	63
Figure 2.17– $I_{SG}$ , $IG$ is removed and then inserted. Scenarios 6 & 7 . . . . .	63
Figure 2.18– $I_{SG}$ . $SG$ smallest contribution = 0.4A. Scenario 3 . . . . .	64
Figure 2.19– $I_{IG}$ , $IG$ biggest contribution =6.9A. Scenario 3 . . . . .	64
Figure 2.20–Transition between Scenarios 4 and 5 . . . . .	64
Figure 2.21–Transition between Scenarios 6 and 7 . . . . .	64
Figure 3.1 – Transient frequency following load removal . . . . .	68
Figure 3.2 – SG and IG feeding the load . . . . .	68
Figure 3.3 – Lab Assembly (Front View) . . . . .	69
Figure 3.4 – Synchronous and Induction Generators in Parallel Operation Mode . . . . .	70
Figure 3.5 – Electronic Board MP410T and Connections . . . . .	71
Figure 3.6 – Speed Control Loop . . . . .	72
Figure 3.7 – Voltage Control Loop . . . . .	72
Figure 3.8 – V-Curve of $SG$ or $SM$ . . . . .	73
Figure 3.9 – Frequency Control Loop . . . . .	74
Figure 3.10–Ballast load circuit . . . . .	75
Figure 3.11–Ballast Load Performance . . . . .	76
Figure 3.12–Ballast Load Control . . . . .	77

Figure 3.13– $V_{bl}$ as Fire Angle $90^\circ$ . . . . .	77
Figure 3.14– $DCM_{SG}$ Current Operation . . . . .	78
Figure 3.15–Energy Regeneration Scheme . . . . .	78
Figure 3.16–Increasing frequency . . . . .	80
Figure 3.17–Ballast load actuation . . . . .	80
Figure 3.18–Voltage $V_{bl}$ across BL . . . . .	80
Figure 3.19–Frequency control ERS . . . . .	80
Figure 3.20–Voltage $V_{dc}$ and Current $I_{ac}$ . . . . .	81
Figure 3.21– $V_{bl}$ -IG operates alone . . . . .	81
Figure 3.22–Voltage $V_{pp}$ -IG alone . . . . .	82
Figure 3.23–BL control-IG alone . . . . .	82
Figure A.1 –Ramp Type Firing Circuit . . . . .	88
Figure A.2 –Waveforms and Firing Angle . . . . .	88
Figure A.3 –Synchronism Transformer . . . . .	89
Figure A.4 –General view of Synchronism Transformer . . . . .	89
Figure A.5 –Motor Armature Circuit and Diagram of the Drive System Mechanical Part . . . . .	90
Figure A.6 –Block diagram of the drive mechanical part . . . . .	91
Figure A.7 –Representation of the Motor Mechanical Part in pu . . . . .	92
Figure A.8 –Block Diagram of the DC Motor Armature Circuit . . . . .	94
Figure A.9 –Reduced Voltage step Applied to the Armature Circuit . . . . .	94
Figure A.10 –Current Response for a Voltage step Applied to the Armature Circuit . . . . .	94
Figure A.11 –Schematic Block Diagram of the Independent Excitation DC Motor . . . . .	95
Figure A.12 –Complete Block Diagram of Controlled Drive . . . . .	96
Figure A.13 –Current Regulation Loop . . . . .	97
Figure A.14 –Current Transducer . . . . .	98
Figure A.15 –Implementation of Current Regulator . . . . .	102
Figure A.16 –Speed Regulation Loop . . . . .	104
Figure A.17 –Implementation of Speed Regulator . . . . .	106
Figure A.18 –General Diagram . . . . .	109
Figure A.19 –Speed and Current Waveforms . . . . .	110
Figure A.20 – $DCM$ coupled with $SG$ and a Resistive Load . . . . .	111
Figure B.1 –Basic Organization of Control Circuit. . . . .	115
Figure B.2 –Blocks Diagram of Control Circuit using the TCA 785 and 555. . . . .	116
Figure B.3 –Internal Diagram of TCA 785. . . . .	118
Figure B.4 –Waveforms Diagram for TCA 785. [1] . . . . .	119
Figure B.5 –TCA 785 Wrapping and Pins . . . . .	119
Figure B.6 –CI 555 as Monostable . . . . .	122
Figure B.7 –Monostable with Adjustable output Pulse Width. . . . .	123

Figure B.8–Internal Diagram of TIL111. . . . .	123
Figure B.9–Attack stage circuit. . . . .	124
Figure B.10–Control Voltage Circuit. . . . .	125
Figure B.11–Block Diagram of Complete Control Circuit . . . . .	125
Figure B.12–Firing Circuit Diagram . . . . .	126
Figure B.13–Voltage Sources for Firing Circuit Diagram . . . . .	126
Figure C.1 –Auxiliary Circuit Mounted in the Laboratory . . . . .	129
Figure C.2 –Generator Time Constant Determination . . . . .	130
Figure C.3 –Simplified Block Diagram of Voltage Regulation . . . . .	131
Figure C.4 –Full Wave Three-phase Rectifier with thyristor [2] . . . . .	131
Figure C.5 –Full Blocks Diagram of Voltage Regulation System . . . . .	132
Figure C.6 –Value of $\tau_{gs}$ and Relation between the large and the Small Time Constants . . . . .	134
Figure C.7 –Graetz Bridge with Thyristor and 220 V Grid Voltage . . . . .	136
Figure C.8 –Voltage regulator . . . . .	138
Figure C.9 –Voltage Regulator Topology with “T” Filter in the Reference Channel .	138
Figure C.10–Voltage Regulator Topology . . . . .	141
Figure C.11–Voltage Regulator System for Synchronous Machine . . . . .	141
Figure D.1 –Full Blocks Diagram of DC Machine . . . . .	144
Figure D.2 –Implemented Drive System . . . . .	145
Figure D.3 –Control Circuit . . . . .	146
Figure D.4 –Conjugate (t) versus Speed (n) Diagram . . . . .	146
Figure D.5 –Closing of Converters I and II . . . . .	147
Figure D.6 –Commutation Switch S1 . . . . .	147
Figure D.7 –Control Circuit . . . . .	148
Figure D.8 –Resistance to Energy Dissipation in Machine Field Circuit . . . . .	149
Figure D.9 –Rotation Inversion using the Armature Current Inversion . . . . .	150
Figure D.10–Rotation Inversion using the Field Current Inversion . . . . .	150
Figure E.1 –No load test and locked rotor test circuit . . . . .	151
Figure E.2 –Induction Motor Equivalent Circuit . . . . .	151
Figure E.3 –Results of no-Load Test: W1+W2 vs Voltage Applied . . . . .	152
Figure E.4 –Equivalent Circuit – No-Load Test . . . . .	153
Figure E.5 –Equivalent Circuit Locked Rotor Test . . . . .	154
Figure E.6 –IM Winding Connection . . . . .	154
Figure E.7 –Magnetization branch power factor . . . . .	158
Figure E.8 –Parameters of Induction Motor . . . . .	159
Figure E.9 –Resistors bank and IM currents in scenarios C as Table 1.10 . . . . .	163
Figure F.1 –Scenario 1B . . . . .	166
Figure F.2 –Scenario 2B . . . . .	166

Figure F.3 – Scenario 3B . . . . .	167
Figure F.4 – Scenario 1C . . . . .	167
Figure F.5 – Scenario 2C . . . . .	167
Figure F.6 – Scenario 3C . . . . .	168

# List of Tables

Table 1.1 – Terminal Descriptions of SEMIKRON MP410T Electronic Board . . . . .	32
Table 1.2 – Electronic Control Board Configuration . . . . .	33
Table 1.3 – $DCM_{IG}$ ( <i>Direct Current Motor coupled with induction generator</i> ) Data plate . . . . .	35
Table 1.4 – $DCM_{SG}$ ( <i>Direct current motor coupled with synchronous generator</i> ) Data plate . . . . .	36
Table 1.5 – $IG$ ( <i>Induction Generator</i> ) Data plate . . . . .	36
Table 1.6 – $SG$ ( <i>Synchronous Generator</i> ) Data plate . . . . .	36
Table 1.7 – Load Data plate . . . . .	36
Table 1.8 – Load Data plate . . . . .	36
Table 1.9 – Operational scenarios in controlled mode and three resistors bank as load	45
Table 1.10–Operational scenarios in controlled mode and three resistors bank and induction motor as load . . . . .	46
Table 1.11–Operational scenarios in controlled mode and a resistor bank . . . . .	47
Table 2.1 – Scenarios and Transitions . . . . .	60
Table 3.1 – Equipment Data Plates . . . . .	70
Table 3.2 – Electronic Control Board Configuration . . . . .	75
Table A.1–DC Motor Data . . . . .	97
Table A.2–Current Regulator Parameters . . . . .	101
Table A.3–Complementary Current Regulator Data . . . . .	103
Table A.4–Speed Regulator Parameters . . . . .	106
Table A.5–Speed Regulator Parameters . . . . .	108
Table B.1–Pulse width from pins 14 and 15 related to capacitor C12 values, [3] . .	121
Table C.1–Excitation Parameters of Salient Poles Synchronous Generator . . . . .	130
Table C.2–Excitation Parameters of Salient Poles Synchronous Generator . . . . .	133
Table C.3–Excitation Parameters of Salient Poles Synchronous Generator . . . . .	133
Table C.4–Regulator Parameters Adjustments and Optimization [4]. . . . .	136
Table C.5–Optimized Voltage Regulator Parameters . . . . .	137
Table C.6–Voltage Regulator Adjustments . . . . .	141
Table D.1–Motor Data . . . . .	145
Table D.2–Speed Regulator Parameters . . . . .	145
Table D.3–Current Regulator Parameters . . . . .	145
Table D.4–Cause and Effect Matrix . . . . .	148
Table E.1–No load Test . . . . .	152
Table E.2–Current Regulator Parameters . . . . .	153
Table E.3–Average Resistance . . . . .	154

# List of abbreviations and acronyms

$BL$	<i>Ballast load</i>	28
$CT$	<i>Current transformer</i>	97
$DCG_{SG}$	<i>Direct current generator coupled with synchronous generator</i>	65
$DCM$	<i>Direct Current Motor</i>	26
$DCM$	<i>Direct current motor</i>	50
$DCM_{IG}$	<i>Direct Current Motor coupled with induction generator</i>	15
$DCM_{SG}$	<i>Direct current motor coupled with synchronous generator</i>	15
$E$	<i>DC supply voltage</i>	99
$ERS$	<i>Energy regeneration system</i>	28
$E_{DCM}$	<i>Direct current motor voltage</i>	90
$E_N$	<i>Rated voltage</i>	93
$E_{SGf}$	<i>Synchronous generator field terminal voltage</i>	131
$E_{SG}$	<i>Synchronous generator electromotive force</i>	73
$E_{pp}$	<i>Phase-phase voltage</i>	135
$FPSO$	<i>Floating production storage and offloading</i>	27
$IG$	<i>Induction Generator</i>	15
$IG$	<i>Gate current</i>	116
$IM$	<i>Induction motor</i>	40
$I_{AK}$	<i>Locked rotor current</i>	95
$I_C$	<i>Capacitor current</i>	39
$I_{IG}$	<i>Induction generator current</i>	39
$I_N$	<i>Rated Current</i>	93
$I_{SG}$	<i>Synchronous generator current</i>	39
$I_{ac}$	<i>Line current across the ac converter side</i>	81
$I_a$	<i>Armature current</i>	90
$I_{bl}$	<i>Ballast load current</i>	80
$I_{cc}$	<i>Generator field circuit current</i>	128
$I_{exc}$	<i>excitation current</i>	135
$I_{f1}$	<i>Field current 1</i>	79
$I_{f2}$	<i>Field current 2</i>	79
$I_{fDCMIG}$	<i>Field current of direct current motor coupled with induction generator</i>	27
$I_f$	<i>Field current</i>	73
$I_{load}$	<i>Load current</i>	10
$I_m$	<i>Magnetization Current</i>	152
$I_{rm}$	<i>Magnetization branch current across resistance</i>	158

$I_{xm}$	<i>Magnetization branch current across inductor</i>	158
$I_{aDCMIG}$	<i>Direct current motor induction generator armature current</i>	48
$I_{C1}$	<i>Capacitor current 1</i>	39
$I_{C2}$	<i>Capacitor current 2</i>	39
$I_{dW_{MT}}$	<i>Induction motor reactive current</i>	39
$I_n$	<i>Rated Current</i>	110
$I_{W_{IG}}$	<i>Induction generator active current</i>	39
$I_{W_{MT}}$	<i>Induction motor active current</i>	39
$I_{W_{SG}}$	<i>Synchronous generator active current</i>	39
$I_{W_{loadR}}$	<i>R Load Active current</i>	39
$K_{pmax}$	<i>maximum regulator gain</i>	139
$K_{pmin}$	<i>minimum regulator gain</i>	140
$K_p$	<i>regulator gain</i>	141
$K_p$	<i>Voltage regulator gain</i>	134
$K_t$	<i>Temperature correction factor for 40 degree C</i>	160
$L_a$	<i>Armature circuit inductance</i>	90
$L_d$	<i>Smoothing reactor inductance</i>	97
$L_{fd}$	<i>Field inductor</i>	132
$L_s$	<i>Separated field inductance</i>	97
$PI$	<i>Proportional-integral regulator</i>	76
$PIG$	<i>Induction generator power</i>	27
$PSG$	<i>Synchronous generator power</i>	39
$P_{DCMIG}$	<i>Power of direct current motor coupled with induction generator</i>	39
$P_{DCMSG}$	<i>Power of direct current motor coupled with synchronous generator</i>	39
$P_{av}$	<i>attrition and ventilation losses</i>	152
$P_{bl}$	<i>Ballast load power</i>	76
$P_{hf}$	<i>hysteresis and Foucault losses</i>	157
$P_{in}$	<i>Motor input power</i>	161
$P_{jstator}$	<i>No Load Stator Joules Losses</i>	156
$P_{mec}$	<i>Mechanical power</i>	111
$P_{nl}$	<i>No load losses</i>	156
$P_{out}$	<i>Motor output power</i>	161
$P_{tl}$	<i>Total losses</i>	161
$P_{tl}$	<i>Total losses</i>	159
$P_{win}$	<i>Winding losses</i>	159
$P_{win40C}$	<i>Corrected winding losses for 40 degree C</i>	160
$Q$	<i>Reactive power</i>	155
$Q_m$	<i>No load Reactive Power in Magnetization Branch</i>	157
$RB$	<i>Resistor bank</i>	68

$RM_1$	<i>integral branch steady resistor of voltage regulator</i>	140
$RM_2$	<i>Integral branch adjustment resistor of voltage regulator</i>	137
$R_{SH}$	<i>Shunt resistor</i>	94
$R_{aj}$	<i>adjustment resistance of voltage regulator</i>	139
$R_a$	<i>Armature circuit resistance</i>	90
$R_{fd}$	<i>Field resistor</i>	131
$R_{fdmed}$	<i>Measured field electrical resistance</i>	128
$R_{q1}$	<i>Proportional branch adjustment resistor of voltage regulator</i>	137
$R_{ti}$	<i>total resistor value of integral branch</i>	140
$R_{tp}$	<i>total resistor value of proportional branch</i>	139
$R_d$	<i>Phase resistance in delta connection</i>	153
$R_m$	<i>Motor Average Measured Resistance</i>	153
$R_y$	<i>Phase resistance in star connection</i>	153
$SG$	<i>Synchronous Generator</i>	15
$SM$	<i>Synchronous machine</i>	89
$SM$	<i>Synchronous motor</i>	72
$SV$	<i>Synchronous voltage</i>	116
$SW$	<i>Interconnection switch</i>	43
$SW_a$	<i>Interchangeable switch</i>	83
$T_c$	<i>Load torque</i>	90
$T_{fr}$	<i>Friction torque</i>	90
$T_m$	<i>Motor torque</i>	110
$T_n$	<i>Motor rated torque</i>	110
$U_2$	<i>AC supply voltage</i>	99
$U_a$	<i>Direct current motor armature voltage</i>	72
$U_{na}$	<i>Feedback speed signal</i>	77
$V_1$	<i>Sawtooth voltage</i>	116
$V_2$	<i>Rectangular pulse</i>	116
$V_3$	<i>Rectangular wave</i>	116
$V_4$	<i>Rectangular pulses train</i>	116
$V_5$	<i>Amplified rectangular pulses train</i>	116
$VC$	<i>Control voltage</i>	116
$VL$	<i>Load voltage</i>	116
$V_{DCMSG}$	<i>Voltage of direct current motor coupled with synchronous generator</i>	79
$V_{IG}$	<i>Induction generator voltage</i>	61
$V_{Ri}$	<i>Gain of the current regulator</i>	96
$V_{Rn}$	<i>Gain of the speed regulator</i>	95
$V_{SG}$	<i>Synchronous generator voltage</i>	10
$V_{blRMS}$	<i>RMS ballast load voltage</i>	76

$V_{cc}$	<i>Control voltage of thyristor firing system</i>	87
$V_{dc}$	<i>Direct current voltage</i>	48
$V_{fd}$	<i>Generator field terminal voltage</i>	128
$V_{ia}$	<i>Feedback current signal</i>	77
$V_i$	<i>Motor current amplification factor</i>	93
$V_i$	<i>Gain of machine electric part</i>	96
$V_{pn}$	<i>Phase neutral voltage</i>	61
$V_{pp}$	<i>Phase-phase voltage</i>	61
$V_{ref}$	<i>Reference Voltage</i>	130
$V_{sa}$	<i>Generator output voltage</i>	131
$V_s$	<i>Gain of the static converter</i>	96
$V_t$	<i>Transducer output voltage</i>	131
$V_{aDCMIG}$	<i>DCM armature voltage coupled with IG</i>	27
$V_{t1}$	<i>Voltage signal from the frequency transducer (position 1)</i>	77
$V_{t2}$	<i>Voltage signal from the frequency transducer (position 2)</i>	83
$\Theta_0$	<i>Magnetization Branch Power Factor Angle</i>	158
$\beta_{RM2}$	<i>adjustable resistor of integral branch</i>	137
$\dot{I}_a$	<i>Synchronous generator armature current</i>	73
$\eta_{IG}$	<i>IG efficiency</i>	39
$\eta_{SG}$	<i>SG efficiency</i>	39
$\eta_{group}$	<i>Group efficiency</i>	39
$\tau_H$	<i>Accelerating time constant</i>	91
$\tau_a$	<i>Inductor circuit or armature time constant</i>	92
$\tau_e$	<i>Equivalent time constant</i>	104
$\tau_{gi}$	<i>Filter time constant of the current transducer</i>	96
$\tau_{gn}$	<i>Filter time constant of the speed transducer</i>	96
$\tau_{gs1}$	<i>Filter time constant of the reference channel of the speed loop</i>	95
$\tau_{gs2}$	<i>Filter time constant of the reference channel of the current loop</i>	95
$\tau_{gs}$	<i>Smoothing time constant</i>	132
$\tau_i$	<i>Current regulator time constant</i>	96
$\tau_n$	<i>Time constant of the speed regulator</i>	96
$\tau_{ss}$	<i>Firing circuit time constant</i>	96
$f_{SG}$	<i>Synchronous generator frequency</i>	10
$i_a$	<i>Armature current in pu</i>	92
$m$	<i>Motor torque in pu</i>	92
$n.a.$	<i>Not applicable</i>	44
$n_{IG}$	<i>Induction generator speed</i>	40
$n_{REF}$	<i>Reference speed</i>	96
$n_{SG}$	<i>Synchronous generator speed</i>	61

$n_u$	<i>Speed in pu</i>	96
$r_1$	<i>Stator winding resistance</i>	154
$r_{140C}$	<i>Corrected stator winding resistance for 40 degree C</i>	160
$r_2'$	<i>Rotor winding resistance referred to stator winding</i>	155
$r_{2'40C}$	<i>Corrected rotor winding resistance referred to stator for 40 degree C</i>	160
$r_m$	<i>Magnetization branch resistance</i>	158
$t_c$	<i>Load torque in pu</i>	96
$vi$	<i>Signal from the current transducer</i>	97
$x_1$	<i>Stator winding reactance</i>	155
$x_2'$	<i>Rotor winding reactance referred to stator winding</i>	155
$x_m$	<i>Magnetization branch reactance</i>	159
$I_a'$	<i>Direct current motor armature current</i>	73
$RM_2''$	<i>Integral branch adjustment resistor of current regulator</i>	102
$RM_2'$	<i>Integral branch adjustment resistor of speed regulator</i>	106
$R_{aj}''$	<i>adjustment resistance of current regulator</i>	102
$R_{aj}'$	<i>adjustment resistance of speed regulator</i>	107
$R_{q1}''$	<i>Proportional branch adjustment resistor of current regulator</i>	102
$R_{q1}'$	<i>Proportional branch adjustment resistor of speed regulator</i>	106
$R_{q2}''$	<i>Proportional branch steady resistor of current regulator</i>	103
$R_{q2}'$	<i>Proportional branch steady resistor of speed regulator</i>	107
$V1'$	<i>Rectangular pulse</i>	117
$V2'$	<i>Wider Rectangular pulse</i>	117
$V3'$	<i>Wider Rectangular pulse</i>	117
$V4'$	<i>Wider Rectangular pulse</i>	117
$V_{bl_{RMS}}'$	<i>Phase-neutral RMS ballast load voltage</i>	76
$\tau'$	<i>Generator field time constant</i>	128
$\tau'_i$	<i>Regulator time constant</i>	132
MHPP	<i>Micro-Hydro Power Plants</i>	26

# List of symbols

$B$	Resultant torque	90
$F(s)$	Transfer function	134
$J$	Inertia moment, motor plus load	90
$L$	Inductor	79
$M$	Torque	73
$M_n$	Rated torque	91
$N_n$	Rated speed	110
$U$	Counter electromotive force	90
$\Delta V$	Voltage error signal	131
$\Theta_{med}$	Measured winding temperature	129
$\Theta_{ref}$	Reference temperature resistance	128
$\alpha$	thyristor firing angle	79
$\alpha_u$	Value in pu of the thyristor firing angle	99
$\eta$	motor efficiency	111
$\mu$	Overlap angle	99
$\phi$	Machine flux	48
$\sigma$	Sum of small time constant	133
$k$	Proportionality constant 0	111
$n_0$	No load speed	90
$t$	Time	110
$w$	Rotation $\frac{rad}{s}$	90
$\sigma'$	Sum of small time constant of speed regulator	104
$k''''$	Proportionality constant 4	112
$k'''$	Proportionality constant 3	111
$k''$	Proportionality constant 2	111
$k'$	Proportionality constant 1	111
$n$	Speed	73

# Contents

<b>1</b>	<b>ANALYSIS OF SYNCHRONOUS AND INDUCTION GENERATORS IN PARALLEL OPERATION MODE IN AN ISOLATED ELECTRIC SYSTEM</b> . . . . .	<b>29</b>
<b>1.1</b>	<b>Introduction</b> . . . . .	<b>29</b>
<b>1.2</b>	<b>Isolated Electric System</b> . . . . .	<b>30</b>
<b>1.3</b>	<b>Digital Control Board</b> . . . . .	<b>31</b>
1.3.1	MP410T Electronic Board Parameterization . . . . .	32
1.3.2	Voltage and Speed Control Loops . . . . .	33
1.3.3	Arrangement . . . . .	34
<b>1.4</b>	<b>Data Plate</b> . . . . .	<b>35</b>
<b>1.5</b>	<b>Equations - Part I</b> . . . . .	<b>36</b>
1.5.1	Capacitor Bank Sizing . . . . .	37
1.5.2	Resistive Divider Sizing . . . . .	37
<b>1.6</b>	<b>Equations - Part II</b> . . . . .	<b>38</b>
<b>1.7</b>	<b>Equations - Part III</b> . . . . .	<b>40</b>
<b>1.8</b>	<b>The Experiment and Schemes</b> . . . . .	<b>40</b>
1.8.1	Methods of IG Connection into the Electric System . . . . .	41
1.8.2	Experiment Data . . . . .	44
<b>1.9</b>	<b>Results</b> . . . . .	<b>48</b>
<b>1.10</b>	<b>Conclusion</b> . . . . .	<b>53</b>
<b>2</b>	<b>LOAD AND GENERATION TRANSIENTS OF SYNCHRONOUS AND INDUCTION GENERATORS IN PARALLEL OPERATION MODE IN AN ISOLATED ELECTRIC SYSTEM</b> . . . . .	<b>55</b>
<b>2.1</b>	<b>Introduction</b> . . . . .	<b>55</b>
<b>2.2</b>	<b>Isolated Electric System</b> . . . . .	<b>56</b>
<b>2.3</b>	<b>Data Plate</b> . . . . .	<b>56</b>
<b>2.4</b>	<b>Equation - Part I</b> . . . . .	<b>56</b>
<b>2.5</b>	<b>Equation - Part II</b> . . . . .	<b>56</b>
<b>2.6</b>	<b>Experiment and Schemes</b> . . . . .	<b>57</b>
<b>2.7</b>	<b>Voltage and Speed Control Loops</b> . . . . .	<b>58</b>
<b>2.8</b>	<b>Experimental Data</b> . . . . .	<b>59</b>
<b>2.9</b>	<b>Results</b> . . . . .	<b>61</b>
<b>2.10</b>	<b>Conclusion</b> . . . . .	<b>65</b>

<b>3</b>	<b>ALTERNATIVES TO CONTROL THE FREQUENCY INCREASE IN AN ELECTRIC SYSTEM WITH SYNCHRONOUS AND INDUCTION GENERATORS IN PARALLEL OPERATION MODE . .</b>	<b>66</b>
<b>3.1</b>	<b>Introduction . . . . .</b>	<b>66</b>
<b>3.2</b>	<b>Frequency Increase . . . . .</b>	<b>67</b>
<b>3.3</b>	<b>Laboratory Experiments . . . . .</b>	<b>67</b>
3.3.1	General Scheme . . . . .	68
3.3.1.1	Data Plates . . . . .	70
3.3.1.2	Digital Control Boards . . . . .	71
3.3.1.3	Analogical Control Board . . . . .	71
3.3.1.4	Speed Control Loop . . . . .	72
3.3.1.5	Voltage Control Loop . . . . .	72
3.3.1.6	Ballast Load Control Loop . . . . .	74
3.3.1.7	Control Board Parametrization . . . . .	74
3.3.2	Ballast Load Control Experiment . . . . .	75
3.3.3	$DCM_{SG}$ Speed Regulator . . . . .	77
3.3.4	Energy Regeneration Experiment . . . . .	78
<b>3.4</b>	<b>Results . . . . .</b>	<b>79</b>
<b>3.5</b>	<b>Conclusion . . . . .</b>	<b>82</b>

## **APPENDIX 86**

	<b>APPENDIX A – FILTERS AND REGULATORS PROJECT . . . . .</b>	<b>87</b>
<b>A.1</b>	<b>Introduction . . . . .</b>	<b>87</b>
<b>A.2</b>	<b>Ramp Firing Circuit . . . . .</b>	<b>87</b>
<b>A.3</b>	<b>Synchronism Transformer . . . . .</b>	<b>88</b>
<b>A.4</b>	<b>Current and Speed Regulators of DC machine project . . . . .</b>	<b>89</b>
A.4.1	Introduction . . . . .	89
A.4.2	Motor Block Diagram . . . . .	89
A.4.3	Armature Circuit Equations . . . . .	92
A.4.4	Complete Block Diagram with Regulators, Filters and Transducers . . . . .	95
<b>A.5</b>	<b>Current Regulator and Filters Project of DC Machine (practical case) 96</b>	
A.5.1	Current Regulator Parameters . . . . .	101
A.5.2	Current Regulator Arrangement . . . . .	101
A.5.2.1	Calculus of $RM_2''$ and $Rq_1''$ . . . . .	102
<b>A.6</b>	<b>Speed Regulators and Filters Project of DC machine (practical case) Project . . . . .</b>	<b>104</b>
A.6.1	Capacitors calculus . . . . .	105

A.6.2	Speed Regulator Parameters . . . . .	106
A.6.2.1	Calculus of $RM'_2$ and $R'_{q1}$ . . . . .	106
A.6.3	General Arrangement . . . . .	108
<b>A.7</b>	<b>Results . . . . .</b>	<b>108</b>

**APPENDIX B – ANALOGICAL CONTROL BOARD (FIRING CIRCUIT) . . . . . 115**

<b>B.1</b>	<b>Introduction . . . . .</b>	<b>115</b>
<b>B.2</b>	<b>Stage Descriptions . . . . .</b>	<b>117</b>
B.2.1	Pulse generation by TCA 785 . . . . .	117
B.2.2	Integrated Circuit Characteristics . . . . .	117
<b>B.3</b>	<b>Operation of TCA 785 . . . . .</b>	<b>120</b>
<b>B.4</b>	<b>Equations . . . . .</b>	<b>121</b>
<b>B.5</b>	<b>The Pulse Enlargement Stage using the Integrated Circuit 555 . . .</b>	<b>122</b>
<b>B.6</b>	<b>Coupling Stage with TIL111 . . . . .</b>	<b>123</b>
<b>B.7</b>	<b>Attack Stage . . . . .</b>	<b>124</b>
<b>B.8</b>	<b>Control Voltage . . . . .</b>	<b>124</b>
<b>B.9</b>	<b>General Overview . . . . .</b>	<b>125</b>
<b>B.10</b>	<b>Conclusion . . . . .</b>	<b>127</b>

**APPENDIX C – VOLTAGE REGULATORS AND FILTERS PROJECT TO SYNCHRONOUS MACHINE . . . . . 128**

<b>C.1</b>	<b>Introduction . . . . .</b>	<b>128</b>
<b>C.2</b>	<b>Calculus of Generator Field Resistance and Inductance . . . . .</b>	<b>128</b>
<b>C.3</b>	<b>Voltage Regulators and Filters Project . . . . .</b>	<b>130</b>
C.3.1	Introduction . . . . .	130
C.3.2	Voltage Regulator Optimization . . . . .	131
C.3.3	Practical Implementation of Voltage Regulator . . . . .	137
<b>C.4</b>	<b>Results . . . . .</b>	<b>140</b>
<b>C.5</b>	<b>Conclusion . . . . .</b>	<b>142</b>

**APPENDIX D – FOUR-QUADRANT REGENERATIVE DRIVEN SYSTEM FOR DC MACHINE APPLYING SPEED REVERSION USING EITHER ARMATURE CURRENT REVERSION OR FIELD CURRENT REVERSION . . . . . 143**

<b>D.1</b>	<b>Introduction . . . . .</b>	<b>143</b>
<b>D.2</b>	<b>Block Diagram of Controlled Drive System for use in DC Machine .</b>	<b>143</b>
<b>D.3</b>	<b>Laboratory Implementation . . . . .</b>	<b>144</b>
<b>D.4</b>	<b>Full Hardware of Implemented Drive System . . . . .</b>	<b>145</b>

<b>D.5</b>	<b>Speed Inversion by Armature Current Inversion</b>	<b>146</b>
<b>D.6</b>	<b>Rotation Inversion using the Field Current Inversion</b>	<b>148</b>
<b>D.7</b>	<b>Results</b>	<b>149</b>
<b>D.8</b>	<b>Conclusion</b>	<b>149</b>
	<b>APPENDIX E – INDUCTION MOTOR PARAMETERS</b>	<b>151</b>
<b>E.1</b>	<b>No Load and Locked Rotor Tests</b>	<b>151</b>
E.1.1	No Load Test	151
E.1.2	Locked Rotor Test	153
<b>E.2</b>	<b>Stator and Rotor Parameters</b>	<b>153</b>
<b>E.3</b>	<b>Power and Losses Calculus</b>	<b>156</b>
E.3.1	No Load Reactive Power	157
E.3.2	Magnetization Branch	157
<b>E.4</b>	<b>Parameters of Induction Motor</b>	<b>159</b>
<b>E.5</b>	<b>Induction Motor Efficiency</b>	<b>159</b>
E.5.1	Temperature Correction Factor and Resistance Correction	160
<b>E.6</b>	<b>Corrected Winding Losses for 40 °C and Total Losses</b>	<b>160</b>
<b>E.7</b>	<b>Motor Efficiency Estimate</b>	<b>161</b>
<b>E.8</b>	<b>Induction Motor Currents</b>	<b>162</b>
	<b>APPENDIX F – SOLVING EQUATIONS WITH MATLAB</b>	<b>164</b>
<b>F.1</b>	<b>Introduction</b>	<b>164</b>
<b>F.2</b>	<b>Equations</b>	<b>164</b>
F.2.1	Electrical system feeding three resistor banks	164
F.2.2	Electrical system feeding three resistor banks and an induction motor	164
F.2.3	Power and Efficiencies	165
<b>F.3</b>	<b>Matlab Code</b>	<b>165</b>
F.3.1	Electrical system feeding three resistor banks	165
F.3.2	Electrical system feeding three resistor banks and an induction motor	166
	<b>BIBLIOGRAPHY</b>	<b>169</b>

# Introduction

In recent years, self-excited induction generators have been employed as suitable isolated power sources in *MHPP (Micro-Hydro Power Plants)* and wind energy applications [5, 6, 7, 8, 9, 10, 11]. In wind power generating systems, the physical size of the individual machines operating at maximum efficiency and dealing with regular routine maintenance related to necessary interruptions, future growth and reliability are reasons for them to be operated in parallel [12, 13, 14].

The studies related to *IG* and *SG* in parallel operation mode [15, 16, 17, 18, 19, 20, 21, 22] show a newer knowledge border, that show the results and behavior of this kind of generation topology, including simulation results for an *MHPP*. Overall, one of the main contributions of this work is the use of actual control loops in practical experiments involving *SG* and *IG* in parallel operation and their optimization and adjustments [4, 23]. These control loops and experiments were mounted in the Laboratory of research development of electrical didactic laboratory of Federal University of Itajubá.

This work is focused on the operational behavior of two different kinds of generators operating in parallel mode, their roles within the electric system, their controls and characteristics of each generator, some transients and their effects, as well as studies and implementations of control alternatives in order to avoid the undesirable transient effects.

As basis of the target study, this work presents various experiments accomplished in this cited laboratory, which are related to *DCM (Direct Current Motor)* and their speed and current control loops. The *DCM* are used as primary machine to *SG* and *IG*. Then, it is essential that *DCM<sub>SG</sub>* has speed control loop and *DCM<sub>IG</sub>* can be driven manually due to their functional characteristics.

The *SG* requires synchronous speed rotation in its shaft regardless to load transients or any other disturbs on going in the electric system. On the contrary, the *SG* does not operate. The *SG* shaft speed is sensible to disturbs and any other changes on going in the electric system. It means that, speed regulation or speed control loop is required for the *SG* primary machine or *DCM<sub>SG</sub>* in order to keep its shaft synchronous speed.

On the other hand, *IG* has different functional characteristics that make it able to supply active power taking only into account its shaft speed be higher than synchronous speed. As *IG* shaft speed increases above the synchronous speed, the supply power is higher. The other characteristic is that, regardless of load changes or disturbs on going in the electric system, its shaft speed and power supply is the same for the *IG*. Then, these functional characteristics do not require any *IG* shaft automatic speed regulation. It means that its primary machine or *DCM<sub>IG</sub>*, in the case of these experiments studied in

this work, do not need automatic speed regulation or any speed control loop. From these cited reasons, the  $DCM_{IG}$  speed is not automatically controlled, differently of the  $DCM_{SG}$  speed that is automatically controlled. The control of  $DCM_{IG}$  speed is done manually by open control loop. The two methods used to change the  $DCM_{IG}$  speed are: the  $V_{aDCMIG}$  (*DCM armature voltage coupled with IG*) method and the field flux or  $I_{fDCMIG}$  (*Field current of direct current motor coupled with induction generator*) method.

In general, the generators used in the industry are driven by gas or steam turbines. One of the main characteristics of these turbines is the availability of keeping the machine shaft speed even in adverse conditions as in load transients. The cited turbine speed variation does not overcome ten percent independently of electrical system transients, [24]. Then, in order to do the  $DCM_{IG}$  closer to turbine behavior in the experiment implemented in laboratory, two methods of  $DCM_{IG}$  speed elevation were studied in order to rise the  $PIG$  (*Induction generator power*) supplied. First, the machine field flux is decreased and, the second, the  $DCM_{IG}$  armature voltage  $V_{aDCMIG}$  is increased. The increase of  $V_{aDCMIG}$  has better results than decrease of machine field flux.

In the experiments of this work, the wound rotor machine was used instead of squirrel cage rotor machine. The wound rotor machine can have an extra advantage that is the high startup torque due to resistors that can be connected at the induction machine rotor circuit [25]. In this way, the induction machine can start directly as motor and it can turn a  $IG$  by increase of speed up to this speed exceeds the synchronous speed as detailed in chapter 1. Besides of likely higher wound rotor machine cost, the unique technical considerable difference between the two machines considered in this work is that the wound rotor machine can have a higher startup torque and then it permits an additional option of synchronism between the  $IG$  and  $SG$ , that is the method of direct startup as mentioned in chapter 1. Then, except that mentioned difference, the results obtained with wound rotor machine can be also considered identical to results with squirrel cage rotor machine. Considering that explanation, the results of this work are valid to as wound rotor machine as squirrel cage rotor machine.

One of the potential motivations for this study is to identify a potential alternative capable of optimizing the main electric system currently adopted in oil platforms or  $FPSO$  (*Floating production storage and offloading*), making them cheaper, simpler, lighter and more efficient. The oil platforms use traditionally three of four  $SG$ s in parallel operation mode.

Analysis of a generator's power balance and its interactions is presented in this work in various operational scenarios. The results enable comparisons of the two methods of induction generator speed control, by either the autotransformer method or the field flux variation method. The former results in a larger range of speed and power from the induction generator. Therefore, it has more desirable features for actual operational

conditions.

In order to provide a wider analysis of generators' behavior under transient conditions, this work shows the results of experiments and analysis about various operational scenarios, some of which have challenging conditions to be overcome, that is the case of increasing frequency which will be detailed in this work. The last chapter shows two ways to control the system frequency when a frequency increase appears as a result of some specific operative condition as detailed in this work.

As consequences of the frequency increase cited in chapter 2, this work also shows two other experiments and analysis of how to control the frequency increase in an electric system. The first is the insertion of a *BL (Ballast load)* control system and the second, the insertion of an energy regenerating system *ERS (Energy regeneration system)* to enable the system to return regenerative energy to the grid. Then, the former is more appropriate for an isolated electric system and the latter is a didactic alternative and serves as basis of comparison and evaluation. Both experiments achieved the expected results and enabled system frequency control while the system voltage were kept.

In addition, this work shows six appendixes to the chapters 1, 2 and 3, as follow: the appendix A says about filter and regulator project for direct current motor, DC motor, appendix B says about analogical control Board for current and voltage control loops, appendix C says about voltage regulators project to synchronous machine, appendix D shows studies about a practical case using *DCM* controls for driving in four quadrants [26], appendix E calculates the induction motor parameters used in one of the experiments of chapter 1 and appendix F shows the Matlab codes used to solve the equation system indicated in chapters 1 and 2. Thus, these additional studies provide the basis of knowledge [27] for the analysis of synchronous and induction generators in parallel operation mode in an isolated electric system. These generators feed either a resistive load or a resistive load and an induction motor together.

# 1 Analysis of Synchronous and Induction Generators in Parallel Operation Mode in an Isolated Electric System

## 1.1 Introduction

This work is composed of analysis over an electric system that includes an induction motor, a resistive load and an autotransformer connected to a diodes bridge to feed the  $DCM_{IG}$  armature, what permits to increase manually the  $IG$  electric power limits, [28], [29] with better efficiency. Therefore, this work shows the  $IG$  supplying more active power than it was shown in [28] and an induction motor inserted in experiment what enables an wider analysis of the system behavior.

Two methods of  $DCM_{IG}$  speed elevation were studied in order to rise the  $PIG$  supplied. First, the machine field flux is decreased and, the second, the  $DCM_{IG}$  armature voltage  $V_{aDCMIG}$  is increased. The increase of  $V_{aDCMIG}$  has better results than decrease of machine field flux.

This work presents results that show additional remarkable characteristics by operation in parallel mode between one  $SG$  and one  $IG$ . Some characteristics, such as reduced weight and size, easier maintenance, and shorter manufacturing and delivery time are more associated with induction generators and are relevant to  $MHPP$  as demonstrated in general introduction and they could also be to oil platforms. Besides, it has absence of dc supply for excitation and better transient performances [20], [8].

In this chapter, the three different methods of  $IG$  connection into the electric system were studied as follow: (i) direct startup as a motor and rising the induction motor speed up to induction motor turns  $IG$ , (ii) synchronism of self-excited  $IG$  with the electric system and (iii) adjustment of  $IG$  speed at synchronous speed and  $IG$  connection into the system;

In the experiments of this chapter, the wound rotor machine was used instead of squirrel cage rotor machine. The wound rotor machine can have an extra advantage that is the high startup torque due to resistors that can be connected at the induction machine rotor circuit [25]. For this work, the unique differential advantage by the use of this kind of machine is making the first method of  $IG$  connection into the electric system available, (i) direct startup as a motor and rising the induction motor speed up to it turns  $IG$ .

A potential application of this cited generator topology is in  $MHPP$ , which has

already been partially tested as cited in general introduction.

Therefore, the study target is concerned for analysing various aspects of generators topology and operating, involving an induction generator in parallel with a synchronous generator for application in an isolated electric system, and establish the operational viability aspects, advantages and challenges.

## 1.2 Isolated Electric System

The isolated electric system was mounted in laboratory as Figure 1.1 and sized as shown in sections 1.5 and 1.6. The automatic controls of the system consist of a voltage control loop and a speed control loop as shown in Figure 1.1. In this chapter, the three electric system settings are shown in Figure 1.10, Figure 1.11 and Figure 1.12 will be studied. The data plates of the principal equipment are shown from Table 1.3 to Table 1.6.

The electronic control boards shown in Figure 1.1 are indicated in 1.1. The parametrizations used in both are shown in Table 1.2, except for the references of voltage and speed for each one of control loops which are respectively 65.5 and 65.2 as shown in Table 1.2.

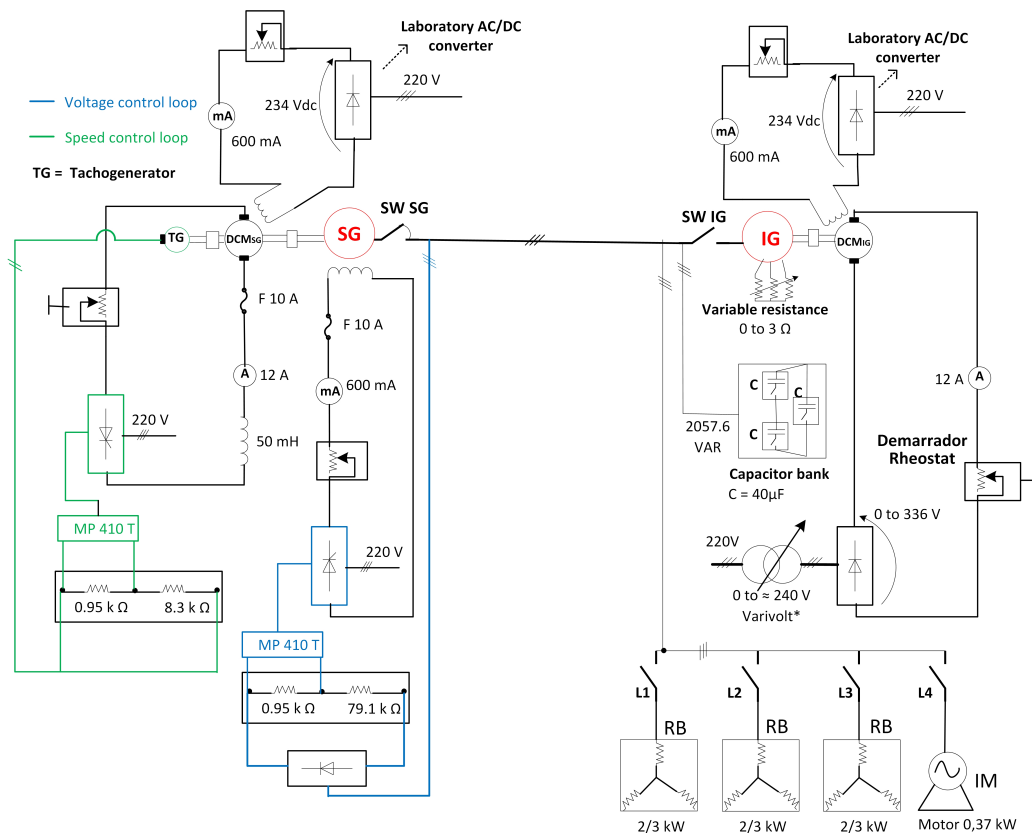


Figure 1.1 – Electric Scheme

\*Note: The maximum varivolt output voltage shown in Figures 1.1, 1.11, 1.12 and 2.3 is a bit upper than 240 V.

### 1.3 Digital Control Board

The digital control board MP 410T aims to control the three-phase thyristor bridge firing angle. After the correct connections between the thyristors bridge and the electronic board, the MP 410T board can be set as shown in Table 1.1, so that all firing gates from thyristors bridge operate properly. It means that all firing angle turn itself controlled by the MP 410T electronic board. All reference signals from control loops are connected to MP 410T such as speed and field voltage references. This kind of electronic board are inserted in the circuit as part of speed and voltage control loops as shown in Figures 1.2 and 1.3. The correct connections and electronic board configuration are necessary to proper operation of MP 410T. The terminal descriptions of electronic boards MP 410T follow in the Table 1.1.

Note: The analogical control board will be used in the experiments described in chapter 3 and it will be detailed in appendix A.

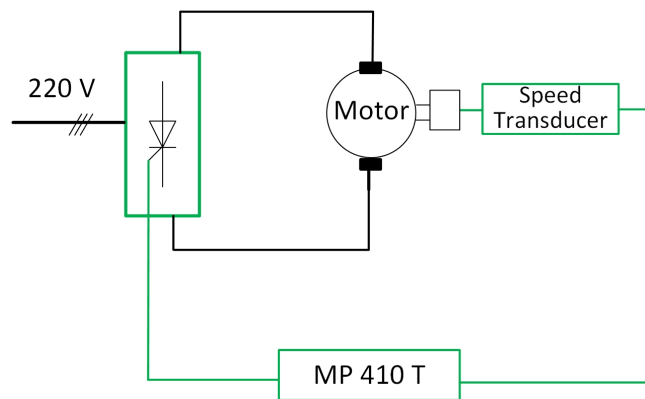


Figure 1.2 – MP 410T in Speed Control loop

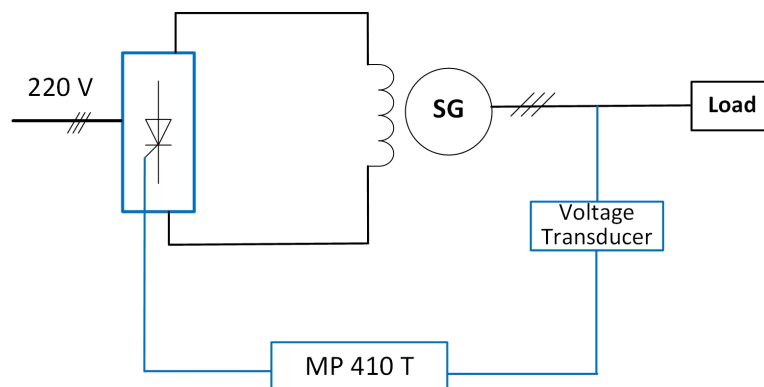


Figure 1.3 – MP 410T in Voltage Control loop

Table 1.1 – Terminal Descriptions of SEMIKRON MP410T Electronic Board

Terminal	Name	Description
1	10	10 V voltage source to 3 and 5 outputs
2	VCC	5 V voltage source to 3 and 5 outputs
3	LIM	Limitation display
4	F_RAMP	Running display
5	INHI_OUT	Inhibition display
6	GND	Earth to 3 and 5 outputs
7	INHI_IN	inhibitory input
8	TERMO	Thermostate input
9	START_STOP	Start stop input
10	POT_KEY	The reference value is put in through by potentiometer or keyboard. Once set STARTER the energy save mode is disabled.
11	GND	Earth to 1 and 4 inputs
12	RS485+	Positive terminal to RS485 bar
13	RS485-	Negative terminal o RS485 bar
14	5	Voltage source of 5 V
15	-5	Voltage source of -5 V
16	CON_IN_TEMPE	Temperature sensor input
17	AGND	Temperature sensor earth
18	IN_0_5	Reference value input to the range 0V to 5V
19	IN_0_10	Reference value input to the range 0V to 10V
20	AGND	Reference value earth
21	INTI+	Pos <sup>1</sup> terminal of analog <sup>2</sup> differential current input
22	INTI-	Neg <sup>3</sup> terminal of analog. differential current input
23	START_STOP	START_STOP input
24	AGND	Voltage analogical input Earth
25	L1	Analogical current input for current transformer
26	L2	Analogical current input for current transformer
27	COM	Common to current analog. input to current transformer

<sup>1</sup> positive

<sup>2</sup> negative

<sup>3</sup> analogical

### 1.3.1 MP410T Electronic Board Parameterization

The MP 410T board was parametrized as shown in Table 1.2.

Table 1.2 – Electronic Control Board Configuration

Memory Position	Name ( abbreviation at display)	Value (unit)
0	Local Remote (LR)	0(0=local)
1	Adres (Ad)	1(default)
2	Configuration 9 (CF)	1B6C
3	Phase Difference (DY)	0°
4	Auto Manual (Am)	0(0=auto)
5	Peak (P)	66.0%
6	Time Peak (PS)	0s(default)
7	Pedestal (D)	66.0%
8	Ramp Up (RU)	0s
9	Ramp Down (Rd)	0s
10	Lim Intensity (CL)	0
11	Max Intensity (Cm)	0
12	AL Temperature (HL)	0=non(default)
13	Com Temperature (Hm)	0
14	AL_ Failure Phase (PA)	0=non(default)
15	AL_ Failure Thiristor (SA)	0=non(default)
16	Energy Saving (ES)	0
17	Regulation Mode (Rm)	1(1=voltage)
18	Linear (LI)	1(1=yes)
19	Reference Value (E)	65.2%(speed) or 65.5%(voltage)
20	KP_ Intensity (PC)	non used
21	TI_ Intensity (IC)	non used
22	TD_ Intensity (DC)	non used
23	LIM_ Voltage (VL)	1(1=yes)
24	MAX_ Voltage (Vm)	99.9%
25	KP_ Voltage (PV)	0.10 both controller
26	TI_ Voltage (IV)	0.04s both controller
27	TD_ Voltage (DV)	0.0
28	Input_ Intensity (CI)	0 (default)

### 1.3.2 Voltage and Speed Control Loops

The Figure 1.4 and Figure 1.5 show the close control loop used to control the *SG* voltage and frequency via electronic boards which are shown in Figure 1.10, Figure 1.11 and Figure 1.12.

Note: In Appendix C, an analogical control board was used in the generator field voltage control loop instead of digital control board as this one described here. In addition, that regulator was parametrized by symmetrical optimization technique. The information contained in Appendix C adds this issue.

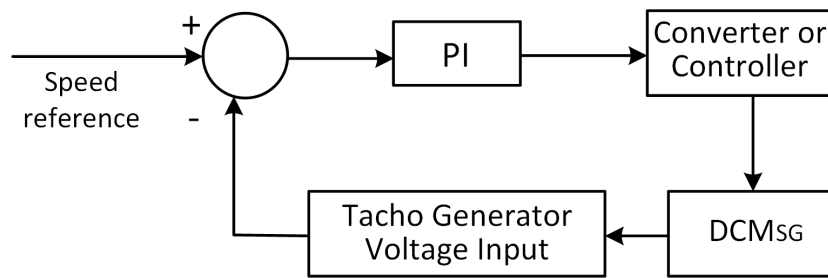


Figure 1.4 – Speed Control Loop

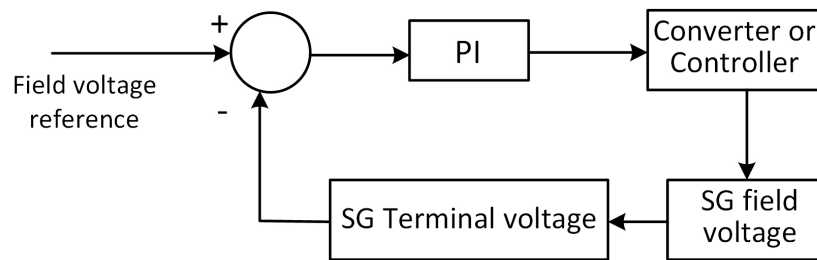


Figure 1.5 – Field Voltage Control Loop

The figure 1.6 shows the configuration 1B6C used for the two thyristor-converter bridges which were used in these control loops.

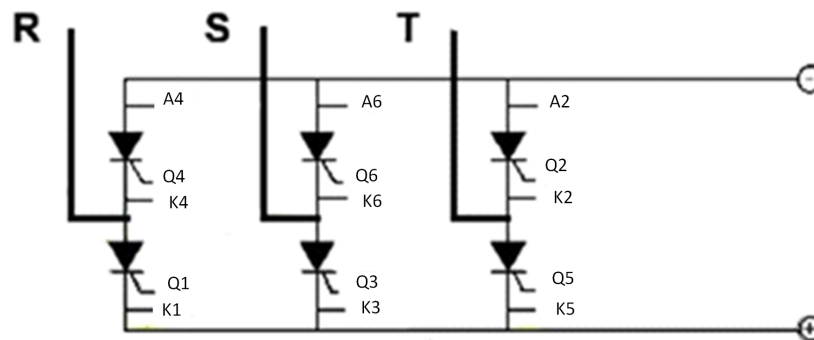


Figure 1.6 – Converter Configuration used for control Operational Scenarios

### 1.3.3 Arrangement

The figure 1.7 shows the connections arrangement of MP410T electronic board.

Figure 1.8 show the circuit boards with the respective working point or reference points defined during parameterization for the speed control loop, 65.2, and the voltage control loop, 65.5.

The master and slave behavior between generators were realized, considering that the *SG* is the master for the system frequency and voltage. The *IG* is master for the active power and the slave for the system frequency and voltage. *SG* determines the frequency and voltage, while *IG* controls active power supplied to load.

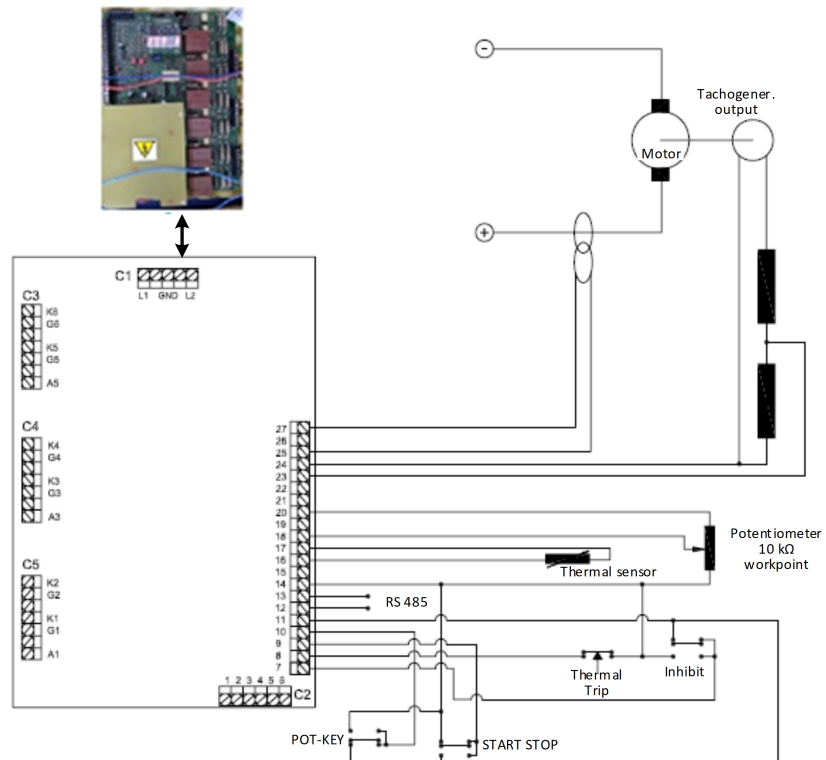
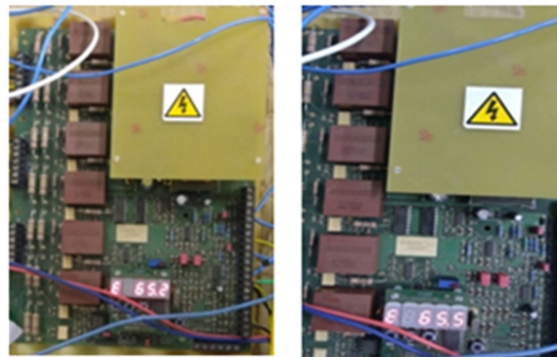


Figure 1.7 – Electronic Board MP410T and Connections



(a) Speed Control Loop (b) Voltage Control Loop

Figure 1.8 – Circuit boards MP410T used to implement the Control Loops

## 1.4 Data Plate

In tables 1.3 to 1.8 are shown the main equipment’s data plates. The tables 1.7 and 1.8 show the loads data plates that are used in the experiments along this work.

Table 1.3 –  $DCM_{IG}$  Data plate

Direct Current Motor IG				
220 V	7.72 A	1500 rpm	1.7kW	600 mA

Table 1.4 –  $DCM_{SG}$  Data plate

Direct Current Motor SG				
220 V	9.1 A	2.0 kW	1800 rpm	600 mA

Table 1.5 –  $IG$  Data plate

Induction Generator (IG)					
220 V	7.5 A	1.86 kW	1410 rpm	0.8 PF	50 Hz

Table 1.6 –  $SG$  Data plate

Synchronous Generator (SG)					
230 V	5,0 A	2,0 kVA	1800 rpm	0,8 PF	60 Hz
Vfield: 220 V			Ifieldmax: 600 mA		

Table 1.7 – Load Data plate

Resistive Load		
Load 1 (kW)	Load 2 (kW)	Load 3 (kW)
2/3	2/3	2/3

Table 1.8 – Load Data plate

Induction Motor			
0.37 kW	1715 rpm	Cos $\phi$ 0.71	60 Hz

## 1.5 Equations - Part I

Follow the main equations:

- Direct Current Motor

$$n = \frac{E}{k \times \phi} \quad (1.1)$$

$$n = \frac{U_a - (\sum R_a) \times I_a}{k \times \phi} \quad (1.2)$$

$$C_{conjugate} = k \times \phi \times I_a \quad (1.3)$$

- Synchronous Generator

$$\dot{E} = \dot{U}_a + (R_a + jX_s) \times \dot{I}_a \quad (1.4)$$

- Induction Generator

$$S_{slip}\% = \frac{n_s - n_{IG}}{n_s} \times 100 \quad (1.5)$$

$$n_s = \frac{120 \times f_{SG}}{P_{\text{number of poles}}} \quad (1.6)$$

### 1.5.1 Capacitor Bank Sizing

As informed at the *IG* data plate,  $\cos\phi=0.8$ , then  $\sin\phi=0.6$ . The reactive power is calculated to attend the reactive demand of the Induction Machine [30].

$$Q = \sqrt{3} \times V \times I \times \sin\Phi \therefore Q = \sqrt{3} \times 220 \times 7.5 \times 0.6 = 1714.7 \text{ Var} \quad (1.7)$$

$$Q_{\text{generated}} = F_c \times Q \therefore F_c = 1.2 \quad (1.8)$$

For the induction machine coupled to a resistive load, it is necessary a reactive power generation to be approximately 2057.6 VAR as demonstrated below. The 50 Hz was used in the calculus because it is one of the frequencies used in the experiments and it is that which results in the biggest capacitance.

$$Q_{\text{generated}} = 1.2 \times 1714.7 = 2057.6 \text{ Var} \quad (1.9)$$

$$Q_{\text{generated}} = \frac{3 \times V^2}{X_c} \quad (1.10)$$

$$X_c = \frac{3 \times 220^2}{2057.6} = 70.6 \Omega \quad (1.11)$$

$$C = \frac{1}{2 \times \pi \times f \times X_c} = \frac{1}{2 \times \pi \times 50 \times X_c} \quad (1.12)$$

$$= \frac{1}{2 \times \pi \times 50 \times 70.6} \cong 40\mu\text{F per phase} \quad (1.13)$$

### 1.5.2 Resistive Divider Sizing

- Field Control Loop Resistive Divider as shown in Figures 1.10, 1.11 and 1.12.

$$(1k\Omega + r_1) - > 300 V_{(\text{outputvoltage})} \quad (1.14)$$

$$r_2(1k\Omega) - > 4V_{(\text{MP410T-VOLTAGE-LIMIT})} \quad (1.15)$$

$$r_1 = 74 \text{ k}\Omega \text{ and } r_2 = 1 \text{ k}\Omega \quad (1.16)$$

- Resistor Power Sizing:

$$P_{power} = \frac{300^2}{(75 \times 10^3)} = 1.2 \text{ W} \quad (1.17)$$

- The resistors that were selected based on the sized resistor, were:

$$r_1 = 79.1 \text{ k}\Omega \text{ } r_2 = 947 \text{ }\Omega \quad (1.18)$$

- Speed Control Loop Resistive Divisor as shown in Figure 1.10, 1.11 and 1.12.

$$(1 \text{ k}\Omega + r_1) - > 36 \text{ V}_{(\text{tachogenerator output voltage})} \quad (1.19)$$

$$r_2(1 \text{ k}\Omega) - > 4 \text{ V}_{(\text{MPT410 voltage limit})} \quad (1.20)$$

$$r_1 = 8 \text{ k}\Omega \text{ and } r_2 = 1 \text{ k}\Omega \quad (1.21)$$

- Resistor Power sizing:

$$P_{power} = \frac{36^2}{(9 \times 10^3)} = 1.14 \text{ W} \quad (1.22)$$

- Based on the sized resistor, the following resistors were chosen:

$$r_1 = 8.3 \text{ k}\Omega \text{ and } r_2 = 947 \text{ }\Omega \quad (1.23)$$

## 1.6 Equations - Part II

Follow the system of equations to calculate the power and efficiencies shown in Tables 1.9, 1.10 and 1.11 for each generator and entire group of machines.

$$I_{SG}^2 = Iw_{SG}^2 + I_{c1}^2 \quad (1.24)$$

$$I_{IG}^2 = Iw_{IG}^2 + I_{c2}^2 \quad (1.25)$$

$$I_c = I_{c1} + I_{c2} \quad (1.26)$$

$$Iw_{loadR} = Iw_{SG} + Iw_{IG} \quad (1.27)$$

$$I_c - Idw_{MT} = Ic_1 + Ic_2 \quad (1.28)$$

$$Iw_{loadR} + Iw_{MT} = Iw_{SG} + Iw_{IG} \quad (1.29)$$

The  $I_{SG}$  (*Synchronous generator current*),  $I_{IG}$  (*Induction generator current*),  $I_C$  (*Capacitor current*) and  $Iw_{loadR}$  (*R Load Active current*) are measured values and these are shown in Tables 1.9, 1.10 and 1.11. The  $Idw_{MT}$  (*Induction motor reactive current*) and  $Iw_{MT}$  (*Induction motor active current*) are values calculated as appendix E and these are also shown in Table 1.11.

Then, the system has 4 four variables and 4-four equations. Then, for each scenario, the four variables,  $Iw_{SG}$  (*Synchronous generator active current*),  $Ic_1$  (*Capacitor current 1*),  $Iw_{IG}$  (*Induction generator active current*) and  $Ic_2$  (*Capacitor current 2*), were calculated by Matlab software as appendix F and these are shown in Table 1.9, 1.10 and 1.11.

The entire group efficiency  $\eta_{group}$  (*Group efficiency*) and the efficiency of each subgroup,  $\eta_{SG}$  (*SG efficiency*) and  $\eta_{IG}$  (*IG efficiency*), were calculated based on  $PIG$ ,  $PSG$  (*Synchronous generator power*),  $P_{DCMSG}$  (*Power of direct current motor coupled with synchronous generator*), and  $P_{DCMIG}$  (*Power of direct current motor coupled with induction generator*), as follows.

$$P_{SG} = \sqrt{3} \times V_{SG} \times Iw_{SG} \quad (1.30)$$

$$P_{IG} = \sqrt{3} \times V_{IG} \times Iw_{IG} \quad (1.31)$$

$$P_{DCMSG} = Va_{DCMSG} \times Ia_{DCMSG} \quad (1.32)$$

$$P_{DCMIG} = Va_{DCMIG} \times Ia_{DCMIG} \quad (1.33)$$

$$\eta_{group\%} = \frac{P_{SG} + P_{IG}}{P_{DCMSG} + P_{DCMIG}} \times 100 \quad (1.34)$$

$$\eta_{SG\%} = \frac{P_{SG}}{P_{DCMSG}} \times 100 \quad (1.35)$$

$$\eta_{IG\%} = \frac{P_{IG}}{P_{DCMIG}} \times 100 \quad (1.36)$$

## 1.7 Equations - Part III

The equations and calculus used to determine the *IM* (*Induction motor*) parameters and *IM* equivalent circuit such as the primary and secondary impedances and also the primary and secondary currents are showed in Appendix E.

## 1.8 The Experiment and Schemes

The experiment was mounted in the laboratory as shown in Figure 1.9 a) and b). The detailed circuit is shown in Figures 1.10, 1.11 and 1.12.

Figure 1.9 b) shows another experiment view, including the taco generator and its connections. The detailed circuits are shown in Figures 1.10, 1.11 and 1.12.

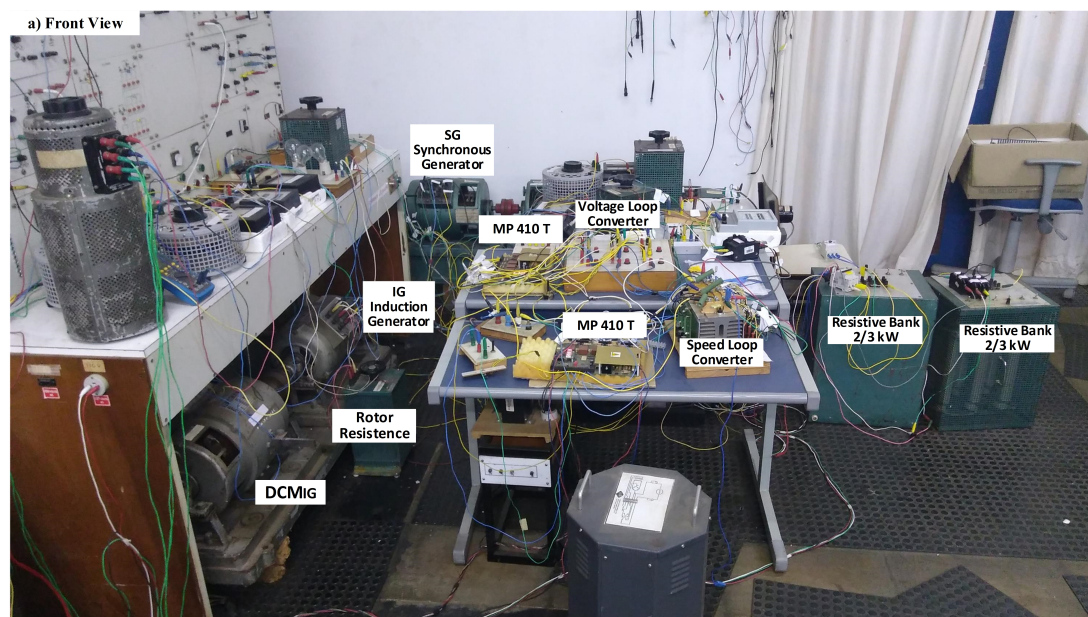
The power from *IG*, *PIG*, was limited because the  $I_{fDCMIG}$  reached the maximum value in accordance with  $DCM_{IG}$  current specifications. This limited speed from  $DCM_{IG}$  was a challenge because the low speed resulted in low contribution from *PIG*. Then, it was necessary to elevate the  $DCM_{IG}$  speed,  $n_{IG}$  (*Induction generator speed*).

Then, the methodology consists of implementing the comparative analysis of the power and efficiencies, starting with an analysis between the *PIG* from the scheme in Figure 1.10 and *PIG* from the schemes in Figure 1.11 and Figure 1.12, covering the scenarios shown in Table 1.11, Table 1.9 and Table 1.10 respectively.

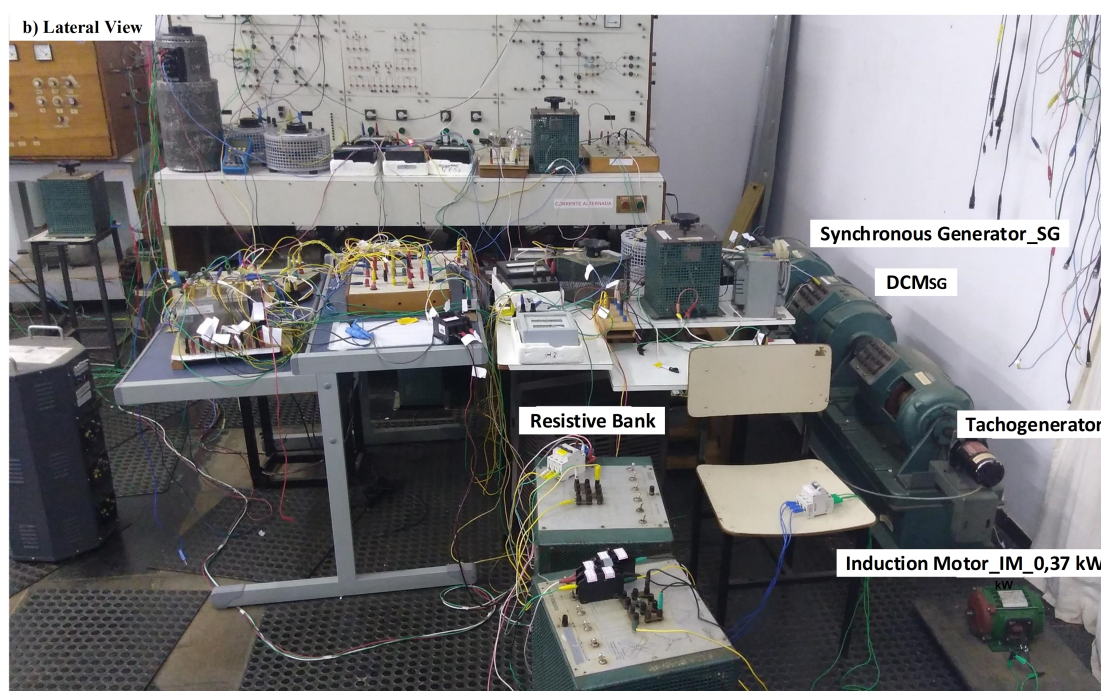
Finally, a comparative efficiency analysis was conducted for two subgroups, one composed of *IG* and a  $DCM_{IG}$  and the other composed of *SG* and a  $DCM_{SG}$ . These analyses are done over the scenarios related to the scheme in Figure 1.10, the scheme in Figure 1.11 and the scheme in Figure 1.12.

Thus, the increase of  $DCM_{IG}$  speed results in increase of the *PIG* contributions and *IG* subgroup efficiencies such as they are shown in the results.

The Figure 1.11 and Figure 1.12 show the schemes implemented in the laboratory to overcome the challenge related to limitation of *IG* speed [28] such as bringing the experiment closer to actual conditions and taking into advantages of *IG* power capacity. It was used as an autotransformer connected to a diodes bridge to vary the voltage applied on the  $DCM_{IG}$  armature circuit and obtain a higher speed and *PIG*.



(a) Front View



(b) Lateral View

Figure 1.9 – Laboratory assembly in the laboratory of research development of electrical didactic laboratory of Federal University of Itajubá

### 1.8.1 Methods of IG Connection into the Electric System

This work studies three different methods of *IG* connection into the electric system such as: (i) direct startup as a motor and rising the *IG* speed, (ii) synchronism of self-excited *IG* with the electric system and (iii) adjustment of *IG* speed at synchronous speed and connect it into the system [28].

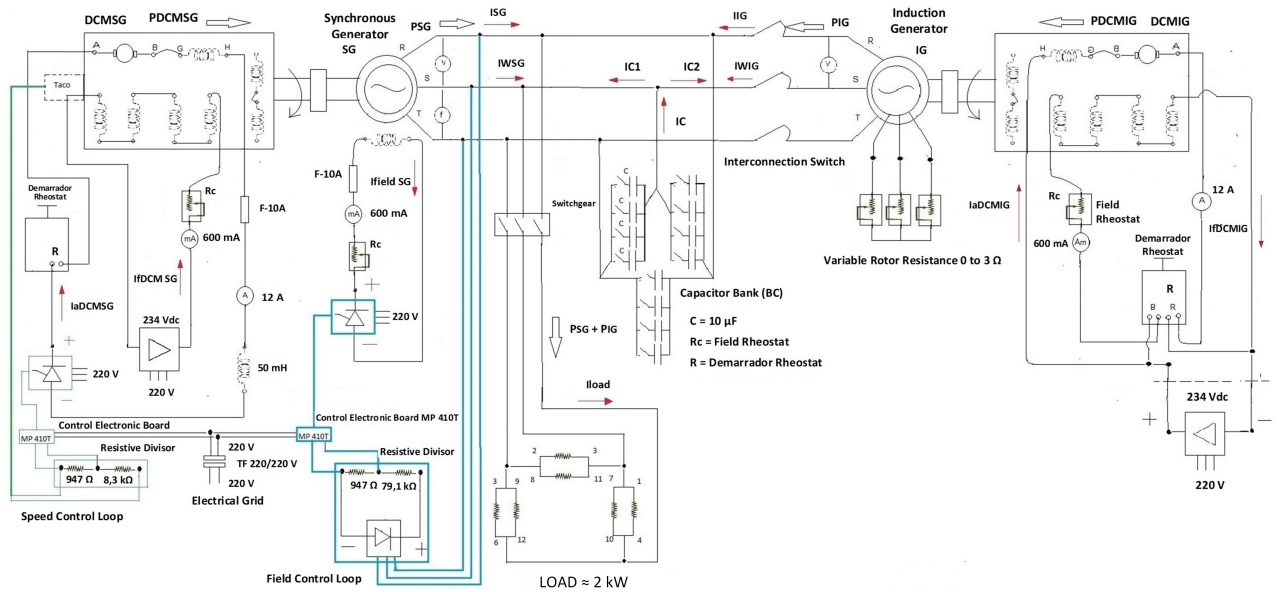


Figure 1.10 – Synchronous and Induction Generators in parallel Operation Mode with Steady Armature Voltage for  $DCM_{IG}$  (Variation of  $DCM_{IG}$  field flux by field Rheostat)

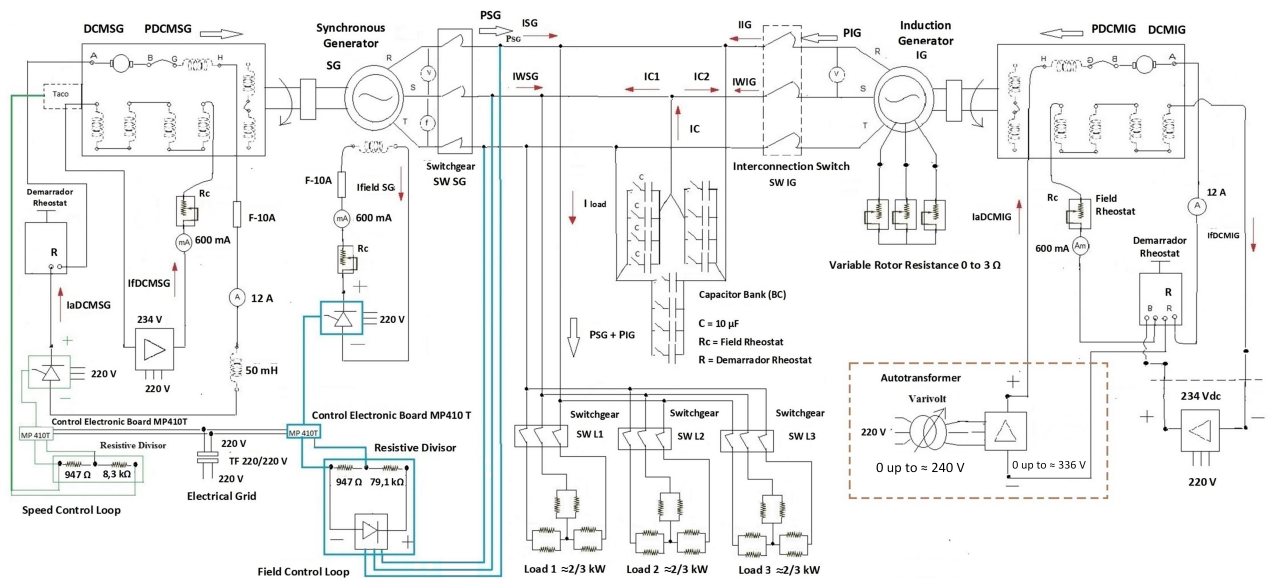


Figure 1.11 – Synchronous and Induction Generators in Parallel Operation mode with Variable Armature Voltage for  $DCM_{IG}$  ( $DCM_{IG}$  Steady field flux)

- Direct Startup

For this option, the induction machine is started up directly as motor. In this case, rotor resistance was necessary to reach the required torque for start up as shown in Figure 1.12. After start up, the  $IG$  speed is raised by manual command up to it overcomes the synchronous speed. In this moment, the induction motor becomes the  $IG$ .

- Synchronism of self-excited  $IG$  with the Electric System

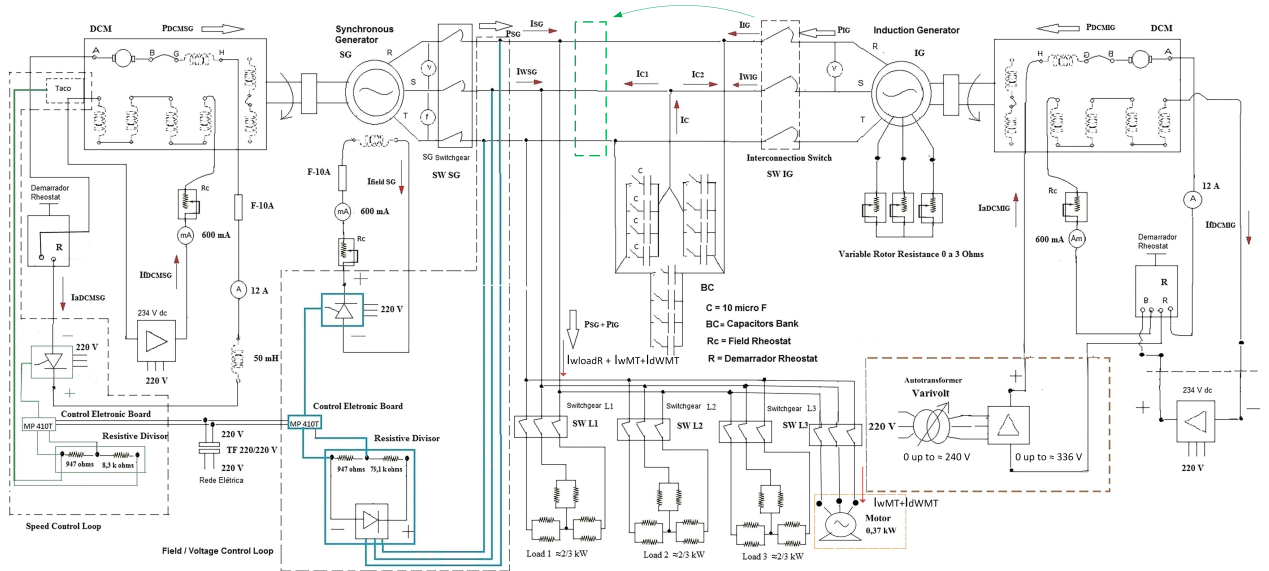


Figure 1.12 – Synchronous and Induction Generators in Parallel Operation mode with Variable Armature Voltage for  $DCM_{IG}$  and an Induction Motor as Load ( $DCM_{IG}$  Steady field flux)

For this option, the induction generator is auto-excited and the capacitor bank is required and connected in the  $IG$  directly as well as the interconnection switch,  $SW$  (Interconnection switch), is placed beside of capacitor bank as shown in Figure 1.12 by green arrow. For this option, it was used a synchroscope for closing the interconnection switch.

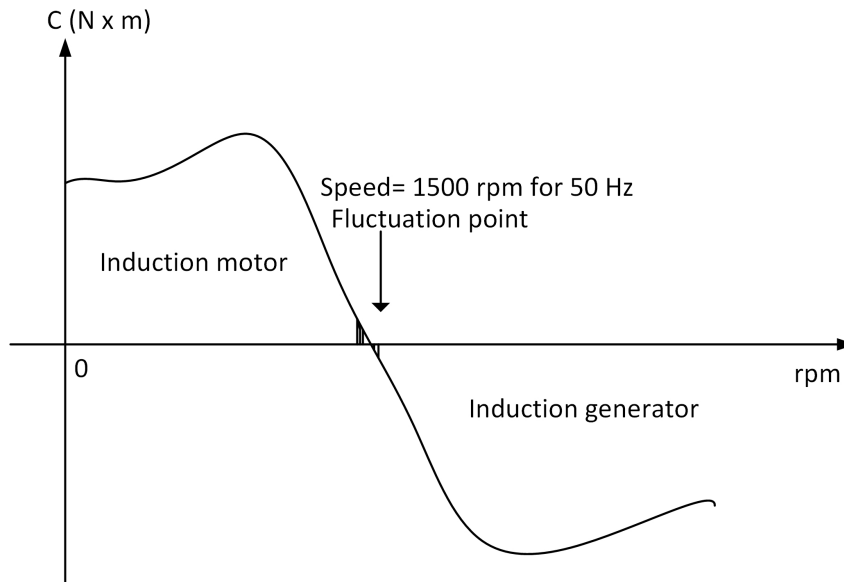


Figure 1.13 – Conjugate vs rpm - Induction Motor and Generator

- Adjustment of IG Speed at Synchronous Speed

Considering the scheme shown in the Figure 1.12, the  $IG$  speed was led to close and below the fluctuation point, it means some value close to point where the torque or

conjugate is null as it can be seen in Figure 1.13 below. The fluctuation point is at the intersection with rpm axis. The interconnection switch shown in Figure 1.12 was closed when the Induction motor speed is in the fluctuation area. From this  $IG$  speed, the  $DCM_{IG}$  speed should be raised up to overcome the fluctuation point to become the induction motor an induction generator.

For this option, the  $IG$  is not auto-excited, the reactive is obtained from the grid.

## 1.8.2 Experiment Data

The experimental data obtained in the laboratory are shown in Table 1.11, Table 1.9 and Table 1.10. The Table 1.9 shows the data obtained from the scheme in Figure 1.11, Table 1.10 shows the data obtained from the scheme in Figure 1.12 and Table 1.11 shows the data obtained from the scheme in Figure 1.10. The unique difference between Figure 1.11 and Figure 1.12 is the presence of  $IM$  in Figure 1.12 as additional load. The difference between the Figure 1.10 and the others is basically the presence of an autotransformer in the  $DCM_{IG}$  field circuit and an additional motor as load in Figure 1.12.

The autotransformer is responsible for applying a voltage range directly on the  $DCM_{IG}$  armature to obtain a larger speed range of the  $DCM_{IG}$  and to push more power to the  $IG$ , keeping the  $DCM_{IG}$  parameters into the rated values. Hence, the elevation of  $IG$  speed and power depend on  $DCM_{IG}$  armature voltage,  $V_{aDCMIG}$ . It means that the  $DCM_{IG}$  speed control method used for the scheme in Figure 1.10 is different of the method used in the Figures 1.11 and 1.12. The  $IG$  speed of scheme shown in Figure 1.10 depends on just the  $DCM_{IG}$  field flux because  $V_{aDCMIG}$  is steady. The  $DCM_{IG}$  field flux is adjusted manually and  $V_{aDCMIG}$  as well.

In summary, the Table 1.11 shows the data obtained from the scheme shown in Figure 1.10 that has the 234  $V_{dc}$  steady source; Table 1.9 and Table 1.10 show respectively the data obtained from the schemes shown in Figure 1.11 and Figure 1.12. These schemes have an autotransformer and a diodes bridge as substitute of the 234  $V_{dc}$  steady source shown in Figure 1.10. The difference between Figures 1.11 and 1.12 is the induction motor that is inserted as additional load in Figure 1.12.

Then, from these three schemes, the data obtained from each operation scenario into a same scheme are analyzed and compared among themselves. The generators performances between different schemes are analyzed and compared considering the similar operational scenarios under tests and the respective schemes' differences. The results are shown along this work.

Note: The abbreviations *n.a.* (*Not applicable*) shown in scenarios 1, 1C and 1B of tables 1.9, 1.10 and 1.11 refer to values not used in  $SG$  and  $IG$  power graphics. The cited graphics are based on the scenarios 2 onwards.

Table 1.9 – Operational scenarios in controlled mode and three resistors bank as load

	Scenario 1B	Scenario 2B	Scenario 3B	Scenario 4B	Scenario 5B	Scenario 6B	Scenario 7B	Scenario 8B	Scenario 9B
SG and IG in parallel and no load	SG and IG in parallel and load in <sup>1</sup>	SG and IG in parallel and load in <sup>1</sup>	SG and IG in parallel and load in <sup>1</sup>	SG and IG in parallel and load in <sup>1</sup>	SG and IG in parallel and load in <sup>1</sup>	SG and IG in parallel and load in <sup>1</sup>	SG and IG in parallel and load in <sup>1</sup>	SG alone and load in <sup>1</sup>	SG alone and no load <sup>2</sup>
Results	Scenario 1B	Scenario 2B	Scenario 3B	Scenario 4B	Scenario 5B	Scenario 6B	Scenario 7B	Scenario 8B	Scenario 9B
$V_{SG}$ (V)	220.0	220.0	220.0	220.0	220.0	220.0	220.0	220.0	220.0
$f_{SG}$ (Hz)	60	60	60	60	60	60	60.0	60.0	60.0
$I_{fieldSG}$ (mA)	190	320	300	300	320	350	370	340	100
$V_{aDCMSG}$ (V)	272.9	275.0	276.2	276.8	277.5	278.0	280.7	278.5	270.0
$I_{aDCMSG}$ (A)	2.0	2.5	3.8	4.7	6.2	7.4	9.5	10.6	2.0
$I_{fDCMSG}$ (mA)	510.0	530.0	520.0	520.0	515.0	510.0	515.0	515.0	515.0
$V_{IG}$ (V)	220.0	220.0	220.0	220.0	220.0	220.0	220.0	n.a.	n.a.
$f_{IG}$ (Hz)	60	60	60	60	60	60	60	n.a.	n.a.
$n_{IG}$ (rpm)	1793	1896	1878	1857	1848	1821	1794	n.a.	n.a.
$V_{aDCMIG}$ (V)	291.3	323.6	316.7	308.3	301.3	293.0	284.1	n.a.	n.a.
$I_{aDCMIG}$ (A)	0.5	8.0	7.0	6.0	4.7	3.5	2.0	n.a.	n.a.
$I_{fDCMIG}$ (mA)	330.0	330.0	330.0	330.0	330.0	330.0	330.0	n.a.	n.a.
$I_{WloadR}$ (A)	0.0	5.0	5.0	5.0	5.0	5.0	5.0	5.0	0.0
$I_{IG}$ (A)	2.4	5.8	5.1	4.4	3.7	2.9	2.4	0.0	0.0
$I_{SG}$ (A)	2.9	1.5	2.0	2.8	3.6	4.5	5.6	7.4	4.0
$IC$ (A)	5.4	5.4	5.4	5.4	5.4	5.4	5.4	5.4	4.0
$I_{WSG}$ (A)	0.0	1.05	1.48	1.97	2.47	3.32	4.65	5.03	0.0
$IC1$ (A)	2.9	1.13	1.60	2.13	2.66	3.03	3.13	5.40	4.0
$IC2$ (A)	2.4	4.26	3.80	3.27	2.74	2.37	2.27	0.0	0.0
$I_{WIG}$ (A)	0.0	3.95	3.51	3.03	2.53	1.68	0.35	0.0	0.0
$PSG$ (W)	0.0	400.5	565.5	750.0	939.8	1266.6	1770.1	1915.8	0.0
$PIG$ (W)	0.0	1504.8	1335.8	1155.3	965.5	638.67	135.17	0.0	0.0
$P_{DCMSG}$ (W)	545.8	687.5	1049.6	1301.0	1665.0	2057.2	2666.7	2962.7	543.4
$P_{DCMIG}$ (W)	145.7	2588.8	2216.9	1849.8	1416.1	1025.5	568.2	0	0.0
$\eta_{GROUP}$ (%)	0.0	58.15	58.33	60.47	61.84	61.80	58.89	64.66	0.0
$\eta_{SG}$ (%)	0.0	58.25	53.88	57.65	56.44	61.57	66.38	64.66	0.0
$\eta_{IG}$ (%)	0.0	58.12	60.43	62.45	68.18	62.28	23.79	n.a.	n.a.

<sup>1</sup> 40  $\mu$ F / phase

<sup>2</sup> 30  $\mu$ F/phase

Table 1.10 – Operational scenarios in controlled mode and three resistors bank and induction motor as load

	Scenario 1C SG and IG in parallel and no R load. <sup>1</sup>	Scenario 2C SG and IG in parallel mode and load in. <sup>1</sup>	Scenario 3C SG and IG in parallel mode and load in. <sup>1</sup>	Scenario 4C SG and IG in parallel mode and load in. <sup>1</sup>	Scenario 5C SG and IG in parallel mode and load in. <sup>1</sup>	Scenario 6C SG and IG in parallel mode and load in. <sup>1</sup>	Scenario 7C SG and IG in parallel mode and load in. <sup>1</sup>	Scenario 8C SG alone and load in. <sup>1</sup>	Scenario 9C SG alone and no load. <sup>2</sup>
Results	220.0	220.0	220.0	220.0	220.0	220.0	220.0	220	220.0
$V_{SG}$ (V)	60	60	60	60	60	60	60	60	60
$f_{SG}$ (Hz)	170	420	410	400	400	430	475	390	100
$I_{fieldSG}$ (mA)	278.9	277.0	277.5	280.5	281.0	281.1	282.9	279.2	271.7
$V_{aDCMSG}$ (V)	2.0	2.9	4.0	5.0	6.3	7.6	9.6	10.5	2.0
$I_{aDCMSG}$ (A)	530.0	530.0	530.0	530.0	530.0	520.0	520.0	520.0	515.0
$V_{IG}$ (V)	220.0	220.0	220.0	220.0	220.0	220.0	220.0	0.0	n.a.
$f_{IG}$ (Hz)	60	60	60	60	60	60	60	0.0	n.a.
$n_{IG}$ (rpm)	1803	1893	1868	1857	1843	1821	1793	0.0	n.a.
$V_{aDCMIG}$ (V)	288.9	330.0	318.0	310.0	302.3	295.2	285.9	0.0	n.a.
$I_{aDCMIG}$ (A)	1.0	8.0	7.0	6.0	4.7	3.5	2.0	0.0	n.a.
$I_{fDCMIG}$ (mA)	330.0	330.0	330.0	330.0	330.0	330.0	330.0	0.0	n.a.
$I_{wloadR}$ (A)	0.0	5.0	5.0	5.0	5.0	5.0	5.0	5.0	0.0
$I_{wMT}$ (A)	0.2	0.2	0.2	0.2	0.2	0.2	0.2	0.2	0.0
$I_{dwMT}$ (A)	1.23	1.23	1.23	1.23	1.23	1.23	1.23	1.23	0.0
$I_{IG}$ (A)	2.3	6.0	5.0	4.4	3.6	2.9	2.3	0.0	0.0
$I_{SG}$ (A)	2.8	0.7	1.6	2.3	3.3	4.1	5.3	6.7	4.0
$IC$ (A)	5.4	5.4	5.4	5.4	5.4	5.4	5.4	5.4	4.0
$I_{WSG}$ (A)	1.55	0.65	1.29	1.99	3.04	3.74	4.95	5.23	0.0
$IC1$ (A)	2.33	0.28	1.03	1.17	1.29	1.66	1.88	4.2	4.0
$IC2$ (A)	1.85	3.91	3.14	3.00	2.88	2.51	2.29	0.0	0.0
$I_{wIG}$ (A)	-1.37	4.55	3.91	3.22	2.16	1.45	0.25	0.0	0.0
$PSG$ (W)	591.2	247.97	490.34	753.80	1156.9	1428.7	1887.8	1991.7	0.0
$PIG$ (W)	-521.1	1733.5	1491.1	1227.7	824.52	552.74	93.68	0.0	0.0
$P_{DCMSG}$ (W)	557.8	803.30	1110.0	1402.5	1770.3	2136.4	2715.8	2931.6	624.5
$P_{DCMIG}$ (W)	288.9	2640.0	2226.0	1860.0	1420.8	1033.2	571.8	0.0	0.0
$\eta_{GROUP}$ (%)	0.0	57.55	59.40	60.73	62.09	62.52	60.27	67.59	0.0
$\eta_{SG}$ (%)	0.0	30.87	44.17	53.75	65.35	66.88	69.51	67.59	0.0
$\eta_{IG}$ (%)	0.0	65.66	66.99	66.00	58.03	53.50	16.38	0.0	n.a.

<sup>1</sup> 40  $\mu$  F / phase

<sup>2</sup> 30  $\mu$ F/phase

Table 1.11 – Operational scenarios in controlled mode and a resistor bank

	Scenario 1	Scenario 2	Scenario 3	Scenario 4	Scenario 5	Scenario 6	Scenario 7	Scenario 8
	SG and IG in parallel mode and no load. <sup>1</sup>	SG and IG in parallel mode $I_{IG} = 5.3 \text{ A}$ . <sup>1</sup>	SG and IG in parallel mode $I_{IG} = 4.5 \text{ A}$ . <sup>1</sup>	SG and IG in parallel mode $I_{IG} = 4.0 \text{ A}$ . <sup>1</sup>	SG and IG in parallel mode $I_{IG} = 3.5 \text{ A}$ . <sup>1</sup>	SG and IG in parallel mode $I_{IG} = 3.2 \text{ A}$ . <sup>1</sup>	SG alone and load in <sup>1</sup>	SG alone and no load <sup>1</sup>
Results	Scenario 1	Scenario 2	Scenario 3	Scenario 4	Scenario 5	Scenario 6	Scenario 7	Scenario 8
$V_{SG}$ (V)	228.0	228.0	228.0	228.0	228.0	228.0	228.0	228.0
$f_{SG}$ (Hz)	55	55	55	55	55	55	55	55
$I_{fieldSG}$ (mA)	380	510	500	500	510	580	400	100
$V_{aDCMSG}$ (V)	232.1	234.0	237.6	239.5	239.4	243.0	239.0	232.4
$I_{aDCMSG}$ (A)	0.0	4.7	6.8	8.0	9.5	12.0	12.0	2.0
$I_{fDCMSG}$ (mA)	450	420	450	440	440	440	420	420
$V_{IG}$ (V)	228.0	228.0	228.0	228.0	228.0	228.0	0.0	0.0
$f_{IG}$ (Hz)	55	55	55	55	55	55	0.0	0.0
$n_{IG}$ (rpm)	1679	1720	1707	1693	1683	1663	0	0
$V_{aDCMIG}$ (V)	232.1	225.4	226.8	228.2	229.8	231.2	0.0	0.0
$I_{aDCMIG}$ (A)	0.0	9.8	7.4	6.0	4.2	2.3	0.0	0.0
$I_{fDCMIG}$ (mA)	250	100	200	220	245	310	0.0	0.0
$I_{load}$ (A)	0.0	5.0	5.0	5.0	5.0	5.0	5.0	0.0
$I_{IG}$ (A)	3.5	5.3	4.5	4.0	3.5	3.2	0.0	0.0
$I_{SG}$ (A)	1.9	2.2	3.0	3.5	4.3	5.3	7.3	5.2
$IC$ (A)	5.2	5.2	5.2	5.2	5.2	5.2	5.2	5.2
$I_{WSG}$ (A)	n.a.	2.05	2.68	3.06	3.86	4.91	5.00	0.00
$IC1$ (A)	n.a.	0.79	1.34	1.70	1.89	2.00	5.20	5.2
$IC2$ (A)	n.a.	4.40	3.86	3.50	3.31	3.20	0.00	0.00
$I_{WIG}$ (A)	n.a.	2.94	2.32	1.94	1.14	0.10	0.00	0.00
$PSG$ (W)	n.a.	809.9	1059.5	1207.5	1525.3	1938.1	1998.4	0.0
$PIG$ (W)	n.a.	1.164.7	915.04	767.07	449.27	36.48	0.00	0.0
$P_{DCMSG}$ (W)	n.a.	1099.8	1615.7	1916.0	2274.3	2916.0	2868.0	464.8
$P_{DCMIG}$ (W)	n.a.	2208.9	1678.3	1369.2	965.2	531.8	0.0	0.0
$\eta_{GROUP}$ (%)	n.a.	59.68	59.94	60.10	60.95	57.27	68.85	n.a.
$\eta_{SG}$ (%)	n.a.	73.64	65.58	63.02	67.07	66.46	68.85	n.a.
$\eta_{IG}$ (%)	n.a.	52.73	54.52	56.02	46.55	6.9	n.a.	n.a.

<sup>1</sup> 40  $\mu$  F / phase

## 1.9 Results

The results show graphs, analysis of configurations presented in Figure 1.10, Figure 1.11 and Figure 1.12 and analysis of contribution from each generator for each arrangement of load, that is either a resistive bank or three resistive banks added with an induction motor.

All graphs obtained from scheme in Figure 1.10 [28] are based on a system frequency of 55 Hz. For the others experiments from Figures 1.11 and Figure 1.12, the system frequency is 60 Hz. Then, the synchronous speed for the experiments from Figure 1.10 is 1650 rpm, see the equation 1.6, and 1800 rpm for the other experiments.

In order to highlight the contributions from autotransformer and Diodes Bridge to the experiments, it will be presented some analysis based on graphs and experiment results.

Figure 1.14 shows that the *PIG* was limited to 1164 W in scenario 2 from Table 1.11 because the over current of  $I_{aDCMIG}$  (*Direct current motor induction generator armature current*) 9.8 A, that is a value greater than the rated  $I_{aDCMIG}$  of 7.72 A as Table 1.3. To overcome this barrier, an autotransformer and a diodes bridge were installed to widen the voltage range applied over the  $DCMIG$  armature, as shown in Figure 1.11 and Figure 1.12. The armature voltage range with the autotransformer and diodes bridge can vary from 0 to 336  $V_{dc}$  (*Direct current voltage*). This range is bigger than the previous case with  $V_{aDCMIG}$  of 234  $V_{dc}$ . As the  $DCMIG$  speed,  $n_{IG}$ , is directly proportional to  $V_{aDCMIG}$ , 1.2, the  $n_{IG}$  is elevated proportionally with the  $V_{aDCMIG}$ , as shown in scenarios 2 to 8 from Table 1.9 and Table 1.10. Then, in this latter method,  $I_{aDCMIG}$  variation depends on the load conjugate variation only, whereas the  $DCMIG$  flux,  $\phi$ , remains constant as 1.3.

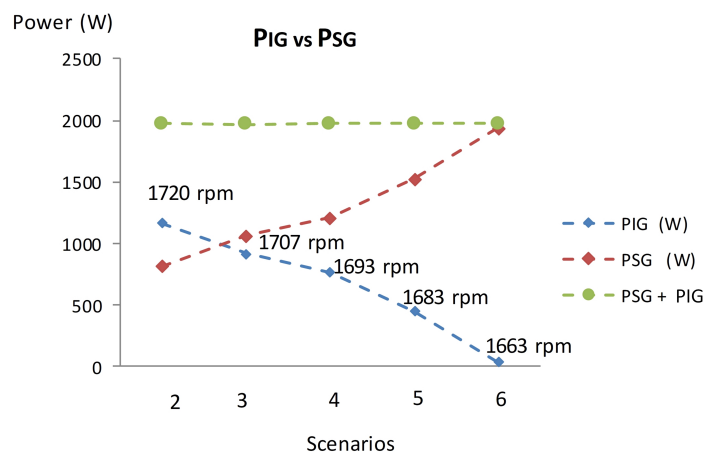


Figure 1.14 – *PIG* vs *PSG* with  $DCMIG$  Field Variation and  $V_{aDCMIG}$  kept Constant

Figure 1.15 and Figure 1.16 shows that the power range supplied from *IG*, *PIG*,

through the autotransformer method, is greater than  $PIG$  of  $234 V_{dc}$  steady source method. Consequently, the  $PSG$  supplied from this autotransformer method is lower than the  $PSG$  supplied from  $234 V_{dc}$  steady source method. Both methods feed the entire resistive load as shown in Figure 1.14 and Figure 1.15, and the resistive and motor load as shown in Figure 1.16.

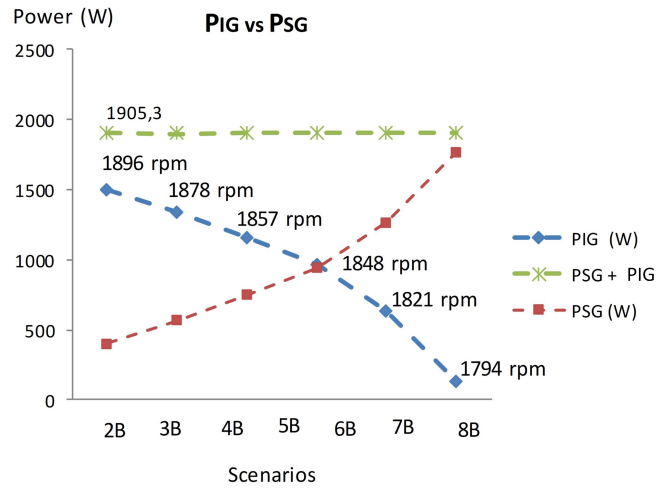


Figure 1.15 –  $PIG$  vs  $PSG$  with  $V_{aDCMIG}$  Variation and Field flux kept Constant (Only resistive load)

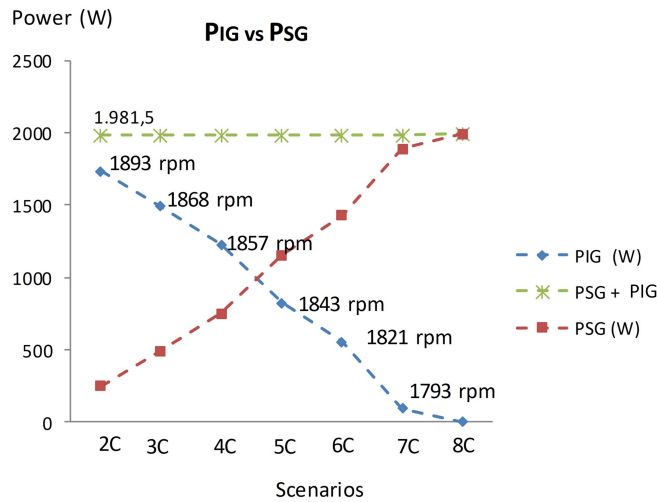


Figure 1.16 –  $PIG$  vs  $PSG$  with  $V_{aDCMIG}$  Variation and Field Flux kept Constant (Resistive load & IM)

In Figure 1.17, Figure 1.19 and Figure 1.20 show the comparative results of  $IG$  and  $SG$  primary machine output power,  $P_{DCMIG}$  vs  $P_{DCMSG}$ . These performances are similar to  $PIG$  and  $PSG$  performances shown in Figure 1.14, Figure 1.15 and Figure 1.16. The  $P_{DCMIG}$  in Figure 1.17 elevates because a field flux decreases and  $V_{aDCMIG}$  kept constant.

The  $P_{DCMIG}$  in Figure 1.19 and Figure 1.20 elevates because of the  $V_{aDCMIG}$  increases, which is manually adjusted by the autotransformer shown in Figure 1.11 and Figure 1.12.

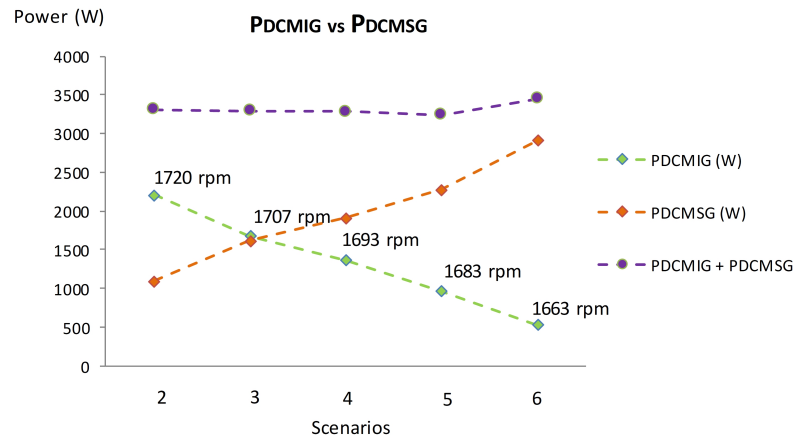


Figure 1.17 –  $P_{DCMIG}$  vs  $P_{DCMSG}$  with  $DCM_{IG}$  Field Flux Variation and  $V_{aDCMIG}$  Kept Constant

Figure 1.18 shows that the system voltage and frequency are kept the same even with the resistive load is connected or disconnected, showing a good regulation control in system voltage and frequency [28]. This voltage and frequency performance was realized in all scenarios of load transients with the loads shown in Tables 1.9, 1.10 and 1.11.

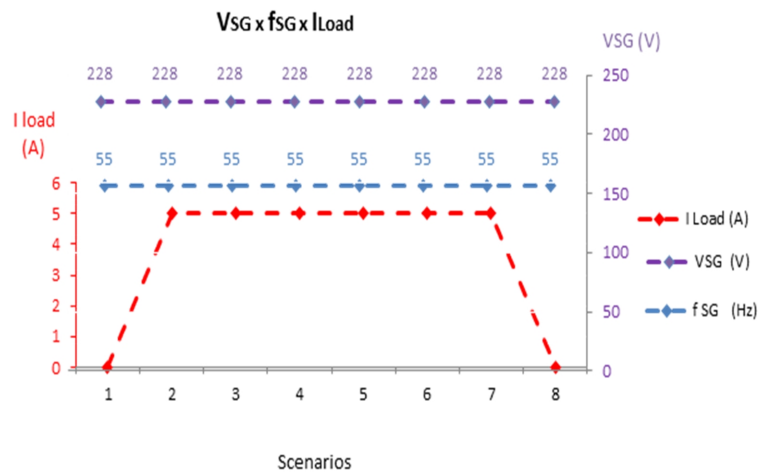


Figure 1.18 –  $V_{SG} \times f_{SG} \times I_{load}$

The efficiency results shown in Figure 1.21, Figure 1.22 and Figure 1.23 show each subgroup efficiency for each scenario and load conditions. Each subgroup efficiency is resulted from relation between a generator and its respective *DCM* (*Direct current motor*) as shown in equations 1.32 and 1.33.

In summary, the following scenarios are shown: scenarios 2 to 7 (without autotransformer), scenarios 2B to 8B (with autotransformer and just resistive load) and scenarios 2C to 8C (with autotransformer, resistive load and induction motor).

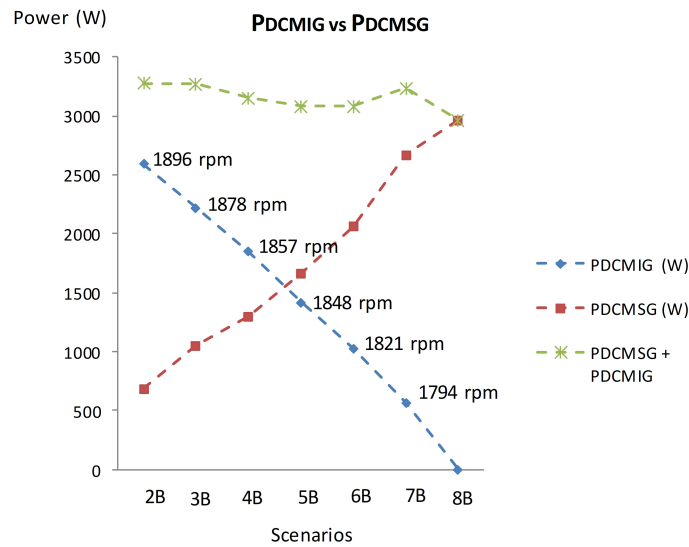


Figure 1.19 –  $P_{DCMIG}$  vs  $P_{DCMSG}$  with  $V_{aDCMIG}$  Variation and Field Flux Kept Constant (Only resistive load)

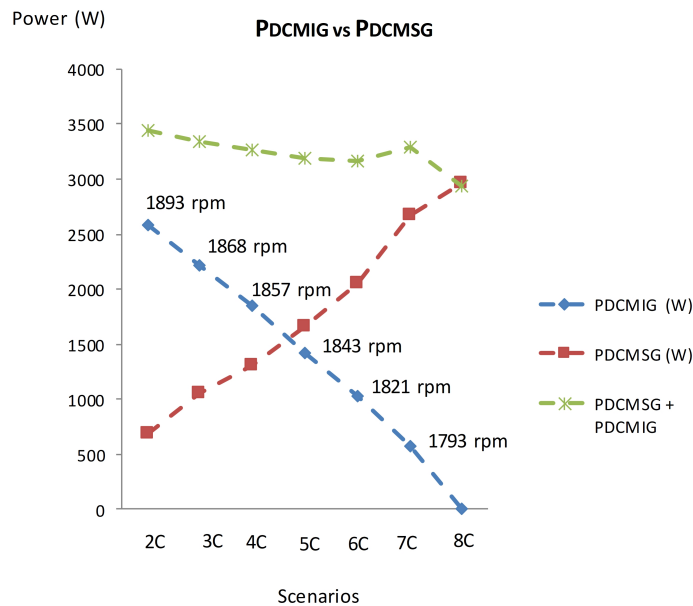


Figure 1.20 –  $P_{DCMIG}$  vs  $P_{DCMSG}$  with  $V_{aDCMIG}$  Variation and Field Flux Kept Constant (Resistive load plus IM)

The  $IG$  subgroup efficiencies shown in Figure 1.22 and Figure 1.23 are bigger than  $IG$  subgroup efficiencies from similar scenarios in Figure 1.21. Moreover, the elevation of power from  $IG$  due to the increase of  $DCM_{IG}$  speed,  $n_{IG}$ , is more representative of actual conditions. For instance, the turbines can assume whatever speed required from generators in offshore platforms.

The reduction of losses resulted in better  $IG$  subgroup efficiency as shown in Figure

1.22 and Figure 1.23. Figure 1.21 shows the machine's efficiencies when the  $I_{fDCMIG}$  or field flux decreases to elevate the speed. The efficiency improves when the  $V_{aDCMIG}$  elevation method is applied as shown in Figure 1.22 and Figure 1.23.

The efficiencies shown in Figure 1.22 and Figure 1.23 are higher than the efficiency presented in Figure 1.21, that indicates the  $DCM_{IG}$  speed range is more restricted [28].

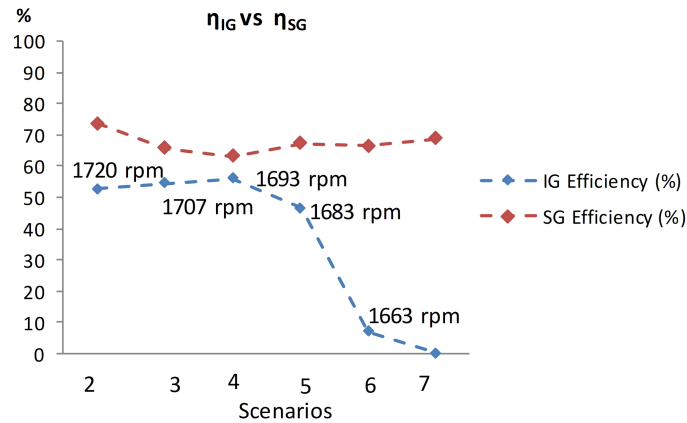


Figure 1.21 –  $n_{IG}$  vs  $n_{SG}$  with  $DCM_{IG}$  Field Flux Variation and  $V_{aDCMIG}$  Kept Constant

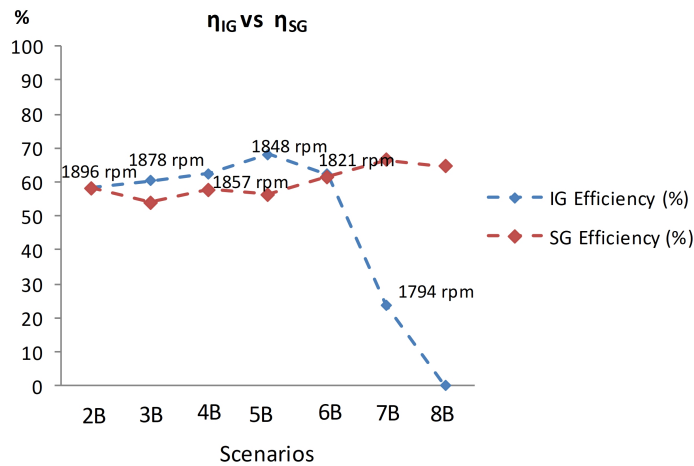


Figure 1.22 –  $n_{IG}$  vs  $n_{SG}$  with  $V_{aDCMIG}$  Variation and Field Flux kept Constant (Only resistive load)

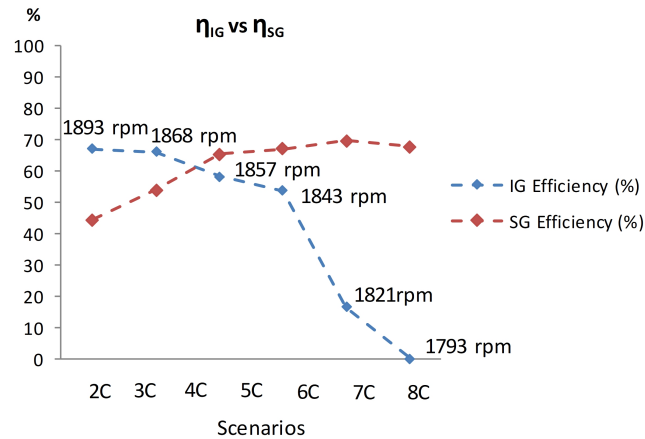


Figure 1.23 –  $n_{IG}$  vs  $n_{SG}$  with  $V_{a_{DCMIG}}$  Variation and Field Flux kept Constant (Resistive load plus IM)

## 1.10 Conclusion

The cited electric system shows voltage and frequency regulation for each scenario transition as demonstrated in Figure 1.18, tables 1.9, 1.10 and 1.11 and respective analysis.

$SG$  presented the master behavior for the system frequency and voltage as [28].  $IG$  did the master behaviour for the active power and slave behavior for the system frequency and voltage.  $SG$  controls the system voltage and frequency and  $IG$  follows the voltage and frequency defined by  $SG$ . The  $IG$  establishes the active power supplied to the system and the  $SG$  complements the rest of active power and reactive power required. The  $PSG$  depends on the  $IG$  shaft speed imposed by  $DCM_{IG}$ . The  $PSG$  and the system voltage and frequency are controlled respectively by field voltage and speed control loops presented in Figure 1.10, Figure 1.11 and Figure 1.12.

It was realized a bigger  $PIG$  range in the scenarios shown in Table 1.9 and in Table 1.10, than the scenarios shown in Table 1.11 due to  $V_{a_{DCMIG}}$  elevation method. The  $PSG$  fulfilled the load power automatically from the  $PIG$  manually adjusted by autotransformer.

The field flux variation method of  $DCM_{IG}$ , [28], does not result in  $P_{DCMIG}$  increase, whereas the  $V_{a_{DCMIG}}$  elevation method results in increase of  $P_{DCMIG}$ ,  $PIG$  and  $IG$  subgroup efficiency. The increase of  $PIG$  is resulted from  $IG$  speed increase,  $n_{IG}$ , that was obtained by elevation of  $V_{a_{DCMIG}}$  as shown in Figure 1.15, Figure 1.16, Figure 1.19 and Figure 1.20.

The use of  $V_{a_{DCMIG}}$  method, instead of  $V_{dc}$  steady source or flux ( $I_{f_{DCMIG}}$ ) reduction method, enables to reach the  $I_{a_{DCMIG}}$  limit of 8.0 A and 1893 rpm of  $DCM_{IG}$  shaft speed. It is higher than the  $DCM_{IG}$  speed from  $V_{dc}$  steady source, see Figure 1.21.

The efficiencies from the  $V_{a_{DCMIG}}$  elevation method were greater than those from

the scheme with  $V_{dc}$  steady source [28], as shown in Figure 1.22 and Figure 1.23.  $V_{aDCMIG}$  elevation method does not have the additional current losses that the  $V_{dc}$  steady source method have.

The  $V_{dc}$  steady source method consist of reduction of field flux  $\phi$ ,  $I_{fDCMIG}$ , and increasing of  $I_{aDCMIG}$  as 1.3. Then, the  $IG$  speed,  $n_{IG}$ , is increased as equation 1.2.

The main losses for the  $V_{dc}$  steady source method are related to higher  $I_{aDCMIG}$  elevation,  $P_{(w)} = Ra * I_{aDCMIG}^2$ , than the  $I_{aDCMIG}$  elevation caused by  $V_{aDCMIG}$  elevation method. Then, by use of  $V_{dc}$  steady source method, the  $I_{aDCMIG}$  is elevated due to reduction of  $I_{fDCMIG}$ . The higher  $I_{aDCMIG}$  is, the higher losses are. Then, as the losses of  $V_{aDCMIG}$  elevation method are lower, the efficiencies are higher.

As shown in power performance graphs related to  $V_{aDCMIG}$  elevation method, Figure 1.15, Figure 1.16, Figure 1.19 and Figure 1.20, the  $P_{IG}$  and  $P_{DCMIG}$  are more representative of actual operation conditions.

All of the followings three different methods of  $IG$  connection into the electric system were implemented and the results were satisfactory: (i) direct startup as a motor and rising the induction motor speed up to it turns  $IG$ , (ii) synchronism of self-excited  $IG$  with the electric system and (iii) adjustment of  $IG$  speed at synchronous speed and  $IG$  connection into the system;

## 2 Load and Generation Transients of Synchronous and Induction Generators in Parallel Operation Mode in an Isolated Electric System

### 2.1 Introduction

This section presents an analysis of load and generation transients in an isolated electric system with a parallel connection of one synchronous generator and induction generator, each one coupled to a dc machine or primary machine as well as to a capacitor bank. A resistive load is connected to the system. Changes in the load were intentionally provoked. Then, each generator was removed, one at a time, and reconnected. The results are shown here and the respective curves are analysed.

The results show the performance and responses of the cited system regarded to either transients from load changes or from partial generation withdrawal [31].

Differently of scheme shown in Figure 1.10, the schemes shown in Figures 1.11, 1.12, 3.4 and in the Figure 2.3 have an autotransformer for actuating directly in  $V_{aDCMIG}$  and permitting a greater speed elevation range and, then, a higher power contribution from the *IG*. Furthermore, the current resistor bank consists of three individual bank resistors connected in parallel, as presented in Figure 2.3 [28].

In the experiments of this chapter, the first method of *IG* connection into the electric system was implemented, (i) direct startup as a motor and rising the induction motor speed up to it turns *IG*. As the wound rotor machine was used instead of squirrel cage rotor machine, that first method can be used to the experiments described here. As already informed in general introduction and in chapter 1, the wound rotor machine can have an extra advantage that is the high startup torque due to resistors that can be connected at the induction machine rotor circuit [25].

One of the motivations of this study is related to the main advantages of induction generators over synchronous generators which are: brushless construction with squirrel-cage rotor, reduced size and weight, absence of DC supply for excitation, reduced maintenance cost, and better transient performance [8]. As previously informed, the use of wound rotor machine does not make invalid the results obtained in this work for squirrel cage rotor machine because the functioning of both machines is the same, except the

possibility of increasing of wound rotor startup torque.

Then, this work presents conclusions about the system performance regarding to load and generation transients.

## 2.2 Isolated Electric System

The isolated electric system was sized as shown by the equations and data given in the following paragraphs. The equations are based on calculations in [32].

The system automatism consists of a voltage control loop and a speed control loop. Both are inserted in the *SG* scheme, as shown in Figure 2.3.

The data plates of the principal equipment are shown in Tables 1.3 to Table 1.7.

The speed and voltage control loops are presented respectively in Figure 2.4 and Figure 2.5.

The voltage and speed electronic control boards are shown in Figure 2.1, Figure 2.2 and Figure 2.3.

The parametrization used in both electronic control boards was shown in chapter 1, except de reference values of voltage and speed. The references of voltage and speed control loops are respectively 68.6 and 60.1.

## 2.3 Data Plate

The equipment's data plates are shown in tables 1.3 to 1.8. The tables 1.7 and 1.8 show the loads data plates that are used in the experiments along this work.

## 2.4 Equation - Part I

The equations of this section are the same used in the previous chapter as shown in section 1.5.

## 2.5 Equation - Part II

The equations 2.1, 2.2, 2.3 and 2.4 together with the equations 2.5 to 2.11 were employed to calculate the power and efficiencies as shown in the Table 2.1 for each generator and the entire group of machines.

$$I_{SG}^2 = Iw_{SG}^2 + I_{c1}^2 \quad (2.1)$$

$$I_{IG}^2 = Iw_{IG}^2 + I_{c2}^2 \quad (2.2)$$

$$I_c = I_{c1} + I_{c2} \quad (2.3)$$

$$I_{load} = Iw_{loadR} = Iw_{SG} + Iw_{IG} \quad (2.4)$$

As  $I_{SG}$ ,  $I_{IG}$ ,  $I_c$  and  $Iw_{loadR}$  are measured values, (see Table 2.1), the system has four variables and four equations. Then, for each scenario, the four variables  $Iw_{SG}$ ,  $I_{c1}$ ,  $Iw_{IG}$  and  $I_{c2}$  were calculated by Matlab software as appendix F and result in values shown in Table 2.1.

The entire group efficiency and the efficiency of each subgroup were calculated based on  $PIG$ ,  $PSG$ ,  $P_{DCMSG}$ , and  $P_{DCMIG}$  as follows.

$$PSG = \sqrt{3} \times V_{SG} \times Iw_{SG} \quad (2.5)$$

$$PIG = \sqrt{3} \times V_{IG} \times Iw_{IG} \quad (2.6)$$

$$P_{DCMSG} = Va_{DCMSG} \times Ia_{DCMSG} \quad (2.7)$$

$$P_{DCMIG} = Va_{DCMIG} \times Ia_{DCMIG} \quad (2.8)$$

$$\eta_{group\%} = \frac{P_{SG} + P_{IG}}{P_{DCMSG} + P_{DCMIG}} \times 100 \quad (2.9)$$

$$\eta_{SG\%} = \frac{P_{SG}}{P_{DCMSG}} \times 100 \quad (2.10)$$

$$\eta_{IG\%} = \frac{P_{IG}}{P_{DCMIG}} \times 100 \quad (2.11)$$

## 2.6 Experiment and Schemes

The experiment was mounted in the laboratory as shown in Figures 2.1, 2.2 and 2.3.

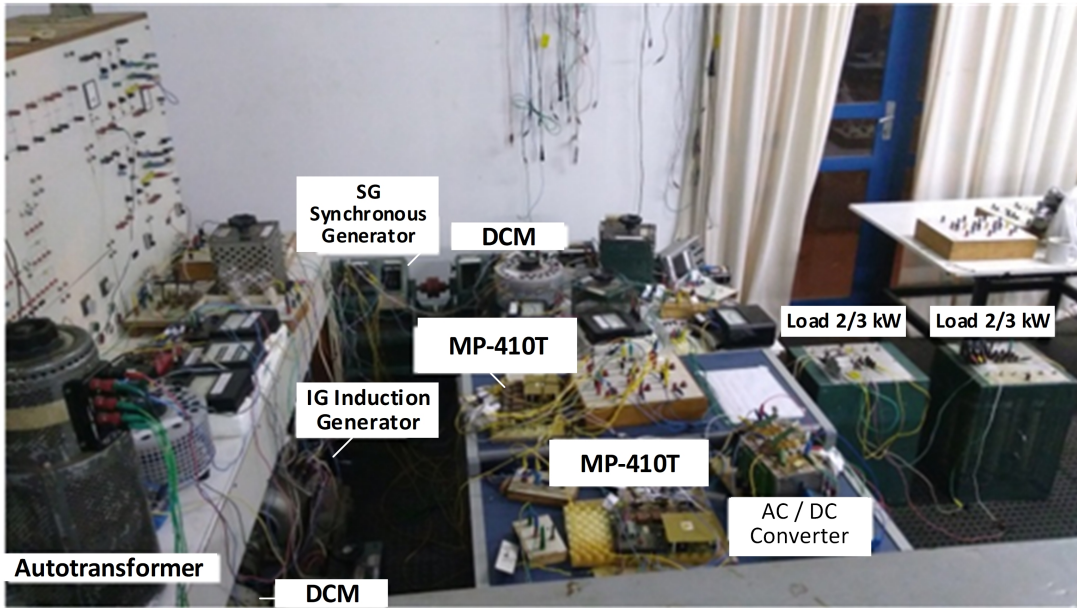


Figure 2.1 – Laboratory Assembly

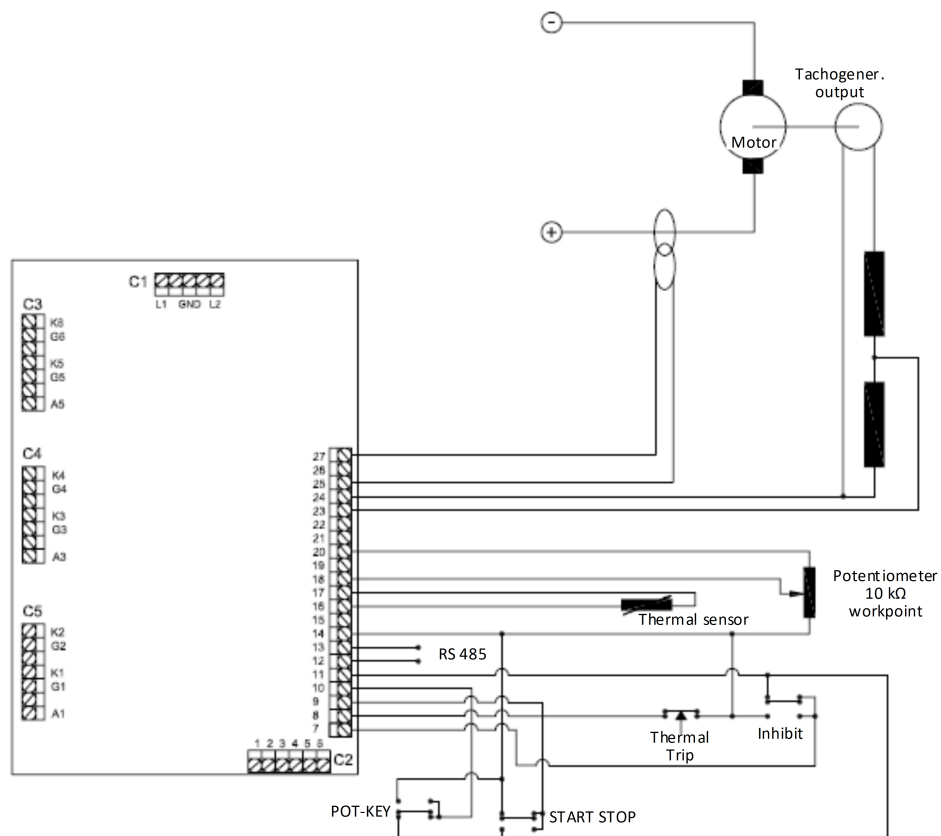


Figure 2.2 – Connections Arrangement of MP410T and Devices

## 2.7 Voltage and Speed Control Loops

The Figures 2.4 and 2.5 show the close control loop used to control the *SG* speed and voltage via electronic boards.

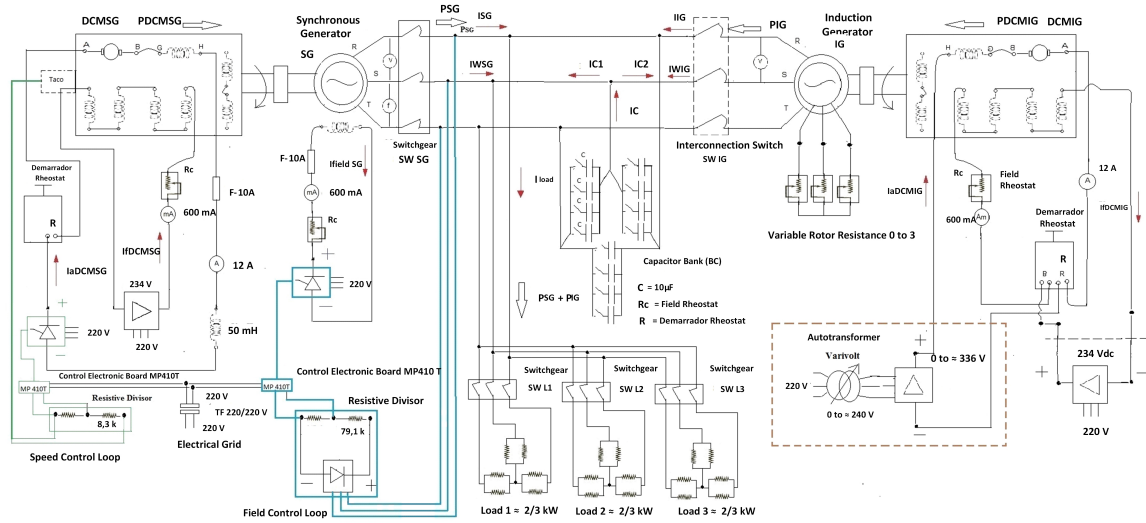


Figure 2.3 – Synchronous and Induction Generators in Parallel Operation Mode

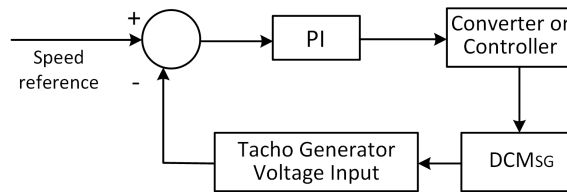


Figure 2.4 – Speed Control Loop

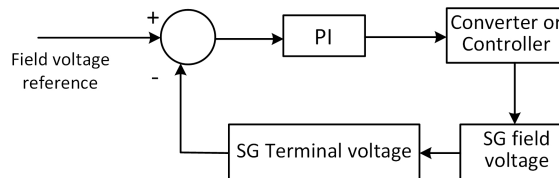


Figure 2.5 – Field Voltage Control Loop

The master and slave behavior of the generators (*SG* is the master and *IG* is the slave for the system frequency and voltage) as well as the *IG* is the master for the active power supply as verified and detailed in chapter 1 of this work. The frequency and voltage are determined by *SG*, while the active power consumed at load is supplied by the *IG* and complemented by *SG*.

## 2.8 Experimental Data

The laboratorial data are shown in Table 2.1.

Table 2.1 – Scenarios and Transitions

	Scenario 1	Scenario 2	Scenario 3	Scenario 4	Scenario 5	Scenario 6	Scenario 7
Results	Scenario 1	Scenario 2	Scenario 3	Scenario 4	Scenario 5	Scenario 6	Scenario 7
$V_{SG}$ & $V_{IG}$ (V)	228.0	228.0	228.0	228.0	204.0	228.0	228.0
$f_{SG}$ (Hz)	55	55	55	55	53.3	55	55
$I_{fieldSG}$ (mA)	380	500	550	520	600	510	420
$V_{aDCMSG}$ (V)	238.4	240.2	235.3	238.0	234.1	238.3	241.5
$I_{aDCMSG}$ (A)	2.0	4.7	3.0	4.9	0.0	3.6	12.0
$I_{fDCMSG}$ (mA)	450	450	450	450	450	450	450
f IG (Hz)	55	55	55	55	53	55	0.0
n I G (rpm)	1650	1731	1746	1724	1697	1747	1954
$V_{aDCMIG}$ (V)	299.5	323.3	334.4	323.1	322.2	323.5	333.5
$I_{aDCMIG}$ (A)	1.9	7.0	8.6	6.8	8.0	8.2	0.0
$I_{fDCMIG}$ (mA)	400	380	380	380	380	380	370
$I_{load}$ (A)	0.0	5.1	5.1	5.1	4.5	5.1	5.1
$I_{IG}$ (A)	3.1	5.6	6.9	5.6	6.5	6.4	0.0
$I_{SG}$ (A)	1.9	1.7	0.4	1.6	0	0.9	7.3
$IC$ (A)	5.1	5.1	5.1	5.1	4.4	5.1	5.1
$I_{WSG}$ (A)	n.a.	1.32	0.3967	1.14	0.0	0.8396	5.1
$IC1$ (A)	1.9	1.06	0.0513	1.14	0.0	0.3241	5.1
$IC2$ (A)	3.1	4.14	5.05	3.96	4.4	4.7759	0
$I_{WIG}$ (A)	n.a.	3.77	4.70	3.96	4.65	4.26	0
$PSG$ (W)	n.a.	524.91	156.65	449.50	0.0	331.57	2038.60
$PIG$ (W)	n.a.	1489.10	1857.40	1564.50	1643.0	1682.50	0.0
$P_{DCMSG}$ (W)	n.a.	1128.9	705.90	1166.20	0.0	857.88	2898.0
$P_{DCMIG}$ (W)	n.a.	3168.30	2875.80	2197.10	2577.60	2652.70	0.0
$\eta_{GROUP}$ (%)	n.a.	46.87	56.23	59.88	61.70	57.37	69.50
$\eta_{SG}$ (%)	n.a.	46.50	22.19	38.54	n.a.	38.65	69.50
$\eta_{IG}$ (%)	n.a.	47.00	64.59	71.21	61.70	63.42	n.a.

<sup>1</sup> 40  $\mu$  F / phase

## 2.9 Results

For each scenario and transition indicated in Table 2.1, the respective voltage and current signal and their transition waveforms are shown below.

The oscilloscope configurations are:  $I_{IG}$ ,  $I_{SG}$  and  $I_{load}$ : 100mV/A and 500mV/division.  $V_{pn}$  (Phase neutral voltage): 100 V/division or 50V/division.  $n_{SG}$  (Synchronous generator speed): 550 rpm/division.

Note: As the generators are in parallel connection,  $V_{SG}=V_{IG}$  (Induction generator voltage) =  $V_{pp}$  (Phase-phase voltage) =  $V_{pn} * \sqrt{3}$

- Load Transients: The load changes consist of removal and insertion of 2/3 kW. The other 4/3 kW remain connected. Figures 2.6, 2.7, 2.8 and 2.9 show  $I_{IG}$ ,  $I_{SG}$  and  $V_{pn}$  for scenarios 1 and 2. The figures show the actual state and values of these parameters in accordance with Table 2.1. The  $I_{IG}$  is advanced from  $V_{pn}$  because the reactive bank supply during these scenarios. In scenarios 1 (no load) and scenario 2 (low resistive load),

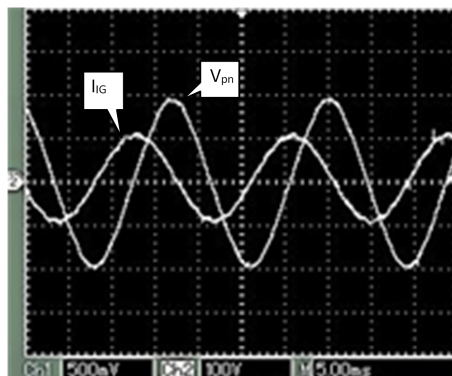


Figure 2.6 –  $I_{IG}$  and  $V_{pn}$  (Scenario 1)

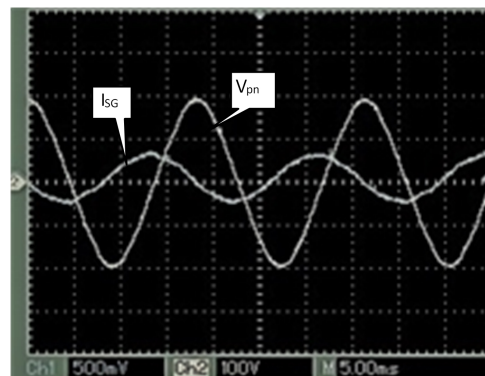


Figure 2.7 –  $I_{SG}$  and  $V_{pn}$  (Scenario 1)

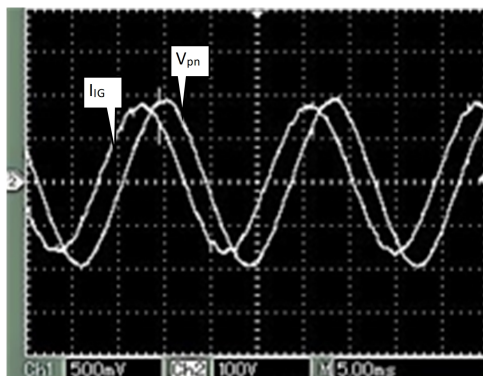


Figure 2.8 –  $I_{IG}$  and  $V_{pn}$  (Scenario 2)

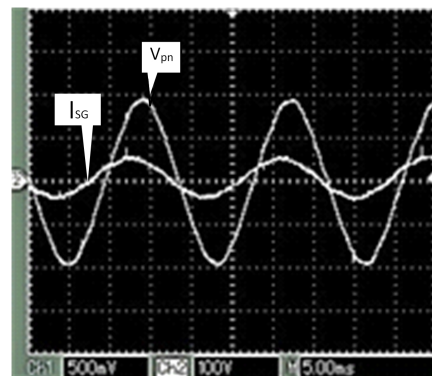


Figure 2.9 –  $I_{SG}$  and  $V_{pn}$  (Scenario 2)

Figure 2.10 reveals the automatic  $I_{SG}$  regulation upon removal and insertion of 2/3 kW from the resistor bank. Figure 2.11 shows that  $I_{IG}$  remains the previous values with an identical load change.

Figures 2.10 and 2.11 also show that  $V_{pn}$  keeps a constant value. This means that the system regulation for load changes is managed solely by  $SG$ . The  $V_{pn}$  and  $V_{IG}$  remains constant.

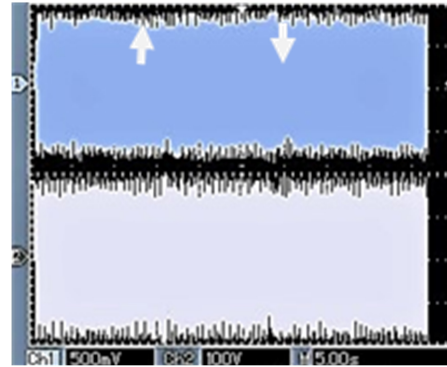
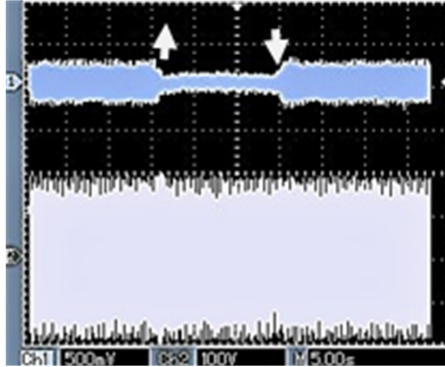


Figure 2.10 – Channel 1-  $I_{SG}$ , Channel 2-  $V_{pn}$ . (2/3 kW is removed and then inserted) (Scenario 2)

Figure 2.11 – Channel 1-  $I_{IG}$ , Channel 2-  $V_{pn}$ . (2/3 kW is removed and then inserted) (Scenario 2)

Figure 2.12 shows that  $I_{IG}$  does not change with removal and insertion of load. All the  $PIG$  that feed the load before the load change, still feeding the load after the load change. The  $SG$  just participates this by complementing the load power required.

Figure 2.13 shows that  $I_{SG}$  adjustments for the load change in order to provide the increased power required by the load.

Figures 2.12 and 2.13 also show that  $n_{SG}$  does not change, and the  $SG$ 's controls regulate the speed to synchronous speed for 55 Hz, 1650 rpm, always when the load changes.

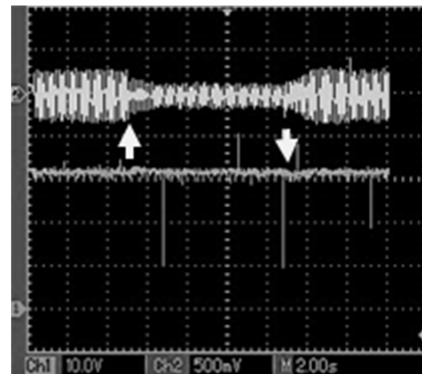
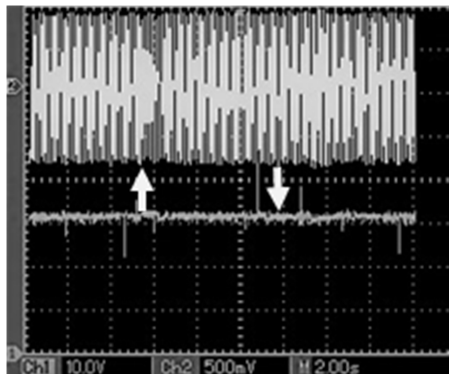


Figure 2.12 – Channel 1-  $n_{SG}$ , Channel 2-  $I_{IG}$ . (2/3 kW is removed and then inserted.) (Scenario 2)

Figure 2.13 – Channel 1-  $n_{SG}$ , Channel 2-  $I_{SG}$ . (2/3 kW is removed and then inserted.) (Scenario 2)

- Generation Transients: The changes created in the generation system consist of removal and insertion of each generator.

Figure 2.14 shows that when  $SG$  is removed, the voltage system has a small drop and the voltage regulation is lost. This shows that the voltage regulation is the sole responsibility of  $SG$ . During the period that  $IG$  operates alone, the frequency is bigger as observed in chapter 3 and Figure 3.23. A lower system voltage is still remaining due to  $IG$  excited by capacitor bank and in operation.

Figure 2.15 shows the regulation of  $V_{pn}$  from the  $SG$  (master) when the  $IG$  (slave) is removed.

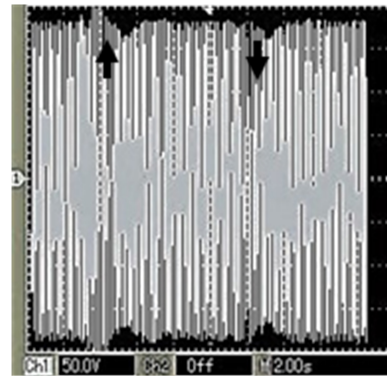
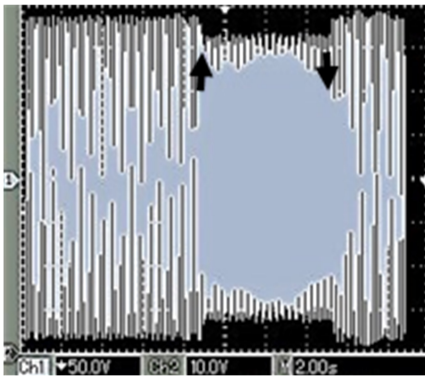


Figure 2.14 –  $V_{pn}$ ,  $SG$  is removed and then Figure 2.15 –  $V_{pn}$  in load.  $IG$  is removed and then inserted. Scenarios 4 & 5

Figure 2.16 reveals good speed regulation from the  $SG$  when the  $IG$  is removed and inserted.

Figure 2.17 shows that  $I_{SG}$  assumes the  $IG$  load when  $IG$  is removed. In contrast to  $IG$ ,  $SG$  realizes the  $IG$  is out and regulates itself to meet the demand and keeping the previous voltage and speed as shown in Figure 2.17, Figure 2.18 and Table 2.1.

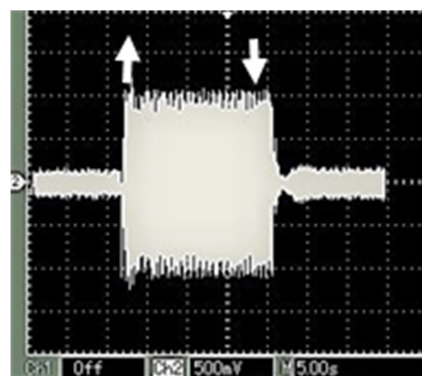
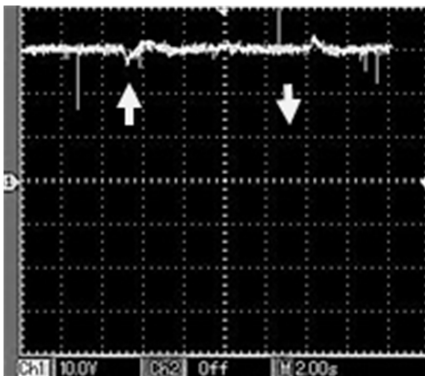


Figure 2.16 –  $SG$  speed.  $IG$  is removed and Figure 2.17 –  $I_{SG}$ ,  $IG$  is removed and then inserted. Scenarios 6 & 7

Figures 2.18 and 2.19 show  $I_{SG}$  and  $I_{IG}$ , which are representing respectively, the smallest  $I_{SG}$  and the biggest  $I_{IG}$  obtained in the experiment.

Note: In the case of Figure 2.18, the oscilloscope scale was set to 1000mV/A.

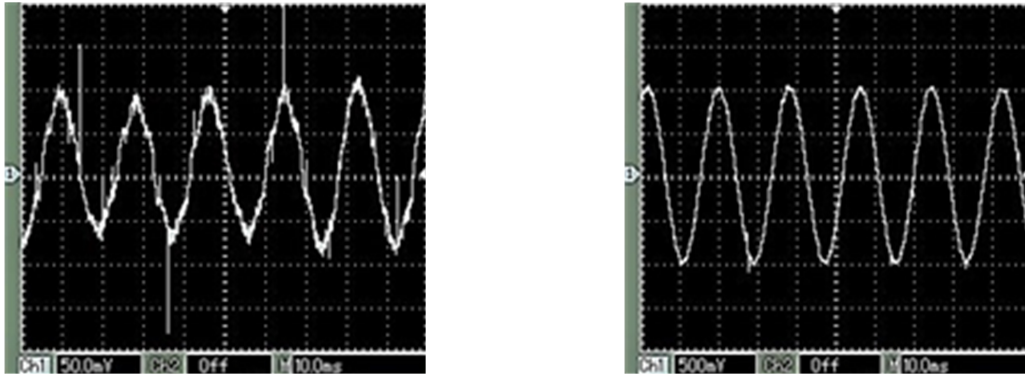


Figure 2.18 –  $I_{SG}$ .  $SG$  smallest contribution = 0.4A. Scenario 3  
 Figure 2.19 –  $I_{IG}$ ,  $IG$  biggest contribution = 6.9A. Scenario 3

Figure 2.20 indicates that  $IG$  continues supply a steady power to the load, even with the  $SG$  removed. As  $SG$  is out, the system loses the voltage and frequency regulation. In this condition, the system voltage and frequency are imposed by  $IG$ .

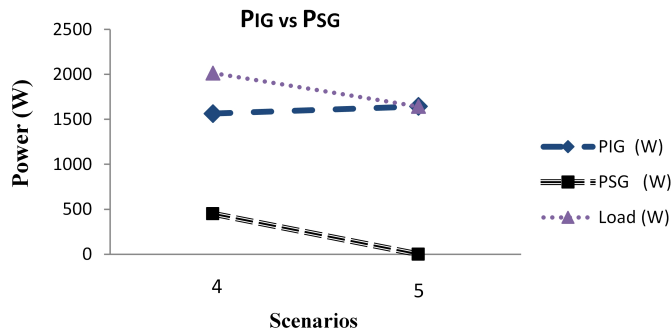


Figure 2.20 – Transition between Scenarios 4 and 5

On the contrary, Figure 2.21 shows the transition between the scenarios 6 and 7, it means when  $IG$  is disconnected,  $SG$  assumes the full load and still regulates the system voltage and frequency.

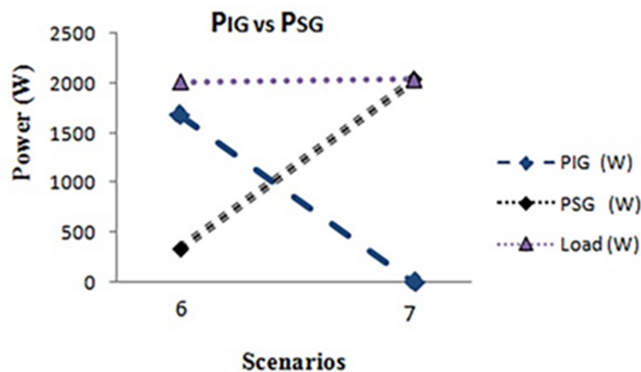


Figure 2.21 – Transition between Scenarios 6 and 7

## 2.10 Conclusion

Regarding to load changes, with removal and insertion of load, the *SG* can regulate the system voltage and frequency. The  $I_{SG}$  adjustments to the new load demand, while the  $I_{IG}$  keeps the previous values during transients. *IG* continues to supply the same power previously set for.

Regarding to *IG* transients, *IG* removed or inserted, *SG* and its system can regulate the system voltage and frequency. This is running even if the *IG* is fully loaded or *IG* is removed abruptly.

Regarding to *SG* transients, *SG* removed or inserted, *IG* is not capable of maintaining the system voltage and frequency, because *IG* does not have the voltage and frequency controls as the *SG* has. In this situation, the system frequency falls slightly as well as the system voltage.

In addition, when the system has no load or has only 2/3 kW and the two machines operating in parallel, when  $P_{DCMIG}$  is elevated to a value bigger than 600 W, the system frequency exceeds 55 Hz. Then, the *IG* and  $DCM_{IG}$  group motorizes the *SG*, and the  $DCM_{SG}$  operates as a no load  $DCG_{SG}$  (*Direct current generator coupled with synchronous generator*). As it is shown in the scheme shown in Figure 2.3, there is not no other way besides the load for receiving the generated power. Moreover, as the converter is operating as rectifier instead of inverter, the generated energy does not have another way to be regenerated or dissipated, then, the system frequency increases. When the system has 2/3 kW or 2kW connected, it is realized that the frequency does not exceed the rated value. In this case, all generated power is being consumed by loads. It consists of scenarios two to seven as shown in Table 2.1. Therefore, when  $P_{DCMIG}$  is adjusted to a value bigger than load power, the system frequency exceeds 55 Hz.

In the next chapter, it will be shown two systems capable to regulate the system frequency in an electric system, the one of them is able to regulate the system frequency in an isolated electric that uses *BL* (energy dissipation) and the other uses energy regeneration to the grid. It requires interconnected system. This latter serves as a didactic alternative only.

# 3 Alternatives to Control the Frequency Increase in an Electric System with Synchronous and Induction Generators in Parallel Operation Mode

## 3.1 Introduction

Based on [33], this chapter aims to demonstrate the increase in the frequency of events that can appear in an isolated electric system composed of a *SG* in parallel with an *IG*, the causes of this increase and two alternative methods of tackling this problem. To achieve this, this work presents laboratory experiments that show how to control the system frequency while maintaining the rated system voltage. The frequency increase observed in this work is due to the generated power exceeding the load demand as result of either generation in excess supplied by induction generator or a relevant load disconnected from the system at the moment that the *SG* has no power capacity for balancing the system power. This work then presents two alternative ways to control the system frequency: by ballast load control or by returning regenerative energy to the grid. This work also analyses an experiment involving *SG* removal while the *IG* is still operating and evaluates the consequences for the system frequency and voltage. Two suggested improvements are cited for implementation in future works.

Some of the works related to *SG* and *IG* in parallel operation mode implemented in the laboratory include speed and voltage control loops respectively applied on the *SG* primary machine and the *SG* field circuit [31, 29, 28, 34, 25, 35]. Increasing frequencies were observed in [31, 29]. The initial idea for the project of *BL* to frequency regulation was shown in [29], but it was not developed, implemented or described, as shown in the current chapter. The idea adopted in the current chapter was suggested as future work in [31] and [29].

In addition, the *BL* method was used in [9] to regulate only the voltage in an isolated grid fed by an *IG*, whereas this work uses a *BL* to regulate the frequency in an isolated grid fed by either an *IG* and an *SG* in parallel mode or by an *IG* alone.

Based on the prior experiments involving *IG* and *SG* in parallel operation, manual *IG* speed control is a third and more usual alternative to control the system frequency, which has already been accomplished in [10, 29, 28, 34]. In brief, this third alternative must obey the following rule: *IG* speed can rise up to the *PIG* limit, which corresponds to

when the minimum *PSG* is supplied. Thus, the system frequency does not increase since the *SG* continues to supply any amount of power. On the contrary, the system frequency is increased.

Although there are some prior works on *SG* and *IG* in parallel operation mode that report simulated or practical experiments [22, 16, 17, 18, 19, 20, 21, 31, 29, 28, 34], none of these studies investigate all the practical causes of frequency increase that can appear in the system due to the presence of an *IG*, as well as alternative schemes to control the increasing frequency of events. Thus, this work intends to show the causes of frequency increase that can appear in an isolated electric system due to the presence of an *IG*, as well as, two alternative schemes implemented in the laboratory to control the increasing frequency.

The two laboratory experiments shown in the chapter are: first, the insertion of a *BL* control system and second, the insertion of an energy regenerating system (*ERS*) to enable the system to return regenerative energy to the grid. Both experiments achieved the expected results and enabled system frequency control while maintaining the system voltage control.

As already said in introduction of this thesis, this study is important in showing the causes of frequency increase and to show a method of *BL* control that is useful for *MHPP* application as cited in [9], [16], and [17], whose generation could be composed for *IG* and *SG* in parallel operation mode.

## 3.2 Frequency Increase

The main causes of frequency increase investigated in this work are as follows: (i) the elevation of generated *PIG* and the lack of *PSG* capacity to automatically compensate for the increase in *PIG*, for a steady load; and (ii), abrupt removal of the load, which leaves the lack of *PSG* capacity to automatically compensate for the removal of load power from electric system, resulting in a frequency increase, as shown in Figure 3.1. In order to ensure that the system voltage and frequency are constant and regulated in this generator topology, the *SG* needs to continue to supply at least, a minimum amount of power to the system. On the contrary, if the *IG* is supplying more power than that demanded by normal loads connected, the synchronous machine is motorized and the system frequency increases.

## 3.3 Laboratory Experiments

The normal operation of the *SG* and *IG* in parallel mode is summarized in Figure 3.2 considering the following clarifications. First, as the *PIG* decreases by acting on the

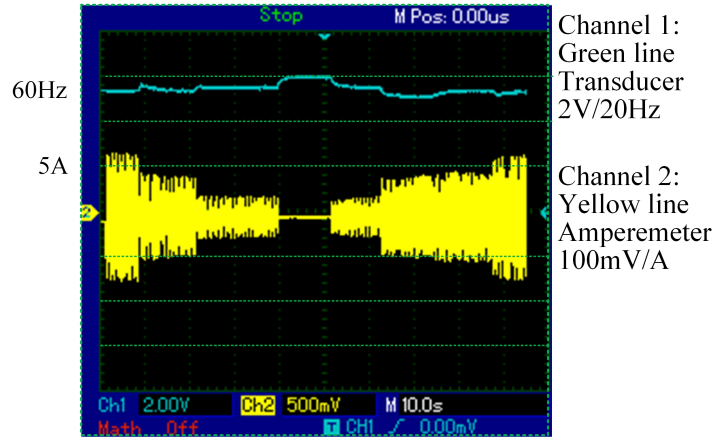


Figure 3.1 – Transient frequency following load removal

speed of the *IG* primary machine  $DCM_{IG}$ , the *PSG* increases automatically by actuation in the  $DCM_{SG}$  speed control loop in such a manner that the sum of the generated power results in the power required by the load, 2 kW. Second, the frequency and voltage are determined by the *SG*, while the active power consumed by the load is supplied by the *IG* and complemented by the *SG*. Third, when the *IG* is disconnected, the *SG* assumes the full load and continues regulating the system voltage and frequency as shown in [31, 29, 28] and [34]. On the contrary, the *IG* is not able to regulate these parameters as shown in [31].

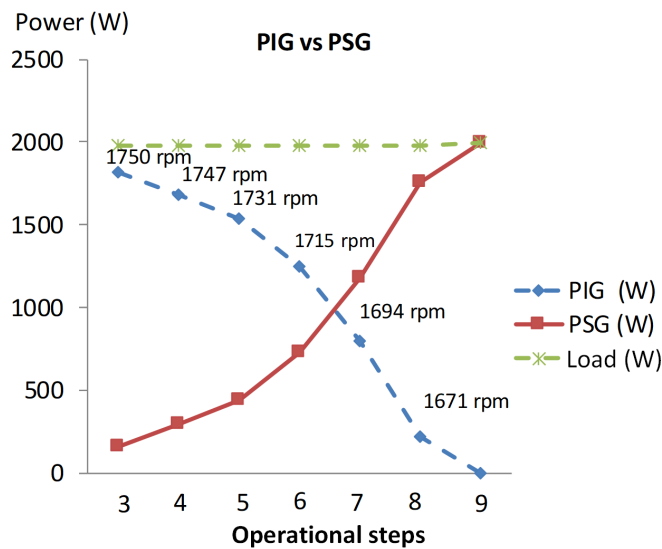


Figure 3.2 – SG and IG feeding the load

### 3.3.1 General Scheme

The electric system mounted in the laboratory is shown in Figures 3.3 and 3.4. It consists of one *SG*, one *IG*, one capacitor bank, three resistor banks *RB* (*Resistor*

*bank*)s, one ballast load *BL*, one induction motor *IM*, three converters, one analogical regulator for one speed control loop, one digital control board for one voltage control loop, one digital control board for one *BL* control loop, and instruments and devices such as ammeter, voltmeters, and rheostats.

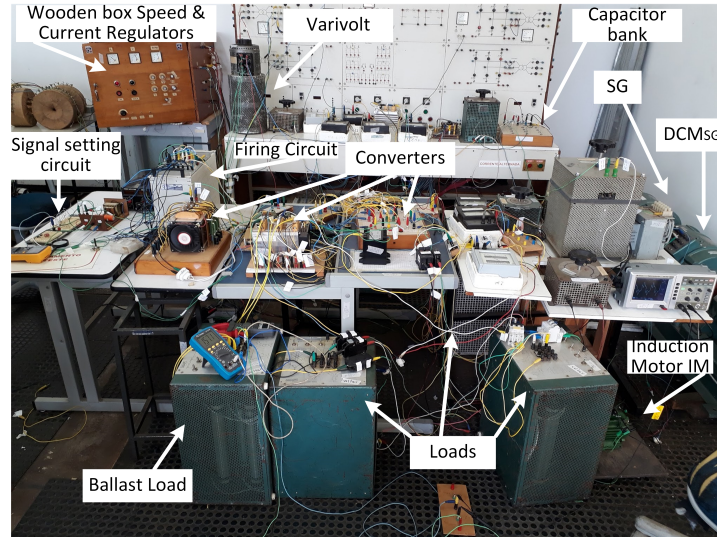


Figure 3.3 – Lab Assembly (Front View)

Figure 3.3 shows the general circuit used to develop and test the laboratory experiments performed in this work, mainly those implemented to control the system frequency when it deviates from the rated value. Figure 3.4 shows all the control loops, namely the speed control loop (in green), the voltage control loop (in blue), and the *BL* control loop (in red). The capacitor was sized to supply 2057.6 VAR. This reactive power is required by the *IG* when feeding the resistive load with 7.5 A.

The three closed loops, control boards, and the detailed circuit used in each experiment are summarized below

Based on the Figure 3.4, note that the  $DCM_{IG}$  is driven manually by an auto-transformer which applies a voltage of 0 to 336 V on the  $DCM_{IG}$  armature, which result in the speed setting and allows delivery of the corresponding power to the system, as shown in [34].

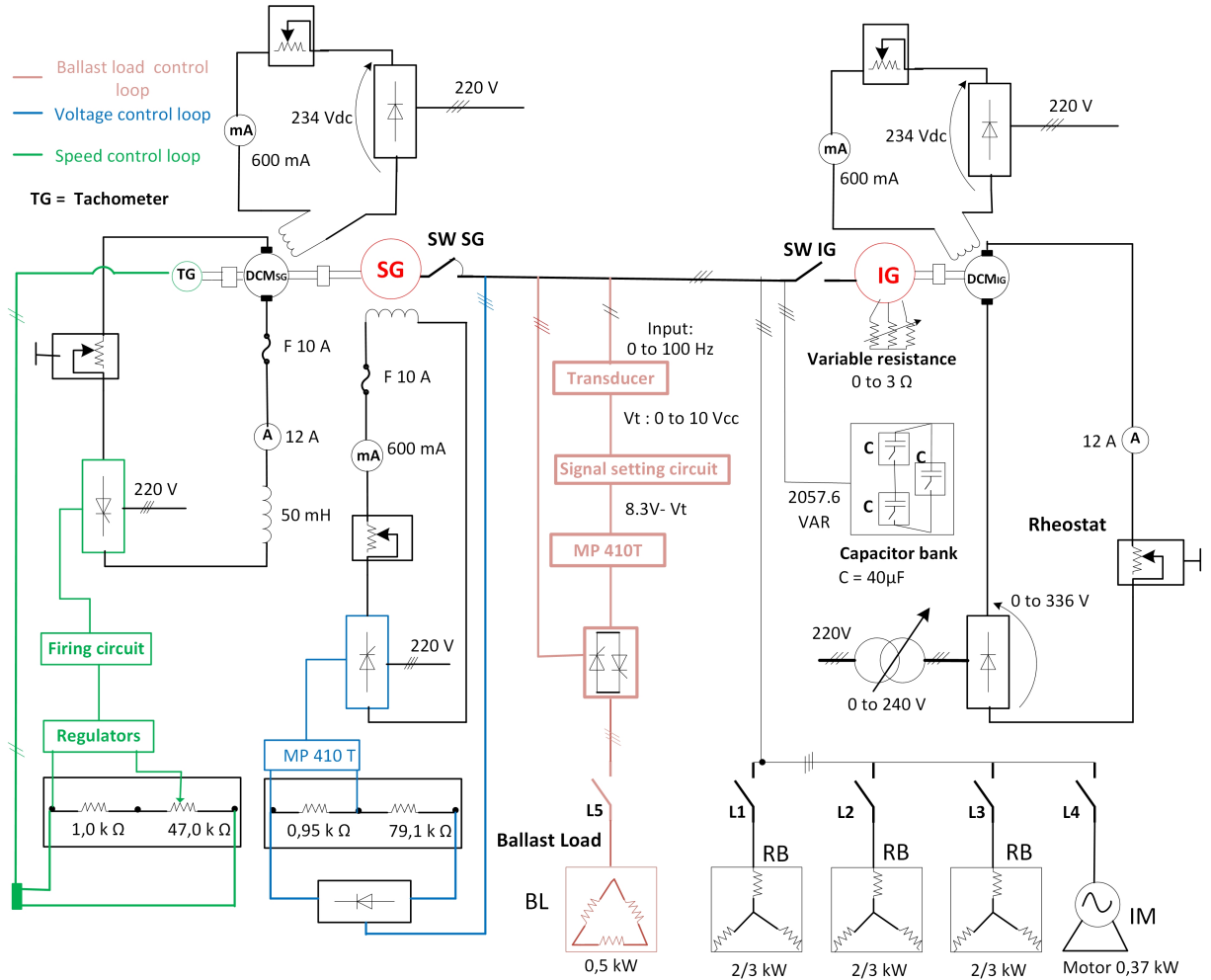


Figure 3.4 – Synchronous and Induction Generators in Parallel Operation Mode

### 3.3.1.1 Data Plates

The equipment data plates used in the experiments are shown in Table 3.1.

Table 3.1 – Equipment Data Plates

<b>Direct Current Motor <math>I_G</math></b>						
220 V	7.72 A	1.7 kW	1500 rpm	600 mA	$I_{fieldmax}$	
<b>Direct Current Motor <math>S_G</math></b>						
220 V	9.1 A	2.0 kW	1800 rpm	600 mA	$I_{fieldmax}$	
<b>Induction Generator <math>I_G</math></b>						
220 V	7.5 A	1.86 kW	1410 rpm	0.8 pF	50Hz	
<b>Synchronous Generator <math>S_G</math></b>						
230 V	5.0 A	2.0 kVA	1800 rpm	0.8 pF	60 Hz	
$V_{field}: 220 V$			$I_{fieldmax}: 600 mA$			
<b>Load (kW)</b>			<b>Ballast Load (kW)</b>			
Load 1	Load 2	Load 3	Load 5			
2/3	2/3	2/3	0.5			
<b>Induction Motor (<math>IM</math>)</b>						
0.37 kW	1715 rpm		0.71 (PF)		60 Hz	

### 3.3.1.2 Digital Control Boards

A digital MP 410T voltage control board manufactured by Semikron is used to control the *SG* voltage as shown in Figure 3.5. The same kind of digital board shown in Figure 3.5 is used to control the *BL*. This kind of digital board is used in all the experiments reported in this work.

The digital control board MP 410T attends the same goal of analogical firing circuit and regulators together. In other words, MP 410T controls the firing angle of thyristors in order to apply the correct voltage across DCM, primary machine of *SG* or *IG* in response to required speed defined by speed regulator, for instance.

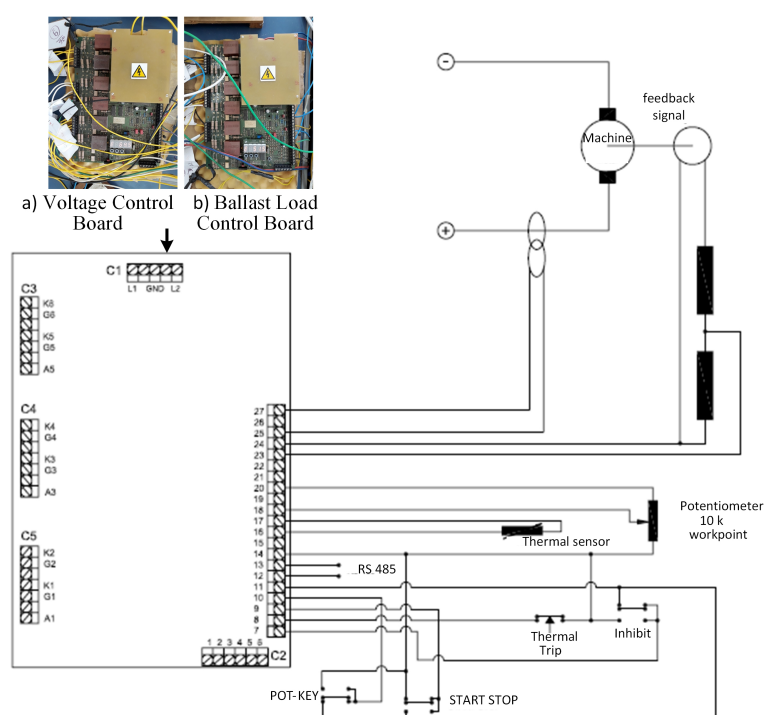


Figure 3.5 – Electronic Board MP410T and Connections

### 3.3.1.3 Analogical Control Board

The analogical control board used as speed and current regulators in speed control loop, see Figure 3.4, was totally developed in the laboratory of research development of electrical didactic laboratory of Federal University of Itajubá, as detailed and demonstrated in Appendixes A, B and D. This cited analogical control board was mounted in an wooden box as shown in Figure 3.3.

The firing circuit shown in Figure 3.4 works together with analogical regulator, appendixes A, B and D in order to control the thyristor firing angle and consequently the applied voltage across machine terminals. This firing circuit was manufactured by Datapool, located in Itajubá-MG, Brazil, and it is similar to firing circuit shown in Figure

B.12 of Appendix B, that was totally developed and tested in the laboratory of research development of electrical didactic laboratory of Federal University of Itajubá.

### 3.3.1.4 Speed Control Loop

Figure 3.6 shows the use of closed speed control loop highlighted in green in Figure 3.4, to control the *SG* speed via analogical regulator, firing circuit board and thyristor bridge as detailed in [4, 23]. This speed control loop controls the *SG* direct current motor, *DCM<sub>SG</sub>*, using (3.1) as the basis of control. As the tachometer [36] measures the trend of the speed decrease, the speed control loop commands the  $U_a$  (*Direct current motor armature voltage*) elevation, indicated by the red up arrow in (3.1), what result in the same motor speed indicated by the reference speed.

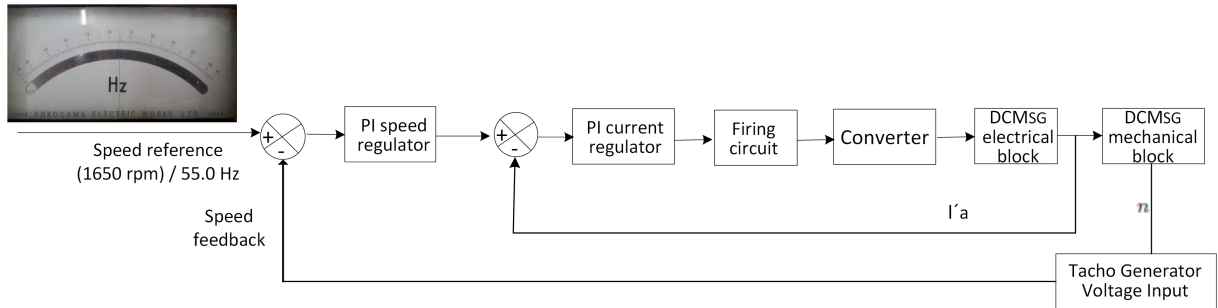


Figure 3.6 – Speed Control Loop

$$n = \frac{U_a \uparrow - (\sum R_a) I'_a}{k\phi} \quad (3.1)$$

### 3.3.1.5 Voltage Control Loop

Figure 3.7 shows the use of the closed voltage control loop, highlighted in blue in Figure 3.4, to control the system voltage via the *SG* field control using an electronic board as shown in Figure 3.5. This control loop is removed in the *SG* removal experiment.

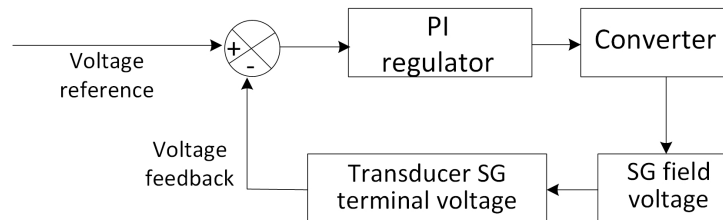


Figure 3.7 – Voltage Control Loop

In addition, this voltage control loop controls the synchronous-machine-terminal voltage through field current settings that result in the terminal voltage equal to voltage reference manually adjusted in the MP410T electronic board. This *SG* field current control is based on the V-curve of the *SG* or *SM* (*Synchronous motor*) as shown in Figure 3.8.

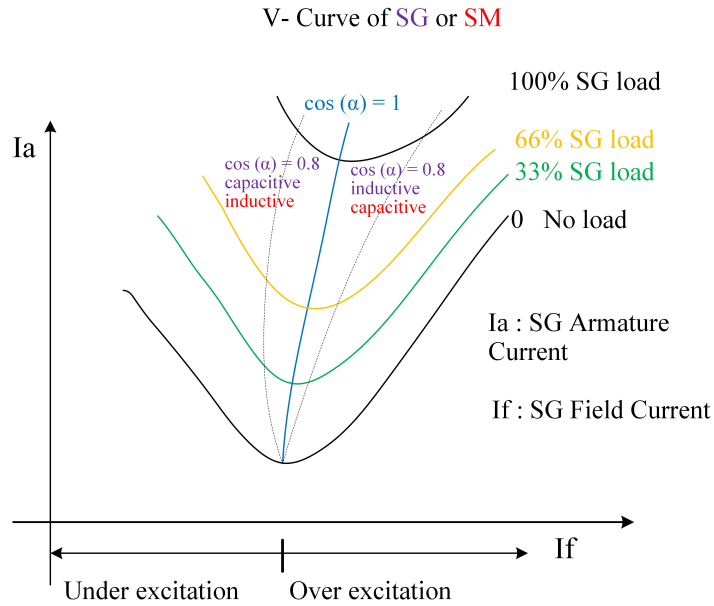


Figure 3.8 – V-Curve of *SG* or *SM*

Note: The V curves of the *SG* and *SM* are very similar. In this case, they are considered identical except for the power factor curves which are permuted as shown in Figure 3.8, [25]. The red colour is associated with the *SM* and the purple colour with the *SG*.

For instance, when more one resistor bank *RB* is inserted in the system, the system's load departs from 33% and reaches 66% of 2kW, and the system voltage  $V_{SG}$  given in (3.2) tends to fall a bit as indicated by the blue and brown arrows in (3.4) and (3.2) respectively. Then, the voltage control loop measures this decreasing trend and increases the field current  $I_f$  (*Field current*) so that the flux  $\phi$  rises and the  $V_{SG}$  keeps the same value. In summary, the load rises, the *M* rises as indicated by the blue arrow in (3.4),  $I'_a$  (*Direct current motor armature current*) rises as indicated by the brown arrow in (3.4), the *SG* speed (*n*) tends to decrease as indicated by the green arrow in (3.3), and the voltage drop across the armature impedance  $\dot{I}_a \times (Ra + jXa)$  rises,  $\dot{I}_a$  (*Synchronous generator armature current*). So, the voltage control loop commands the  $I_f$  elevation, resulting in elevation of  $\phi$  as indicated by the red arrow in (3.3). Thus, the voltage control loop raises the electromotive force  $E_{SG}$  (*Synchronous generator electromotive force*), maintaining  $V_{SG}$  at the same value or at a value equal to the reference voltage [28].

$$\dot{V}_{SG} = \dot{E}_{SG} - \dot{I}_a \uparrow \times (Ra + jXa) \quad (3.2)$$

$$E_{SG} = k \times n \downarrow \times \phi \uparrow \quad (3.3)$$

$$M\uparrow = k \times \phi \times I_a'\uparrow \tag{3.4}$$

### 3.3.1.6 Ballast Load Control Loop

In addition to the *BL* control loop highlighted in red in Figure 3.4, Figure 3.9 shows the closed control loop used to control the frequency via the *BL* connected to the system as shown in Figure 3.4. This control loop does not participate in the energy regeneration experiment, in which the control was run in manual mode.

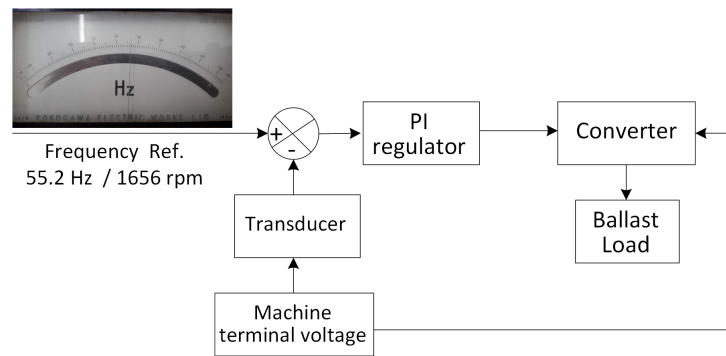


Figure 3.9 – Frequency Control Loop

Note that the reference frequency was adjusted to 55.2 Hz so that the *BL* control loop assumes the frequency control instead of the speed control loop. At a working point greater than 55.2 Hz, this control loop performs the system frequency regulation and regulates it to 55.2 Hz as shown in Figure 3.9. At a working point lower than 55.0 Hz, the speed control loop performs the system frequency regulation and regulates the speed and system frequency to 1650 rpm and 55.0 Hz, respectively. This small difference does not affect the cited electrical system but is relevant for the correct functioning of the control. This measurement is accomplished by a high-accuracy frequency meter because, in other ways, it is not perceptible. This BL control is described in more detail forward.

### 3.3.1.7 Control Board Parametrization

All the required parametrization configured in the laboratory for the two MP410T electronic control boards is shown in Table 3.2. This parametrization is addressed to the voltage control loop as addressed to the *BL* control loop. The rest of the MP410T parametrization consists of default values that are not shown in this Table 3.2. These ones can be found in [28, 23]. All of the values below were experimentally adjusted with satisfactory dynamic system stability.

Table 3.2 – Electronic Control Board Configuration

Memory Position	Name (abbreviation at display)	Value (unit)
1	Local or Remote ( <i>LR</i> )	Local (0)
2	Configuration 9 ( <i>CF</i> )	1B6C (Graetz (voltage)) W3C(antiparallel (BL))
16	Reference Value ( <i>E</i> )	64.5% (voltage) 51.5% ( <i>BL</i> )
19	KP_Voltage ( <i>PV</i> )	0.05 (voltage) 0.2 (BL)
20	TI_Voltage ( <i>IV</i> )	0.1s

### 3.3.2 Ballast Load Control Experiment

Regarding the frequency elevation scenario described previously, the inclusion of a frequency regulation system is necessary in order to keep the frequency stable at rated values. In this case, a BL is used to control the frequency. This option, shown in Figure 3.10, is able to control the load within the *BL* power range. It is controlled in such a manner that the frequency is kept at the rated values.

The *BL* is connected in parallel to the principal loads of the generators. In the frequency control loop is set to a reference frequency and the feedback frequency is obtained by signal from a frequency transducer connected to the principal generator terminals as shown in Figure 3.10.

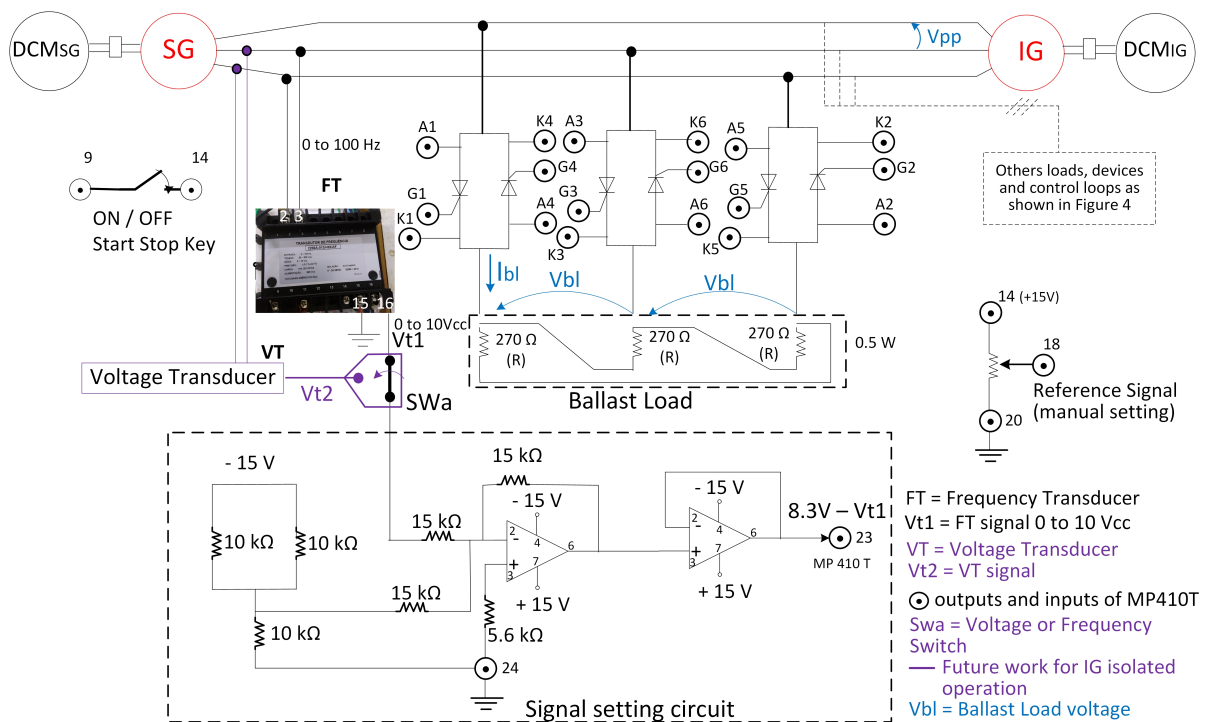


Figure 3.10 – Ballast load circuit

The control system actuates the thyristors, as a result of an increase or decrease of the system frequency, and results in setting of the system frequency. This consists of

a load power increase in the system when the system frequency is above the reference frequency, as shown in Figure 3.11.

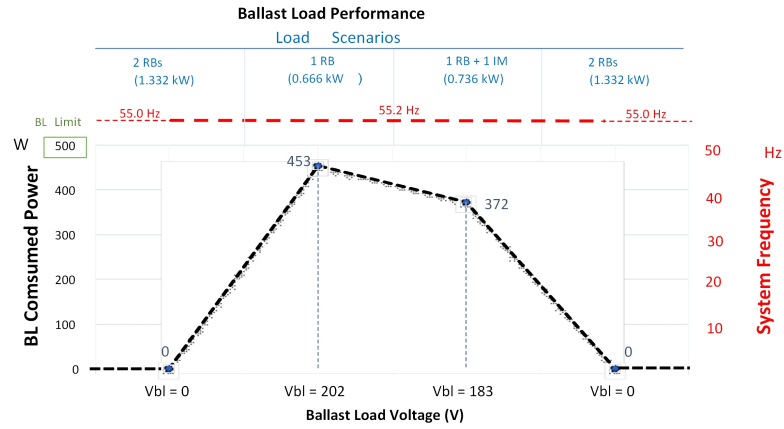


Figure 3.11 – Ballast Load Performance

As long as  $V_{bl_{RMS}}$  (*RMS ballast load voltage*) increases, the consumed load power  $P_{bl}$  (*Ballast load power*) increases, as shown by (3.5), up to the available limit, which is 0.5 kW. Then, as  $P_{bl}$  increases, the load increases and then the system frequency decreases to the reference frequency. The part of Figure 3.10 highlighted in purple is proposed as a future work.

$$P_{bl} = \frac{3 \times V_{bl_{RMS}}^2}{R} \quad (3.5)$$

The figures 3.12 and 3.13 show the frequency control technique of *BL*. Figure 3.12 shows how to control the phase-neutral RMS voltage  $V'_{bl_{RMS}}$  (*Phase-neutral RMS ballast load voltage*) over the *BL*. This  $V'_{bl_{RMS}}$  is chosen and shown in 3.12 and 3.13 only to demonstrate, in an easier way, the functioning principle of voltage control over the *BL*, instead of using the real BL phase-phase voltage  $V_{bl_{RMS}}$ , as shown in Figure 3.10, which comes from the delta connection. These can be seen in the results section. Then, the functioning principle is the same for  $V_{bl_{RMS}}$  as for  $V'_{bl_{RMS}}$ .

Hence, the control system receives the system voltage feedback signal and compares it with the reference frequency, which results in an error value, which is processed by the *PI* (*Proportional-integral regulator*) and the firing circuit that controls the firing angle of antiparallel thyristors, generating an applied voltage over the load as shown in Figure 3.12. Note that the voltage  $V'_{bl_{RMS}}$  is applied to the load in a progressive way until the maximum  $V'_{bl_{RMS}}$ , and consequently the maximum load power seen by generators, is reached. Figure 3.13 shows the expected phase-neutral voltage waveform applied to the BL connected in star, as the firing angle is 90°. In the results section, real waveforms of  $V_{bl_{RMS}}$  obtained from the scheme in Figure 3.10 will be shown and analysed.

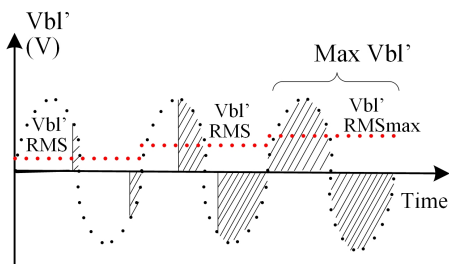


Figure 3.12 – Ballast Load Control

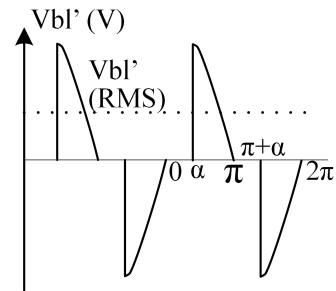


Figure 3.13 –  $V_{bl'}$  as Fire Angle  $90^\circ$

The voltage setting circuit shown in Figure 3.10 obtains the voltage signal  $Vt1$  (*Voltage signal from the frequency transducer (position 1)*) from the frequency transducer and generates  $8.3 \text{ V} - Vt1$  as the output signal. The voltage setting circuit was implemented to correct the control system functioning. This is an alternative that involves energy dissipation for system frequency control.

### 3.3.3 $DCM_{SG}$ Speed Regulator

For the normal functioning of an electric system, it is necessary for the analogical speed regulator circuit to control the  $DCM_{SG}$  speed as shown in Figure 3.14. Then, the control signal from 0 to 10 V to fire the thyristors comes from regulators inside the wooden box shown in Figure 3.4. This signal goes to the firing circuit, TCA 785, which commands the thyristors that are applying the direct current voltage,  $V_{dc}$ , on the  $DCM_{SG}$  so that the  $DCM_{SG}$  and  $SG$  speed can be controlled as already shown in [34].

The speed regulator circuit is composed of two regulators in cascade [4, 23] as follow: The first of them is the speed regulator, which receives the  $U_{na}$  (*Feedback speed signal*), from the tachometer [36]. The second is the current regulator, which receives the feedback current signal,  $V_{ia}$  (*Feedback current signal*), from the current transformer TC 30/5A, diode bridge, and signal buffer as shown in Figure 3.14. This cascade regulator generates the 0 to 10 V signal and sends it to pin 11 of TCA 785, which commands the thyristors as already explained. All wooden-box devices are highlighted in purple in Figure 3.14. The wooden box is shown in Figure 3.3.

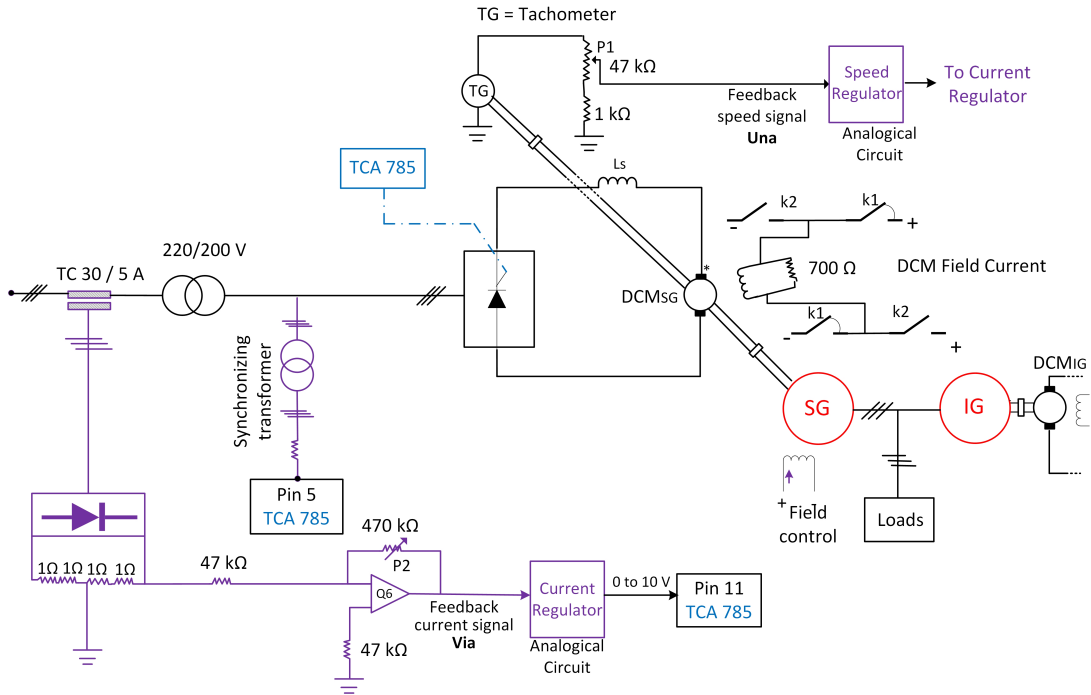


Figure 3.14 –  $DCM_{SG}$  Current Operation

### 3.3.4 Energy Regeneration Experiment

Figure 3.15 shows part of circuit shown in Figure 3.14 to detail the energy regeneration scheme and functioning as well as the frequency elevation process.

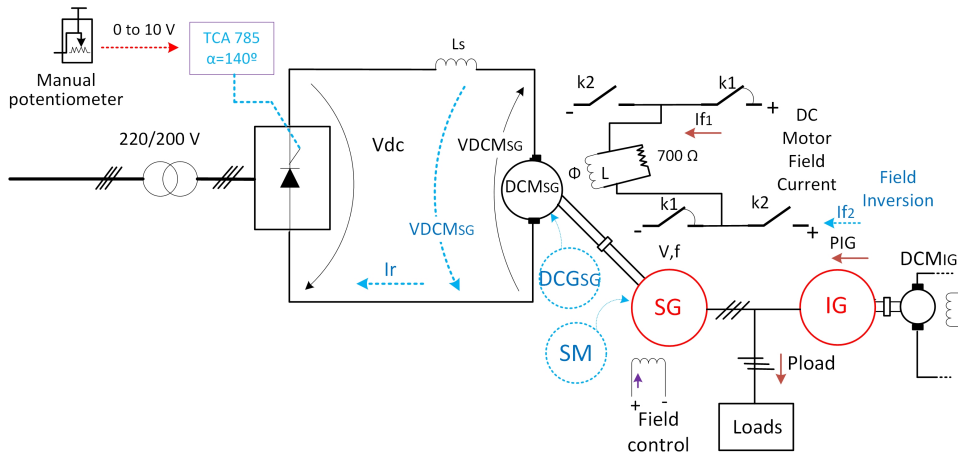


Figure 3.15 – Energy Regeneration Scheme

The *ERS* is an alternative way to control the system frequency elevation for the electric system proposed in this work, which is a result of decompensation between generation and demands inherent in this scheme involving the *IM*, resistive loads, and different generators in parallel operation mode, as already detailed. This frequency control alternative is based on the regeneration principle instead of the dissipation principle used in *BL* control.

During the normal operation based on Figures 3.4 and 3.14, the *IG* is powered by the *DCM<sub>IG</sub>* to supply more power *PIG* to the system, which only has a load of 2/3 kW connected. It is managed in such a way that the *SG* is motorized and becomes a *SM*, the *DCM<sub>SG</sub>* becomes the *DCG<sub>SG</sub>*, and, because the energy generated by the *DCG<sub>SG</sub>* is blocked by the  $V_{dc}$  and  $V_{DCMSG}$  (*Voltage of direct current motor coupled with synchronous generator*) sense, the system frequency is increased to 56 Hz.  $V_{dc}$  is given by (3.6), where the phase-phase voltage is  $V_{pp}$  and the thyristor firing angle is  $\alpha$ .

The appendix D adds this content using another and similar practical experiment totally developed in the Laboratory of research development of electrical didactic laboratory of Federal University of Itajubá, in which the four quadrants operations of *DCM* is more detailed.

$$V_{dc} = 1.35 \times V_{pp} \times \cos(\alpha) \quad (3.6)$$

Then, to control the system frequency, the firing circuit TCA 785 is changed to manual position, the firing angle is adjusted manually to 140°, and the switches K1 and K2 are commutated in order to change the field sense over the *DCM<sub>SG</sub>* which results in a change of the  $V_{DCMSG}$  voltage sense applied on *DCM<sub>SG</sub>*, see the blue arrow shown in Figure 3.15. So, this  $V_{DCMSG}$  transition enables the current  $I_r$  into the circuit composed of the converter and the *DCM<sub>SG</sub>*, as shown in Figure 3.15. This results in the return of regenerative energy to the grid, causing the system frequency drop to 55.0 Hz, the reference value. Then, in the third stage, the switches K1 and K2 are commutated again, which results in a new inversion of the *DCM<sub>SG</sub>* field sense, the inversion of  $V_{DCMSG}$ , leading to an interruption of the current circulation between the converter and the *DCM<sub>SG</sub>* and an interruption of the return of the regenerative energy to the grid. So, the system frequency rises to 56 Hz again.

In order to avoid the field over voltage across  $L$  given by (3.7) during the field sense change,  $I_{f1}$  (*Field current 1*) to  $I_{f2}$  (*Field current 2*), shown in Figure 3.15, the resistor 700  $\Omega$  was inserted into the *DCM<sub>SG</sub>* field circuit. This resistor attenuates the current variation during the transition time interval.

$$V_L = L \times \frac{di_{f1,2}}{dt} \quad (3.7)$$

## 3.4 Results

In Figure 3.16, the system frequency rises when the *IG* speed rises and its power flows to the system. The system has one 2/3-kW RB connected. The system voltage is

maintained at 220 V due to the voltage control loop from the synchronous machine. At this moment, it is acting as a *SM*.

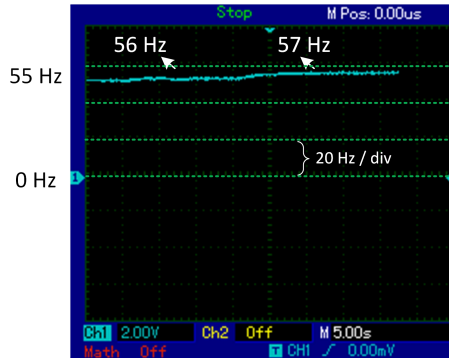


Figure 3.16 – Increasing frequency

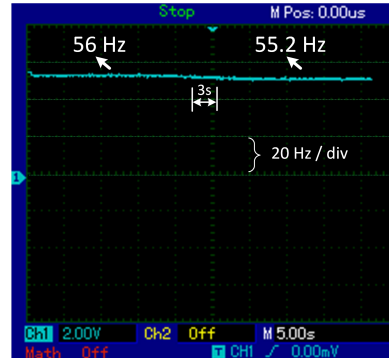


Figure 3.17 – Ballast load actuation

Figure 3.17 shows the ballast load control actuation. Firstly, *BL* control is acting and the frequency remains stable at 55.2 Hz. After a period of time, the thyristor firing pulses connected to the *BL* are blocked, which results in elevation of the system frequency to 56 Hz. In the following, *BL* control is activated and controls the system frequency again, returning it to 55.2 Hz. The system voltage remains at 220 V due to the *SG* voltage control loop actuation. In this interval, the synchronous machine is acting as the *SM* and the *DCM<sub>SG</sub>* is acting as the generator *DCM<sub>SG</sub>*, as shown in Figure 3.15. The scenario consists of  $V_{bl_{RMS}} = 155$  V,  $P_{bl} = 267$  W and  $I_{bl}$  (*Ballast load current*) (line) = 0.8 A.

Figure 3.18 shows the phase-phase voltage  $V_{bl_{RMS}}$  across the *BL* to regulate the system frequency. The system has one-2/3 kW *RB*. The system voltage remains at 220 V due to the voltage control loop actuation. The synchronous machine is acting as a *SM*, as shown in Figure 3.15. The scenario consists of  $V_{bl_{RMS}} = 155$  V,  $P_{bl} = 267$  W and  $I_{bl}$  (line) = 0.8 A.

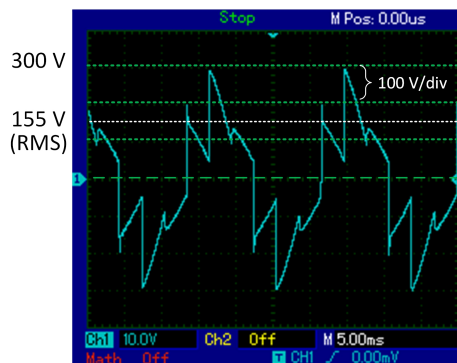


Figure 3.18 – Voltage  $V_{bl}$  across BL



Figure 3.19 – Frequency control ERS

The Figure 3.19 shows the result of the *ERS*. Firstly, the system is operating with 56.5 Hz, one *RB* connected as the load, and the voltage control loop keeping the system voltage at 220 V. Next, the switches K1 and K2 are commutated in order to change the field sense over the *DCM<sub>SG</sub>*, which results in a change of the  $V_{DCMSG}$ . Then, this  $V_{DCMSG}$

transition allows the current to circulate in the circuit composed of the converter and the  $DCM_{SG}$ , as shown in Figure 3.15. So, it results in the return of regenerative energy to the grid, causing the system frequency drop to 55.0 Hz, the reference value. Then, in the third stage, the switches K1 and K2 are commutated again, resulting in a new inversion of the  $DCM_{SG}$  field sense and the inversion of  $V_{DCMSG}$ , leading to an interruption of the current circulation between the converter and the  $DCM_{SG}$  and to an interruption of the return of regenerative energy to the grid. So, the system frequency changes to 56.5 Hz again.

Figure 3.20 shows the direct current voltage  $V_{dc}$  over the dc converter side as  $\alpha$  is  $140^\circ$ . This means that the converter is operating as an inverter, taking energy out to the grid. This angle  $\alpha$  was previously manually adjusted to  $140^\circ$ . The  $I_{ac}$  (*Line current across the ac converter side*), is also shown. Firstly, the system is operating at 56.5 Hz, with one  $RB$  connected as the load and the voltage control loop keeping the system voltage at 220 V. This figure shows the moment when the  $ERS$  returns the system frequency to the reference value.

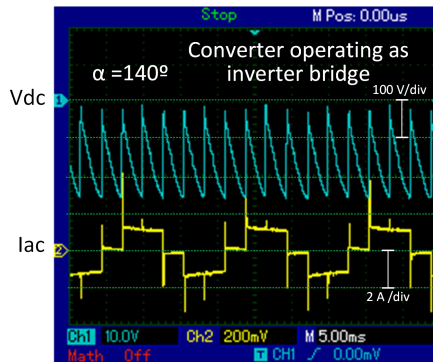


Figure 3.20 – Voltage  $V_{dc}$  and Current  $I_{ac}$

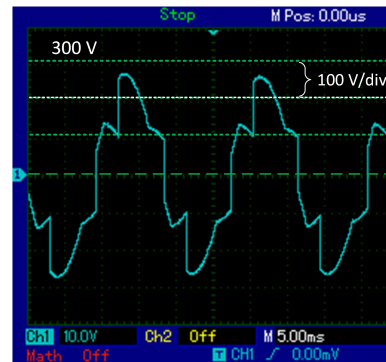


Figure 3.21 –  $V_{bl}$  -IG operates alone

Figure 3.21 shows the phase-phase voltage  $V_{bl_{RMS}}$  across the  $BL$  to regulate the system frequency as the  $SG$  has been removed and the  $IG$  is operating alone. The system has one-2/3 kW  $RB$  connected. The scenario consists of  $V_{bl_{RMS}} = 205$  V,  $P_{bl} = 448$  W and  $I_{bl}$  (line) = 1.0 A.

Figure 3.22 shows the system voltage  $V_{pp}$  varying from 205 V with the  $BL$  connected to 250 V without the  $BL$  and when the  $SG$  has been removed and the  $IG$  is operating alone. In the last stage, the  $BL$  control returns and the system voltage  $V_{pp}$  returns to 205 V as well. The phase-phase voltage  $V_{bl_{RMS}}$  across  $BL$   $V_{bl_{RMS}}$  regulates the system frequency when the  $SG$  has been removed and the  $IG$  is operating alone. The system has one 2/3-kW  $RB$ . The Scenario is composed of  $V_{bl_{RMS}} = 205$  V,  $P_{bl} = 448$  W and  $I_{bl}$  (line) = 1.0 A.

Figure 3.23 shows the  $BL$  control actuation to keep the system frequency at 55.2 Hz when the  $SG$  has been removed and the  $IG$  is operating alone. The  $BL$  thyristor firing

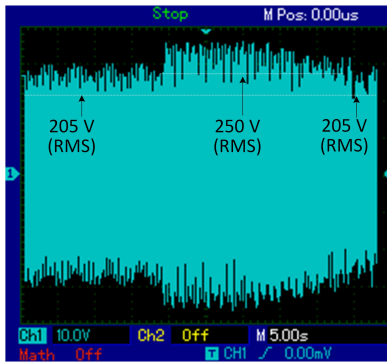


Figure 3.22 – Voltage  $V_{pp}$ -IG alone

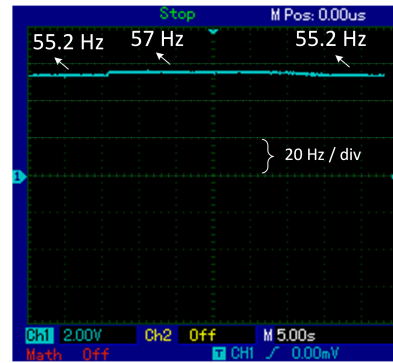


Figure 3.23 – BL control-IG alone

pulses are blocked, which results in elevation of the system frequency to 57 Hz. In the following, *BL* control is activated and acting in the system frequency again, returning it to 55.2 Hz. The system voltage  $V_{pp}$  varies from 205 V with *BL* to 250 V without *BL* and then when the *BL* control returns, it changes the system voltage  $V_{pp}$  to 205 V as well. The system has one-2/3 kW *RB* connected. The scenario is composed of  $V_{bl_{RMS}} = 205$  V,  $P_{bl} = 448$  W and  $I_{bl}$  (line) = 1.0 A.

### 3.5 Conclusion

The laboratory experiments were designed as two alternatives to control the system frequency which were successfully implemented.

Based on these experiments, when the frequency rises, the *SG* and  $DCM_{SG}$  become the *SM* and  $DCG_{SG}$ , respectively, due to excess of generation in the system caused by the *IG*.

To tackle the system frequency elevations due to the specific transients as also mentioned in chapter 2, two contingencies were implemented in laboratory, the first experiment consist of frequency control via ballast load in which was used a resistor bank, frequency converter and a digital control board MP 410T. The second experiment is an energy regeneration to the grid that consist of an analogical control board that is detailed in appendix A, a firing circuit and a resistor to protect the  $DCM_{SG}$  when the field inversion of DC machine is done. Both control the system frequency when the generated power is bigger than the demanded power.

In the case of the ballast load method, the process happens automatically, when the frequency goes up, the ballast load enters into system to decrease and control the frequency system. In the case of energy regeneration method, when the frequency goes up, the DC machine field is inverted via manual switch as already detailed in this chapter 3, the additional energy flows via converter whose firing angle was previously adjusted to  $140^\circ$ . Then, the system frequency is controlled into rated frequency, 55.0 Hz.

The results show that frequency control using a *BL* gives good performance, maintaining or controlling the system frequency in a stable way, while the system rated voltage is kept constant by the *SG* voltage control loop.

Unlike the *BL* method, which uses dissipation of energy, the *ERS* uses energy regeneration to achieve success. The *ERS* regulates the frequency faster than *BL* method: the *ERS* approach takes 1s and the *BL* method takes 3s to regulate the frequency, as shown in Figures 3.19 and 3.17 respectively. Both of these methods maintain the rated voltage in steady state using the voltage control loop of the *SG*.

The *BL* and *ERS* methods maintain the frequency controlled. The first keeps the frequency controlled in 55.2 Hz and the second keeps it in 55.0 Hz. This difference 0.2 Hz is important in order to avoid improper interference between the two control loops. This conclusion was obtained empirically.

It also was carried out an additional experiment that consisted of the removal of the *SG*, during operation of the *SG* and *IG* in parallel, in order to analyse the effects on the system voltage and frequency with and without *BL* control. When the *IG* operates alone, the system loses control of the voltage since the *SG* field control is not acting. In this case, although the system rated frequency is being controlled by the *BL* method, the system voltage  $V_{pp}$  varies considerably, from 205 to 250 V. When the *SG* has to be removed, the use of system voltage control scheme described in [10] and highlighted in purple in Figure 3.11 is strongly recommended. In order to use the cited voltage control scheme, the  $SW_a$  (*Interchangeable switch*) switch has to be changed from the *Vt1* to the *Vt2* (*Voltage signal from the frequency transducer (position 2)*) as shown in Figure 3.11.

The regulation frequency techniques described in this work were applied at the laboratory scale. The frequency range varied from 1 to 2 Hz in these experiments so that the proposed frequency control scheme could be validated. However, the techniques demonstrated here can be applied over a larger frequency range with similar results.

As previously informed, the *BL* method is more appropriate for an isolated electric system and the *ERS* method is a didactic alternative and serves as base of comparison and evaluation.

In future work, the automatic *IG* speed control is recommended for implementation as an alternative control method and as a continuation of this approach, in order to avoid *SG* synchronous machine motorization and an increase in system frequency. Therefore, this cited *IG* speed reference control would have the aim of changing the *IG* speed reference automatically instead of using the manual *IG* speed control.

# Conclusion

After the studies of DC machines regulators project (appendix A), thyristor firing circuit (appendix B), voltage regulators and filters project to synchronous machine (appendix C) and four-quadrant operations for DC machines (appendix D) was possible implement the target experiment of this work which consist of laboratorial scheme of induction and Synchronous generators in parallel operation mode feeding inductive and resistive loads. This experiment was target of analysis and studies of generation and load transients and specific contingencies for this kind of generators topology.

The main conclusions about the experiments are:

1. The *SG* presents a master behavior for the system frequency and voltage. *IG* does a master behavior for the active power supply and slave behavior for the system frequency and voltage. *SG* controls the system voltage and frequency and *IG* establishes the active power supplied to the system and *SG* complements the rest of active power and reactive power required;
2. The  $V_{aDCMIG}$  elevation method resulted in increase of  $P_{DCMIG}$ ,  $PIG$  and higher *IG* subgroup efficiency than the  $I_{fDCMIG}$  reduction method [28]. The increase of  $P_{DCMIG}$  and  $PIG$  are consequences of *IG* speed increase,  $n_{IG}$ , that was obtained by elevation of  $V_{aDCMIG}$ .
3. When the *IG* generates more than the load demand, the system frequency grows up and stays out of rated system frequency. The *IG* motorizes synchronous machine and  $DCM_{SG}$  operates as a no load  $DCG_{SG}$ ;
4. In the scenarios "*IG* out and *IG* in", *SG* and its system can regulate the system voltage and frequency and *SG* keeps running even if the *IG* is fully loaded and is removed abruptly. On the contrary, when the *SG* is disconnected, the system voltage and frequency go out of control.
5. Three control loops were implemented in lab to control the parallel operation of synchronous and induction generators, voltage and speed control loops and *BL* control loop.
6. Three different methods of *IG* connection into the electric system were studied as follow: (i) direct startup as a motor and rising the speed up to it turns *IG*, (ii) synchronism of self-excited *IG* with the electric system and (iii) adjustment of *IG* speed at synchronous speed and connection into the system;

7. It was used an original method to find power and efficiencies values of different equipment in different scenarios as demonstrated in chapters 1, 2 and complemented by appendix F;
8. The frequency elevation was checked when load transients happen in specific scenarios or *PIG* is bigger than load demand as demonstrated in chapters 2 and 3;
9. The effects of frequency elevation were cancelled due to implementation in lab of two methods of frequency control, these ones were compared, and their results shown.

Based on the results obtained, the operation in parallel of induction and synchronous generators in an isolated electric system is technically viable in *MHPP* and it should be economic advantageous for *MHPP* and other applications due to some reasons such as: the *IG* final price is so lower than *SG* final price even to big machines 25 MW (information has obtained from Brazil traditional machine supplier), *IG* maintenance is simpler and consequently cheaper and *IG* is lighter than *SG*. Beyond, The *IG*'s reply for short circuit events is better than *SG*'s one because the *IG* contributes less than *SG* to short circuit power, [20]. Otherwise, mainly for greater applications as oil platforms and *FPSO*, there are other equipment and accessories that may be required, such as capacitor bank, switches and filters which should be also considered for a more deeper economic and technical evaluation.

In the case of *SG* to be removed and the *IG* is operating alone and feeding the load as mentioned in chapter 3, the system voltage vary from 205 V to 250 V in spite of system frequency is in control, 55.2 Hz, by ballast load control. Then, the voltage range is so larger and for this specific scenario and reason, it is recommended the use of voltage control system which was detailed in [9]. The voltage control system can be interchangeable with the frequency control system used in this work by handling of a switch  $SW_a$  presented in chapter 3. It means that when the *IG* operates alone, it is recommended the use of voltage control system instead of frequency control system through by use of the cited interchangeable switch  $SW_a$ . It is expected that voltage keeps controlled in rated voltage, 220V, and system frequency varies a little bit such as 2 Hz to 3 Hz as in [9].

The chapter 3 is important in showing the causes of frequency increase and to show a method of *BL* control that could be useful for *MHPP* application as cited in [9], [16], and [17], whose generation could be composed for *IG* and *SG* in parallel operation mode. Thus, this *BL* method could be applicable in *MHPP* such as Boa Esperança and Lajeado Farms, cited in [9]. The *ERS* shown in this paper serves as a didactic application only.

# Appendix

# APPENDIX A – Filters and Regulators Project

## A.1 Introduction

In this appendix, two kinds of analogical filters and regulators for a DC motor will be studied, namely a speed regulator that is composed of a speed control loop and current regulators [37]. Both loops, the current control loop and speed control loop aim to control the DC motor speed.

These loops will be used in primary machines that will serve as the primary drives of induction and synchronous generators. The primary machines used in the experiments are independent excitation ones. They are proper to speed control because their speed is basically controlled by armature current or field flux variation.

Initially, in this appendix will be present some devices required in DC motor controllers such as a ramp type firing circuit and synchronism transformer.

And then, it will be followed by practical cases and instructions of how design the analogical speed and current DC machine regulators and how define filters, capacitors, resistors and others necessary devices to implement the regulators. In add, all of the time constants and gains values will be estimated or calculated and the experiments will be didactically presented.

All the issues studied in this appendix are based on original and practical-case projects carried out and tested in the Laboratory of research development of electrical didactic laboratory of Federal University of Itajubá.

The analogical voltage regulator will be shown in appendix C.

## A.2 Ramp Firing Circuit

The ramp-type firing system are used in all the experiments accomplished in this work and its functioning shown in Figure A.1 was implemented either with an analogical circuit detailed in appendix B and chapter 3 or inside of the electronic board MP 410T algorithm used in chapters 1, 2 and 3:

The intersection of the DC level with a ramp, which is internally generated in the TCA 785 integrated circuit, produces the pulses. The  $V_{cc}$  (*Control voltage of thyristor firing system*) is the output of the current regulator. Three TCA 785 integrated circuits

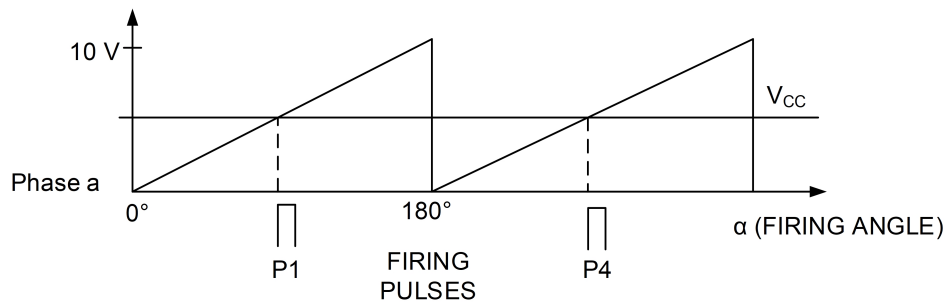


Figure A.1 – Ramp Type Firing Circuit

should be used to produce six firing pulses for the Graetz converter bridge that is built by thyristors. The pulses generated by TCA 785 are P1 and P4 for the thyristors 1 and 4; P3 and P6 for the thyristors 3 and 6; and P5 and P2 for the thyristors 5 and 2 respectively. This is the explanation of the firing circuit pulse generation stage.

The other additional firing circuit functions such as enlargement of pulses, galvanic isolation of pulses and pulse amplification will be shown in details in appendix B.

### A.3 Synchronism Transformer

The synchronism transformer function causes a  $30^\circ$  displacement on the grid voltage signal in order to synchronize this grid voltage and the interested start points with the thyristor firing angle, as demonstrated in Figure A.2. This kind of transformer is shown in Figure A.3 and it will be used in this work as a device necessary in the driven system.

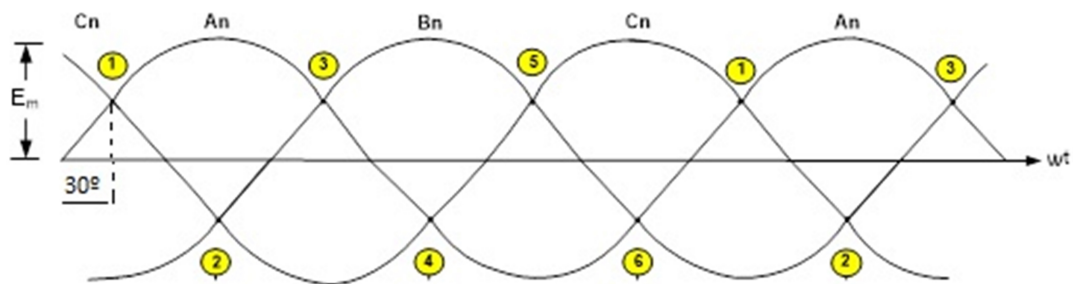
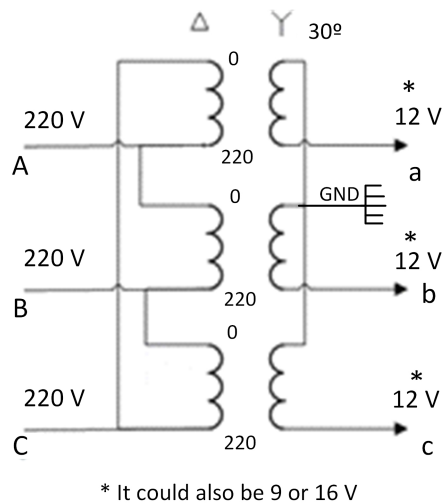


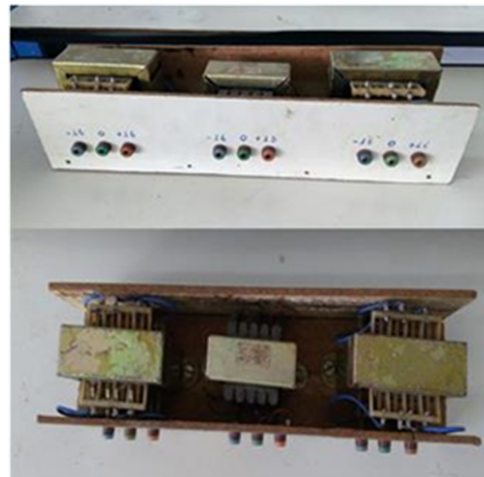
Figure A.2 – Waveforms and Firing Angle

This kind of transformer is used in practically all experiments carried out in this work.

Figure A.4 shows the synchronism transformer in a typical diagram which will be used in the experiments. Each TCA 785 controls the two thyristors connected to its respective phase, e.g., the TCA 785 located in phase a controls the two thyristor firing angles located in phase a, thyristors 1 and 4. For more details, see the Figure B.12 of appendix B.



(a) Synchronism Transformer Diagram



(b) Synchronism Transformer Views

Figure A.3 – Synchronism Transformer

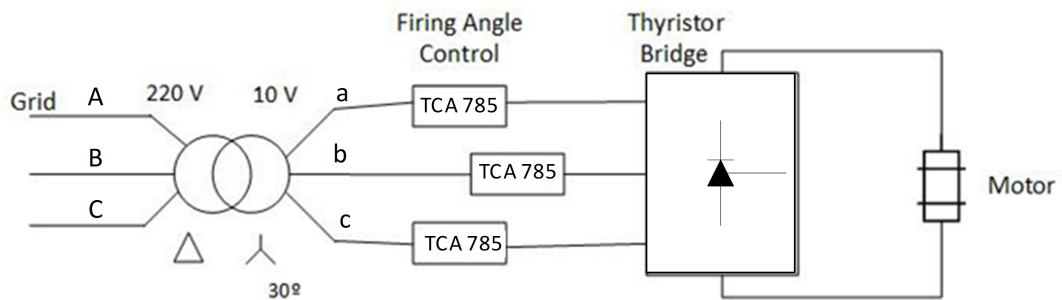


Figure A.4 – General view of Synchronism Transformer

## A.4 Current and Speed Regulators of DC machine project

### A.4.1 Introduction

The digital regulators were implemented in [38] and in the chapters 1, 2 and 3. The analogical current and speed regulators of DC machine will be described and detailed in this appendix and it was implemented in chapter 3.

### A.4.2 Motor Block Diagram

Figure A.5 shows the motor armature circuit and the driven system of *DCM*, *SM* (*Synchronous machine*) and load. The diagram of the driven system mechanical part is also presented in [38, 39].

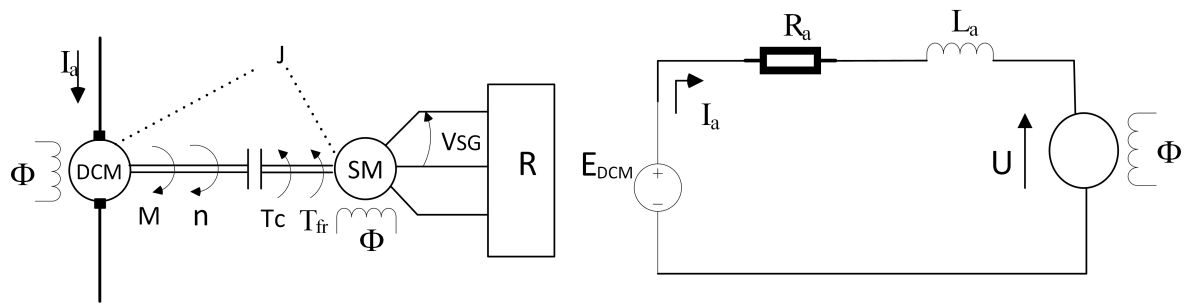


Figure A.5 – Motor Armature Circuit and Diagram of the Drive System Mechanical Part

where:

$U$  Counter electromotive force [V]

$E_{DCM}$  (Direct current motor voltage) [V]

$R_a$  (Armature circuit resistance)

$L_a$  (Armature circuit inductance)

$\phi$  Motor flux

$I_a$  (Armature current)

$M$  Motor torque

$T_c$  (Load torque)

$T_{fr}$  (Friction torque)

$J$  Moment of inertia (motor + load)

$n$  Speed [rpm]

$\omega$  Rotation [rad/s]

$B$  Resultant torque

Also:

$$M = k \times \phi \times I_a \quad (\text{A.1})$$

For the accelerating torque:

$$M - T_c = B \quad (\text{A.2})$$

$$B = J \times \frac{d\omega}{dt} \quad (\text{A.3})$$

$$\omega = \frac{2 \times \pi}{60} \times n_0 \times \frac{n}{n_0} \quad (\text{A.4})$$

where:

$n_0$  No load speed [rpm]

$M_n$  Rated torque.

$$B = M_n \times \frac{B}{M_n} \quad (\text{A.5})$$

Substituting A.4 and A.5 into A.3 results in:

$$M_n \times \frac{B}{M_n} = J \times \frac{d_{\frac{2\pi}{60} \times n_0 \times \frac{n}{n_0}}}{dt} \quad (\text{A.6})$$

$$M_n \times \frac{B}{M_n} = J \times \frac{2\pi \times n_0}{60 \times n_0} \times \frac{dn}{dt}$$

$$n = \frac{n_0}{M_n} \times \frac{1}{\frac{2\pi J n_0}{60 M_n}} \int B \cdot dt \quad (\text{A.7})$$

The  $\tau_H$  (*Accelerating time constant*) is defined as:

$$\tau_H = \frac{2\pi J n_0}{60 M_n} \quad (\text{A.8})$$

This time constant may be interpreted as the time required for the motor to reach no load speed from rest, as it is accelerated by a resultant torque equal to the rated motor torque.

$$n = \frac{n_0}{M_n \tau_H} \int B \cdot dt \quad (\text{A.9})$$

Figure A.6 shows the block diagram related to the motor mechanical part.

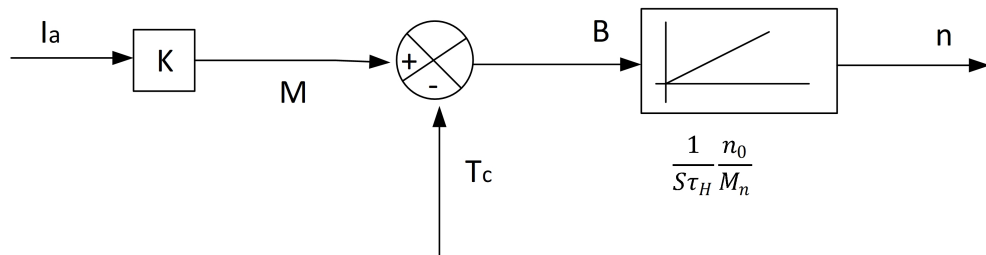


Figure A.6 – Block diagram of the drive mechanical part

Setting the values in pu (per unit) for the current, load torque, speed and motor torque results in:

$$\frac{I_a}{I_N} = i_a(\text{pu})$$

$$\frac{T_c}{M_n} = t_c(pu)$$

$$\frac{B}{M_n} = b(pu)$$

$$\frac{n}{n_0} = n_u(pu)$$

$$\frac{M}{M_n} = m(pu)$$

The mechanical block diagram of Figure A.6 can be represented in pu as shown in Figure A.7.

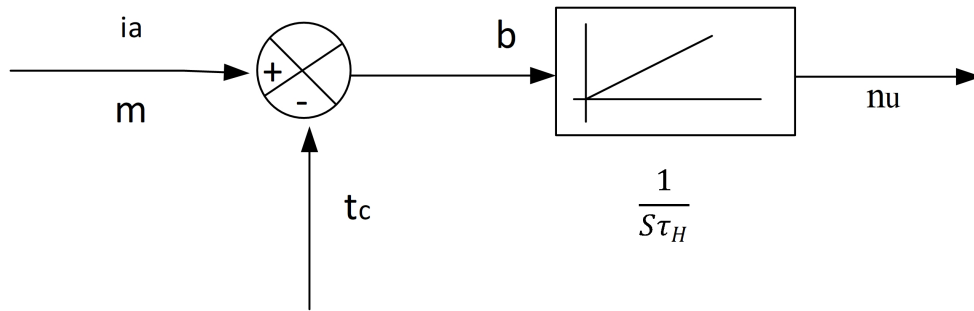


Figure A.7 – Representation of the Motor Mechanical Part in pu

Notes: 1- All variables from Figure A.6 are shown in Figure A.7 in per unit mode and lower-case letters. 2- The variables  $i_a$  (*Armature current in pu*) and  $m$  (*Motor torque in pu*) are equal.

### A.4.3 Armature Circuit Equations

In order to define the  $\tau_a$  (*Inductor circuit or armature time constant*) and the block diagram, the calculus are shown in the following.

$$E_{DCM} = R_a I_a + L_a \frac{dI_a}{dt} + U \quad (A.10)$$

Applying the Laplace transform results in:

$$E_{DCM} = R_a I_a(S) + S L_a I_a(S) + U(S)$$

$$E_{DCM} = U(S) = I_a(S) [R_a + S L_a]$$

$$i_{a(S)} = \frac{E_{DCM}(S) - U(S)}{R_a + SL_a} \quad (\text{A.11})$$

Defining  $\tau_a$ :

$$\tau_a = \frac{L_a}{R_a} \quad (\text{A.12})$$

$$I_a(S) = \frac{E_{DCM}(S) - U(S)}{1 + S\tau_a} \times \frac{1}{R_a} \quad (\text{A.13})$$

$$\frac{I_a}{I_N} \times I_N = \frac{E_{DCM} - U}{R_a} \times \frac{E_N}{E_N} \times \frac{1}{1 + S\tau_a}$$

$$\frac{I_a}{I_N} = \frac{E_{DCM} - U}{E_N R_a} \times \frac{E_N}{I_N} \times \frac{1}{1 + S\tau_a}$$

$$\frac{I_a}{I_N} = \frac{E_{DCM} - U}{E_N} \times \frac{E_N}{R_a I_N} \times \frac{1}{1 + S\tau_a}$$

The armature current  $I_a$  seems to be normalized by the current  $I_N$  (*Rated Current*). Voltages  $E_{DCM}$  and  $U$  are also normalized by the voltage  $E_N$  (*Rated voltage*). The normalized values are set as:

$$I_a = \frac{I_a}{I_N} \quad (\text{A.14})$$

$$e = \frac{E_{DCM}}{E_N} \quad (\text{A.15})$$

$$u = \frac{U}{E_N} \quad (\text{A.16})$$

$$V_i = \frac{E_N}{R_a I_N} \quad (\text{A.17})$$

where  $V_i$  (*Motor current amplification factor*).

The block diagram of the DC motor armature circuit is shown in Fig. A.8.

The factor  $\frac{V_i}{1+S\tau_a}$  can be considered a delay element of the 1st order. The time constant  $\tau_a$  can be determined in one of two alternative ways:

a) Measuring  $L_a$  and  $R_a$ ;

b) Applying a reduced voltage step in the armature circuit at the moment that the rotor of the motor is blocked.

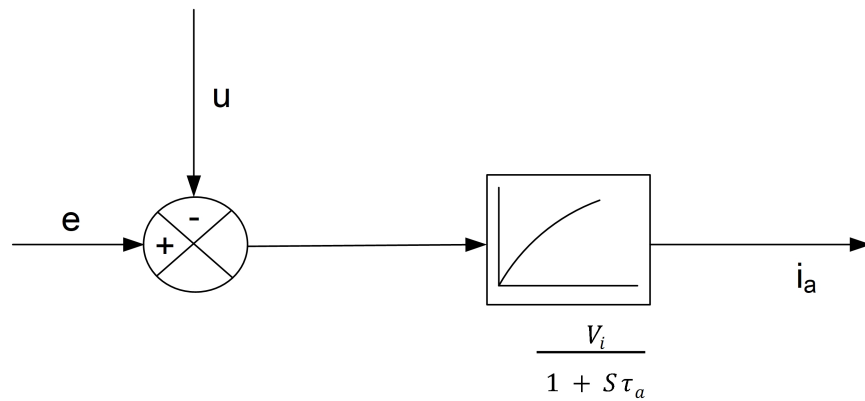


Figure A.8 – Block Diagram of the DC Motor Armature Circuit

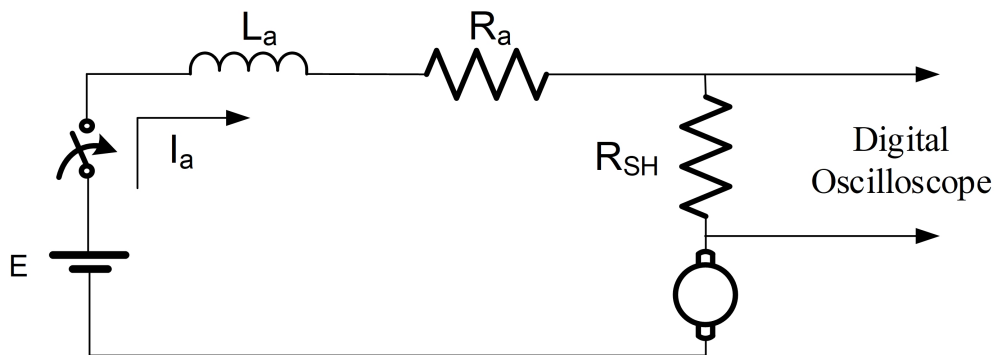


Figure A.9 – Reduced Voltage step Applied to the Armature Circuit

Figure A.9 shows the reduced voltage step applied to the armature circuit.

The current  $i_a$  is captured through an oscillograph or digital oscilloscope (voltage drop in the  $R_{SH}$  (*Shunt resistor*)). The shunt resistor  $R_{SH}$  can be replaced by a current Hall sensor, which is a usual alternative. Figure A.10 shows the expected time transient response.

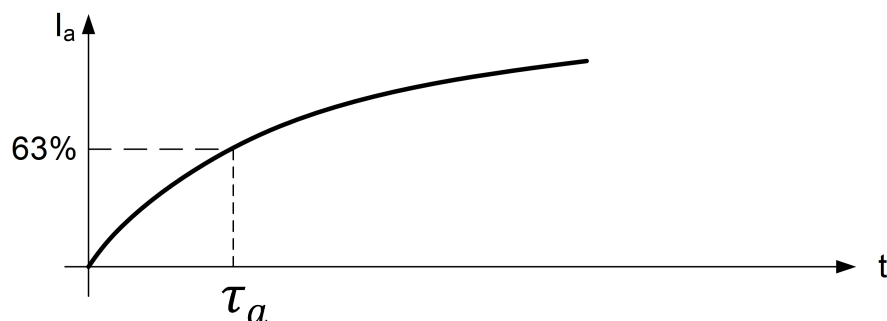


Figure A.10 – Current Response for a Voltage step Applied to the Armature Circuit

Marking up to 63% of the regime value and checking the corresponding time on

the horizontal axis that corresponds to a time constant  $\tau_a$ .

$$i_a = \frac{e - u}{1 + s\tau_a} V_i \quad (\text{A.18})$$

An interpretation of the constant  $V_i$  is given in A.18. The  $V_i$  is a multiplicative factor when the motor has the rotor locked and with rated voltage applied to the armature.

$$I_{AK} = \frac{E_N}{R_a} \quad (\text{A.19})$$

$$\frac{I_{AK}}{I_N} = \frac{E_N}{R_a I_N} \quad (\text{A.20})$$

Comparing (A.19) and (A.17) results in:

$$I_{AK} = V_i I_N \quad (\text{A.21})$$

Thus, the  $V_i$  factor can be interpreted as the multiplicative factor of the rated current to get a  $I_{AK}$  (*Locked rotor current*), when nominal voltage is applied to the armature circuit (starting current in pu).

Figure A.11 shows the schematic diagram of the separated excitation DC motor with rated flux and considering the normalized magnitudes (pu) in lower case letters.

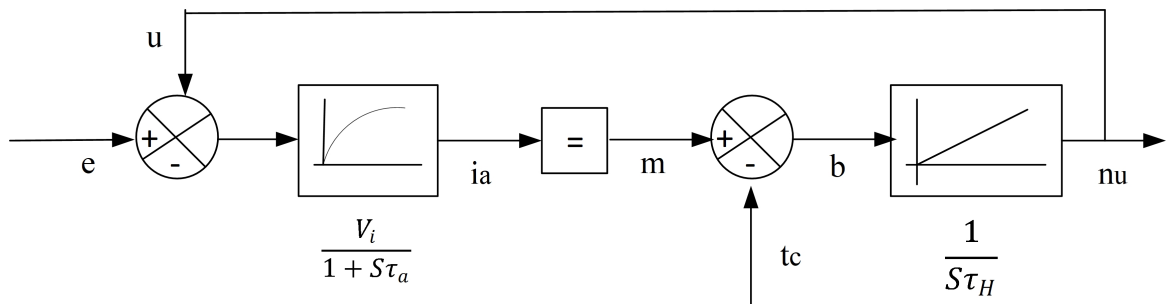


Figure A.11 – Schematic Block Diagram of the Independent Excitation DC Motor

#### A.4.4 Complete Block Diagram with Regulators, Filters and Transducers

Figure A.12 shows the complete block diagram of the controlled drive.

where:

$\tau_{gs1}$  (*Filter time constant of the reference channel of the speed loop*)

$\tau_{gs2}$  (*Filter time constant of the reference channel of the current loop*)

$V_{Rn}$  (*Gain of the speed regulator*)

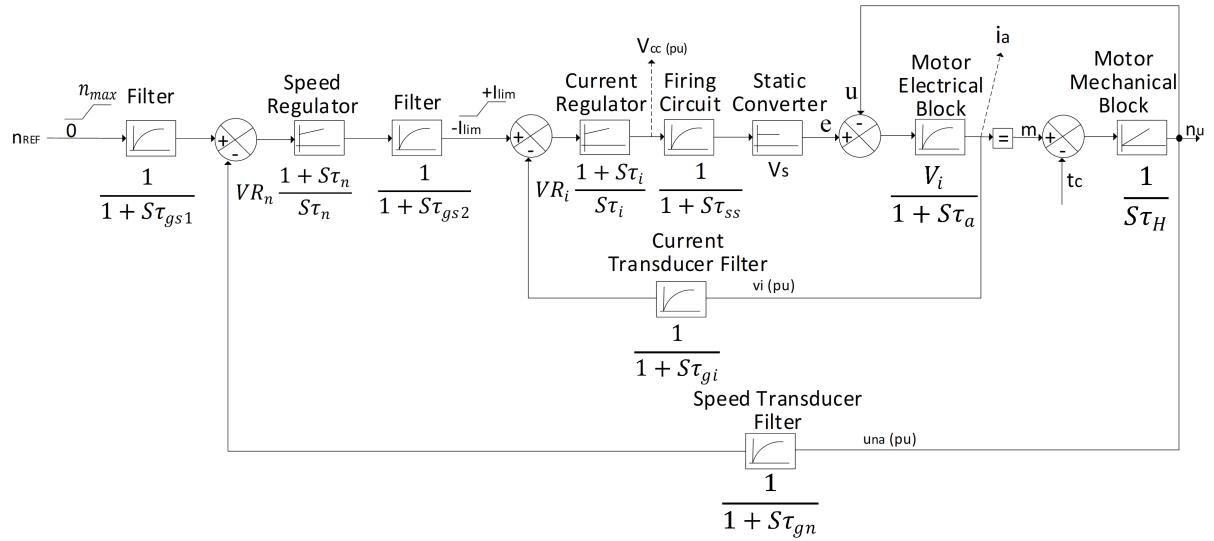


Figure A.12 – Complete Block Diagram of Controlled Drive

$V_{Ri}$  (Gain of the current regulator)

$\tau_n$  (Time constant of the speed regulator )

$\tau_i$  (Current regulator time constant)

$\tau_{gn}$  (Filter time constant of the speed transducer )

$\tau_{gi}$  (Filter time constant of the current transducer)

$\tau_{ss}$  (Firing circuit time constant )

$V_s$  (Gain of the static converter)

$\tau_a$  Inductor circuit or armature time constant

$V_i$  (Gain of machine electric part)

$V_{cc}$  Control voltage of thyristor firing circuit

$i_a$  Armature current in pu

$t_c$  (Load torque in pu)

$n_u$  (Speed in pu)

$n_{REF}$  (Reference speed)

The regulators shown in Fig. A.12 were considered as PI (proportional integral) and their parameters will be determined by the design procedure in this work.

## A.5 Current Regulator and Filters Project of DC Machine (practical case)

In this appendix will be described the current control loop with current regulators and filters parameters project [39].

Figure A.13 shows the current regulation loop and Table A.1 shows the DC motor data.

The current transducer is a diode bridge connected between a resistor and the

Table A.1 – DC Motor Data

Power (kW)	Rated current (A)	Rated speed (rpm)	No load speed (rpm)	Voltage (V)	Armature resistance ( $\Omega$ )	Armature inductance (mH)	Accel. <sup>1</sup> time constant $T_H$ (s)	Rated torque Nm	J inertial moment ( $kg.m^2$ )
1.7	7.72	1500	1770	220 V	7.0	490	1.54	10.8	0.09

<sup>1</sup> accelerating

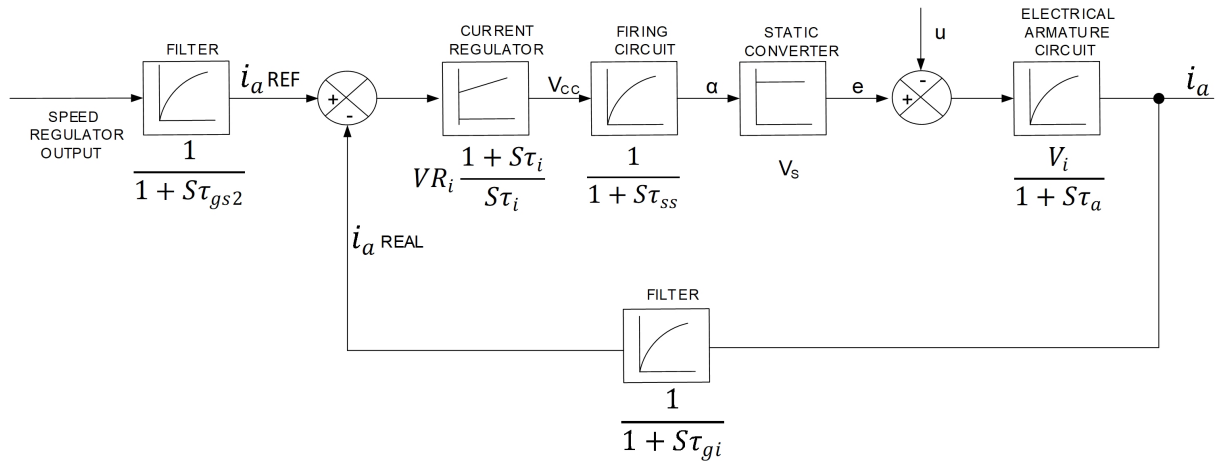


Figure A.13 – Current Regulation Loop

alternating current side. The diode bridge is fed by the 30/5 A *CT (Current transformer)* secondary. Figure A.14 shows the current transducer connected in a typical DCM driven circuit.

where:

$L_d$  (*Smoothing reactor inductance*)

$L_s$  (*Separated field inductance*)

The  $v_i$  (*Signal from the current transducer*) has a 1/6 cycle ripple wave. Thus, the filter time constant of the current transducer is:

$$\tau_{gi} \leq \frac{1}{2} \frac{\text{period}}{\text{number of pulses}} (s) \tag{A.22}$$

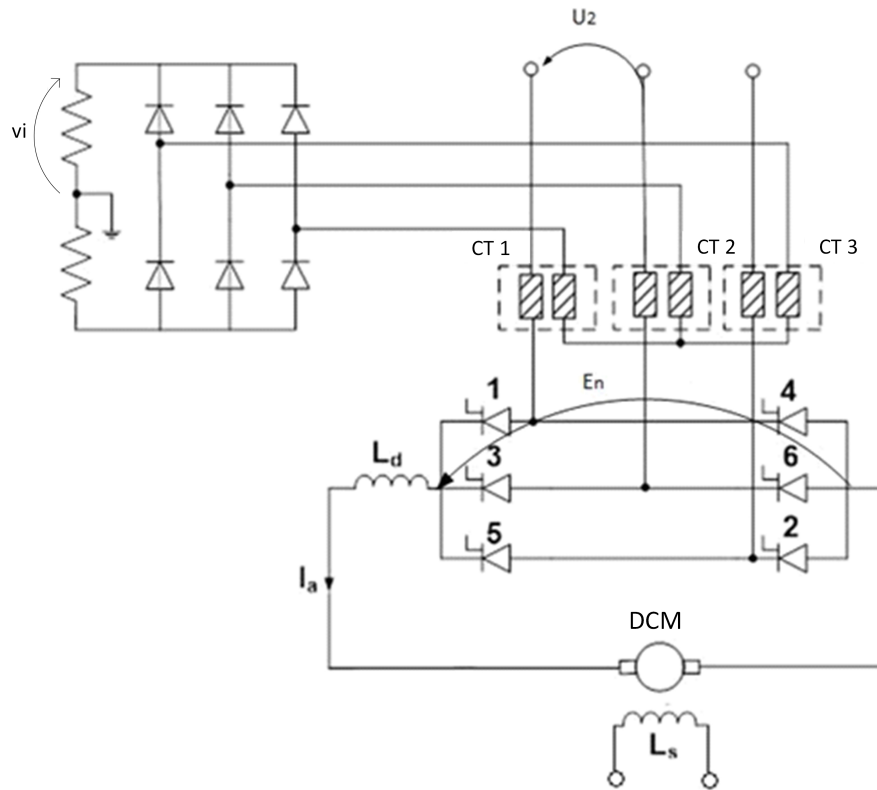


Figure A.14 – Current Transducer

$$\tau_{gi} \leq \frac{1}{2} \times \frac{16.7 \times 10^{-3}}{6} \quad (s) \quad \therefore \tau_{gi} \leq 1.39 \text{ ms}$$

For 60 Hz, a period of 16.7 ms and a six-pulse bridge, the filter time constant of the current transducer is then adopted as:

$$\tau_{gi} \leq 1.39 \text{ ms} \quad (\text{A.23})$$

The firing circuit cannot instantly respond to the change in the firing angle  $\alpha$ . This time constant can vary in the range of zero to one sixth of a cycle. Thus, the time constant of the firing circuit  $\tau_{ss} = 2.5 \text{ ms}$  is defined.

From the armature resistance  $R_a$  and armature inductance  $L_a$ , the inductor circuit time constant  $\tau_a$  was obtained measuring  $L_a$  and  $R_a$  and calculated as demonstrated below.

$$\tau_a = \frac{L_a}{R_a} = \frac{490 \times 10^{-3}}{7} \quad (\text{A.24})$$

$$\tau_a = \frac{L_a}{R_a} = 70 \text{ ms} \quad (\text{A.25})$$

This constant  $\tau_a$  was calculated considering the total inductance  $L_a$  in series with the armature circuit, which corresponds to the inductance of the machine added to the inductance of the external smoothing reactor.

Considering  $E_N$  equal to the rated voltage at the rectifier bridge output, the  $V_i$  (motor current amplification factor) is:

$$V_i = \frac{E_n}{R_a \times I_a} = \frac{220}{7 \times 7.72} = 4.07 \quad (\text{A.26})$$

The gain of the converter  $V_s$  is obtained as follow, considering that the overlapping effect is neglected.  $E$  (*DC supply voltage*) is given by equation:

$$E = 1.35 \times U_2 \times \cos\alpha \quad (\text{A.27})$$

$U_2$  (*AC supply voltage*) is applied on the converter bridge:

$$\frac{dE}{d\alpha} = -1.35 \times U_2 \times \sin\alpha \quad (\text{A.28})$$

Multiplying part by part by  $\frac{\pi}{E_N}$  results in:

$$\frac{d\left(\frac{E}{E_N}\right)}{d\left(\frac{\alpha}{\pi}\right)} = -1.35 \times \frac{U_2}{E_N} \times \pi \times \sin\alpha \quad (\text{A.29})$$

In order to define  $U_2$ , the *AC* supply voltage applied on the converter bridge and neglecting the overlap angle  $\mu$ , the following equation is used:

As  $E_n = 220V$  and considering the firing angle  $\alpha = 30^\circ$

$$220 = 1.35 \times U_2 \times \cos(30^\circ) \therefore U_2 = 188 V \quad (\text{A.30})$$

Then, considering  $\alpha_u$  equal to  $\alpha_u = \frac{\alpha}{\pi}$  and substituting Equation A.30 in A.29, results in:

$$\frac{d_e}{d\alpha_u} = -1.35 \times \frac{188}{220} \times \pi \sin\alpha \therefore \frac{d_e}{d\alpha_u} = -1.15\pi \sin\alpha \quad (\text{A.31})$$

resulting in:

$$V_S = \left| \frac{d_e}{d\alpha_u} \right| = 1.15 \times \pi \times \sin\alpha$$

When  $\alpha = 90^\circ$ , the maximum gain is:

$$V_{S1} = \frac{d_e}{d\alpha_u} = 1.15 \times \pi \therefore V_{S1} = 3.61 \quad (\text{A.32})$$

For  $\alpha = 30^\circ$ , the gain is given by:

$$V_{S2} = \frac{d_e}{d\alpha_u} = 1.15 \times \pi \times 0.5 \therefore V_{S2} = 1.80 \quad (\text{A.33})$$

The average gain of static converter  $V_s$  can be determined as:

$$V_s = \frac{V_{S1} + V_{S2}}{2} = 2.71 \quad (\text{A.34})$$

The current regulation system gain is then obtained:

$$V_{sia} = V_s \times V_i = 2.71 \times 4.07 = 11.03 \quad (\text{A.35})$$

The sum of the small-time constants  $\alpha$  is:

$$\sigma = \tau_{ss} + \tau_{gi} = 2.5 + 1.39 \therefore \sigma = 3.89 \quad (\text{A.36})$$

Then:

$$\frac{\tau_a}{4\sigma} = \frac{70}{4 \times 3.89} = 4.50 > 1 \quad (\text{A.37})$$

According to Table 6.3 from [4], the regulator type  $PI$  should be adopted.

According to Table 6.4 from [4], the gain and the time constant of the regulator  $V_{Ri}$  can be obtained:

$$V_{Ri} = \frac{\tau_a}{2 \times V_{sia} \times \sigma} = \frac{70}{2 \times 11.03 \times 3.89} = 0.8 \quad (\text{A.38})$$

Then, the current regulator time constant  $\tau_i$  is:

$$\tau_i = 4 \times \sigma \times \frac{\tau_a}{\tau_a + 3 \times \sigma} = 4 \times 3.89 \times \frac{70}{70 + 3 \times 3.89} = 13.34ms \quad (\text{A.39})$$

The time constant value of the reference channel filter [ms] is:

$$\tau_{gs2} = 4 \times \sigma \times (1 - e^{-(\frac{\tau_a}{4 \times \sigma} - 1)}) \quad (\text{A.40})$$

$$\tau_{gs2} = 4 \times 3.89 \times (1 - e^{-(\frac{70}{4 \times 3.89} - 1)}) = 15.09ms \quad (\text{A.41})$$

Capacitors Calculus

- Reference value filter:

$$C_s = \frac{R_{S1} + R_{S2}}{R_{S1} \times R_{S2}} * \tau_{gs2} \quad (\text{A.42})$$

$$C_s = \frac{22 + 22}{22 \times 22} \times 15.09 \mu F = 1.37 \mu F \quad (\text{A.43})$$

- Current transducer filter

$$C_i = \frac{R_{i1} + R_{i2}}{R_{i1} \times R_{i2}} * \tau_{gi} \quad (\text{A.44})$$

$$C_i = \frac{15 + 15}{15 \times 15} \times 1.39 \therefore C_i = 0.19 \mu F \quad (\text{A.45})$$

The closest and chosen capacitors values were  $C_s = 1.22 \mu F$  and  $C_i = 0.22 \mu F$  as shown in Fig. A.15.

### A.5.1 Current Regulator Parameters

In summary, the current regulator parameters are shown in Table A.2:

Table A.2 – Current Regulator Parameters

Type	Gain ( $V_{Ri}$ )	Time Constant ( $\tau_i$ )	Reference channel Filter time constant ( $\tau_{gs2}$ )	Feedback channel filter time constant ( $\tau_{gi}$ )
PI	0.8	13.34	15.09	1.39

### A.5.2 Current Regulator Arrangement

Figure A.15 shows the current regulator. Its inner current loop structure was proposed by [4].

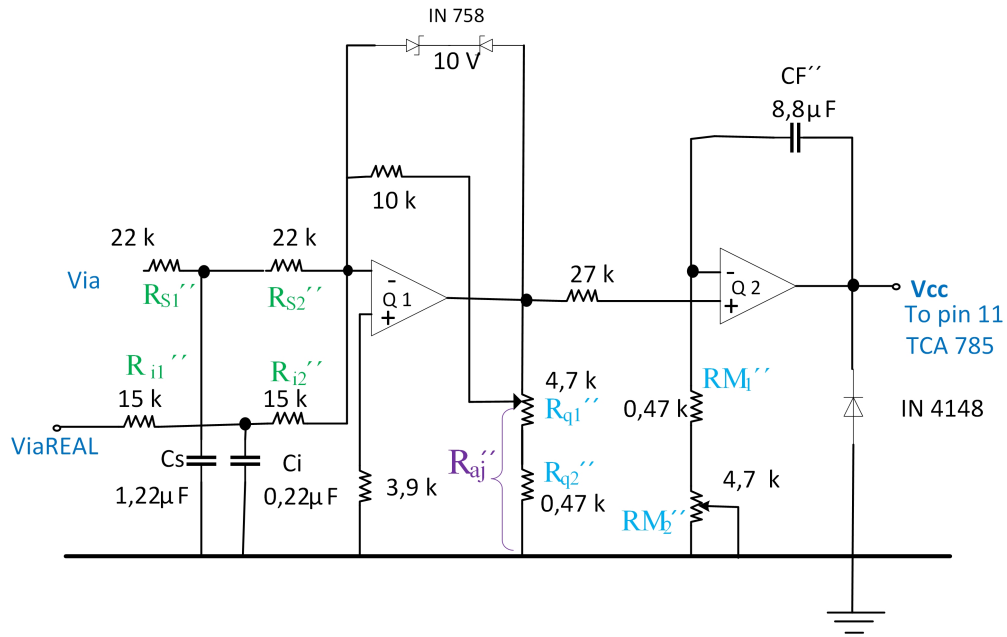


Figure A.15 – Implementation of Current Regulator

#### A.5.2.1 Calculus of $RM_2''$ and $Rq_1''$

In order to make the adjustment of  $RM_2''$  (*Integral branch adjustment resistor of current regulator*) and  $Rq_1''$  (*Proportional branch adjustment resistor of current regulator*), the specific values of each one of these resistors will be calculated.

$RM_2''$  was obtained as:

$$\tau_n = (RM_1'' + RM_2'') \times CF'' \quad (\text{A.46})$$

$$RM_1'' + RM_2'' = \frac{\tau_i}{CF''} = \left( \frac{13.34 \times 10^{-3}}{8.8 \times 10^{-6}} \right) = 1.52 \text{ k}\Omega \quad (\text{A.47})$$

$$RM_2'' = \frac{\tau_i}{CF''} - RM_1'' = 1520 - 470 = 1.05 \text{ k}\Omega \quad (\text{A.48})$$

The  $R_{aj}''$  (*adjustment resistance of current regulator*) was calculated as:

$$R_{aj}'' = \frac{(R_F'' \times (R_{q1}'' + R_{q2}''))}{(V_{Ri} \times (R_{i1}'' + R_{i2}''))} \quad (\text{A.49})$$

$$R_{aj}'' = \frac{(10 \times (4.7 + 0.47))}{(0.8 \times (15 + 15))} \times 10^3 \quad (\text{A.50})$$

$$R_{aj}'' = 2.15 \text{ k}\Omega \quad (\text{A.51})$$

Then, as  $R''_{q2}$  (*Proportional branch steady resistor of current regulator*)=470  $\Omega$

$$R''_{q1} + R''_{q2} = 2150 \Omega \quad (\text{A.52})$$

$$R''_{q1} = 2150 - 470 \Omega \quad (\text{A.53})$$

$$R''_{q1} = 1.68 \text{ k}\Omega \quad (\text{A.54})$$

Adopting the  $V_{Ri}$  as the variable in evidence, it will be possible to find the  $V_{Ri}$  limits by just changing  $R''_{aj}$  as follows.

Equation A.49 and isolating the variable  $V_{Ri}$ , it results in:

$$V_{Ri} = \frac{(R''_F \times (R''_{q1} + R''_{q2}))}{(R''_{aj} \times (R''_{i1} + R''_{i2}))} \quad (\text{A.55})$$

For the minimum  $R''_{aj}$ =0.47 k  $\Omega$ , the maximum  $V_{Ri}$  is:

$$V_{Ri}max = \frac{(10 \times (4.7 + 0.47))}{(0.47 \times (15 + 15))} = 3.6 \quad (\text{A.56})$$

For the maximum  $R''_{aj}$ = 4.8 k  $\Omega$ , the minimum  $V_{Ri}$  is:

$$V_{Ri}min = \frac{(10 \times (4.7 + 0.47))}{(5.17 \times (15 + 15))} = 0.33 \quad (\text{A.57})$$

Thus, as the defined resistors, the  $V_{Ri}$  can vary from 0.33 to 3.6.

The current regulator data are given in Table A.3.

Table A.3 – Complementary Current Regulator Data

Optimized $R''_{aj}$	$R''_{q1}$	$RM''_2$	Optimized gain ( $V_{Ri}$ )	Minimum gain ( $V_{Ri}min$ )	Maximum gain ( $V_{Ri}max$ )
2.15 k $\Omega$	1.68 k $\Omega$	1.05 k $\Omega$	0.8	0.33	3.6

## A.6 Speed Regulators and Filters Project of DC machine (practical case) Project

In order to define the parameters of speed filters and regulators [38, 39, 37], the current loop will be replaced by a first order delayed block whose equivalent time constant is  $\tau_e$  (*Equivalent time constant*) as in [4]:

$$\tau_e = 2 \times \sigma + \frac{1}{2} \times \tau_{gs2} \quad (\text{A.58})$$

$$\tau_e = 2 \times 3.89 + \frac{1}{2} \times 15.09 \approx 15 \text{ ms} \quad (\text{A.59})$$

In that way, the speed block diagram can be represented as in Figure A.16, [40]:

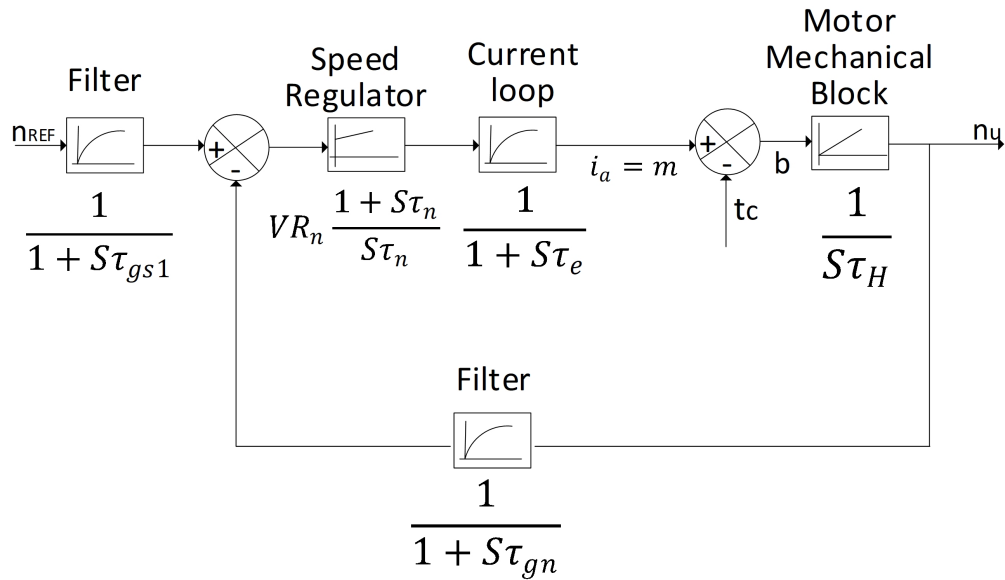


Figure A.16 – Speed Regulation Loop

The speed transducer filter time constant is  $\tau_{gn} = 100$  ms.

The speed loop has the following time constants:

$\tau_H$  (accelerating time constant) = 1.54 s

$\tau_e$  (equivalent time constant of current stabilization loop) = 15 ms

$\tau_{gn}$  (speed transducer filter time constant) = 100 ms

The small-time constants  $\tau_e$  and  $\tau_{gn}$  will be replaced by representative time constant  $\sigma'$  as follows:

$$\sigma' = \tau_e + \tau_{gn} \quad (\text{A.60})$$

$$\sigma' = 15 + 100 = 115 \text{ ms} \quad (\text{A.61})$$

As the division  $\frac{\tau_H}{4 \times \sigma'} = \frac{1.54}{4 \times 0.115} = 3.34 > 1$ , then, in accordance with Table 6.3 from [4], a proportional-integral regulator (PI) should be used.

From Table 6.4 from [4], the optimized gain and time constant of the regulator are:

$$V_{RN} = \frac{\tau_H}{2 \times \sigma'} = \frac{1.54}{2 \times 0.115} = 6.7 \quad (\text{A.62})$$

$$\tau_n = 4 \times \sigma' = 460 \text{ ms} \quad (\text{A.63})$$

The speed transducer is a tachogenerator coupled with the DC motor shaft. The filter was used to reduce the high wave that was part of the tachogenerator output voltage. The considered time constant was:

$$\tau_{gn} = 100 \text{ ms} \quad (\text{A.64})$$

The reference channel filter has the following time constant:

$$\tau_{gs1} = 4 \times \sigma' \times (1 - e^{-(\frac{\tau_H}{4 \times \sigma'})^{-1}}) = 416 \text{ ms} \quad (\text{A.65})$$

### A.6.1 Capacitors calculus

Adopting the resistances  $R'_{s1} = R'_{s2} = 100 \text{ k}\Omega$  as part of the reference value filter and  $R'_{i1} = R'_{i2} = 100 \text{ k}\Omega$  as part of the speed transducer filter, it results in:

- Reference value filter capacitor:

$$C_n = \frac{R'_{s1} + R'_{s2}}{R'_{s1} \times R'_{s2}} * \tau_{gs1} = 8.32 \text{ }\mu\text{F} \quad (\text{A.66})$$

The closest capacitor value was got by four capacitors  $2.2 \text{ }\mu\text{F}$  in parallel, resulting in  $8.8 \text{ }\mu\text{F}$ .

- Speed transducer filter capacitor:

$$C_L = \frac{R'_{i1} + R'_{i2}}{R'_{i1} \times R'_{i2}} * \tau_{gn} = 2.2 \text{ }\mu\text{F} \quad (\text{A.67})$$

## A.6.2 Speed Regulator Parameters

In summary, the speed regulator parameters are shown in Table A.4.

Table A.4 – Speed Regulator Parameters

Type	Gain ( $V_{RN}$ )	Time Constant ( $\tau_n$ )	Reference channel Filter time constant ( $\tau_{gs1}$ )	Speed transducer filter time constant ( $\tau_{gn}$ )
PI	6.7	460	416	100

Figure A.17 shows the speed regulator. This speed regulator structure was proposed by [4]

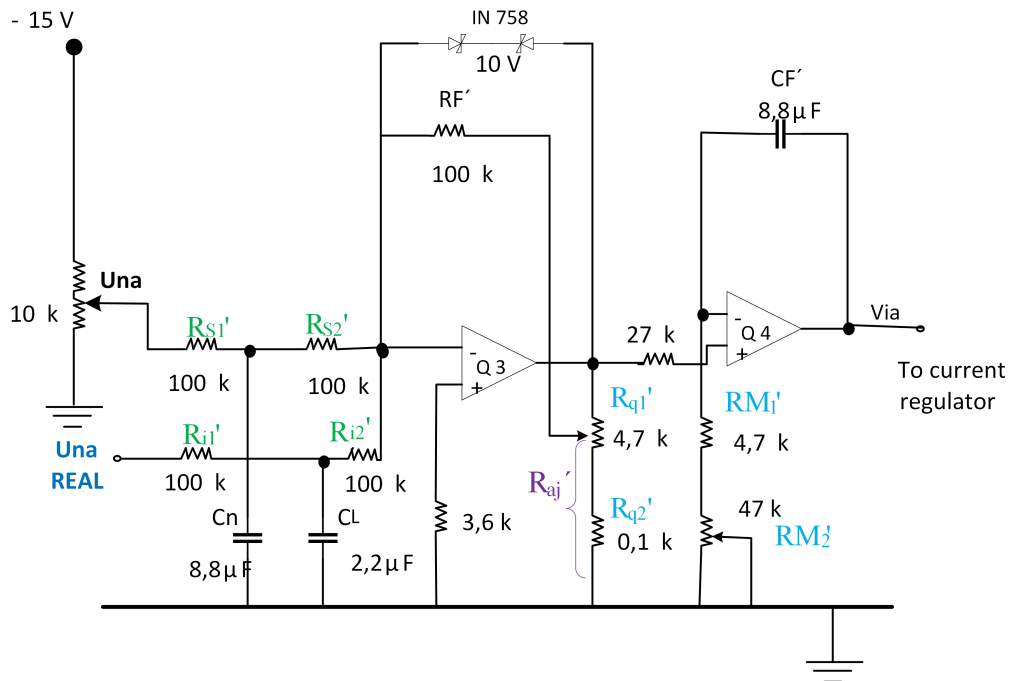


Figure A.17 – Implementation of Speed Regulator

### A.6.2.1 Calculus of $RM_2'$ and $R_{q1}'$

In order to do the adjustment of  $RM_2'$  (*Integral branch adjustment resistor of speed regulator*) and  $R_{q1}'$  (*Proportional branch adjustment resistor of speed regulator*), the specific values for each of these resistors will be calculated.

$RM_2'$  was obtained as follow:

$$\tau_n = (RM_1' + RM_2') \times CF'$$

$$(RM_1' + RM_2') = \frac{\tau_n}{CF'} = \frac{460 \times 10^{-3}}{8.8 \times 10^{-6}} = 52.27 \text{ k}\Omega \quad (\text{A.68})$$

$$RM'_2 = \frac{\tau_n}{CF'} - RM'_1 = 52.27 - 4.7 = 47.57 \text{ k}\Omega \quad (\text{A.69})$$

Note: The  $RM'_2$  was adjusted in 47.0 k $\Omega$ , the maximum value available.

Follow the calculus used to calculate the adjustment resistance  $R'_{aj}$  (*adjustment resistance of speed regulator*) and  $R'_{q1}$ :

$$R'_{aj} = \frac{(R_F \times (R'_{q1} + R'_{q2}))}{(V_{RN} \times (R'_{i1} + R'_{i2}))} \quad (\text{A.70})$$

$$R'_{aj} = \frac{(100 \times (4.7 + 0.10))}{(6.7 \times (100 + 100))} \times 10^3 = 358.2 \text{ }\Omega \quad (\text{A.71})$$

Then, as  $R'_{q2}$  (*Proportional branch steady resistor of speed regulator*)=100.0  $\Omega$ , the adjusted  $R'_{q1}$  is

$$R'_{q1} = 358.2 - 100 \text{ }\Omega \quad (\text{A.72})$$

$$R'_{q1} = 258.2 \text{ }\Omega \quad (\text{A.73})$$

Adopting the variable  $V_{Rn}$  as not defined, it will be possible to find the  $V_{Rn}$  limits by changing of the  $R'_{aj}$  as follow:

Using Equation A.70 and isolating the variable  $V_{Rn}$  results in:

$$V_{Rn} = \frac{(R_F \times (R'_{q1} + R'_{q2}))}{(R'_{aj} \times (R'_{i1} + R'_{i2}))} \quad (\text{A.74})$$

For the minimum  $R'_{aj}$ =0.10 k  $\Omega$ , the  $V_{Rn}$  max is:

$$V_{Rnmax} = \frac{(100 \times (4.7 + 0.10))}{(0.10 \times (100 + 100))} = 24 \quad (\text{A.75})$$

For the maximum  $R'_{aj}$ =4.8 k $\Omega$ , the  $V_{Rn}$  min is:

$$V_{Rnmin} = \frac{(100 \times (4.7 + 0.10))}{(4.8 \times (100 + 100))} = 0.5 \quad (\text{A.76})$$

Thus, as the defined resistors for the controller, the  $V_{Rn}$  can vary from 0.5 to 24.

The  $R'_{aj}$  was empirically defined as  $R'_{aj}$ =600.0  $\Omega$ , which resulted in  $V_{Rn1}$  equal to:

$$V_{Rn1} = \frac{(100 \times (4.7 + 0.10))}{(0.6 \times (100 + 100))} = 4.0 \quad (\text{A.77})$$

Then, instead of considering the optimized value  $V_{Rn} = 6.7$ , (A.62),  $V_{Rn1} = 4.0$  was considered for this practical experiment and the results are shown below.

The speed regulator data follow in Table A.5.

Table A.5 – Speed Regulator Parameters

Optimized $R'_{aj}$	$R'_{q1}$	$RM'_2$	Optimized gain $V_{Rn}$	Minimum gain ( $V_{Rnmin}$ )	Maximum gain ( $V_{Rnmax}$ )
358.2 $\Omega$	258.2 $\Omega$	47.57 k $\Omega$	6.7	0.5	24

### A.6.3 General Arrangement

Figure A.18 shows the general diagram including all the module interconnections [38], [39].

Notes:

1- The P1 value (the maximum speed adjustment) was empirically adjusted as shown in Fig. A.18.

2- By means of P2 shown in Fig. A.18; increasing the gain of Q6, the limit current of main circuit is decreased; in other way, when the gain is decreased, the limit current is increased, see the block diagram in Fig. A.12.

## A.7 Results

Although the optimized gain  $V_{Rn}$  of 6.7 has been calculated, the gain was empirically adjusted to 4.0 with the  $R'_{aj}$  equal to 600  $\Omega$ .

The motor speed and current waveforms for the gain of 4.0 are shown in Fig. A.19 at the moment when the motor is driven by the control system from its rest position. The gain was empirically adjusted to 4.0 with the  $R'_{aj}$  equal to 600  $\Omega$ , which resulted in a satisfactory dynamic response to the current and speed startup transitory, as shown in Fig. A.19, (yellow curve: current and blue curve: speed).



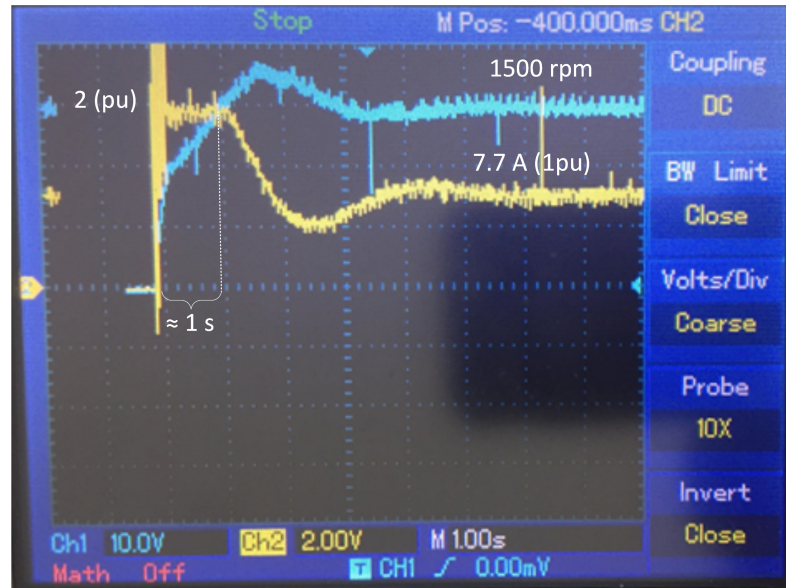


Figure A.19 – Speed and Current Waveforms

Variables:

$T_{fr}$ : Friction torque

$T_m$  (*Motor torque*)

$T_n$  (*Motor rated torque*)

$T_c$ : Load torque

$J$ : Inertial moment

$N_n$ : Rated speed

$n$ : Speed

$t$ : Time

$I_n$  (*Rated Current*)

Note: The motor data are in Table A.1. The balance equation (Newton's second law) of the system is:

$$T_m - T_{fr} - T_C = J \times \frac{d_n}{dt} \quad (\text{A.78})$$

Considerations:

$T_m = 2 \times T_n$  (the limit torque was adjusted by the regulator system by the limit current).

$Torque = k \times \phi \times I$ , considering  $I_{limit} = 2 \times I_n$ .

$T_c$  and  $T_{fr}$  depend on the speed  $n$ . This affirmation was demonstrated in Fig. A.20 and below:

When the *DCM* is coupled with an *SG* that feeds a bank of resistors, it is known that  $T_{fr}$  is proportional to the speed  $n$ . The load torque  $T_c$  is also approximately propor-

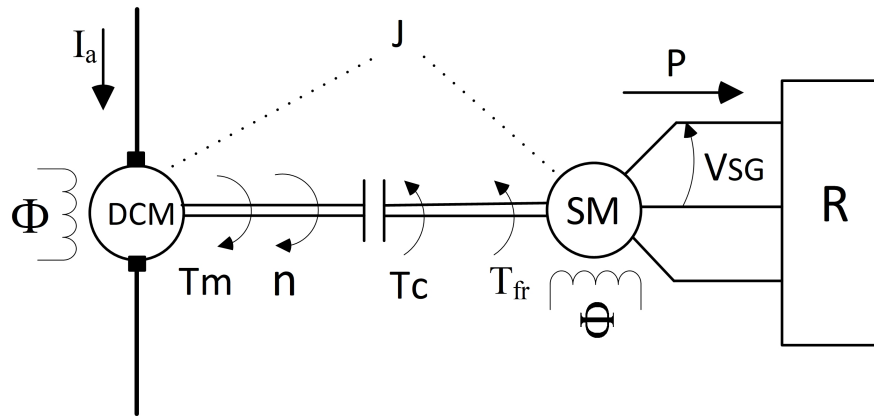


Figure A.20 – DCM coupled with SG and a Resistive Load

tional to the speed  $n$ , as demonstrated below:

$$P = \frac{V_{SG}^2}{R} \quad (\text{A.79})$$

and as  $V_{SG} = k \times n \times \phi$  and as  $\phi = \text{constant}$ , then  $k' = k \times \phi$ , therefore,

$$V_{SG} = k' \times n \quad (\text{A.80})$$

Substituting (A.80) into (A.79) gives:

$$P = \frac{k'^2 \times n^2}{R} \therefore P = k'' \times n^2 \quad (\text{A.81})$$

Note:  $k''$  is the proportionality constant 2.

Considering the steady state conditions,  $T_m$  is equal to  $T_c$ , that result in:

$$T_c = \frac{P_{mec}}{n} \quad (\text{A.82})$$

Note: As  $P_{mec}$  (*Mechanical power*) is equal to  $\frac{P_{elec}}{\eta}$ , the  $\eta$  was considered constant in an average value.

Substituting Equation (A.81) into Equation (A.82), the result is:

$$T_c = \frac{k''' \times n^2}{n} \therefore \quad (\text{A.83})$$

$$T_c = k''' \times n \quad (\text{end of demonstration}) \quad (\text{A.84})$$

Note:  $k'''$  is the proportionality constant 3.

In order to find the motor acceleration time, considering the system configuration shown in Fig. A.17, the following calculation is used.

Substituting  $T_m=2 \times T_n$  into Equation (A.78) results in:

$$2 \times T_n - T_{fr} - T_c = J \times \frac{d_n}{d_t} \quad (\text{A.85})$$

As the magnetic field  $\phi$  is constant, then  $T_{fr}+T_c=(k_1 + k_2) \times n$ , or, in summary:

$$T_{fr} + T_c = k'''' \times n \quad (\text{A.86})$$

Note:  $k''''$  is the proportionality constant 4.

Substituting Equation (A.86) into Equation (A.85) gives:

$$2 \times T_n - k'''' \times n = J \times \frac{d_n}{d_t} \quad (\text{A.87})$$

From Table A.1,  $T_n=10.8$  Nm.

$$J \times \frac{d_n}{d_t} + k'''' \times n = 2 \times 10.8 \quad (\text{A.88})$$

$$\frac{d_n}{d_t} + \frac{k''''}{J} \times n = \frac{21.6}{J} \quad (\text{A.89})$$

For  $k''''$  definition, the motor speed is in rated speed as described below:

$$T_n = k'''' \times \frac{2 \times \pi}{60} \times 1500 \quad (\text{A.90})$$

$$k'''' = \frac{60 \times 10.8}{2 \times \pi \times 1500} \therefore \quad (\text{A.91})$$

$$k'''' = \frac{64.8}{300 \times \pi} = 0.069 \frac{Nm}{\frac{rad}{s}} \quad (\text{A.92})$$

Getting  $J$  of motor plus load from Table A.1 and substituting  $k''''$  from (A.92) into Equation (A.89) gives:

$$\frac{d_n}{d_t} + \frac{0.069}{0.09} \times n = \frac{21.6}{0.09} \quad (\text{A.93})$$

Linear differential equation:

$$\frac{d_n}{d_t} + 0.77 \times n = 240 \quad (\text{A.94})$$

Considering [41], the solution for (A.94) is:

$$n = e^{-\int P d_t} \times \left[ \int Q \times e^{\int P d_t} d_t + C \right] \quad (\text{A.95})$$

Considering [41] and Equation (A.94), P= 0.77 and Q= 240, then:

$$n = e^{-\int 0.77 d_t} \times \left[ \int 240 \times e^{\int 0.77 d_t} d_t + C \right] \quad (\text{A.96})$$

$$n = e^{-0.77t} \times \left[ \int 240 \times e^{0.77t} d_t + C \right] \quad (\text{A.97})$$

$$n = e^{-0.77t} \times \left[ \frac{240 \times e^{0.77t}}{0.77} + C \right] \quad (\text{A.98})$$

$$n = e^{-0.77t} \times \left[ 311.68 \times e^{0.77t} + C \right] \quad (\text{A.99})$$

In order to find the constant C, the boundary condition is used:

$$\text{For } t = 0, n = 0 \quad (\text{A.100})$$

Substituting (A.100) into (A.99) gives:

$$0 = 1 \times [311.68 + C] \quad (\text{A.101})$$

$$C = -311.68 \quad (\text{A.102})$$

Substituting (A.102) into (A.99) gives:

$$n = e^{-0.77t} \times [311.68 \times e^{0.77t} - 311.68] \frac{\text{rad}}{\text{s}} \quad (\text{A.103})$$

Converting  $\frac{\text{rad}}{\text{s}}$  to *rpm* results in:

$$n = e^{-0.77t} \times [311.68 \times e^{0.77t} - 311.68] \times \frac{60}{2 \times \pi} \text{rpm} \quad (\text{A.104})$$

$$n = 2976.32e^{-0.77t} \times [e^{0.77t} - 1] \text{rpm} \quad (\text{A.105})$$

For  $n=1500$  rpm, it gives:

$$1500 = 2976.32e^{-0.77t} \times [e^{0.77t} - 1] \quad (\text{A.106})$$

$$1500 = 2976.32 \times [1 - e^{-0.77t}] \quad (\text{A.107})$$

Solving the equation (A.107) by the iterative method results in:

$$t = 0.91s \quad (\text{A.108})$$

# APPENDIX B – Analogical Control Board (Firing Circuit)

## B.1 Introduction

This appendix presents the concepts of operation and functioning of firing circuit to control the three-phase thyristor bridge firing angle using the integrated circuit TCA 785 and other components, The TCA 785 was developed by ICOTRON-SIEMENS. This firing circuit was implemented and tested in the Laboratory of research development of electrical didactic laboratory of Federal University of Itajubá [42], [43], [3].

This electronic circuit generates all the logic of the command signals that will control the thyristors operation. The aim of the device is to drive the thyristors by using the necessary gate current.

This firing circuit was developed to control the firing angle of thyristors, transistors, and TRIACs continually in the  $0^\circ$  to  $180^\circ$  range. It has a large number of configurations and few external components.

In the first part of this appendix is shown the firing circuit logic and, in the second part, the functions are shown. The most contribution of this appendix is the presentation of a complete firing circuit with all details that becomes possible an easy implementation.

This kind of control board is used in the primary machine of the synchronous generator in order to control the primary machine speed that drives the *SG*. So, this analogical control board is used in chapter 3.

Figure B.1 shows the basic organization of the control circuit in block diagram.

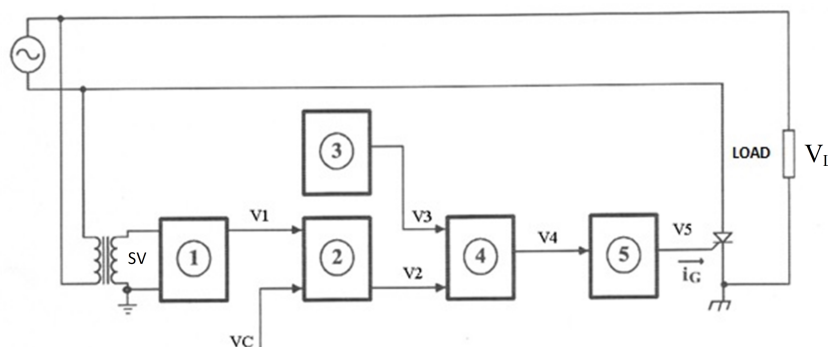


Figure B.1 – Basic Organization of Control Circuit.

Legend

- 1: Function of synchronism and sawtooth wave generation
- 2: Function of comparing
- 3: Oscillator
- 4: Logical block E
- 5: Amplification, isolating and attack

*SV (Synchronous voltage)*

*V1 (Sawtooth voltage)*

*VC (Control voltage)*

*V3 (Rectangular wave)*

*V2 (Rectangular pulse)*

*V4 (Rectangular pulses train)*

*V5 (Amplified rectangular pulses train)*

*IG (Gate current)*

*VL (Load voltage)*

The thyristor bridge is composed of control and power circuits and between them there is an isolation which should be kept, mainly, between the load and the electrical grid. In order to achieve this goal of isolation, the stages of Figure B.1 are coupled by a pulse transformer or by optocouplers (stage 3). For this purpose, an optic coupler TIL 111 (stage 3) produced by Texas Instruments was used.

Besides the optic coupler, independent voltage sources are necessary to supply energy to the stage 4 in order to have an isolation more efficient. In order to reduce the number of components, a TCA 785 and simple rectangular pulses can be used, instead of the rectangular pulses train applied in thyristors. Therefore, this can be achieved using a TCA 785 for stages 1 and 2 and the 555 device set as monostable for stages 3 and 4.

Figure B.2 shows the block diagram of the control circuit using the integrated circuits TCA 785 and 555.

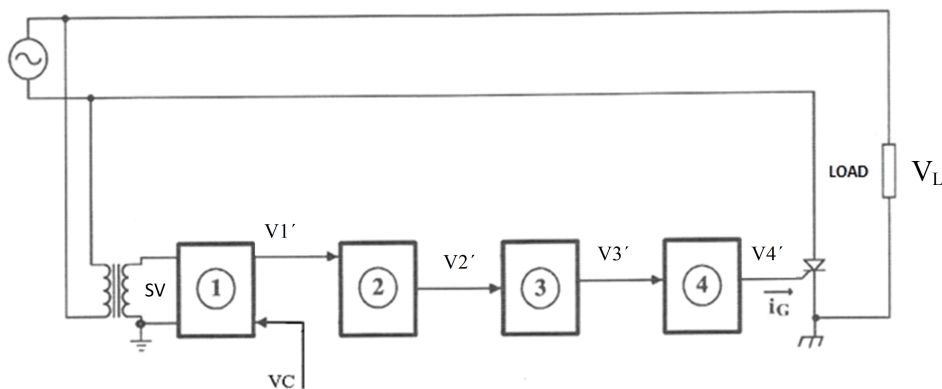


Figure B.2 – Blocks Diagram of Control Circuit using the TCA 785 and 555.

Legend:

1: TCA 785

2: Monostable 555

3: Optic coupler TIL 111

4: Amplification, isolating and attack

*SV*: Synchronous voltage

*V1'* (*Rectangular pulse*)

*V2'* (*Wider Rectangular pulse*), *V3'* (*Wider Rectangular pulse*) and *V4'* (*Wider Rectangular pulse*)

*VL*: Load voltage

## B.2 Stage Descriptions

This section will show the main characteristics of the integrated circuit TCA 785 and its functions.

### B.2.1 Pulse generation by TCA 785

The main TCA 785 function is to control the firing angle of thyristors, TRIACs and transistors continually in the range from  $0^\circ$  to  $180^\circ$ . Its configuration options enable a simplified selection of external devices for connections and disconnections. This keeps the final circuit simpler and smaller than other available options.

### B.2.2 Integrated Circuit Characteristics

The main characteristics of this integrated circuit are:

- Internal required current: 5 mA;
- Digital logic is highly immune to interference;
- Two main outputs with 55 mA current and two other outputs with open collector pins rated to 1.5 mA current;
- Three TCA 785 are needed for a three-phase system;
- The period of the output pulse is defined by the external capacitor;
- The output voltage is adjusted at 3.1 V;
- Simultaneous inhibition of all outputs is possible;
- One output is for TRIACs control.

Figures B.3 and B.4 [1] show the internal diagram and signals in the TCA 785 outputs.

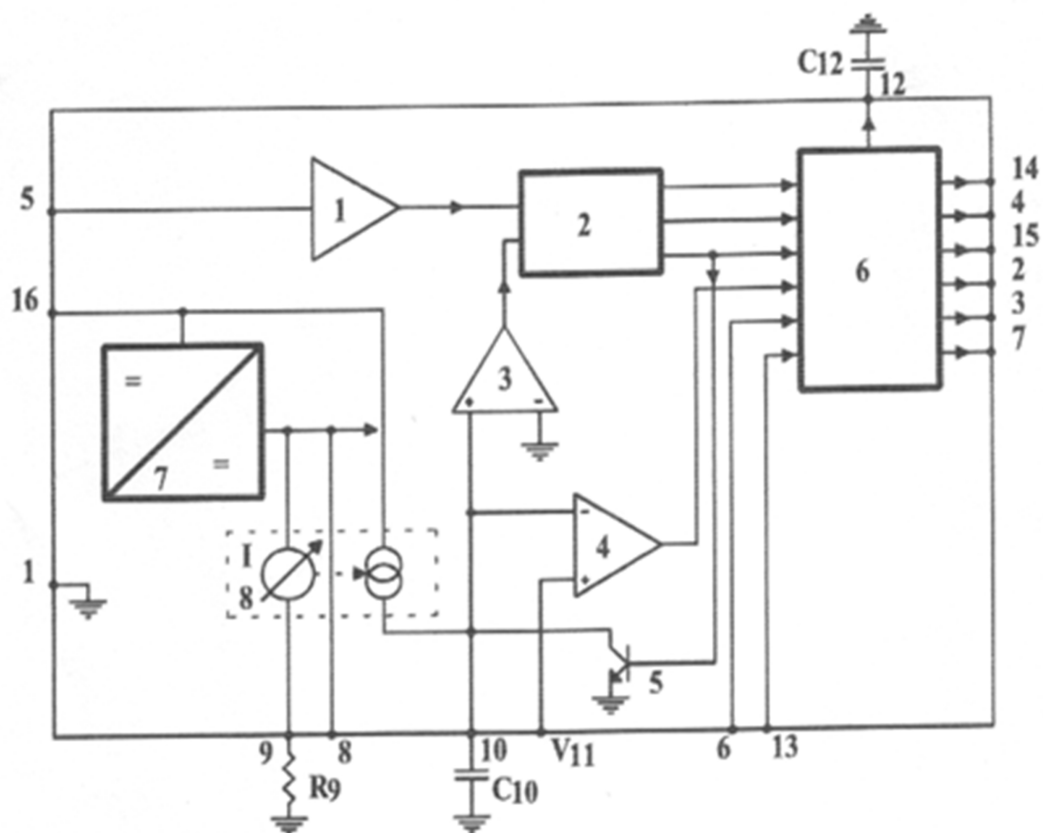


Figure B.3 – Internal Diagram of TCA 785.

Legend:

- 1: Zero detection
- 2: Synchronism memory
- 3: C10 discharge monitoring
- 4: Control comparator
- 5: Synchronizing voltage
- 6: Logical unit
- 7: Voltage internal regulator (3.1 V)
- 8: Steady current source

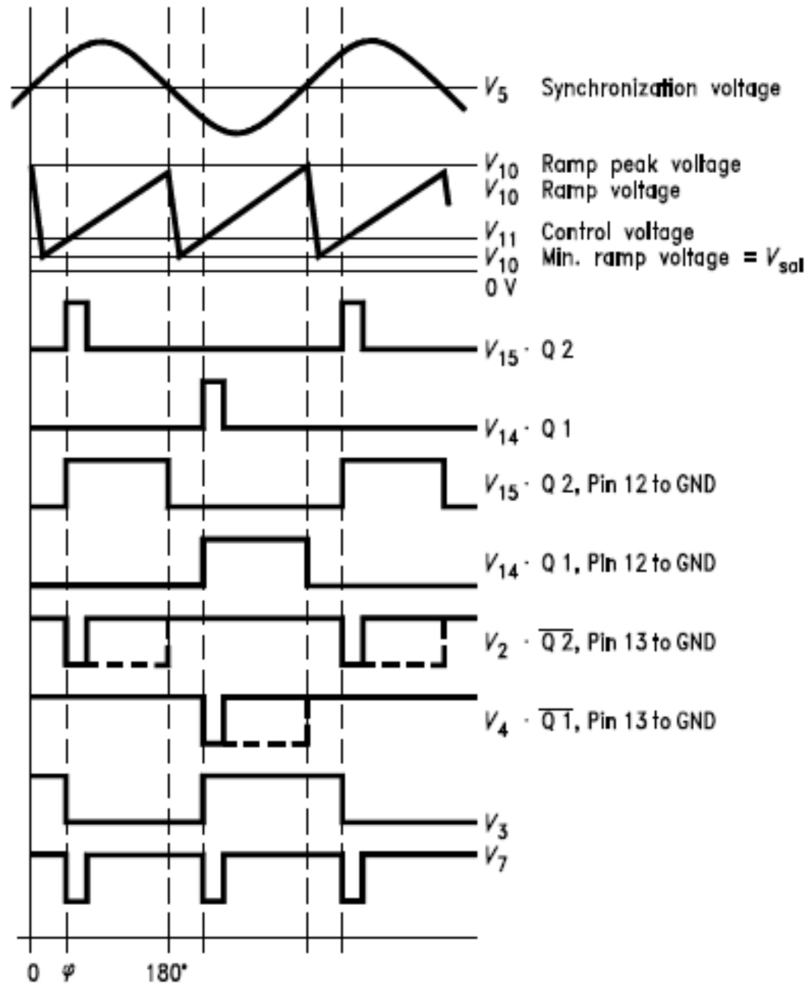


Figure B.4 – Waveforms Diagram for TCA 785. [1]

Figure B.5 shows the TCA 785 pins and wrapping.

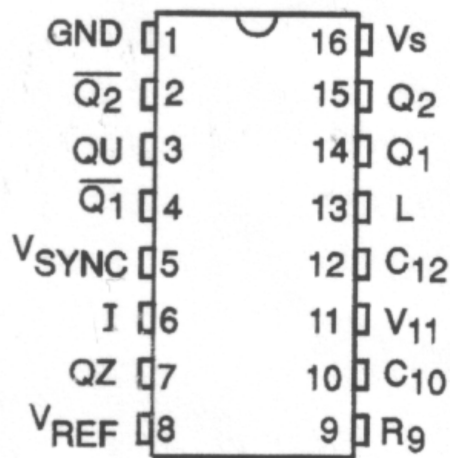


Figure B.5 – TCA 785 Wrapping and Pins

The pins and their functions are as follows:

- 01 Ground
- 02 Pin 15 complementary output with open collector
- 03 Positive pulse output with open collector
- 04 Pin 14 complementary output with open collector
- 05 Synchronism input (antiparallel diodes)
- 06 Inhibits all outputs when they are grounded
- 07 Open collector output to activate TRIACs
- 08 Steady supply 3.1 V
- 09 Potentiometer to ramp adjustment ( $20 < R9 < 500k\Omega$ )
- 10 Capacitor to generate the ramp ( $C10 \leq 0.5\mu F$ )
- 11 Controls voltage input (DC)
- 12 Controls the output pulse width of 14 and 15
- 13 Controls the output pulse width of 02 and 04
- 14 Positive pulse output in the positive half wave
- 15 Positive pulse output in the negative half wave
- 16 DC supply; it is not guaranteed for stabilization

### B.3 Operation of TCA 785

The integrated circuit (IC) feed is done by pin 16 referenced to the ground terminal (pin 1) with a voltage range between 8 V and 18 V. Internally, the IC is fed by a regulated voltage of 3.1 V, regardless of the possible changes in its external feed. The synchronism is obtained by a zero detector (pin 5), which is connected to a synchronism transformer. The ramp generator, whose control is located in the logical unit, consists of a steady current source that charges an external capacitor C10. The charge current is set by an external resistance R9 in order to adjust the ramp amplitude, which goes to zero whenever the synchronism voltage exceeds zero. Then, the group R9 and C10 determine the ramp inclination.

The control comparator compares the ramp voltage and control voltage and when they are equal to each other, the comparator sends pulses to the output through the logical unit. Then, positive pulses appear in the positive half-wave in the synchronism

voltage V15 in pin 15. In addition, positive pulses appear in the negative half-wave in the synchronism voltage V14 in pin 14. V14 and V15 are 180° delayed between themselves. The widths of these pulses are determined by external capacitor C12 connected between pin 12 and the ground pin, as shown in Table 3.1. Their amplitudes are equal to the supplied voltage in pin 16. The pin outputs 14 and 15 have complementary outputs that are respectively in pins 2 and 4. These pins 2 and 4 are an open collector transistor that requires an external resistor connected between pins 2 and 16 in the first case, and between pins 4 and 16 for the second case. The maximum resistor current is 5 mA. The width of the pulses can be controlled by the resistor connected between pins 13 and 16. Pin 6 causes an inhibition of all TCA 785 outputs when it is grounded.

Table B.1 – Pulse width from pins 14 and 15 related to capacitor C12 values, [3]

C12 [pF]	100	220	330	680	1000
Pulses width [ms]	0.080	0.130	0.200	0.370	0.550

To avoid any interference including radio frequencies, it is recommended to install ceramic capacitors at pins 8, 11 and 16, which are rated as follows:  $C8 = 10 \text{ nF}$ ,  $C11 = 100 \text{ nF}$  and  $C16 = 10 \text{ }\mu\text{F} + 10 \text{ nF}$

## B.4 Equations

(a) Charge current of capacitor C10:

$$I_{10} = \frac{V_{ref \times K}}{R9} \quad (\text{B.1})$$

(b) Ramp voltage

$$V_{10} = \frac{V_{ref} \times K \times \Delta t}{R9 \times C10} \quad (\text{B.2})$$

(c) Starting point

$$tz = \frac{R9 \times C10}{V_{ref \times K}} \times V_{11} \quad (\text{B.3})$$

(d) Pulse width

$$T_P = 30 \mu s, \text{ without } C12 \quad (\text{B.4})$$

$$T_P \approx \frac{430 \mu s}{nF} \text{ with } C12 \quad (\text{B.5})$$

where:

$$V_{ref} = V_8 = 3.1 \text{ V}$$

$$K = 1.25$$

$$C_{10} \leq 0.5 \mu\text{F}$$

$$25 \text{ k}\Omega < R_9 < 500 \text{ k}\Omega$$

## B.5 The Pulse Enlargement Stage using the Integrated Circuit 555

The integrated circuit 555 was developed as a unit that has various aims, and is able to operate in large ranges, either monostable or stable.

In Figure B.6, the 555 is operating as monostable, which results in larger pulses than the pulses received in its input. The 555 then causes an enlargement of the TCA 785 pulse that was received in its input. It is possible to adjust the output pulse width from the 555 through the  $50 \text{ k}\Omega$  potentiometer connected between the source  $V_{CC}$  and pin 6 of the 555.

Figures B.6 and B.7 show the 555 operating as monostable and monostable with an adjustable width output pulse.

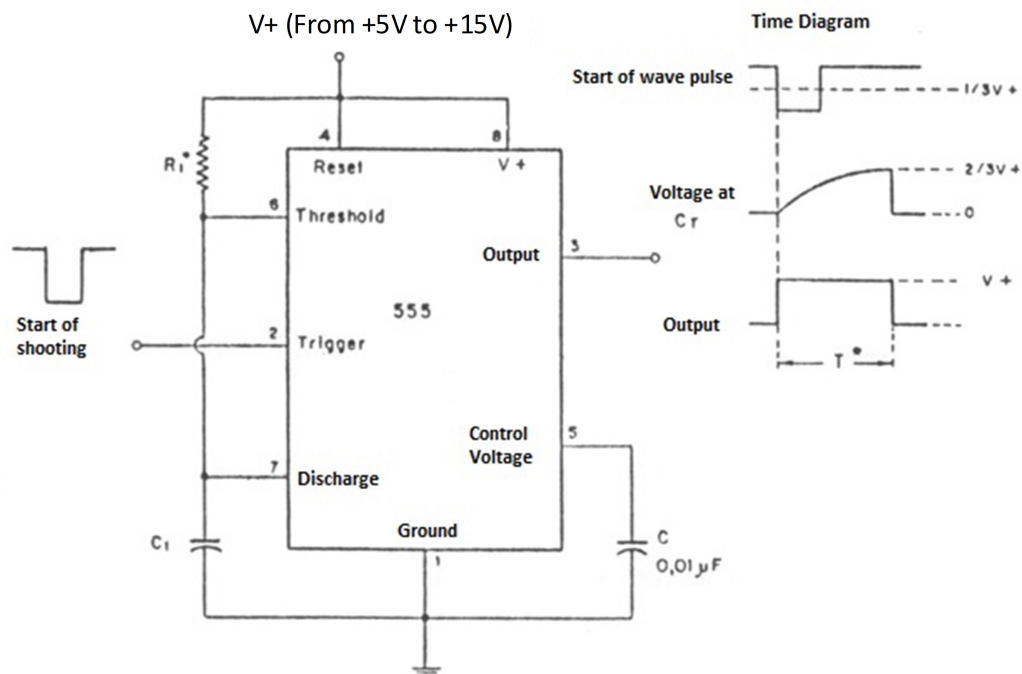


Figure B.6 – CI 555 as Monostable

Note:

The 555 in Figure B.6 is set as:  $T = 1.1 \times R_1 \times C_1$

$R_1$ : Range from  $10 \text{ k}\Omega$  to  $14 \text{ M}\Omega$

C1: Range from 100 pF to 1000  $\mu\text{F}$

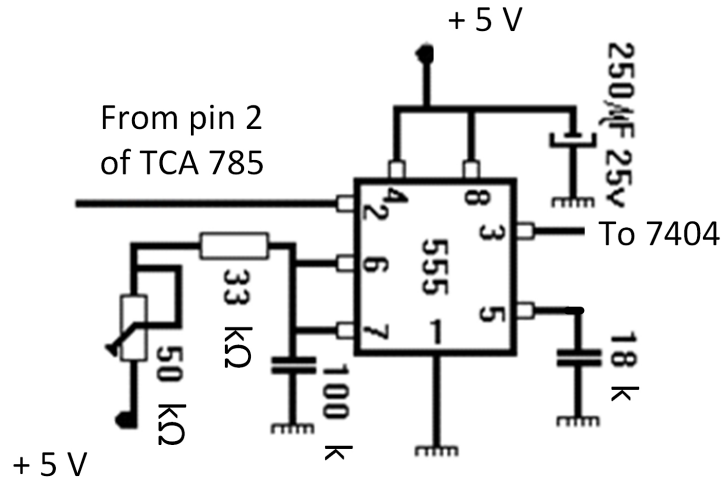


Figure B.7 – Monostable with Adjustable output Pulse Width.

## B.6 Coupling Stage with TIL111

The goal of this stage is the pulse transmission to the next stage and, at the same time, to supply electrical insulation between the high and low power circuits. The TIL111 is an optocoupler that has an infra-red LED between pins 1 and 2 and a photo transistor NPN in pins 4, 5 and 6.

Figure B.8 shows the internal diagram of the TIL111.

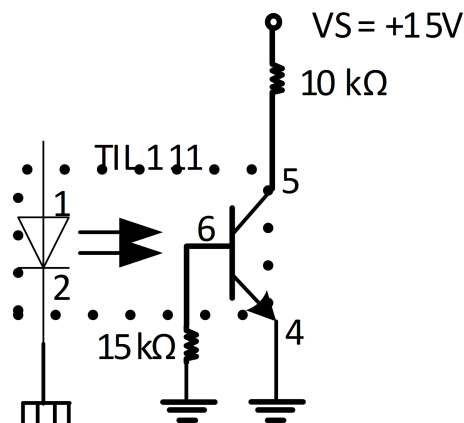


Figure B.8 – Internal Diagram of TIL111.

The diode and the photo transistor of the TIL111 should be fed by independent voltage sources (5V and ground 1, +15V and ground 2).



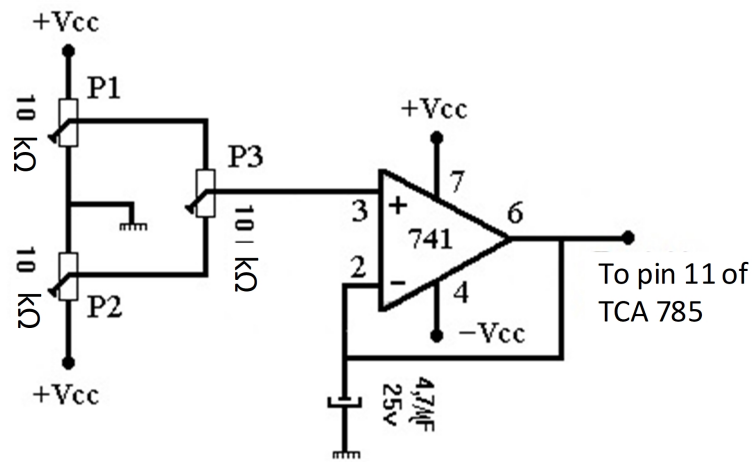


Figure B.10 – Control Voltage Circuit.

### B.9 General Overview

Figure B.11 shows the block diagram.

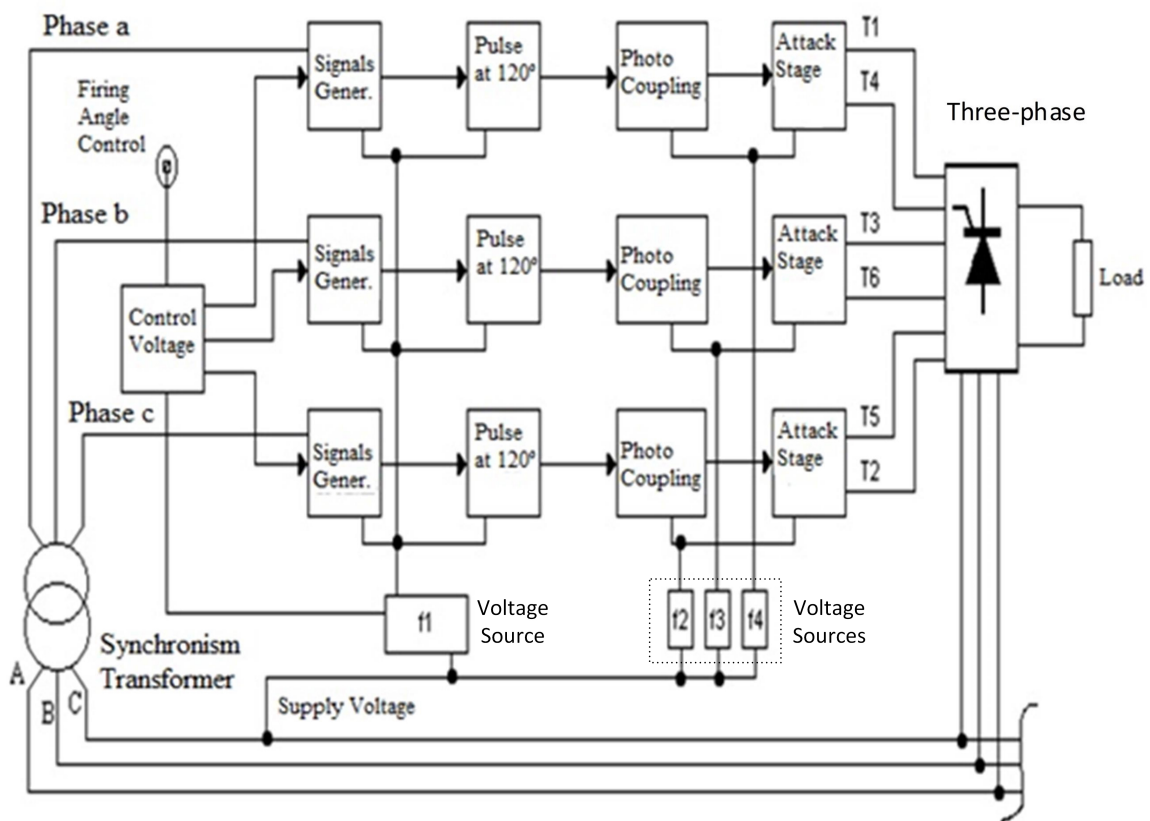


Figure B.11 – Block Diagram of Complete Control Circuit

Figure B.12 shows the electrical diagram of the firing circuit of the thyristor bridge [44], [45], [46]. Figure B.13 also shows the electrical diagrams used for the 6 voltage sources that are shown in Figure B.12.



position between pin 3 of buffer 741 and potentiometers P1 and P3. Sx is in the manual position as demonstrated in Figure B.12. When Sx is in the automatic position, the signal comes from the regulator output instead of potentiometers P1 and P3.

2. P1 serves to adjust the maximum alpha conduction angle and P2 serves to adjust the minimum alpha conduction angle.
3. The integrated circuit TCA 785 is a current version of TCA 780. Both have the same functions and pins.

## B.10 Conclusion

This appendix presented the concepts of operation and functioning of firing circuit to control the three-phase thyristor bridge firing angle using the integrated circuit TCA 785.

This electronic circuit generates all the logic of the command signals that will control the thyristors operation. The aim of the device is to drive the thyristors by using the necessary gate current.

This firing circuit was developed to control the firing angle of thyristors, transistors, and TRIACs continually in the  $0^\circ$  to  $180^\circ$  range. It has a large number of configurations and few external components as demonstrated in this appendix.

The firing circuit logic and functioning algorithm were shown, as well as, the firing circuit and parts of this firing circuit. The most contribution of this appendix is the presentation of complete firing circuit tested and implemented in the Laboratory of research development of electrical didactic laboratory of Federal University of Itajubá with all details that becomes possible a new assembly that can be done for anyone using these same components.

This kind of control board will be used in the primary machine of the synchronous generator in order to control the primary machine speed that will drive the *SG* as shown in chapter 3.

# APPENDIX C – Voltage Regulators and Filters Project to Synchronous Machine

## C.1 Introduction

Generator frequency and voltage regulation means to enable the generator to respond the load disturbances and electrical system variation in a way that the system frequency and voltage can be maintained constant and within the acceptable limits.

This chapter will show a new technique named symmetrical optimization to carry out adjustments of the voltage regulator parameters as shown in [47]. This new technique has already been applied in the speed regulator of a *DCM*. Otherwise, there is nothing about it in the scientific community related to use this technique over generator voltage regulator. Then, this one is the original contribution of this appendix.

This appendix presents theory concepts and practical experiment about the development of analogical automatic voltage regulator applied on the *SG* terminals, which operates in an isolated electric system. Moreover, this kind of voltage regulator and its parameters, such as gain and regulator time constant will be defined and adjusted by this cited technique [4, 47].

The content of this appendix can be used in the experiments with voltage regulator as those shown in chapters 1, 2 and 3 to establish the first approximation of the voltage regulator parameters for *SG* voltage regulator, such as gain and regulator time constant. The final adjustments are always done experimentally (fine adjustment at the workbench).

## C.2 Calculus of Generator Field Resistance and Inductance

Figure C.1 shows the auxiliary circuit mounted in the laboratory to determine the generator field resistance and  $\tau'$  (*Generator field time constant*). As shown in Figure C.1, dividing the  $V_{fd}$  (*Generator field terminal voltage*), by the  $I_{cc}$  (*Generator field circuit current*), the  $R_{fdmed}$  (*Measured field electrical resistance*) is given below:

$$R_{fdmed} = \frac{116.3V}{0.42A} \approx 277 \Omega \quad (C.1)$$

As additional information and to calculate the reference temperature resistance, [48], to 40 °C,  $\Theta_{ref}$ , for the temperature rise test [49, 50], the equation indicated in C.2

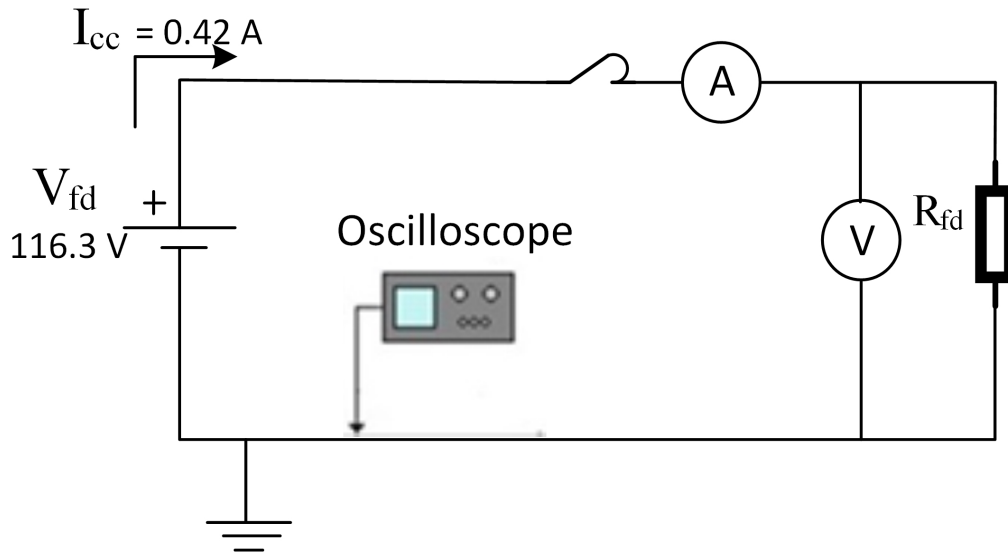


Figure C.1 – Auxiliary Circuit Mounted in the Laboratory

is used:

$$R_{fdref} = R_{fdmed} \times \frac{234.5 + \Theta_{ref}}{234.5 + \Theta_{med}} \quad (C.2)$$

considering:

$R_{fdmed}$  : Measured field electrical resistance

$\Theta_{ref}$  : Reference temperature resistance

$\Theta_{med}$  : Measured winding temperature

The  $277 \Omega$  resistance measured during the experiment was obtained for  $\Theta_{med} = 22.0 \text{ }^\circ\text{C}$ . Otherwise, the reference field resistance for  $40 \text{ }^\circ\text{C}$  is calculated in Equation C.3:

$$R_{fdref} = 277 \times \frac{234.5 + 40.0}{234.5 + 22.0} = 296.4 \Omega \quad (C.3)$$

Note: The field winding is made of copper.

Figure C.2 shows the current  $I_{cc}$  during the field energization transitory.

From Figure C.2, it is found  $\tau' = 160 \text{ ms}$ , that corresponds to time interval to current  $I_{cc}$ , reaches 63 % of steady state current, that is equal to 0.42 A. Once the field resistance and the generator time constant have been defined by Equation C.4, the field inductance is calculated:

$$\tau' = \frac{L_{fd}}{R_{fd}} \quad (C.4)$$

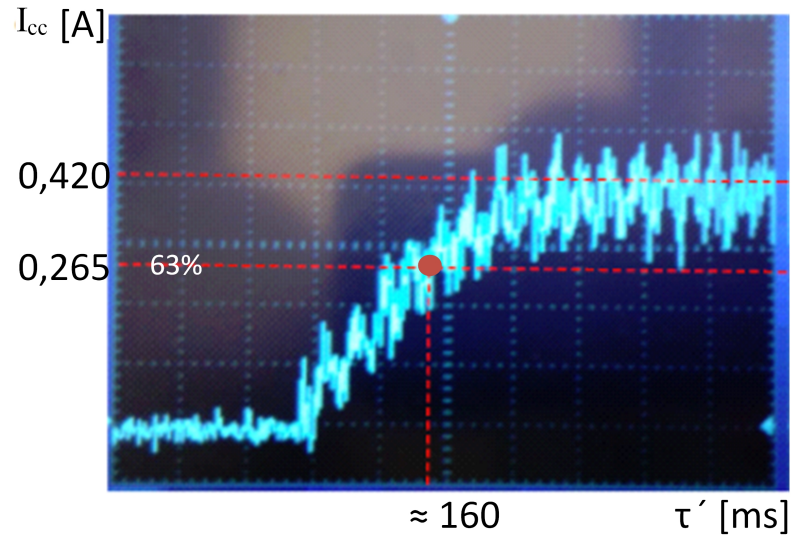


Figure C.2 – Generator Time Constant Determination

Thus, it can be seen that:

$$L_{fd} = \tau' \times R_{fd} = 160.0 \times 10^{-3} \times 277 = 44.3 \text{ H} \quad (\text{C.5})$$

The generator field circuit parameters are shown in Table C.1.

Table C.1 – Excitation Parameters of Salient Poles Synchronous Generator

Generator field resistance	$R_{fd} = 277 \Omega$
Generator field inductance	$L_{fd} = 44.3 \text{ H}$

## C.3 Voltage Regulators and Filters Project

### C.3.1 Introduction

The generator system regulator compares a reference voltage and an output generator voltage; this difference results in control of the synchronous generator excitation voltage to increase or decrease the excitation current in accordance with the desired output voltage  $V_{ref}$  (*Reference Voltage*). In this way, the generator output voltage tends to stay within a predefined voltage range under rated load variations.

Figure C.3 shows a simplified block diagram of the voltage regulation.

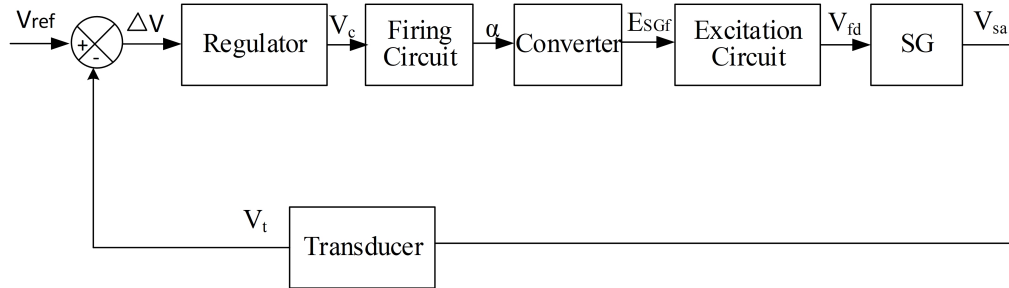


Figure C.3 – Simplified Block Diagram of Voltage Regulation

Legend:

$VC$ : Control voltage;

$V_{fd}$ : Generator field voltage;

$V_{sa}$  (*Generator output voltage*)

$V_t$  (*Transducer output voltage*)

$V_{ref}$ : Reference voltage;

$\Delta V$ : Voltage error signal;

$SG$ : Synchronous generator;

$E_{SGf}$  (*Synchronous generator field terminal voltage*)

$\alpha$ : Firing angle.

Note 1: For  $E_{SGf} = V_{fd}$ , the voltage drop in the cables and connections in the circuit between the field thyristorized converter bridge output and the machine field terminals is neglected; Note 2:  $V_{fd}$  produces field excitation current and, by means of this one, the armature voltage,  $V_{sa}$ , is induced.

### C.3.2 Voltage Regulator Optimization

In the proposed scheme, the full wave three-phase rectifier with thyristor (Graetz) shown in Figure C.4 will be responsible for synchronous generator excitation control.

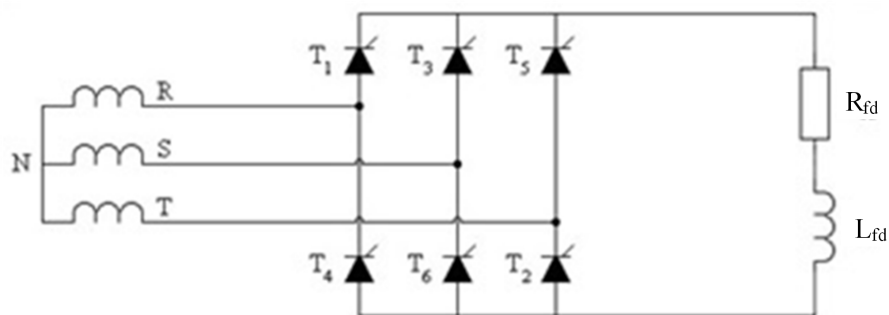


Figure C.4 – Full Wave Three-phase Rectifier with thyristor [2]

Legend

$R_{fd}$  (*Field resistor*)

*L<sub>fd</sub> (Field inductor)*

The thyristor circuit within this topology does not react immediately to variation of the firing angle, whereas after the commutation moment, the pair of thyristors starts conduction just after the conduction of previous couple of thyristors. In general, a typical reaction time value  $\tau_{ss}$  (firing circuit time constant) [51] is:

$$\tau_{ss} = 1.5 \text{ ms}$$

The feedback channel filter time constant,  $\tau_{gi}$ , reduces the ripple due to the function of the transducer diodes bridge. This time constant filters the proportional signal so that the interference can be minimized. In this work  $\tau_{gi}$ , the feedback channel filter time constant, is as shown below [51]:

$$\tau_{gi} = 1.5 \text{ ms}$$

The voltage regulator is responsible for dynamic characteristic compensation of the voltage control loop as shown in Figure C.5:

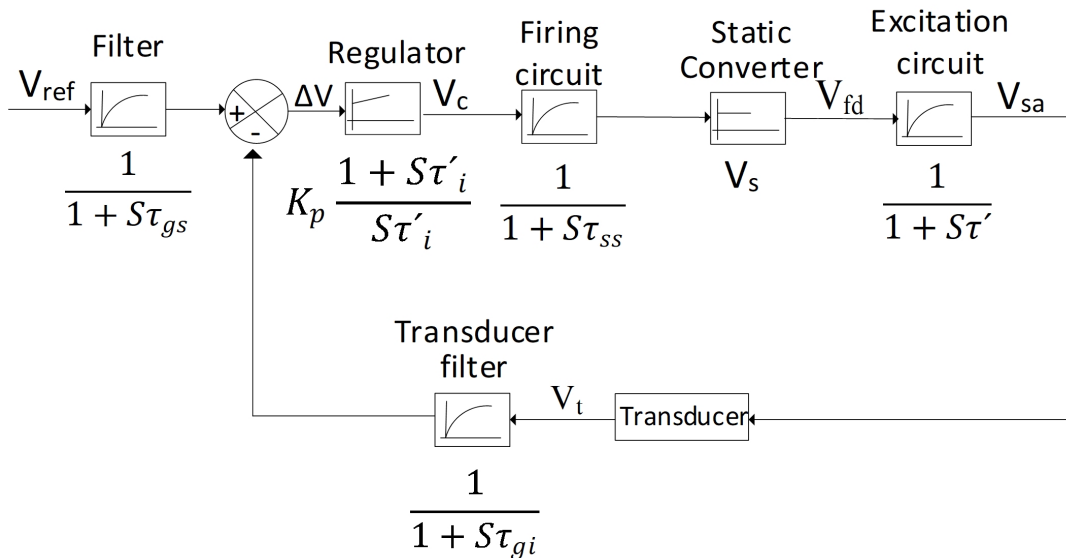


Figure C.5 – Full Blocks Diagram of Voltage Regulation System

Legend:

$\tau'$ : Generator field time constant

$\tau'_i$  (*Regulator time constant*)

$\tau_{gi}$ : Feedback channel filter time constant

$\tau_{gs}$  (*Smoothing time constant*)

$\tau_{ss}$ : Firing circuit time constant

$V_s$ : Gain of static converter

After the filtered reference signal, not considering the regulator and transducer

blocks, if the time constant is more than the sum of the rest of the first order delays (whose blocks have the first-degree polynomial in the denominator), this is termed as a large time constant. The rest of them are called small time constants. The sum of small time constant  $\sigma$  is:

$$\sigma = \tau_{ss} + \tau_{gi} = 3.0 \text{ ms} \quad (\text{C.6})$$

The resulting value from the ratio between the generator field time constant,  $\tau'$  and four times the sum of the small time constants,  $\sigma$  is:

$$\frac{\tau'}{4 \times \sigma} = \frac{160 \times 10^{-3}}{4 \times 3.0 \times 10^{-3}} = 13.3 \quad (\text{C.7})$$

This relation is shown in Figure C.6.

Table C.2 summarizes the time constants of the controlled system [4]:

Table C.2 – Excitation Parameters of Salient Poles Synchronous Generator

Generator field time constant	Large	$\tau' = 160.0 \text{ ms}$
Firing circuit time constant	Small	$\tau_{ss} = 1.5 \text{ ms}$
Time constant of feedback channel filter	Small	$\tau_{gi} = 1.5 \text{ ms}$

The smoothing time constant,  $\tau_{gs}$ , which minimizes the overshoot from the step signal in the loop entry, is:

$$\tau_{gs} = 4 \times \sigma \times \left(1 - e^{-\left(\frac{\tau'}{4\sigma} - 1\right)}\right) \quad (\text{C.8})$$

Substituting the corresponding values in Equation C.8 results in:

$$\tau_{gs} = 4 \times 3.0 \times \left(1 - e^{-\left(\frac{160 \times 10^{-3}}{4 \times 3.0 \times 10^{-3}} - 1\right)}\right) = 12 \text{ ms} \quad (\text{C.9})$$

The smoothing time constant  $\tau_{gs}$  and the resulting value from the ratio between the large and small time constants define the point  $P$  shown in Figure C.6 [4]:

According to Table 6.3 from [4], the  $PI$  regulator should be chosen as shown in Table C.3.

Table C.3 – Excitation Parameters of Salient Poles Synchronous Generator

Type of Regulator		Optimization Method
PI	$\frac{\tau'}{4\sigma} > 1$	Symmetrical optimization ( $SO$ )

When the ratio  $\frac{\tau'}{4\sigma}$  is bigger than 6, this is much greater than 1, ( $\gg 1$ ). Then, the regulator to be chosen would be the P regulator as [4], however, this regulator introduces

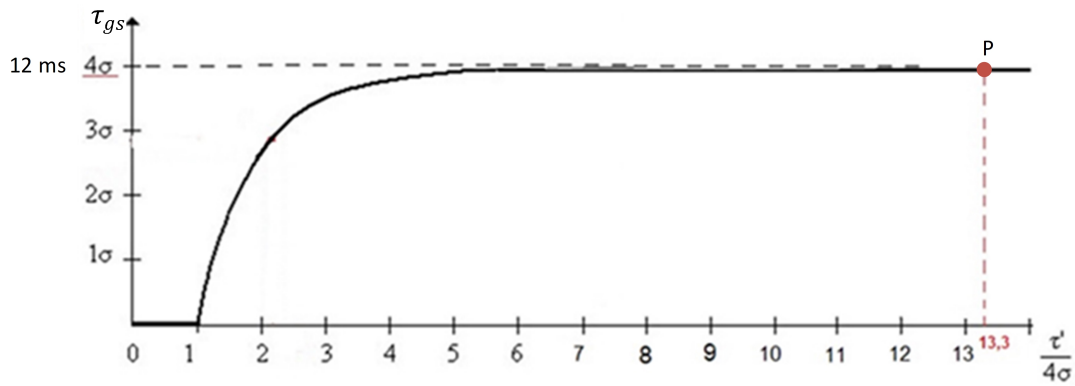


Figure C.6 – Value of  $\tau_{gs}$  and Relation between the large and the Small Time Constants

an error in the steady state response, that result in an undesirable condition. Therefore, the result of ratio  $\frac{\tau'_i}{4\sigma}$  was considered only greater than 1, it means  $> 1$ . For that reason, the *PI* (proportional-integral) regulator and symmetrical optimization (*SO*) method were chosen.

The *PI* regulator adds the pole in the origin, which results in zero error in steady state mode. The *PI* regulator has a proportional part whose response is instantaneous and an integral part whose response is delayed. Then, the *PI* regulator was considered the better regulator for this system.

This *PI* regulator is defined by the following transfer function  $F(s)$ :

$$F(s) = K_p \times \frac{1 + s\tau'_i}{s\tau'_i} \quad (\text{C.10})$$

Legend:

$K_p$  (Voltage regulator gain)

$\tau'_i$ : Regulator time constant

The *PI* regulator or *PI* controller is widely used in electrical drives and it has a phase delay compensation, which results in better transient responses and a small precision variation in steady state. It may, thus, be used to minimize the error in steady state.

After the stage of choosing the controller type and the optimization method to be used, the final definition of the controller can be obtained by adjusting the regulator parameters and applying the selected method.

Otherwise, in order to initialize the regulator optimization, it will be necessary to use the Graetz bridge with thyristors that was presented in Figure C.4. Considering the topology of this bridge, the synchronous generator field terminal voltage,  $E_{SGf}$ , is

calculated by Equation (C.11):

$$E_{SGf} = 1.35 \times E_{pp} \times \cos\alpha \quad (\text{C.11})$$

Developing the expression above:

$$\frac{E_{SGf}}{E_N} = 1.35 \times \frac{E_{pp}}{E_N} \times \left[ \cos \left( \left( \frac{\alpha}{\pi} \right) \times \pi \right) \right] \quad (\text{C.12})$$

$E_N$ : Rated voltage across SG field terminals.

and deriving Equation C.11 against the variable  $\frac{\alpha}{\pi}$ , we obtain the following:

$$\frac{d\left(\frac{E_{SGf}}{E_N}\right)}{d\left(\frac{\alpha}{\pi}\right)} = -1.35 \times \pi \times \frac{E_{pp}}{E_N} \times \left[ \sin \left( \left( \frac{\alpha}{\pi} \right) \times \pi \right) \right] \quad (\text{C.13})$$

Defining  $e = \frac{E_{SGf}}{E_N}$  and  $\alpha_u = \frac{\alpha}{\pi}$  (firing angle, in pu) results in:

$$\frac{d(e)}{d\alpha_u} = -1.35 \times \pi \times \frac{E_{pp}}{E_N} \times [\sin(\alpha)] \quad (\text{C.14})$$

From control theory, the converter gain  $V_s$  is presented as a variation modulus between output variation and input variation:

$$V_s = \left| \frac{d_e}{d\alpha_u} \right| \quad (\text{C.15})$$

Adopting Equation (C.15), Equation (C.14) can be rewritten as:

$$V_s = 1.35 \times \pi \times \frac{E_{pp}}{E_N} \times [\sin(\alpha)] \quad (\text{C.16})$$

The rectifier circuit presented in Figure C.7 has a voltmeter connected to the bridge output terminals in order to measure the voltage, and an amperemeter in series with the positive terminal and with the field generator resistor to measure the  $I_{exc}$  (*excitation current*):

From 113.08 V applied across bridge by varivolt, the measured parameters during the tests were:

- $I_{exc} \approx 0.35$  A - rated excitation current;
- $E_{pp}$  (*Phase-phase voltage*) (ERS, EST, ETR) = 113.50 V phase-phase voltage at the voltage variator output;

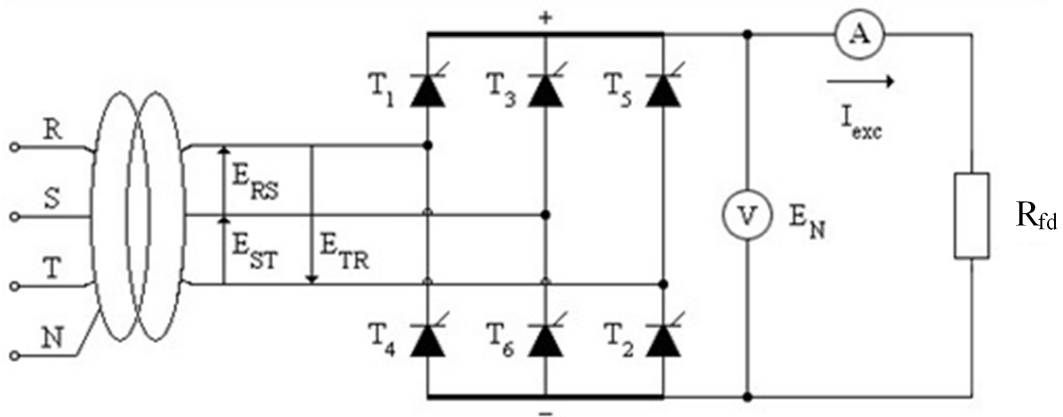


Figure C.7 – Graetz Bridge with Thyristor and 220 V Grid Voltage

- $E_N = 103.74$  V - rated voltage at rectifier bridge output.

Substituting the measured parameters in Equation (C.16) gives:

$$V_s = \left| -1.35 \times \pi \times \frac{113.50}{103.74} \times \sin\alpha \right|$$

The convertor gain  $V_s$  is then:

$$V_s = 4.64 \times \sin\alpha \quad (\text{C.17})$$

In this kind of control, the  $\alpha$  range consists of angles between  $30^\circ$  and  $90^\circ$ , the lower limit is defined by reasons of drive safety, and the upper limit is defined by reasons of continuity of work. Therefore, converter gain is not dimensional and, in general, it is obtained at an intermediate  $\alpha$  value. Thus, the defined value of  $\alpha$  was  $60^\circ$  that result in  $V_s$  equal to:

$$V_s = 4.64 \times \sin 60^\circ = 4.02$$

In this way, the convertor gain will be applied to the voltage regulator gain calculation as shown in Table C.4:

Table C.4 – Regulator Parameters Adjustments and Optimization [4].

Symmetrical optimization	Regulator parameter adjustments	
		$\tau'_i$
Symmetrical functions	$\frac{4\sigma\tau'}{\tau'+3\sigma}$	$\frac{\tau'}{2V_s\sigma}$

Table C.5 – Optimized Voltage Regulator Parameters

Parameters	Proportional-Integral
Voltage regulator optimized gain	$K_p = 6.63$
Regulator time constant	$\tau'_i = 7.7 \text{ ms}$

Referring to Table C.4, the regulator gain  $K_p$  can be calculated as the following equation:

$$K_p = \frac{\tau'}{2 \times V_s \times \sigma} \quad (\text{C.18})$$

$$K_p = \frac{160 \times 10^{-3}}{2 \times 4.02 \times 3.0 \times 10^{-3}} = 6.63$$

Referring again to Table C.4, the voltage regulator time constant,  $\tau'_i$ , is calculated as in the following equation:

$$\tau'_i = \frac{4 \times \sigma \times \tau'}{\tau' + 3 \times \sigma} \quad (\text{C.19})$$

$$\tau'_i = \frac{4 \times 3.0 \times 160}{160 + 3 \times 3.0} \times 10^{-3} = 7.7 \text{ ms}$$

Table C.5 summarizes the classification and optimization parameters needed for the voltage regulator implementation at the workbench.

Considering these results,  $R_{q1}$  (*Proportional branch adjustment resistor of voltage regulator*) and  $RM_2$  (*Integral branch adjustment resistor of voltage regulator*) adjustments will be calculated over the voltage regulators implemented in the laboratory, as shown in Figure C.8.

Note: This cited methodology was developed to analogical regulators. Otherwise, the digital regulators, MP 410T produced by Semikron have parameters adjusted manually, by the use of control keys. In other words, electronic board MP 410T does not require the resistor adjustments  $R_{q1}$  and  $RM_2$  as shown in this cited methodology of this appendix.

### C.3.3 Practical Implementation of Voltage Regulator

The regulator implementation uses the parameters previously calculated as [4]. Thus, to calculate the  $R_{q1}$  and  $RM_2$  (or  $\beta RM_2$  (*adjustable resistor of integral branch*)) adjustments, the parameters previously calculated should be considered, such as gain  $K_p$  and time constant  $\tau'_i$ . Figure C.9 shows the voltage regulator topology that was

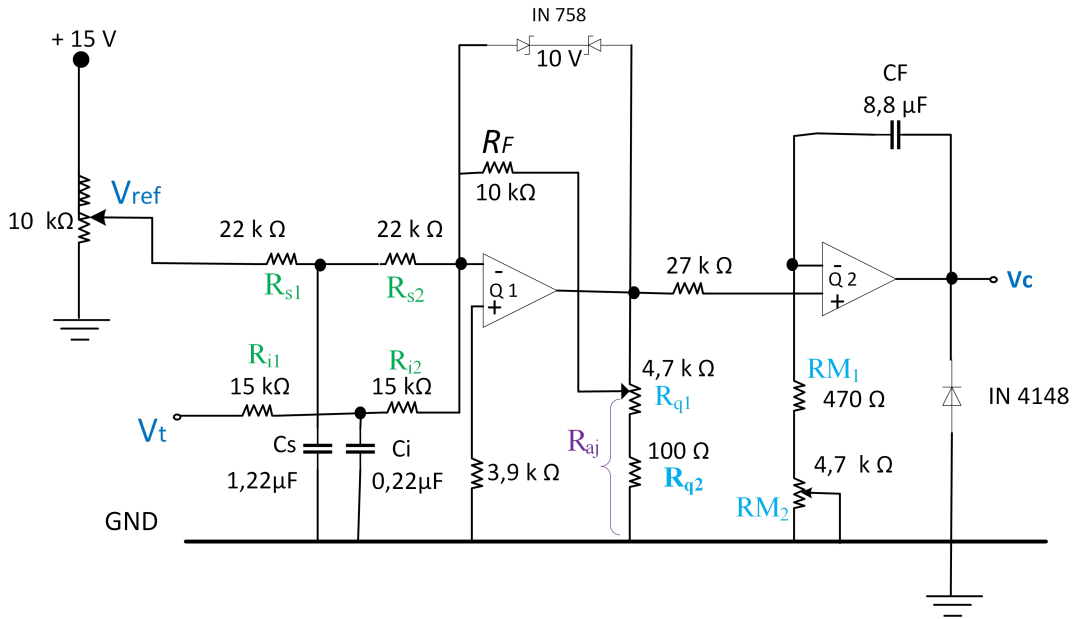


Figure C.8 – Voltage regulator

implemented in the laboratory with the passive filter “T” in the reference channel (blue line) to minimize the maximum peak.

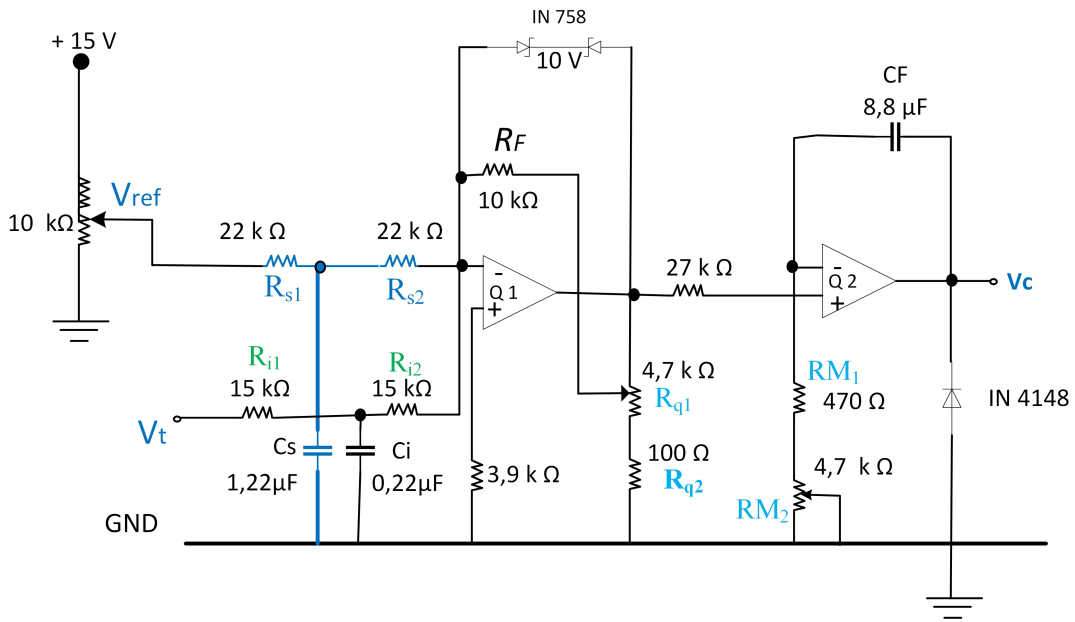


Figure C.9 – Voltage Regulator Topology with “T” Filter in the Reference Channel

With the topology indicated in Figure C.9 [51], it becomes easier to calculate the regulator gain,  $K_p$ . Thus:

$$K_p = \frac{R_F}{a \times (R_{i1} + R_{i2})} \tag{C.20}$$

Isolating the variable  $a$  gives:

$$a = \frac{R_F}{K_p \times (R_{i1} + R_{i2})} \quad (\text{C.21})$$

The resistor value to the gain adjustment can be expressed as  $R_{tp}$  (*total resistor value of proportional branch*),  $R_{tp} = R_{q1} + R_{q2} = 4.8 \text{ k}\Omega$ . This means:

$$R_{aj} = a \times R_{tp} \quad (\text{C.22})$$

Again, isolating the variable  $a$  gives:

$$a = \frac{R_{aj}}{R_{tp}} \quad (\text{C.23})$$

Matching Equations C.23 and C.21 and isolating  $R_{aj}$  (*adjustment resistance of voltage regulator*) gives:

$$\frac{R_{aj}}{R_{tp}} = \frac{R_F}{K_p \times (R_{i1} + R_{i2})} \quad (\text{C.24})$$

$$R_{aj} = \frac{R_F \times R_{tp}}{K_p \times (R_{i1} + R_{i2})} \quad (\text{C.25})$$

$$R_{aj} = \frac{R_F \times (R_{q1} + R_{q2})}{K_p \times (R_{i1} + R_{i2})} \quad (\text{C.26})$$

Substituting the values in Equation C.26 gives:

$$R_{aj} = \frac{10 \times (4.7 + 0.10)}{6.63 \times (15 + 15)} = 241.3 \text{ }\Omega \quad (\text{C.27})$$

Adopting the gain  $K_p$  as not defined, it is possible to find the limits of  $K_p$  by changing  $R_{aj}$  as follows:

Based on Equation C.26 and isolating the variable  $K_p$  results in:

$$K_p = \frac{R_F \times (R_{q1} + R_{q2})}{R_{aj} \times (R_{i1} + R_{i2})} \quad (\text{C.28})$$

For  $R_{aj}=0.10\text{k}\Omega$ , the minimum  $R_{aj}$  value, the  $K_{pmax}$  (*maximum regulator gain*) is:

$$K_{pmax} = \frac{10 \times (4.7 + 0.10)}{0,10 \times (15 + 15)} = 16 \quad (\text{C.29})$$

For  $R_{aj}=4.8k\Omega$ , the maximum  $R_{aj}$  value, the  $K_{pmin}$  (*minimum regulator gain*) is:

$$K_{pmin} = \frac{10 \times (4.7 + 0.10)}{4.8 \times (15 + 15)} = 0.33 \quad (C.30)$$

Then, as the defined resistors for the controller,  $K_p$  can vary from 0.33 to 16.

Adjustment of the time constant causes more stabilization over the output reaction values. Thus, in this way, the regulator time constant  $\tau'_i$  is:

$$\tau'_i = R_{ti} \times C_F \quad (C.31)$$

$$R_{ti} = \frac{\tau'_i}{C_F} \quad (C.32)$$

Where,  $R_{ti}$  (*total resistor value of integral branch*),  $R_{ti} = RM1$  (*integral branch steady resistor of voltage regulator*) +  $\beta RM2$ , and then:

$$\beta RM2 = R_{ti} - RM1 \quad (C.33)$$

Substituting Equation C.32 in Equation C.33 gives:

$$\beta RM2 = \frac{\tau'_i}{C_F} - RM1 \quad (C.34)$$

Then, the adjusted resistor is:

$$\beta RM2 = \frac{7.7 \times 10^{-3}}{8.8 \times 10^{-6}} - 0.47 \times 10^3 = 405 \Omega \quad (C.35)$$

## C.4 Results

The adjustments of  $R_{aj}$  and  $\beta RM2$  are shown in Figure C.10.

Table C.6 shows the values of the gains and adjustments implemented during the voltage regulator implementation stage.

Then, the full implementation of the voltage regulator for the synchronous generator is shown in Figure C.11 [47]:

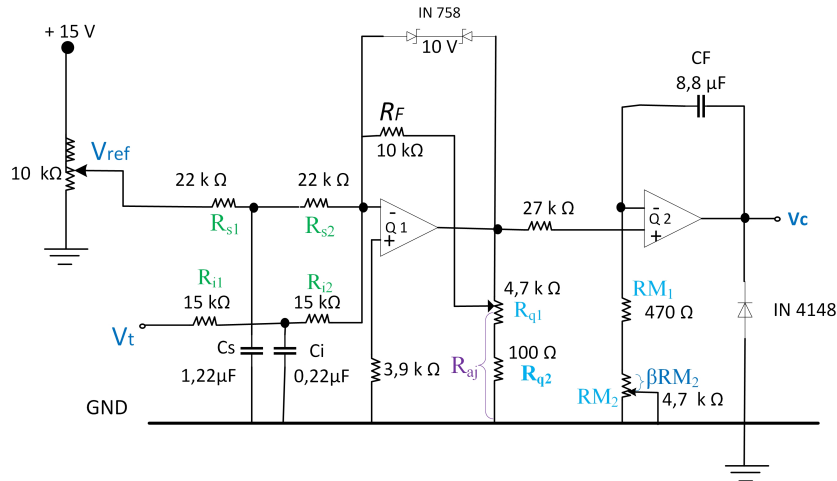


Figure C.10 – Voltage Regulator Topology

Table C.6 – Voltage Regulator Adjustments

Gain adjustment resistor	$R_{aj} = 241.3 \Omega$
Adjusted time constant resistor	$\beta RM2 = 405 \Omega$
Voltage regulator optimized gain	$K_p$ (regulator gain) = 6.63
Maximum regulator gain	$K_{pmax} = 16$
Minimum regulator gain	$K_{pmin} = 0.33$
Regulator time constant	$\tau'_i = 7.7 \text{ ms}$

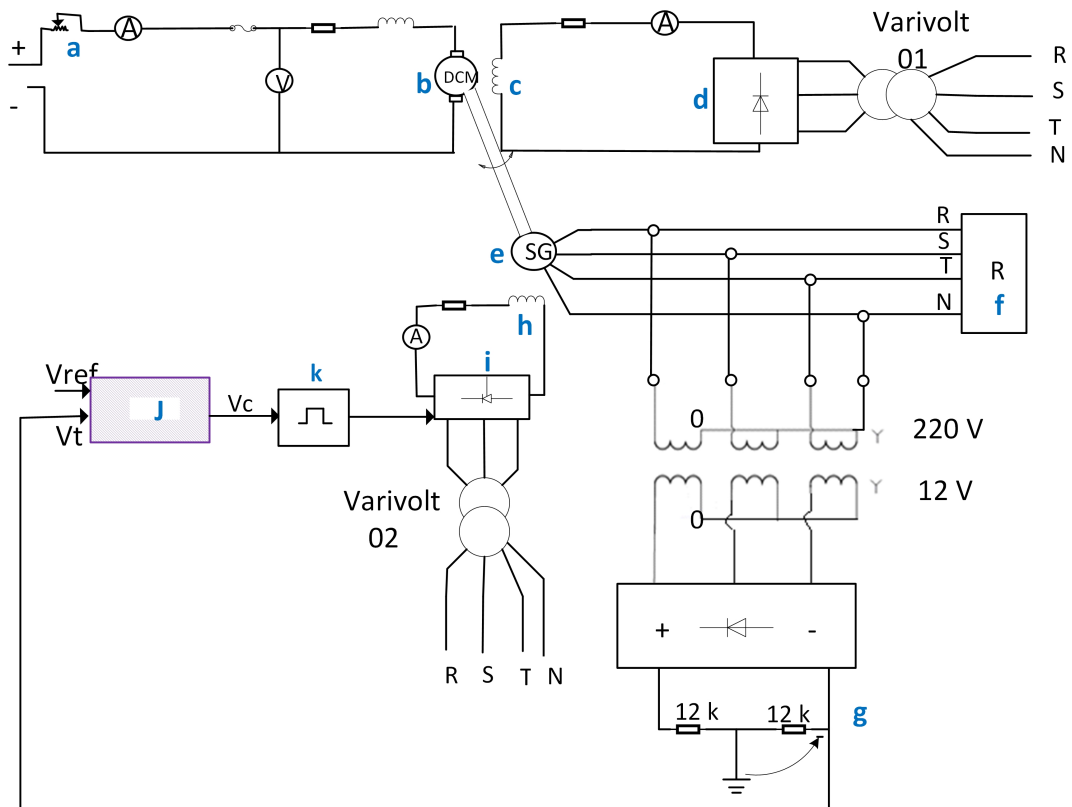


Figure C.11 – Voltage Regulator System for Synchronous Machine

Legend:

a	Rheostat	f	Three-phase load
b	DC motor armature	g	Voltage transducer
c	DC motor field	h	Synchronous generator field
d	Diodes bridge	i	Thyristors bridge
e	Synchronous generator	j	Voltage regulator
		k	Firing Circuit

## C.5 Conclusion

This appendix presented theory concepts and practical experiment mounted in laboratory about the development of an analogical automatic voltage regulator applied on the *SG* terminals, which operates in an isolated electric system. Moreover, the kind of voltage regulator was defined and its parameters as gain and regulator time constant were estimated or calculated using the symmetrical optimization technique [4, 47].

In spite of the analogical voltage regulator parameter optimization procedure has been presented in this appendix, the voltage regulators implemented in laboratory and shown in chapters 1, 2 and 3 were the digital voltage regulator. This kind of regulators uses a Semikron MP 410T board and their parametrization was performed by experimental adjustment method.

Note: The analogical regulators (speed and current regulators) were used in the speed control of the *SG* primary machine, DC motor.

# APPENDIX D – Four-quadrant Regenerative Driven System for DC Machine applying Speed Reversion using either Armature Current Reversion or Field Current Reversion

## D.1 Introduction

A regenerative driven system for DC machines in four quadrants was implemented in the laboratory of research development of electrical didactic laboratory of Federal University of Itajubá, [26]. The speed reversion was done using two distinct methods: the first consisted of armature DC current inversion through the use of two converters, whereas, the second, consisted of inversion of the field current through the use of one converter. The results of both methods are presented, discussed and compared. The symmetrical optimization method [4] was chosen to adjust the regulator parameters.

The controlled drive system for DC machines is widely used in industry, [37, 38, 51, 26]. Speed reversion is needed in many industrial processes. In order to achieve this aim, this work will present the use of the two cited methods to return regenerative energy to the grid during the braking process [26, 40].

The content of this appendix is basis of content shown in chapter 3 which is addressing the subject energy regeneration system to control the frequency increase.

## D.2 Block Diagram of Controlled Drive System for use in DC Machine

Figure D.1 shows the full block diagram of the DC machine:

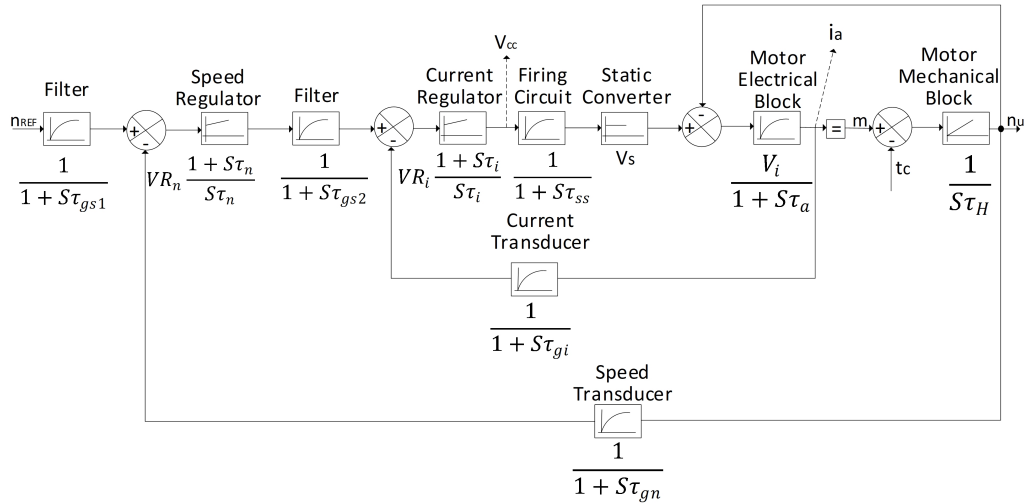


Figure D.1 – Full Blocks Diagram of DC Machine

Legend:

$\tau_{gs1}$  Filter time constant of the reference channel of the speed loop

$\tau_{gs2}$  Filter time constant of the reference channel of the current loop

$V_{Rn}$  Gain of the speed regulator

$V_{Ri}$  Gain of the current regulator

$\tau_n$  Time constant of the speed regulator

$\tau_i$  Current regulator time constant

$\tau_{gn}$  Filter time constant of the speed transducer

$\tau_{gi}$  Filter time constant of the current transducer

$\tau_{ss}$  Time constant of the firing circuit

$V_s$  Gain of the static converter

$\tau_a$  Armature circuit time constant

$V_i$  Gain of machine electric part

$V_{cc}$  Control voltage of thyristor firing system

Note: Figure D.1 shows the PI regulators of DC machine. The motor regulator parameters were obtained by the symmetrical optimization method [4].

### D.3 Laboratory Implementation

In order to implement the system in the laboratory, the following data plates were shown in D.1 to D.3 [40].

Note: All these values were obtained as described in [40] and in appendix A.

Table D.1 – Motor Data

Power	Current	Rated speed	No load speed	Rated voltage	Armature resistance ( $\Sigma R_a$ )
1.7 kW	7.72 A	1500 rpm	1770 rpm	220 V	7.0 $\Omega$

Table D.2 – Speed Regulator Parameters

Type	Gain ( $V_{Rn}$ )	Time constant ( $\tau_n$ )	Reference channel Filter time constant ( $\tau_{gs1}$ )	Speed transducer filter time constant ( $\tau_{gn}$ )
PI	6.7	460 ms	416 ms	100 ms

Table D.3 – Current Regulator Parameters

Type	Gain ( $V_{Ri}$ )	Time constant ( $\tau_i$ )	Reference value filter ( $\tau_{gs2}$ )	Feedback current filter ( $\tau_{gi}$ )
PI	0.8	13.34 ms	15.43 ms	1.39 ms

## D.4 Full Hardware of Implemented Drive System

Figure D.2 shows the implemented drive system and Figure D.3 shows the full hardware of the control system [4], including the control switches.

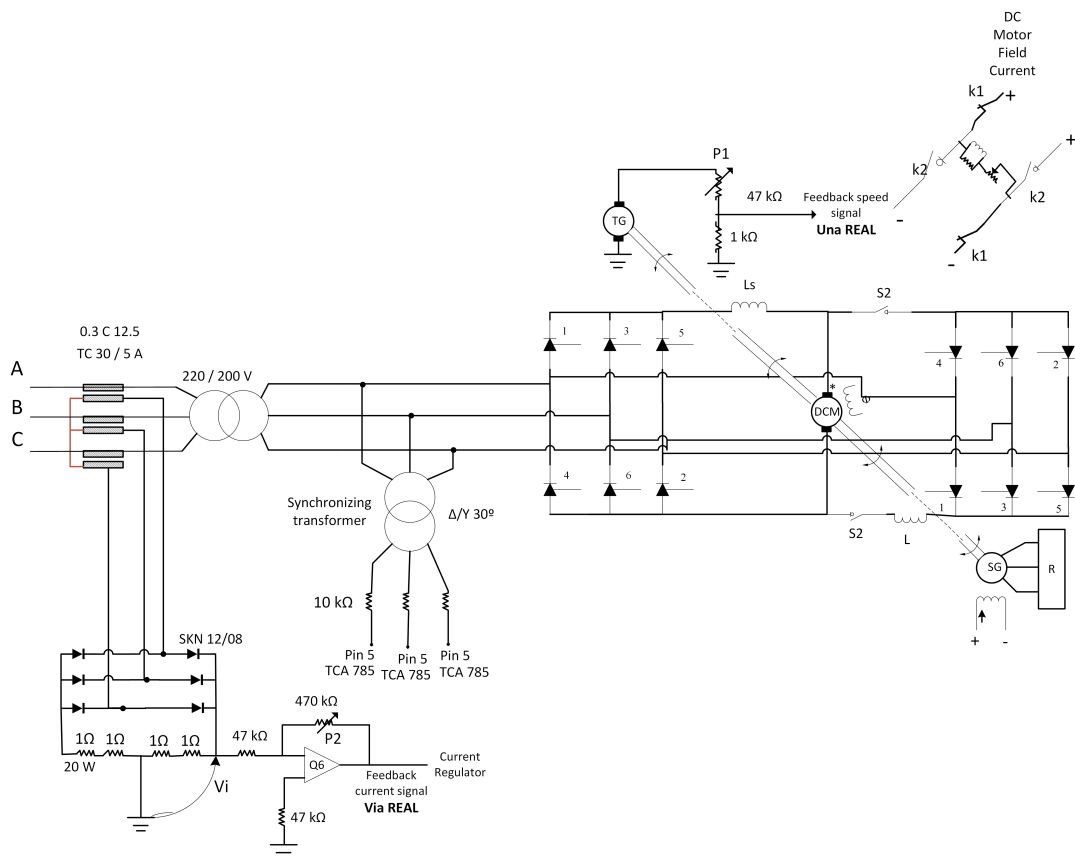


Figure D.2 – Implemented Drive System

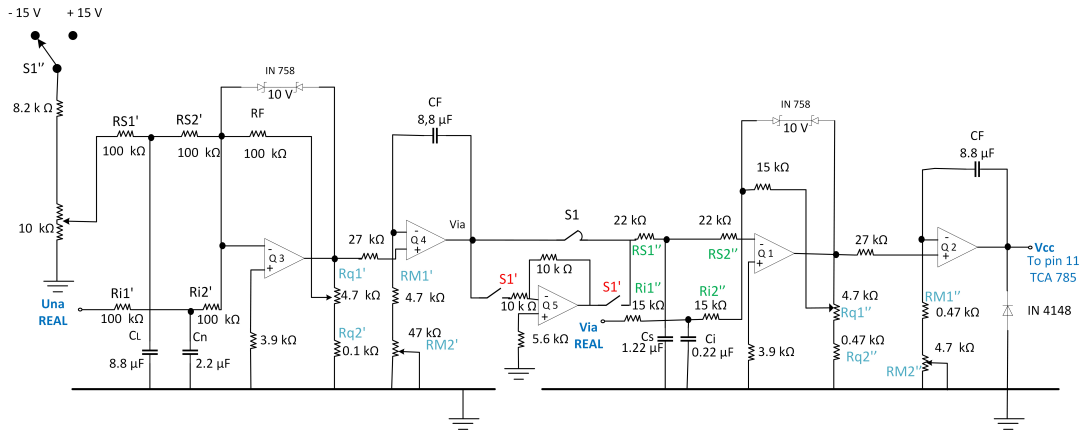


Figure D.3 – Control Circuit

## D.5 Speed Inversion by Armature Current Inversion

Considering the diagram shown in Figure D.4, after the switch  $S1''$  turns from negative to positive, the operations occur as shown in quadrants I, II and III. When the switch  $S1''$  turns from positive to negative, the operations occur as shown in quadrants III, IV and I.

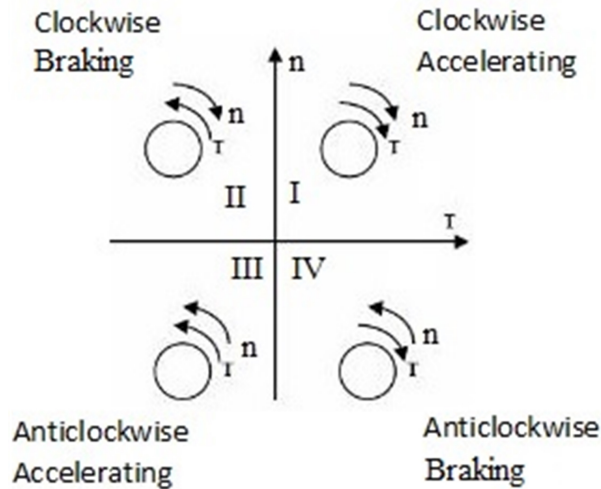


Figure D.4 – Conjugate (t) versus Speed (n) Diagram

In order to clarify Figure D.2, the switch  $S2$  is closed and then converter I and converter II are running one at a time. This system is known as a dual converter, without circulation current.

In this way, if converter I is running, the switch  $S1$  shown in Figure D.3 is close and switches  $S1'$  are open. On the contrary, if converter II is running, the switches  $S1'$  are closed and  $S1$  is open. The switch  $S1''$  enables the speed inversion. The switch  $S1''$  will promote the blockage of the converter pulses I and unblock the converter pulses II as shown in Figure D.5. There is a period of about some milliseconds in which both converters are blocked and, thus, they are not running. Figure D.5 shows this sequence:

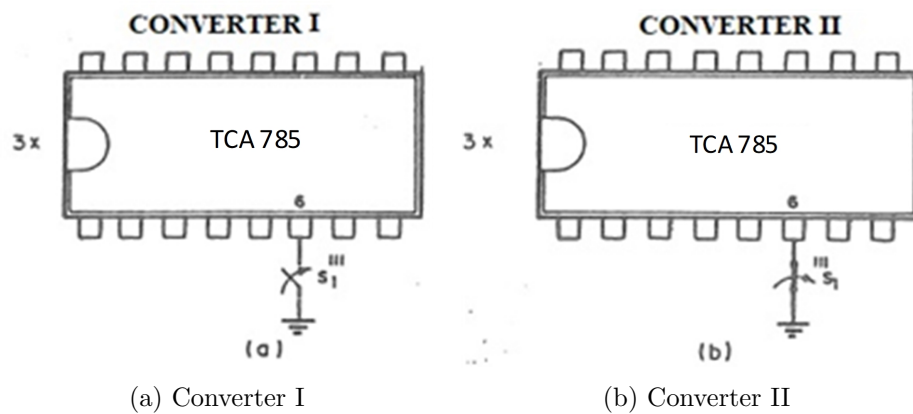


Figure D.5 – Closing of Converters I and II

The commutation switch concentrates the switches  $S_1$ ,  $S_1'$ ,  $S_1''$  and  $S_1'''$ , which are shown in Table D.4 with their operations and interlocks. This kind of switch as shown in Figure D.6 is composed of 2 switches per disc that totalling 6 switches. Thus, it is possible to configure many different combinations among them. Table D.4 shows the open and closed combinations of these switches.

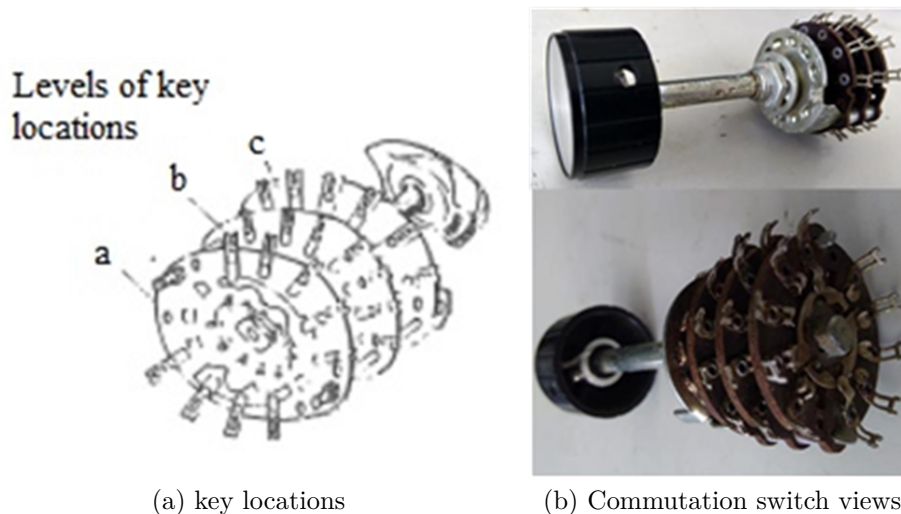


Figure D.6 – Commutation Switch  $S_1$

The bridge firing system was implemented using 3 integrated circuit TCA 785 devices for each converter bridge. Then, when  $S_1'''$  is closed, pin 6 is connected to earth and then bridge I is blocked. In reference to converter II, this is turned on because  $S_1'''$  from Figure D.5b is opening, contrary  $S_1'''$  from Figure D.5a. During commutation between two switches  $S_1'''$  from converters I and II, there is a short period of about 50 ms in which these two switches are kept closed. For this reason, both converters are kept blocked in this period until the total extinction of bridge current that is under operation. The other bridge will just be in operation after the current extinction. The dual converters under

study are rated to run without circulation current. Figure D.6 shows the commutation switch used in the circuit.

In addition, Table D.4 below shows the switch behaviour when  $S1''$  changes its current state.

Table D.4 – Cause and Effect Matrix

S1	S1'	S1''	S1''' Converter I	S1''' Converter II
open	closed	S1'' changes from -15V to +15V	closed	open
closed	open	S1'' changes from +15V to -15V	open	closed

## D.6 Rotation Inversion using the Field Current Inversion

In this case, it is necessary to use only a converter of Figure D.2 and the switches shown in Figure D.2 and Figure D.7. If switch k1 is closed, k2 is open, so the field current is running in a specific direction. On contrary, if switch k2 is closed and k1 is open, then the field current is appearing in another direction. Figure D.7 shows the control circuit.

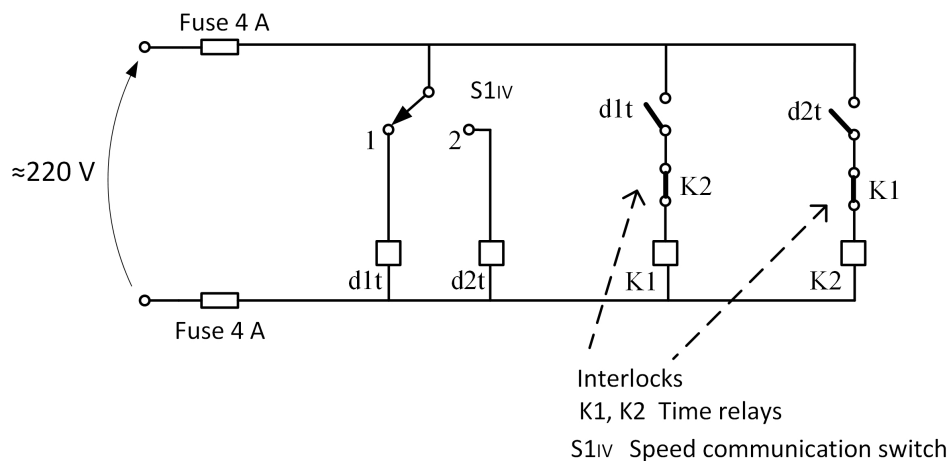


Figure D.7 – Control Circuit

When the commutation switch  $S1^{IV}$  is in position 1, k1 is energized. If  $S1^{IV}$  is in position 2 and then there occurs a delay monitored by the time relay corresponding to about 100 ms, this results in contactor k1 being turned off and contactor k2 turned on. That minimum time is necessary so that stored energy in the field can be discharged. With this aim, the resistance equivalent to  $700 \Omega$  was inserted in parallel to the motor field circuit as shown in Figure D.8.

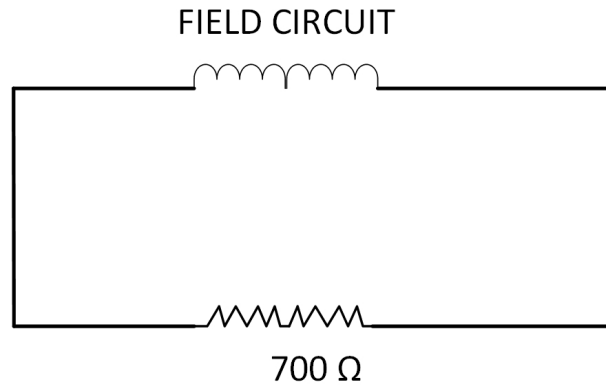


Figure D.8 – Resistance to Energy Dissipation in Machine Field Circuit

## D.7 Results

Figure D.9 shows the speed inversion process in the dual converter (armature current inversion). Figure D.10 shows the cited process related to field current inversion. In Figure D.10, the friction process is used to stop the machine. In this case, the time required is longer than the case in which the regenerative braking occur.

It is also noted that for the braking due to armature current inversion, the period of time required for braking and rotation inversion (quadrants I and II) is different from the period of time corresponding to braking and rotation inversion of the motor in opposite speed direction (quadrants III and IV in Figure D.4. This phenomenon is due to summing or subtracting between the main flux and armature reaction flux. In this way, the resulting flux is bigger in one case than in the other. As the limited current was kept practically constant for both cases, the braking's resulting conjugate was different, which resulted in different rotation inversion periods in these two cases.

In the rotation inversion case using the field current, this cited phenomenon was not observed, which means that the braking and inverted direction acceleration periods are practically equal for both directions.

## D.8 Conclusion

Both of the methods using speed regenerative reversion described in this work have good results. The method that uses field current inversion has a major advantage due to the fact that it uses only one converter. In cases where a high speed is not required to start the braking process, this is the recommended method. There is a new dual converters method in which the change of converters is faster than seen in this work because it can accept circulation current. Implementation of this new method is foreseen as future work.

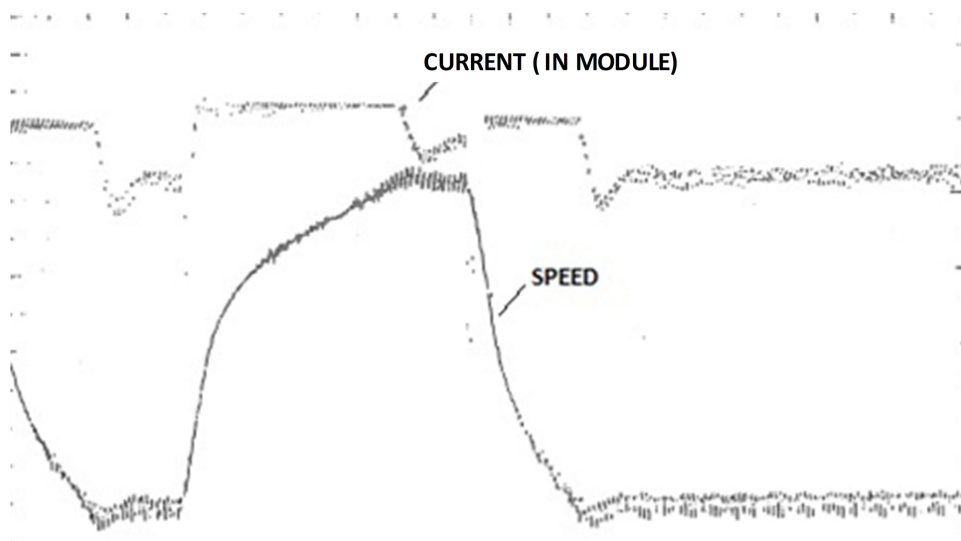


Figure D.9 – Rotation Inversion using the Armature Current Inversion

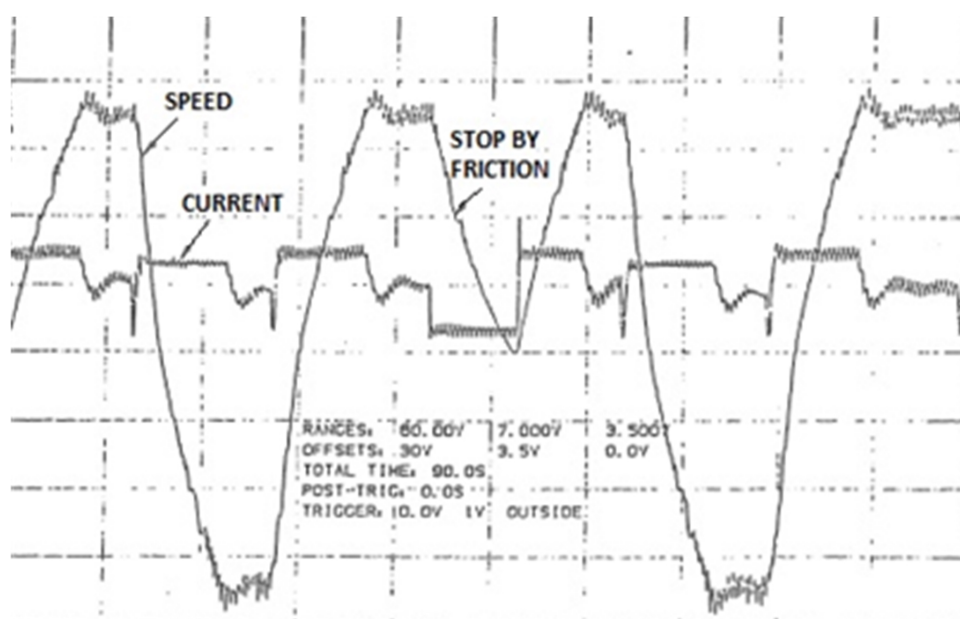


Figure D.10 – Rotation Inversion using the Field Current Inversion

# APPENDIX E – Induction Motor Parameters

The follow calculus was developed as [32] to find the induction motor parameters.

## E.1 No Load and Locked Rotor Tests

The Figure E.1 shows the circuit implemented in laboratory to no load test and locked rotor test. The temperature during the test was  $26^{\circ}C$ .

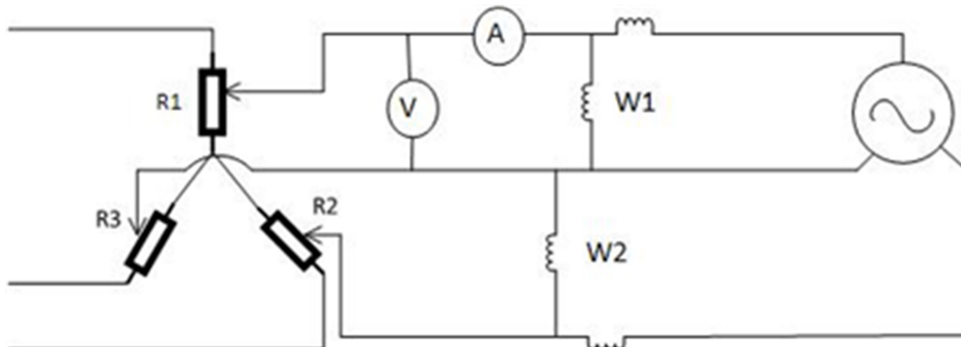


Figure E.1 – No load test and locked rotor test circuit

The Figure E.2 shows the induction motor *IM* equivalent circuit.

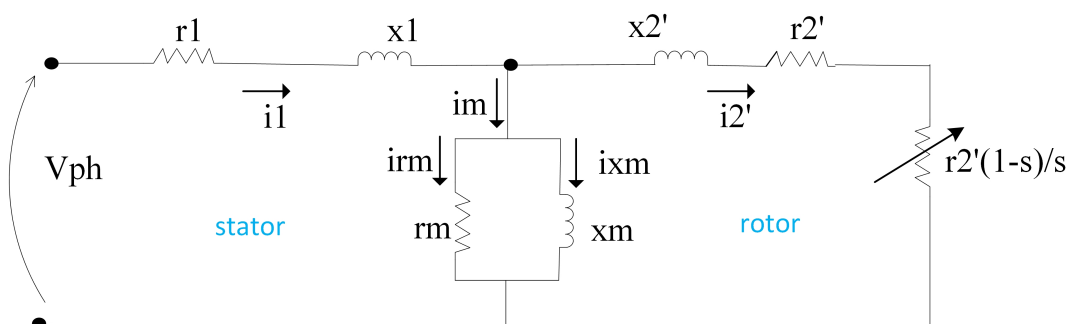


Figure E.2 – Induction Motor Equivalent Circuit

Note:  $V_{ph} = V_{phase}$

### E.1.1 No Load Test

In this section will be presented the no load test and locked rotor test to calculus the IM parameters such as impedances, currents, losses and efficiency

The Table E.1 presented the no load test measurements.

Table E.1 – No load Test

V <sub>applied</sub> (V)	W1 (W)	W2 (W)	A(A)	W1+W2(W)
240	-120.0	+220.0	1.50	100.0
220	-100.0	+170.0	1.35	70.0
200	-70.0	+130.0	1.15	60.0
180	-60.0	+110.0	1.00	50.0
160	-40.0	+80.0	0.90	40.0
140	-30.0	+60.0	0.75	30.0
120	-20.0	+45.0	0.65	25.0
100	-15.0	+30.0	0.55	15.0
80	-10.0	+20.0	0.50	10.0
60	-4.0	+12.5	0.25	8.5
40	0.0	+5.0	0.15	5.0

Figure E.3 shows the curve of voltage applied and power measured by watt-meter (W1) and (W2). Note that the cross of curve and vertical axe result in estimated  $P_{av}$  (*attrition and ventilation losses*). In this case  $P_{av}$  is 3 W as demonstrated in the Figure E.3.

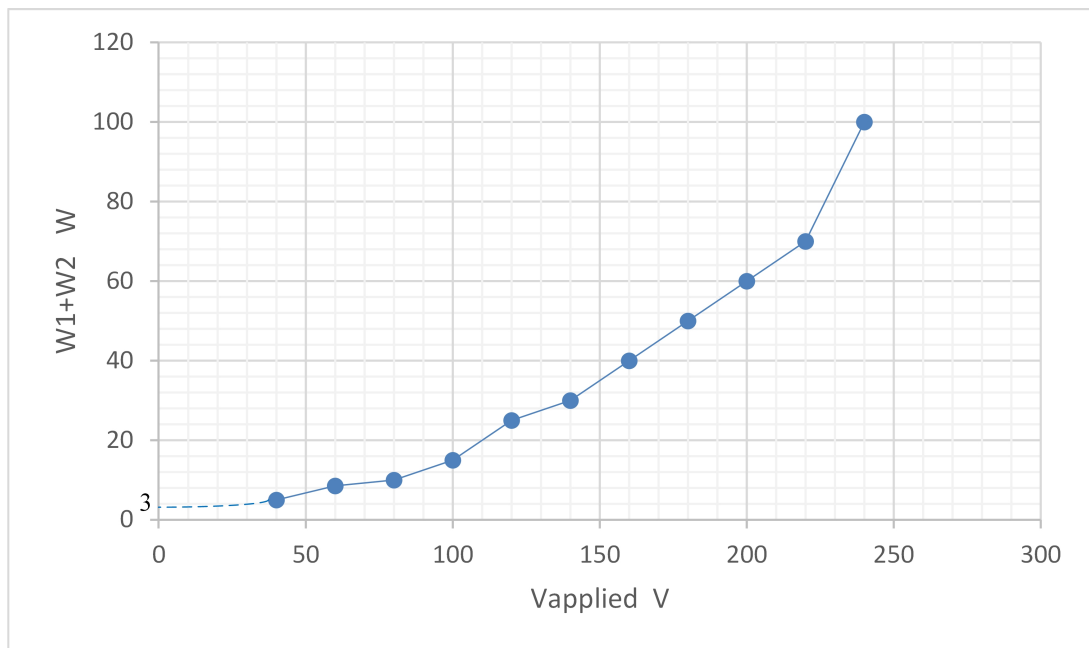


Figure E.3 – Results of no-Load Test: W1+W2 vs Voltage Applied

- Magnetization Current

Note:

$I_m$  (*Magnetization Current*)

$I_m = 1.35$  A as shown in Table E.1.

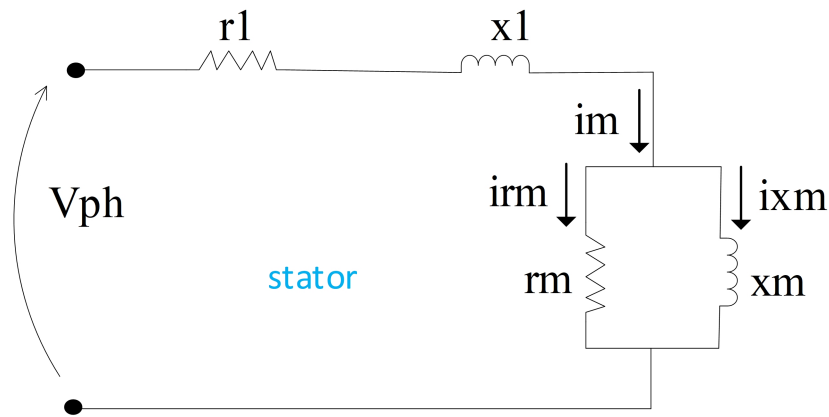


Figure E.4 – Equivalent Circuit – No-Load Test

### E.1.2 Locked Rotor Test

The Table E.2 shows the locked rotor test measurements.

Table E.2 – Current Regulator Parameters

W1 (W)	W2 (W)	V (V)	In (A)	W1+W2 (W)
20	65	39.34	1.80	85

- $I_n$

$$I_n = \frac{P}{\sqrt{3} \times V_{pp} \times \cos\phi \times \eta} \quad (\text{E.1})$$

$$I_n = \frac{370}{\sqrt{3} \times 220 \times 0.71 \times 0.76} \quad (\text{E.2})$$

Note:

$\eta$ : motor efficiency

Figure E.5 shows the induction motor IM equivalent circuit during locked rotor test

## E.2 Stator and Rotor Parameters

Legend:

$R_m$  (Motor Average Measured Resistance)

$R_y$  (Phase resistance in star connection)

$R_d$  (Phase resistance in delta connection)

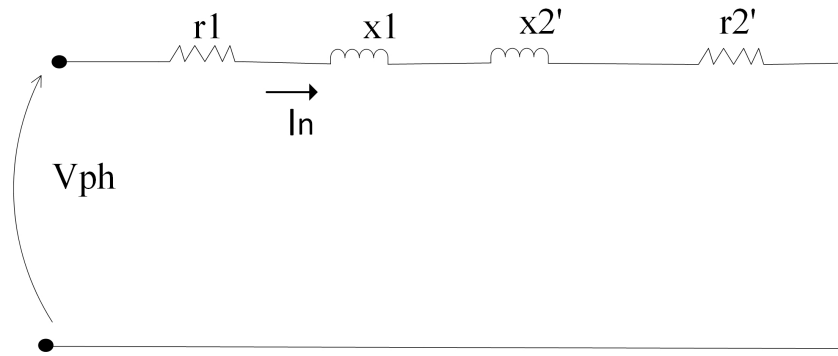


Figure E.5 – Equivalent Circuit Locked Rotor Test

Table E.3 – Average Resistance

$R_{AA'}$	$R_{BB'}$	$R_{CC'}$
10.03	10.30	10.16

$$R_m = \frac{10.03 + 10.3 + 10.16}{3} = 10.16 \Omega \tag{E.3}$$

- $r_1$  (*Stator winding resistance*) Calculus

Follow the calculus memory of stator winding resistor  $r_1$ .

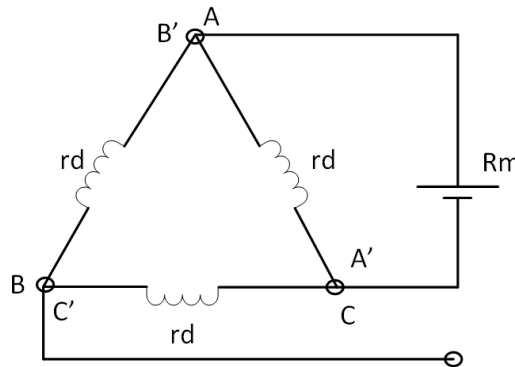


Figure E.6 – IM Winding Connection

$$R_m = \frac{rd \times 2rd}{3rd} \tag{E.4}$$

$$R_m = \frac{2}{3}rd \tag{E.5}$$

$$rd = \frac{3}{2}R_m \tag{E.6}$$

$$\text{As } ry = \frac{1}{3}rd \quad (\text{E.7})$$

And putting (E.6) into (E.7), it has

$$ry = \frac{R_m}{2} = \frac{10.16}{2}$$

$$ry = r1 = 5.08 \Omega \quad (\text{E.8})$$

- $r_2'$  (*Rotor winding resistance referred to stator winding*) Calculus

From Table E.2,  $W1+W2=85$  W

$$W1 + W2 = 3 \times (r1 + r2') \times in^2 \quad (\text{E.9})$$

$$\frac{85}{3 \times 1.8^2} = 5.08 + r2'$$

$$r2' = 3.66 \Omega \quad (\text{E.10})$$

- $Q$  (*Reactive power*)

$$Q = \sqrt{3} \times (W2 - W1) \quad (\text{E.11})$$

From Table E.2,  $W2-W1=45$

$$Q = \sqrt{3} \times (65 - 20) = 77.94 \text{ Var} \quad (\text{E.12})$$

$$Q = 3 \times (x1 + x2') \times In^2 \quad (\text{E.13})$$

- $x_1$  (*Stator winding reactance*) and  $x_2'$  (*Rotor winding reactance referred to stator winding*)

doing (E.13) and (E.2) in (E.14)

$$77.94 = 3 \times (x1 + x2') \times 1.8^2 \quad (\text{E.14})$$

$$(x1 + x2') = 8.01 \Omega \quad (\text{E.15})$$

$$\begin{bmatrix} x1 \mapsto x2' \\ r1 \mapsto r2' \end{bmatrix} \quad (\text{E.16})$$

doing (E.8) and (E.10) in (E.16)

$$\begin{bmatrix} x1 \mapsto x2' \\ 5.08 \mapsto 3.66 \end{bmatrix}$$

$$x1 = \frac{r1 \times x2'}{r2} \quad (\text{E.17})$$

$$x1 = \frac{5.08 \times x2'}{3.66} \quad (\text{E.18})$$

From (E.15) and (E.18), result in

$$5.08 \times x2' + x2' \times 3.66 = 29.32 \quad (\text{E.19})$$

$$x2' \times 8.74 = 29.32 \quad (\text{E.20})$$

$$x2' = 3.35 \Omega \quad (\text{E.21})$$

doing (E.21) in (E.18), result in

$$x1 = \frac{5.08 \times 3.35}{3.66} \quad (\text{E.22})$$

$$x1 = 4.65 \Omega \quad (\text{E.23})$$

### E.3 Power and Losses Calculus

The  $P_{av}$  was defined in Figure E.3 and consist in 3 W.  $P_{nl}$  (*No load losses*) is obtained from no load test for 220 V, it resulted in 70 W ( $W1 + W2$ ).

- $P_{jstator}$  (*No Load Stator Joules Losses*)

$$P_{jstator26^\circ} = 3 \times r1 \times im^2 \quad (E.24)$$

$$P_{jstator26^\circ} = 3 \times 5.08 \times 1.35^2 \quad (E.25)$$

$$P_{jstator26^\circ} = 27.77 \text{ W} \quad (E.26)$$

- $P_{hf}$  (*hysteresis and Foucault losses*)

$$P_{hf} = (W1 + W2) - 3 \times r1 \times im^2 - P_{av} \quad (E.27)$$

$$P_{hf} = 70 - 3 \times 5.08 \times 1.35^2 - 3 \quad (E.28)$$

$$P_{hf} = 39.23 \text{ W} \quad (E.29)$$

### E.3.1 No Load Reactive Power

$$Q_0 = \sqrt{3} \times (W2 - W1) \quad (E.30)$$

From Table E.1,  $W2 - W1 = 270 \text{ W}$

$$Q_0 = \sqrt{3} \times 270 \text{ Var}$$

$$Q_0 = 467.65 \text{ Var} \quad (E.31)$$

### E.3.2 Magnetization Branch

- $Q_m$  (*No load Reactive Power in Magnetization Branch*)

$$Q_m = Q_0 - 3 \times x1 \times I_0^2 \quad (E.32)$$

$$Q_m = 467.65 - 3 \times 4.65 \times 1.35^2 \quad (E.33)$$

$$Q_m = 442.23 \text{ Var} \quad (E.34)$$

- $\Theta_0$  (*Magnetization Branch Power Factor Angle*)

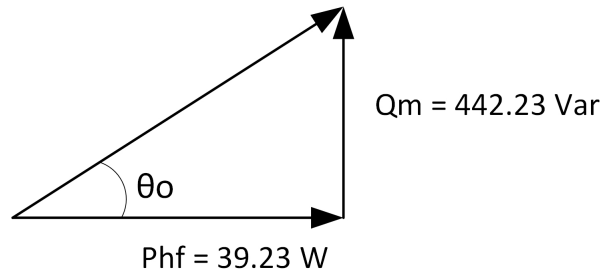


Figure E.7 – Magnetization branch power factor

$$\Theta_0 = \arctan \frac{442.23}{39.23} \quad (\text{E.35})$$

$$\Theta_0 = 84.93^\circ \quad (\text{E.36})$$

- $I_{rm}$  (*Magnetization branch current across resistance*)

$$I_{rm} = I_m \times \cos \Theta_0 \quad (\text{E.37})$$

$$I_{rm} = 1.35 \times \cos 84.93 \quad (\text{E.38})$$

$$I_{rm} = 0.1193 \text{ A} \quad (\text{E.39})$$

- $I_{xm}$  (*Magnetization branch current across inductor*)

$$I_{xm} = I_m \times \sin \Theta_0 \quad (\text{E.40})$$

$$I_{xm} = 1.35 \times \sin 84.93 \quad (\text{E.41})$$

$$I_{xm} = 1.34 \text{ A} \quad (\text{E.42})$$

- $r_m$  (*Magnetization branch resistance*)

$$r_m = \frac{P_{hf}}{3 \times I_{rm}^2} \quad (\text{E.43})$$

$$r_m = \frac{39.23}{3 \times 0.1193^2} \quad (\text{E.44})$$

$$r_m = 918.79 \Omega \quad (\text{E.45})$$

- $x_m$  (Magnetization branch reactance)

$$x_m = \frac{Q_m}{3 \times I_{xm}^2} \quad (\text{E.46})$$

$$x_m = \frac{442.23}{3 \times 1.34^2} \quad (\text{E.47})$$

$$x_m = 82.10 \Omega \quad (\text{E.48})$$

## E.4 Parameters of Induction Motor

Figure E.8 shows all *IM* parameters calculated as resistors, reactance and currents as data obtained during experiment, without temperature correction because the motor operated no load.

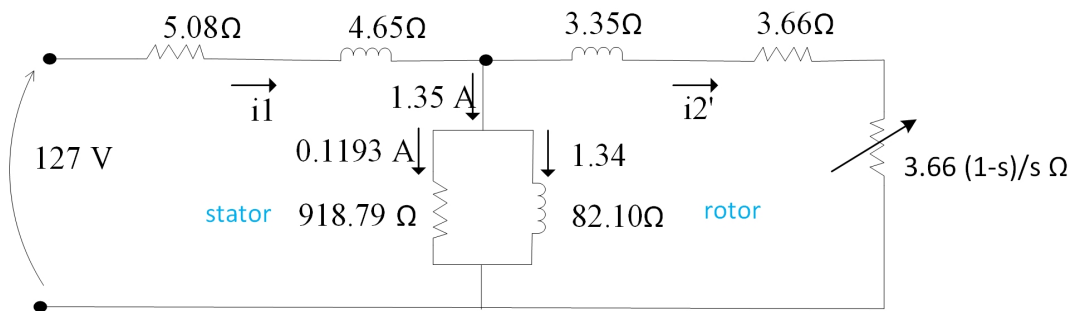


Figure E.8 – Parameters of Induction Motor

## E.5 Induction Motor Efficiency

It will be calculated the temperature correction factor, corrected resistances to 40 °C, corrected winding losses,  $P_{win}$  (Winding losses) 40°C, and total losses,  $P_{tl}$  (Total losses), before induction motor efficiency calculus.

### E.5.1 Temperature Correction Factor and Resistance Correction

The temperature correction factor is used in order to attend the IEC standard,[49, 50], that requires the resistances correction to lead to the starting reference resistance for the temperature rise tests, [50].

- $K_t$  (*Temperature correction factor for 40 degree C*)

$$K_t 40^\circ C = \frac{234.5 + 40}{234.5 + 26} \quad (\text{E.49})$$

$$K_t 40^\circ C = 1.054 \text{ for } r_1 \text{ and } r'_2 \quad (\text{E.50})$$

- $r_1 40C$  (*Corrected stator winding resistance for 40 degree C*)

$$r_1 40^\circ C = r_1 26^\circ \times 1.054 \quad (\text{E.51})$$

$$r_1 40^\circ C = 5.08 \times 1.054 \quad (\text{E.52})$$

$$r_1 40^\circ C = 5.35 \Omega \quad (\text{E.53})$$

- $r'_2 40C$  (*Corrected rotor winding resistance referred to stator for 40 degree C*)

$$r'_2 40^\circ C = r_2 26^\circ \times 1.054 \quad (\text{E.54})$$

$$r'_2 40^\circ C = 3.66 \times 1.054 \quad (\text{E.55})$$

$$r'_2 40^\circ C = 3.86 \Omega \quad (\text{E.56})$$

## E.6 Corrected Winding Losses for 40 °C and Total Losses

- $P_{win40C}$  (*Corrected winding losses for 40 degree C*)

The  $P_{win}$  measured in locked rotor test, Table E.2, need to be corrected for 40 °C. Follow the corrected winding losses for 40 °C.

$$P_{win} 40^{\circ}C = K_t \times P_{win} 26^{\circ}C \quad (E.57)$$

$$P_{win} 40^{\circ}C = 1.054 \times 85 W \quad (E.58)$$

$$P_{win} 40^{\circ}C = 89.59 W \quad (E.59)$$

- $P_{tl}$  (Total losses)

The  $P_{tl}$  calculus:

$$P_{tl} = P_{hf} + P_{av} + P_{win} 40^{\circ}C \quad (E.60)$$

$$P_{tl} = 39.23 W + 3 W + 89.59 W \quad (E.61)$$

$$P_{tl} = 131.82 W \quad (E.62)$$

## E.7 Motor Efficiency Estimate

- $P_{out}$  (Motor output power)
- $P_{in}$  (Motor input power)

Note: (Motor data plate is shown in Table 1.8)

$$\eta = \frac{P_{out}}{P_{in}} \quad (E.63)$$

$$P_{in} = P_{out} + P_{tl} \quad (E.64)$$

$$P_{in} = 370 + 131.82 W \quad (E.65)$$

$$P_{in} = 501.82 W \quad (E.66)$$

$$\eta = \frac{370}{501.82} \quad (\text{E.67})$$

$$\eta = 73.73 \% \quad (\text{E.68})$$

## E.8 Induction Motor Currents

Follow the calculus of  $I_{dw_{MT}}$  and  $I_{w_{MT}}$ . These values are shown in Table 1.10 for all scenarios tested.

- $I_{dw_{MT}}$

$$Q = \sqrt{3} \times 220 \times I_{dw_{MT}} = \sqrt{3} \times (W2 - W1) \quad (\text{E.69})$$

$$Q = \sqrt{3} \times 220 \times I_{dw_{MT}} = 467.65 \quad (\text{E.70})$$

$$I_{dw_{MT}} = 1.23 \text{ A} ** \quad (\text{E.71})$$

Note \*\*: The difference between  $I_{dw_{MT}}$  and  $I_{xm}$  is perfectly acceptable. The difference close to 0.1 A between expected and found values is due to small measurements errors and instruments precision and accuracy errors. It does not affect the presented modelling. Therefore, the results and modelling continue valid.

- $I_{w_{MT}}$

$$P = (W1 + W2) = 70.0 \text{ W} \quad (\text{E.72})$$

$$Q = \sqrt{3} \times (W2 - W1) = 467.6 \text{ W} \quad (\text{E.73})$$

$$S = \sqrt{70.0^2 + 467.6^2} = 472.86 \text{ VA} \quad (\text{E.74})$$

$$\cos\phi = \frac{P}{S} = \frac{70}{472.86} \quad (\text{E.75})$$

$$\cos\phi = 0.148 \quad (\text{E.76})$$

$$I_{w_{MT}} = I_0 \times \cos\phi = 1.35 \times 0.148 \quad (\text{E.77})$$

$$I_{w_{MT}} = 0.20 \text{ A} \quad (\text{E.78})$$

In Figure E.9 is shown the resistor banks current and the no load *IM* current.

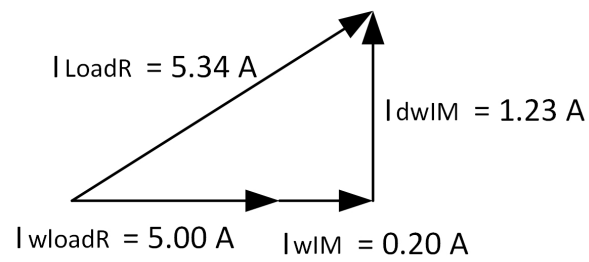


Figure E.9 – Resistors bank and IM currents in scenarios C as Table 1.10

# APPENDIX F – Solving Equations with Matlab

## F.1 Introduction

This appendix demonstrates how the equations indicated in chapter 1 are solved. There will be presented the Matlab code for equation solution used in two typical schemes mounted in laboratory. The first one is focused on electrical system scheme mounted in laboratory for feeding three resistor banks as shown in Figure 1.11. The second is focused on the scheme for feeding three resistor banks and an induction motor together as shown in figure 1.12. In the equation system, there are four known variables and four unknown variables that will be found.

## F.2 Equations

### F.2.1 Electrical system feeding three resistor banks

Based on Figure 1.11, the equations below are formulated to calculate the currents  $I_{w_{SG}}$ ,  $I_{c1}$ ,  $I_{w_{IG}}$ ,  $I_{c2}$ .

$$I_{SG}^2 = I_{w_{SG}}^2 + I_{c1}^2 \quad (\text{F.1})$$

$$I_{IG}^2 = I_{w_{IG}}^2 + I_{c2}^2 \quad (\text{F.2})$$

$$I_c = I_{c1} + I_{c2} \quad (\text{F.3})$$

$$I_{w_{loadR}} = I_{w_{SG}} + I_{w_{IG}} \quad (\text{F.4})$$

### F.2.2 Electrical system feeding three resistor banks and an induction motor

Based on Figure 1.12, the equations below are formulated to calculate the currents  $I_{w_{SG}}$ ,  $I_{c1}$ ,  $I_{w_{IG}}$ ,  $I_{c2}$ . The currents  $I_{dw_{MT}}$  and  $I_{w_{MT}}$  are given values and these were calculated as appendix E.

$$I_{SG}^2 = I_{w_{SG}}^2 + I_{c1}^2 \quad (\text{F.5})$$

$$I_{IG}^2 = Iw_{IG}^2 + I_{c2}^2 \quad (\text{F.6})$$

$$I_c - I_{dwMT} = I_{c1} + I_{c2} \quad (\text{F.7})$$

$$Iw_{loadR} + Iw_{MT} = Iw_{SG} + Iw_{IG} \quad (\text{F.8})$$

### F.2.3 Power and Efficiencies

From the results of previous equations, the power of  $PSG$ ,  $PIG$ ,  $P_{DCMSG}$ ,  $P_{DCMIG}$  and the efficiencies  $\eta_{group}$ ,  $\eta_{SG}$ ,  $\eta_{IG}$  were calculated as equations below.

$$P_{SG} = \sqrt{3} \times V_{SG} \times Iw_{SG} \quad (\text{F.9})$$

$$P_{IG} = \sqrt{3} \times V_{IG} \times Iw_{IG} \quad (\text{F.10})$$

$$P_{DCMSG} = V a_{DCMSG} \times I a_{DCMSG} \quad (\text{F.11})$$

$$P_{DCMIG} = V a_{DCMIG} \times I a_{DCMIG} \quad (\text{F.12})$$

$$\eta_{group\%} = \frac{P_{SG} + P_{IG}}{P_{DCMSG} + P_{DCMIG}} \times 100 \quad (\text{F.13})$$

$$\eta_{SG\%} = \frac{P_{SG}}{P_{DCMSG}} \times 100 \quad (\text{F.14})$$

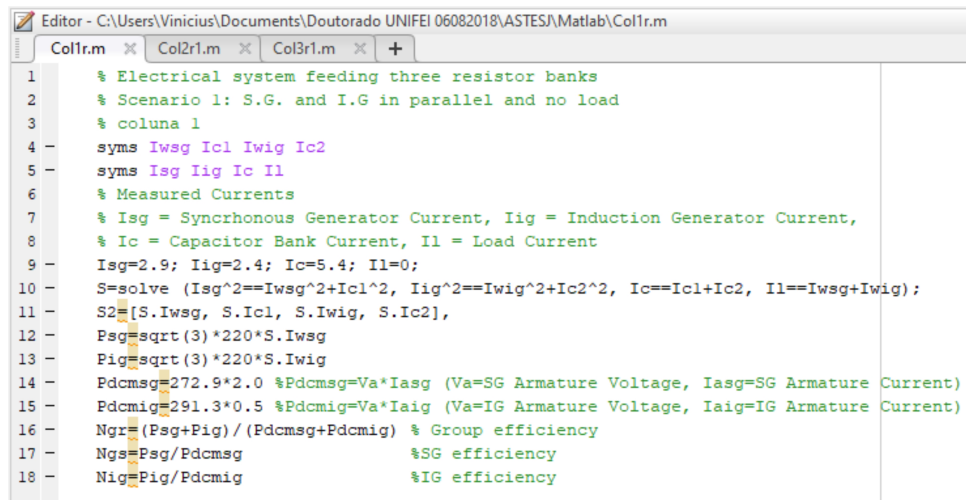
$$\eta_{IG\%} = \frac{P_{IG}}{P_{DCMIG}} \times 100 \quad (\text{F.15})$$

## F.3 Matlab Code

### F.3.1 Electrical system feeding three resistor banks

This section shows the Matlab code used to solve the equations formulated for each scenario. Not make sense to show all scenarios because it would be repetitive and not effective. Then, in order to obtain the results, the new entering data  $Iw_{SG}$ ,  $I_{c1}$ ,  $Iw_{IG}$ ,  $I_{c2}$  from Table 1.9 should be inserted in line 9 of Matlab code, Figures F.1, F.2 or F.3, this code should be run and the viable result should be considered.

- Scenario 1B as Table 1.9, column 1.



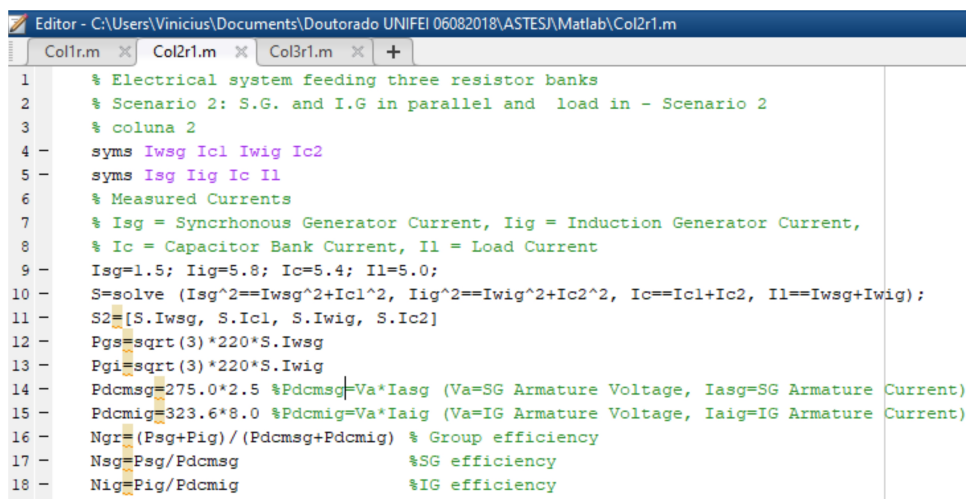
```

Editor - C:\Users\Vinicius\Documents\Doutorado UNIFEI 06082018\ASTESJ\Matlab\Col1r.m
Col1r.m x Col2r1.m x Col3r1.m x +
1 % Electrical system feeding three resistor banks
2 % Scenario 1: S.G. and I.G in parallel and no load
3 % coluna 1
4 - syms Iwsg Icl Iwig Ic2
5 - syms Isg Iig Ic Il
6 % Measured Currents
7 % Isg = Synchronous Generator Current, Iig = Induction Generator Current,
8 % Ic = Capacitor Bank Current, Il = Load Current
9 - Isg=2.9; Iig=2.4; Ic=5.4; Il=0;
10 - S=solve (Isg^2==Iwsg^2+Icl^2, Iig^2==Iwig^2+Ic2^2, Ic==Icl+Ic2, Il==Iwsg+Iwig);
11 - S2=[S.Iwsg, S.Icl, S.Iwig, S.Ic2],
12 - Psg=sqrt(3)*220*S.Iwsg
13 - Pig=sqrt(3)*220*S.Iwig
14 - Pdcmsg=272.9*2.0 %Pdcmsg=Va*Iasg (Va=SG Armature Voltage, Iasg=SG Armature Current)
15 - Pdcmig=291.3*0.5 %Pdcmig=Va*Iaig (Va=IG Armature Voltage, Iaig=IG Armature Current)
16 - Ngr=(Psg+Pig)/(Pdcmsg+Pdcmig) % Group efficiency
17 - Nsg=Psg/Pdcmsg %SG efficiency
18 - Nig=Pig/Pdcmig %IG efficiency

```

Figure F.1 – Scenario 1B

- Scenario 2B as Table 1.9, column 2.



```

Editor - C:\Users\Vinicius\Documents\Doutorado UNIFEI 06082018\ASTESJ\Matlab\Col2r1.m
Col1r.m x Col2r1.m x Col3r1.m x +
1 % Electrical system feeding three resistor banks
2 % Scenario 2: S.G. and I.G in parallel and load in - Scenario 2
3 % coluna 2
4 - syms Iwsg Icl Iwig Ic2
5 - syms Isg Iig Ic Il
6 % Measured Currents
7 % Isg = Synchronous Generator Current, Iig = Induction Generator Current,
8 % Ic = Capacitor Bank Current, Il = Load Current
9 - Isg=1.5; Iig=5.8; Ic=5.4; Il=5.0;
10 - S=solve (Isg^2==Iwsg^2+Icl^2, Iig^2==Iwig^2+Ic2^2, Ic==Icl+Ic2, Il==Iwsg+Iwig);
11 - S2=[S.Iwsg, S.Icl, S.Iwig, S.Ic2]
12 - Pgs=sqrt(3)*220*S.Iwsg
13 - Pgi=sqrt(3)*220*S.Iwig
14 - Pdcmsg=275.0*2.5 %Pdcmsg=Va*Iasg (Va=SG Armature Voltage, Iasg=SG Armature Current)
15 - Pdcmig=323.6*8.0 %Pdcmig=Va*Iaig (Va=IG Armature Voltage, Iaig=IG Armature Current)
16 - Ngr=(Psg+Pig)/(Pdcmsg+Pdcmig) % Group efficiency
17 - Nsg=Psg/Pdcmsg %SG efficiency
18 - Nig=Pig/Pdcmig %IG efficiency

```

Figure F.2 – Scenario 2B

- Scenario 3B as Table 1.9, column 3.

### F.3.2 Electrical system feeding three resistor banks and an induction motor

This section will show the Matlab code used to solve the equations formulated for each scenario. Not make sense to show all scenarios because it would be repetitive and not effective. Then, in order to obtain the new results, the new entering data  $I_{wSG}$ ,  $I_{c1}$ ,  $I_{wIG}$ ,  $I_{c2}$  from Table 1.10 should be inserted in line 9 of Matlab code, Figures F.1, F.2 or F.3, this code should be run and the viable result should be considered.

- Scenario 1C as Table 1.10, column 1.

```

Editor - C:\Users\Vinicius\Documents\Doutorado UNIFEI 06082018\ASTESJA\Matlab\Col3r1.m
Col1r.m x Col2r1.m x Col3r1.m x +
1 % Electrical system feeding three resistor banks
2 % Scenario 3: S.G. and I.G in parallel and load in - Scenario 3
3 % coluna 3
4 syms Iwsg Icl Iwig Ic2
5 syms Isg Iig Ic I1
6 % Measured Currents
7 % Isg = Synchronous Generator Current, Iig = Induction Generator Current,
8 % Ic = Capacitor Bank Current, I1 = Load Current
9 Isg=2.0; Iig=5.1; Ic=5.4; I1=5.0;
10 S=solve (Isg^2==Iwsg^2+Icl^2, Iig^2==Iwig^2+Ic2^2, Ic==Icl+Ic2, I1==Iwsg+Iwig);
11 S2=[S.Iwsg, S.Icl, S.Iwig, S.Ic2],
12 Psg=sqrt(3)*220*S.Iwsg
13 Pgi=sqrt(3)*220*S.Iwig
14 Pdcmsg=276.2*3.8 %Pdcmsg=Va*Iasg (Va=SG Armature Voltage, Iasg=SG Armature Current)
15 Pdcmig=316.7*7.0 %Pdcmig=Va*Iaig (Va=IG Armature Voltage, Iaig=IG Armature Current)
16 Ngr=(Psg+Pig)/(Pdcmsg+Pdcmig) % Group efficiency
17 Nsg=Psg/Pdcmsg %SG efficiency
18 Nig=Pig/Pdcmig %IG efficiency

```

Figure F.3 – Scenario 3B

```

Editor - C:\Users\Vinicius\Documents\Doutorado UNIFEI 06082018\ASTESJA\Matlab\Mot Res\Col1mrr1.m
Col1mrr1.m x Col2mrr1.m x +
1 % Electrical system feeding three resistor banks and an induction motor together
2 % Scenario 1: S.G. and I.G in parallel and no load - Scenario 1
3 % coluna 1
4 syms Iwsg Icl Iwig Ic2
5 syms Isg Iig Ic I1
6 % Measured Currents
7 % Isg = Synchronous Generator Current, Iig = Induction Generator Current,
8 % Ic = Capacitor Bank Current, I1 or (IwloadR) = Load Current
9 Isg=2.8; Iig=2.3; Ic=5.4; I1=0; Idwmt=1.22; Iwmt=0.184;
10 S=solve (Isg^2==Iwsg^2+Icl^2, Iig^2==Iwig^2+Ic2^2, Ic-Iwmt==Icl+Ic2, I1+Iwmt==Iwsg+Iwig);
11 S2=[S.Iwsg, S.Icl, S.Iwig, S.Ic2],
12 Psg=sqrt(3)*220*S.Iwsg
13 Pig=sqrt(3)*220*S.Iwig
14 Pdcmsg=278.9*2.0 %Pdcmsg=Va*Iasg (Va=SG Armature Voltage, Iasg=SG Armature Current)
15 Pdcmig=288.9*1.0 %Pdcmig=Va*Iaig (Va=IG Armature Voltage, Iaig=IG Armature Current)
16 Ngr=(Psg+Pig)/(Pdcmsg+Pdcmig) % Group efficiency
17 Nsg=Psg/Pdcmsg %SG efficiency
18 Nig=Pig/Pdcmig %IG efficiency

```

Figure F.4 – Scenario 1C

- Scenario 2C as Table 1.10, column 2.

```

Editor - C:\Users\Vinicius\Documents\Doutorado UNIFEI 06082018\ASTESJA\Matlab\Mot Res\Col2mrr1.m
Col1mrr1.m x Col2mrr1.m x +
1 % Electrical system feeding three resistor banks and an induction motor together
2 % Scenario: S.G. and I.G in parallel and load in - Scenario 2
3 % coluna 2
4 syms Iwsg Icl Iwig Ic2
5 syms Isg Iig Ic I1
6 % Measured Currents
7 % Isg = Synchronous Generator Current, Iig = Induction Generator Current,
8 % Ic = Capacitor Bank Current, I1 or (IwloadR) = Load Current
9 Isg=0.7; Iig=6.0; Ic=5.4; I1=5.0; Idwmt=1.23; Iwmt=0.2;
10 S=solve (Isg^2==Iwsg^2+Icl^2, Iig^2==Iwig^2+Ic2^2, Ic-Iwmt==Icl+Ic2, I1+Iwmt==Iwsg+Iwig);
11 S2=[S.Iwsg, S.Icl, S.Iwig, S.Ic2],
12 Psg=sqrt(3)*220*S.Iwsg
13 Pig=sqrt(3)*220*S.Iwig
14 Pdcmsg=277*2.9 %Pdcmsg=Va*Iasg (Va=SG Armature Voltage, Iasg=SG Armature Current)
15 Pdcmig=330*8.0 %Pdcmig=Va*Iaig (Va=IG Armature Voltage, Iaig=IG Armature Current)
16 Ngr=(Psg+Pig)/(Pdcmsg+Pdcmig) % Group efficiency
17 Nsg=Psg/Pdcmsg %SG efficiency
18 Nig=Pig/Pdcmig %IG efficiency

```

Figure F.5 – Scenario 2C

- Scenario 3C as Table 1.10, column 3.

```

Editor - C:\Users\Vinicius\Documents\Doutorado UNIFEI 06082018\ASTES\Matlab\Mot Res\Col3mrr1.m
Col1mrr1.m x Col2mrr1.m x Col3mrr1.m x +
1 % Electrical system feeding three resistor banks and an induction motor together
2 % Scenario 3: S.G. and I.G in parallel and load in - Scenario 3
3 % coluna 3
4 - syms Iwsg Icl Iwig Ic2
5 - syms Isg Iig Ic I1
6 % Measured Currents
7 % Isg = Synchronous Generator Current, Iig = Induction Generator Current,
8 % Ic = Capacitor Bank Current, I1 or (IloadR) = Load Current
9 - Isg=1.6; Iig=5.0; Ic=5.4; I1=5.0; Idwmt=1.23; Iwmt=0.2;
10 - S=solve (Isg^2==Iwsg^2+Icl^2, Iig^2==Iwig^2+Ic2^2, Ic-Idwmt==Icl+Ic2, I1+Iwmt==Iwsg+Iwig);
11 - S2=[S.Iwsg, S.Icl, S.Iwig, S.Ic2],
12 - Psg=sqrt(3)*220*S.Iwsg
13 - Pig=sqrt(3)*220*S.Iwig
14 - Pdcmsg=277.5*4.0 %Pdcmsg=Va*Iasg (Va=SG Armature Voltage, Iasg=SG Armature Current)
15 - Pdcmig=318*7.0 %Pdcmig=Va*Iaig (Va=IG Armature Voltage, Iaig=IG Armature Current)
16 - Ngr=(Psg+Pig)/(Pdcmsg+Pdcmig) % Group efficiency
17 - Nsg=Psg/Pdcmsg %SG efficiency
18 - Nig=Pig/Pdcmig %IG efficiency

```

Figure F.6 – Scenario 3C

# Bibliography

- 1 ARCHIVE., D. *TCA 785 Application Notes – SIEMENS*. 2019. Disponível em: <<https://www.datasheetarchive.com/TCA%20785%20application%20note-datasheet.html>>. 12, 118, 119
- 2 MOHAN, N.; UNDELAND, T. M.; ROBBINS, W. P. *Power electronics: converters, applications, and design*. [S.l.]: John wiley & sons, 2003. 13, 131
- 3 LANDER, C. W. *Eletrônica industrial: teoria e aplicações*. [S.l.]: McGraw-Hill, 1988. 15, 115, 121
- 4 FRÖHR, F.; ORTTENBURGUER, F. Introduction to electronic control (in spanish). *Marcombo SA, Siemens Aktiengesellschaft*, 1986. 15, 26, 72, 77, 100, 101, 104, 105, 106, 128, 133, 136, 137, 142, 143, 144, 145
- 5 HAQUE, M. Self-excited single-phase and three-phase induction generators in remote areas. In: IEEE. *2008 International Conference on Electrical and Computer Engineering*. [S.l.], 2008. p. 38–42. 26
- 6 IBRAHIM, K.; LEIDHOLD, R. Variable frequency converter based voltage and frequency regulation of induction generator for stand-alone system application. In: IEEE. *AFRICON 2015*. [S.l.], 2015. p. 1–5. 26
- 7 TOUTI, E. et al. Asynchronous generator model for autonomous operating mode. In: IEEE. *Proceedings of the International Conference on Electronics, Computers and Artificial Intelligence-ECAI 2013*. [S.l.], 2013. p. 1–6. 26
- 8 MACEDO, D. M. "The use of pumps operating as turbines and induction generators in electric power generation" (in portuguese). Master in Science Dissertation, Federal University of Itajubá, UNIFEI. 2004. 26, 29, 55
- 9 Braga, A. V. et al. Isolated induction generator in a rural brazilian area: Field performance tests, doi:10.1016/j.renene.2015.05.057. *Renewable Energy Journal*, 2015. 26, 66, 67, 85
- 10 SIMÕES, M. G.; FARRET, F. A. *Renewable energy systems: design and analysis with induction generators*. [S.l.]: CRC press, 2004. 26, 66, 83
- 11 DEMETRIADES, G. M. The use of induction generators for small-scale hydroelectric schemes in remote areas. In: IEEE. *2000 10th Mediterranean Electrotechnical Conference. Information Technology and Electrotechnology for the Mediterranean Countries. Proceedings. MeleCon 2000 (Cat. No. 00CH37099)*. [S.l.], 2000. v. 3, p. 1055–1058. 26
- 12 LEE, C.-H.; WANG, L. A novel analysis of parallel operated self-excited induction generators. *IEEE Transactions on Energy Conversion*, IEEE, v. 13, n. 2, p. 117–123, 1998. 26
- 13 WANG, L.; LEE, C.-H. Dynamic analyses of parallel operated self-excited induction generators feeding an induction motor load. *IEEE Transactions on Energy Conversion*, IEEE, v. 14, n. 3, p. 479–485, 1999. 26

- 14 CHAKRABORTY, C. et al. Performance of parallel-operated self-excited induction generators with the variation of machine parameters. In: IEEE. *Proceedings of the IEEE 1999 International Conference on Power Electronics and Drive Systems. PEDS'99 (Cat. No. 99TH8475)*. [S.l.], 1999. v. 1, p. 86–91. [26](#)
- 15 GAWANDE, S. et al. Synchronization of synchronous generator and induction generator for voltage & frequency stability using statcom. In: IEEE. *2010 3rd International Conference on Emerging Trends in Engineering and Technology*. [S.l.], 2010. p. 407–412. [26](#)
- 16 ION, C.; MARINESCU, C. Control of parallel operating micro hydro power plants. In: IEEE. *2010 12th International Conference on Optimization of Electrical and Electronic Equipment*. [S.l.], 2010. p. 1204–1209. [26](#), [67](#), [85](#)
- 17 REDDY, P. J.; SINGH, S. Voltage and frequency control of parallel operated synchronous and induction generators in micro hydro scheme. In: IEEE. *2014 International Conference on Computation of Power, Energy, Information and Communication (IC-CPEIC)*. [S.l.], 2014. p. 124–129. [26](#), [67](#), [85](#)
- 18 VANCO, W. E. et al. Experimental analysis of a self-excited induction generators operating in parallel with synchronous generators applied to isolated load generation. *IEEE Latin America Transactions*, IEEE, v. 14, n. 4, p. 1730–1736, 2016. [26](#), [67](#)
- 19 MAGALHÃES, A. S. et al. Parallel operation repowering of synchronous and induction generator. In: IEEE. *2016 IEEE 16th International Conference on Environment and Electrical Engineering (EEEIC)*. [S.l.], 2016. p. 1–6. [26](#), [67](#)
- 20 MELLO, F. P. Induction generators with inherent var generation capabilities an alternative to synchronous generators. XIII Symposium of Specialists in Electric Operational Expansion Planning, Foz do Iguaçu, Brazil. 2014. [26](#), [29](#), [67](#), [85](#)
- 21 WIJAYA, F. D.; GAJAYANA, L. N.; WIJAYA, H. P. Parallel operation synchronous and induction generator on microgrid testbed. In: IEEE. *2017 9th International Conference on Information Technology and Electrical Engineering (ICITEE)*. [S.l.], 2017. p. 1–5. [26](#), [67](#)
- 22 GAWANDE, S.; PORATE, K. Review of parallel operation of synchronous generator and induction generator for stability. In: IEEE. *2009 Second International Conference on Emerging Trends in Engineering & Technology*. [S.l.], 2009. p. 716–721. [26](#), [67](#)
- 23 SILVA, V. Z.; REZEK, Â. J. J.; CAMACHO, C. A. P. Innovative and useful laboratory experiments of electrical machines. Scholar's Press, 2018. [26](#), [72](#), [74](#), [77](#)
- 24 GÜLEN, S. C. *Gas Turbines for Electric Power Generation*. [S.l.]: Cambridge University Press, 2019. [27](#)
- 25 FITZGERALD, A. E. et al. *Electric machinery*. [S.l.]: McGraw-Hill New York, 2003. v. 5. [27](#), [29](#), [55](#), [66](#), [73](#)
- 26 REZEK, Â. J. J. et al. A four quadrant regenerative dc drive by speed reversal using armature current inverting and by means of field current inverter - a comparative analysis (in portuguese). IEEE - INDUSCON/96, São Paulo-SP. INDUSCON/96 Annals. 1996. [28](#), [143](#)

- 27 REZEK, Â. J. J. Fundamentos básicos de máquinas elétricas: teoria e ensaios. *Synergia, Rio de Janeiro-RJ and ACTA, Itajubá-MG*, 2011. 28
- 28 SILVA, V. Z.; REZEK, Â. J. J.; CORRÊA, R. D. L. Analysis of synchronous and induction generators in parallel operation mode in an isolated electric system, doi: 10.1109/pedg.2017.7972459. In: IEEE. *2017 IEEE 8th International Symposium on Power Electronics for Distributed Generation Systems (PEDG)*. [S.l.], 2017. p. 1–8. 29, 40, 41, 48, 50, 52, 53, 54, 55, 66, 67, 68, 73, 74, 84
- 29 SILVA, Â. J. J. R. V. Z.; CORRÊA, R. L. Analysis of synchronous and induction generators in parallel operation mode in an isolated electric system using a ballast load as a regulation system under transient conditions, doi: 10.22270/ijesar.v4i2.112. In: IJESAR. [S.l.], 2018. p. 22–37. 29, 66, 67, 68
- 30 CHAPALLAZ, J.-M.; EICHENBERGER, P.; FISCHER, G. *Manual on pumps used as turbines*. [S.l.]: Vieweg Braunschweig, Germany, 1992. 37
- 31 SILVA, V. Z.; REZEK, Â. J. J.; CORRÊA, R. D. L. Transients analysis of synchronous and induction generators in parallel operation mode in an isolated electric system, doi:10.1109/cobep.2017.8257236. In: IEEE. *2017 Brazilian Power Electronics Conference (COBEP)*. [S.l.], 2017. 55, 66, 67, 68
- 32 OLIVEIRA, J. C.; COGO, J. R.; ABREU, J. P. G. Transformadores, teoria e ensaios. editora edgard blücher ltda. *São Paulo, SP*, 1984. 56, 151
- 33 SILVA, V. Z.; JUNQUEIRA, R. A. J.; OGOULOLA, C. E. G. Alternatives to control the frequency increase in an electric system with synchronous and induction generators in parallel operation mode, doi: 10.1016/j.epsr.2019.106136. *Electric Power Systems Research*, Elsevier, v. 180, 2020. 66
- 34 SILVA, V. Z.; REZEK, Â. J. J.; CORRÊA, R. D. L. Novel analysis of synchronous and induction generators in parallel operation mode in an isolated electric system, doi: 10.25046/aj020625. *ASTES journal*, 2017. 66, 67, 68, 69, 77
- 35 SILVA, V. Z.; REZEK, A. J. J.; CORRÊA, R. L. Novel topology analysis of synchronous and induction generators in parallel operation mode in an offshore isolated electric system. *Annals of CLAGTEE, Mar del Plata Argentina*. 2017. 66
- 36 SILVA, V. Z. Implementation of estimator in c++ as a substitute of tachogenerator to dc motor speed control, (in portuguese). UNIFEI Master in Science Dissertation. 2004. 72, 77
- 37 MORAES, G. G.; FERREIRA, D. C. G.; JÚNIOR, G. S. F. Speed control of dc machine (in portuguese). Electrical engineering final course report, Federal University of Itajuba. 2013. 87, 104, 143
- 38 REZEK, Â. J. J. et al. Modelling and implementation of a series dc motor drive system, doi: 105772/59814. <https://www.intechopen.com>, INTECH, 2015. 89, 104, 108, 143
- 39 REZEK, Â. J. J. Permanent and transitory state analysis of an ac/dc electrical energy conversion (in portuguese). Master in Science Dissertation, EFEI. 1986. 89, 96, 104, 108

- 40 REZEK, Â. J. J. et al. Project and simulation of a controlled drive system to direct current machines (in portuguese). Annals of II Internation Seminary of Electrical Motors and regulatory drives, II SIMEAR, Vol III pages 141-160 – EPUSP, ABINEE TEC/91. 1991. [104](#), [143](#), [144](#)
- 41 SPIEGEL, M. R. Mathematical handbook of formulas and tables. McGraw-Hill, 1968. [113](#)
- 42 MENDONÇA, G. R. S.; REZEK, Â. J. J. Electronic circuit to firing angle command of a three-phase thyristor bridge (in portuguese). Electrical engineering final course report, UNIFEI. 2002. [115](#)
- 43 MALVINO, A. P.; BATES, D. J. *Eletrônica-Vol. 1-8ª Edição*. [S.l.]: McGraw Hill Brasil, 2016. v. 2. [115](#)
- 44 GUIMARÃES, C. A. M. A point-on-wave switching system based on microcomputer (in portuguese). Master in Science Dissertation, UFSC, Florianópolis-SC, Brazil. 1986. [125](#)
- 45 COGO, J. R. Project and implementation of dc transmission system simulator (in portuguese). EFEI/FINEP agreement. 1985. [125](#)
- 46 PINHEIRO, C. A. M.; COGO, J. R. Firing circuit of thyristors in three-phase grid (in portuguese). EFEI. 1985. [125](#)
- 47 CAMACHO, C. A. P.; REZEK, Â. J. J. Use of symmetrical optimization technique to voltage adjust applied on synchronous generator (in portuguese). Master dissertation, Federal University of Itajubá, UNIFEI. 2007. [128](#), [140](#), [142](#)
- 48 ALMEIDA, A. T. L. d. Máquinas síncronas. *Grupo de Estudo em Manutenção Eletro-Eletrônica e Instalações, Universidade Federal de Itajubá*, 2000. [128](#)
- 49 IEC (Ed.). *IEC 60034-2-1 Rotating electrical machines, Standard methods for determining losses and efficiency from tests*. [128](#), [160](#)
- 50 IEC (Ed.). *IEC 60034-1 Rotating electrical machines, Rating and performance*. [128](#), [160](#)
- 51 REZEK, Â. J. J. et al. The modulus optimum (mo) method applied to voltage regulation systems: modeling, tuning and implementation. In: *Proc. International Conference on Power System Transients, IPST*. [S.l.: s.n.], 2001. v. 1, p. 24–28. [132](#), [138](#), [143](#)